

Modelling analysis of heat transfer in polymeric materials exposed to different heating scenarios

Mamadou Ndiaye

A thesis submitted in partial fulfilment of the requirements of the
University of Bolton for the degree of Doctor of Philosophy

School of Engineering,
University of Bolton,
Dean Road, Bolton, BL3 5AB

2016

DECLARATION OF AUTHORSHIP

I declare that the work described in this PhD thesis has not previously been presented in any form to the University or to any other institutional body, whether for assessment or for other purposes. I confirm that the intellectual content of the work is the result of my own effort and of no other person.

Signed

Date

ACKNOWLEDGEMENTS

Praise and glory to the Almighty on whom mercy my life entirely depends.

Completing a thesis such as this requires the understanding and assistance of a great many people. I cannot hope to name all the individuals who have assisted me along the way but wish to pay tributes to many people without whom this achievement would not have been possible.

I would like to thank my supervisors Professor Peter Myler and Professor Baljinder Kandola for their generous and continuous support. Their immense patience and helpful personality are appreciated. I am really indebted to them all for their valuable thoughts and contributions towards the development of my thesis and the knowledge I gain from them. They have helped and taught me not just on research but also a way of life.

I would like to deliver my thanks for help given by Dr. John Milnes and the other members of the Fire group in IMRI at the University of Bolton. I am also thankful to all my colleagues at the School of Engineering for their kindness; Mr Andy Smith, Dr Yassin Osman, Mr Bill Hails, Mr Karl Gregory, Mr Tim Ward, Dr Keith Holmes, Mr Paul Clavell, Dr Zhou Erping, Dr Safa Alhakeem.

Finally, my special thanks go to my parents; my mother Mrs Aissatou Fame, my father Dr Souleymane Ndiaye and my step mother Mrs Dieynaba Ndiaye Diallo, my loved wife Catherine and my children for their sacrifices, continuous prayers, endless love and moral support all the time. I am also thankful to my father-in-law Professor Jean Paul Velly, my brothers Ismael Bashir and his family in Bolton, my brother Fily and my brother Abu Bakr.

Ultimately, I just want to thank Professor Peter Myler and his family because he gave me the opportunity to have this thesis, to learn English, to teach in English, to meet all these knowledgeable people and enjoy the English side of science.

ABSTRACT

Polymers undergo physical, chemical and structural changes when exposed to heat and/or fire. Thermoplastics melt, decompose and burn; thermosets decompose, char and/or burn, depending on the temperature changes due to external incident heat flux.

Detailed in this thesis is a theoretical and numerical heat transfer study, which is undertaken to simulate and experimentally validated temperature variations during melting, decomposition, charring and ignition phases of polymers. For melting, thermoplastic polymers (polypropylene, polyester, polyamide 6, polymethyl methacrylate, polycarbonate and polystyrene) have been used, whereas for decomposition, charring and ignition glass fibre – reinforced epoxy composites have been chosen.

For each case a one-dimensional finite difference method, using Matlab as the operator has been developed to determine the transient temperature distributions within the different types of polymers materials. The convective and radiative heat transfer boundary conditions, at the exposed and unexposed sides of polymer samples, have also been taken into account accordingly. While some experimental results to validate the different numerical models built are from other researchers' work at Bolton, in addition to these, other sets of experiments were specifically developed for this work.

The melting behaviour of thermoplastics has been modelled in two scenarios: (i) vertically oriented sample where melt dripping occurs and (ii) horizontally oriented sample within a contained holder in order that the mass will not escape from the containment region. In the first scenario the sample was placed in a tube furnace, where the radiant heat is uniform on all sides of the sample. This is based on the experimental methodology developed at Bolton University in an earlier project which studied the melt dripping behaviour of polymers. The thermogravimetric and rheological analysis of molten drops had indicated that, depending upon the temperature of the furnace (external heat flux) and the structure of the polymer, in some cases it was pure melting whereas in others it was accompanied by a partial decomposition of the polymer. A one-dimensional finite difference method based on a moving boundary approach has been developed to model the temperatures of the molten drops polymers. The simulated results showed good agreement with the molten drops' temperatures measured by experiments. In addition, using kinetic parameters, degrees of decomposition in drops obtained at different furnace temperatures were also simulated, which were validated with previous experimental results.

For the second scenario, in which the sample is placed horizontally in a container, experiments were conducted using a cone calorimeter with the heat applied only on the top surface, while the other sides of the polymer sample are insulated. A further one-dimensional finite difference method based on a Stefan approach involving phase changing material, has been developed to determine the melting point temperature and to estimate the temperature profile within the polymer slab, to simulate pure melting and melting plus partial decomposition which may or may not catch fire depending upon the degree of decomposition. The predicted results matched well with the experimental results.

Furthermore, the heat transfer model was modified to simulate the temperature profiles through the thickness of a glass fibre - reinforced composite exposed to different heat fluxes in a cone calorimeter. This involved incorporating a kinetic model for the decomposition process taking into consideration the varying thermophysical properties as a function of temperature. This is achieved by using the critical heat flux that is the minimum incident heat flux leading to ignition, in the equation defining the ignition temperature,

The simulated temperature profiles matched well with the experimental results obtained from previous works at the University of Bolton, giving a much better agreement than previously published models describing this condition. Ignition phenomenon is well described by the model showing a jumping step when the composite polymer ignites and burns.

The last part of the work was to simulate the heat transfer in Intumescent coated glass fibre reinforced epoxy composites exposed to heat in a cone calorimeter. On exposure to heat the intumescent coating expands to form a char, the thickness and the thermal conductivity of which, depends on the type of coating. It was not the purpose of this work to model expansion of the coating; rather the emphasis was to understand the thermal barrier efficiency of the expanded char. However, changes to the surface, expansion of the local thickness and char region when exposed to heat were incorporated into the model to gain better agreement with experiment values.

TABLE OF CONTENTS

DECLARATION OF AUTHORSHIP	i
ACKNOWLEDGEMENTS	ii
ABSTRACT	iii
LIST OF FIGURES.....	viii
LIST OF TABLES	xv
Chapter 1: Introduction	1
1.1 Polymeric behaviour on exposure to heat.....	2
1.2 Mathematical modelling process	4
1.3 Aims and objectives.....	7
1.4 Thesis structure.....	8
Chapter 2: Literature review	10
2.1 Kinetics modelling.....	10
2.1.1 Methods of kinetic analysis.	11
2.2 Heat transfer modelling.....	17
2.2.1 Heat transfer modelling in non-charring polymeric materials.....	17
2.2.2 Heat transfer modelling in charring polymeric materials.....	18
2.3 Modelling gas mass transport process	31
2.4 Modelling ignition and combustion processes.....	32
2.6. Modelling melt dripping of thermoplastic polymers.....	39
2.7 Conclusions.....	46
Chapter 3: Experimental procedures and their associated results	47
3.1 Introduction	47
3.2 Melt dripping thermoplastics.....	48
3.2.1 Polymer samples	48
3.2.2 TGA and DSC analysis (Not conducted in this work)	49
3.2.3 Tubular furnace setting for vertical melting drops' temperature measurement.....	51
3.2.4 Measurement of temperatures of horizontally oriented samples exposed to radiant heat in a cone calorimeter	66
3.3 Temperature profiles of glass fibre reinforced resin composite laminates (GRE) exposed to a cone calorimeter.	70
3.3.1 Composite sample.....	70
3.3.2 Cone calorimeter test.....	70
3.3.3 Experimental results.....	70

3.4 GRE with intumescent coatings for thermal barrier protection	73
3.4.1 Intumescent coated glass fibre reinforced epoxy resin composite (GRE) samples.	73
3.4.2 Temperature profile measurement of intumescent coated GRE exposed to a cone calorimeter.	74
3.4.3 Thermophysical properties measurements of GRE, EI, EDI and WI.....	78
3.5 Conclusions.....	82
Chapter 4: Modelling temperature profiles during melting of vertically oriented thermoplastic polymers	84
4.1 Introduction	84
4.2 Modelling for surface temperature estimation	84
4.2.1 Model description.....	84
4.2.2 Formulation and balance equation.....	85
4.2.3 Numerical approach	88
4.2.4. Model validation	97
4.2.5. Analysis and comments.....	101
4.3. Prediction of degree of polymer degradation from predicted temperatures.	102
4.3.1 Introduction	102
4.3.2 Modelling and calculating degree of degradation of thermoplastic polymers.....	102
4.4. Conclusions	112
Chapter 5: Modelling melting, decomposition and combustion of horizontally oriented thermoplastic polymers	113
5.1 Introduction	113
5.2 Mathematical modelling	113
5.2.1 Model description.....	113
5.2.2 Model formulation	115
5.2.3 Numerical methodology for temperature prediction.	117
5.3 Simulations and sensitivity analysis	119
5.3.3 Analysis and comments.....	122
5.3.4 Simulation results	122
5.3.5 Analysis and comments.....	126
5.4 Model validation	126
5.4.1 Comparison between experiment and simulation.....	126
5.4.2 Analysis and comments.....	130
5.5 Conclusions.....	130

Chapter 6: Heat transfer in Glass Reinforced Epoxy (GRE)	131
6.1 Introduction	131
6.2 Model description	132
6.3 Temperature dependent thermophysical properties.....	135
6.4 Numerical resolution.....	137
6.4.1 Simulations and sensitivity analysis.....	139
6.4.2 Simulation results	142
6.5 Model validation	145
6.6 Effect of sample thickness and incident heat on time-to-ignition (TTI).....	150
6.6.1 Effect of the sample thickness changes.....	150
6.6.2 Relationship between TTI and incident heat flux.....	151
6.6.3 Analysis and comments.....	160
6.7 Conclusions.....	160
Chapter 7: Heat transfer in intumescent coated glass reinforced epoxy composite (GRE)	161
7.1 Introduction	161
7.2 Model description	161
7.3 Modelling heat transfer throughout the expanded layer.....	163
7.3.1 Balance equation	163
7.3.2 Moving boundary condition	164
7.4 Modelling heat transfer through the GRE substrate.....	165
7.5 Equation of thermophysical parameters.....	165
7.5.1 WI intumescent coating.....	166
7.5.2 EDI intumescent coating.....	168
7.5.3 EI intumescent coating.....	170
7.6 Numerical resolution.....	172
7.7 Simulation results.....	173
7.8 Model validation	177
7.8.1 Comparison between predicted and experimental results.....	177
7.8.2 Comments.....	180
7.9 Conclusion.....	180
Chapter 8: Conclusions	182
References:	187
Appendix 1: Numerical computation of heat transfer	200

LIST OF FIGURES

Figure 1.1: Thermal response of different polymer types

Figure 1.2: Schematic representation of the heat transfer mechanism within a polymeric sample

Figure 2.1: Schematic representation of heat transfer in non-charring polymeric material exposed to an external heat flux

Figure 2.2: Schematic representation of 1D heat transfer by conduction through the thickness of a wood sample.

Figure 2.3: Schematic representation of 1D heat transfer by conduction through the thickness of a wood sample with char layer.

Figure 2.4: Schematic representation of heat transfer in charring polymeric material exposed to an external heat flux

Figure 2.5: Schematic representation of heat transfer in polymeric material with intumescent coating exposed to an external heat flux.

Figure 2.6: Physical model of melting polymer during burning [195].

Figure 3.1: Schematic of melt dripping experiment in furnace (taken from ref [197]).

Figure 3.2: Calibration curve: Furnace Setting Temperature (FST) vs. temperature of the controller.

Figure 3.3: Schematical view of the tubular furnace coupled to the drops container.

Figure 3.4: Schematic front view of the drops container.

Figure 3.5: Drop temperatures measurement for PMMA at 400°C furnace setting temperature.

Figure 3.6: Temperatures of PMMA molten drops during a period of time.

Figure 3.7: Range of temperatures of molten drops of PMMA at each FST.

Figure 3.8: Temperatures of PET molten drops during a period of time.

Figure 3.9: Range of temperatures of molten drops of PET at each FST.

Figure 3.10: Temperatures of PP molten drops during a period of time.

Figure 3.11: Range of temperatures of molten drops of PP at each FST.

Figure 3.12: Temperatures of PA6 molten drops during a period of time.

Figure 3.13: Range of temperatures of molten drops of PA6 at each FST.

Figure 3.14: Temperatures of PC molten drops during a period of time.

Figure 3.15: Range of temperatures of molten drops of PC at each FST.

Figure 3.16: Temperatures of PS molten drops during a period of time.

Figure 3.17: Range of temperatures of molten drops of PC at each FST.

Figure 3.18: Schematic description of the assemblies of a cone calorimeter [203].

Figure 3.19: Experimental setup for temperature measurements.

Figure 3.20: PP- Surface temperature profiles of sample exposed to 15, 25 and 35kW/m² heat fluxes.

Figure 3.21: PA6- Surface temperature profiles of sample exposed to 15, 25 and 35kW/m² heat fluxes.

Figure 3.22: PET- Surface temperature profiles of sample exposed to 15, 25 and 35kW/m² heat fluxes.

Figure 3.23: Temperature profiles at the top and bottom surface of 3 mm GRE thickness exposed to 15 kW/m² heat flux.

Figure 3.24: Temperature profiles at the top and bottom surface of 3mm GRE thickness exposed to 35kW/m² heat flux.

Figure 3.25: Temperature profiles at the top and bottom surface of 3 mm GRE thickness exposed to 50 kW/m² heat flux.

Figure 3.26: Temperature profiles at the top surface of 3, 4.5, 6 and 7.5mm GRE thicknesses exposed to 35kW/m² heat flux.

Figure 3.27: Temperature profiles at the bottom surface of 3, 4.5, 6 and 7.5mm GRE thicknesses exposed to 35kW/m² heat flux.

Figure 3.28: Temperature profiles at the top side of the GRE coated with 1, 3 and 5mm thicknesses of EI exposed to 50 kW/m² heat flux.

Figure 3.29: Temperature profiles at the bottom side of the GRE coated with 1, 3 and 5mm thicknesses of EI exposed to 50 kW/m² heat flux.

Figure 3.30: Temperature profiles at the top side of the GRE coated with 1, 3 and 5mm thicknesses of EDI exposed to 50 kW/m² heat flux.

Figure 3.31: Temperature profiles at the bottom side of the GRE coated with 1, 3 and 5mm thicknesses of EDI exposed to 50 kW/m² heat flux.

Figure 3.32: Temperature profiles at the top side of the GRE coated with 1, 3 and 5mm thicknesses of WI exposed to 50 kW/m² heat flux.

Figure 3.33: Temperature profiles at the bottom side of the GRE coated with 1, 3 and 5mm thicknesses of WI exposed to 50 kW/m² heat flux.

Figure 3.34 (Taken from reference [202]): Experimental setup for thermal conductivity measurement at a) room temperature and b) elevated temperatures.

Table 3.35: Thermophysical parameters of GRE as a function of temperature.

Table 3.36: Thermophysical parameters of EI as a function of temperature.

Table 3.37: Thermophysical parameters of EDI as a function of temperature.

Table 3.38: Thermophysical parameters of WI as a function of temperature.

Figure 4.1: Schematic top view of furnace and heated polymer slab.

Figure 4.2: Schematic representation of pure melting slab.

Figure 4.3: Schematic representation of melting and degradation of slab.

Figure 4.4: PP-Temperatures profiles simulation at FST of 660, 625, 500, 450 and 350°C.

Figure 4.5: PMMA-Temperatures profiles simulation at FST of 550, 525 and 350°C.

Figure 4.6: PET-Temperatures profiles simulation at FST of 635, 565, 490 and 415°C.

Figure 4.7: PA6-Temperatures profiles simulation at FST of 560, 495 and 425°C.

Figure 4.8: PC-Temperatures profiles simulation at FST of 650, 585 and 415°C.

Figure 4.9: PS-Temperatures profiles simulation at FST of 595, 570, 400 and 300°C.

Figure 4.10: PP- Experimental vs. simulated temperatures at FST of 660, 625, 500, 450 and 350°C.

Figure 4.11: PMMA - Experimental vs. simulated temperatures at FST of 550, 520, 500 and 350°C.

Figure 4.12: PET- Experimental vs. simulated temperatures at FST of 635, 565, 490 and 415°C.

Figure 4.13: PA6 - Experimental vs. simulated temperatures at FST of 560, 595 and 425°C.

Figure 4.14: PC - Experimental vs. simulated temperatures at FST of 650, 585 and 515°C.

Figure 4.15: PS - Experimental vs. simulated temperatures at FST of 595, 570, 400 and 300°C.

Figure 4.16: Experimental vs. simulation of degree of degradation in air atmosphere.

Figure 4.17: Experimental vs. simulation of degree of degradation in nitrogen atmosphere.

Figure 4.18: Experimental vs. simulation of degree of degradation in air atmosphere.

Figure 4.19: Experimental vs. simulation of degree of degradation in nitrogen atmosphere.

Figure 4.20: Experimental vs. simulation of degree of degradation in air atmosphere.

Figure 4.21: Experimental vs. simulation of degree of degradation in nitrogen atmosphere.

Figure 4.22: Experimental vs. simulation of degree of degradation in air atmosphere.

Figure 4.23: Experimental vs. simulation of degree of degradation in nitrogen atmosphere.

Figure 4.24: Experimental vs. simulation of degree of degradation in air atmosphere.

Figure 4.25: Experimental vs. simulation of degree of degradation in nitrogen atmosphere.

Figure 4.26: Experimental vs. simulation of degree of degradation in air atmosphere.

Figure 4.27: Experimental vs. simulation of degree of degradation in nitrogen atmosphere.

Figure 5.1: Horizontal thermoplastic slab insulated at the sides.

Figure 5.2: Matlab programme algorithm.

Figure 5.3: PP- Change of surface temperature versus time when the thermal conductivity is increased or decreased by 10% up to 30%.

Figure 5.4: PP- Change of surface temperature versus time when the heat capacity is increased or decreased by 10% up to 30%.

Figure 5.5: Change in temperatures (%) when the thermal conductivity (k) or the heat capacity (Cp) changes by +/- 10% up to 30%.

Figure 5.6: PP-Simulated surface temperature exposed to 15, 25 and 35kW/m² heat fluxes (ignition is not predicted).

Figure 5.7: PP-Simulated surface temperature exposed to 15, 25 and 35kW/m² heat fluxes (ignition is predicted).

Figure 5.8: PA6- Simulated surface temperature exposed to 15, 25 and 35kW/m² heat fluxes (ignition is not predicted).

Figure 5.9: PA6- Simulated surface temperature exposed to 15, 25 and 35kW/m² heat fluxes (ignition is predicted).

Figure 5.10: PET-Simulated surface temperature exposed to 15, 25 and 35kW/m² heat fluxes (ignition is not predicted).

Figure 5.11: PET- Simulated surface temperature exposed to 15, 25 and 35kW/m² heat fluxes (ignition is predicted).

Figure 5.12: PP- Experimental vs. simulated surface temperature exposed to 15, 25 and 35kW/m² heat fluxes (ignition is not predicted).

Figure 5.13: PP- Experimental vs. simulated surface temperature exposed to 15, 25 and 35kW/m² heat fluxes (ignition is predicted).

Figure 5.14: PA6-Experimental vs. simulated surface temperature exposed to 15, 25 and 35kW/m² heat fluxes (ignition is not predicted).

Figure 5.15: PA6-Experimental vs. simulated surface temperature exposed to 15, 25 and 35kW/m² heat fluxes (ignition is predicted).

Figure 5.16: PET-Experimental vs. simulated surface temperature exposed to 15, 25 and 35kW/m² heat fluxes (ignition is not predicted).

Figure 5.17: PET-Experimental vs. simulated surface temperature exposed to 15, 25 and 35kW/m² heat fluxes (ignition is predicted).

Figure 6.1: Schematic representation of Glass Reinforced Epoxy (GRE).

Figure 6.2: Schematic representation of the heat transfer in GRE, exposed to one sided external heat.

Figure 6.3: Schematic representation of heat transfer model in GRE.

Figure 6.4: Thermal conductivity of GRE as a function of temperature and the averaged value (solid line) used in designed Matlab programme.

Figure 6.5: Heat capacity of GRE as a function of temperature and the averaged value (solid line) used in designed Matlab programme.

Figure 6.6: Density of GRE as a function of temperature and the averaged value (solid line) used in designed Matlab programme.

Figure 6.7: Schematically discretised sample.

Figure 6.8: Matlab programme algorithm.

Figure 6.9: Simulated temperature profiles of GRE exposed to 50kW/m² heat flux.

Figure 6.10: Change of temperature profiles with respect to time when the thermal conductivity is increased or decreased by step of 10% up to 30% from its reference value.

Figure 6.11: Change of temperature profiles with respect to time when the heat capacity is increased or decreased by step of 10% up to 30% from its reference value.

Figure 6.12: Change in temperatures (%) when the thermal conductivity (k) or the heat capacity (Cp) changes by +/- 10%.

Figure 6.13: Simulated surface and bottom temperature profiles of GRE exposed to 15 kW/m² heat flux.

Figure 6.14: Simulated surface and bottom temperature profiles of GRE exposed to 35 kW/m² heat flux.

Figure 6.15: Simulated surface and bottom temperature profiles of GRE exposed to 50 kW/m² heat flux.

Figure 6.16: Simulated top surface temperature profiles of GRE for different samples thicknesses exposed to 35kW/m².heat flux.

Figure 6.17: Simulated bottom surface temperature profiles of GRE for different samples thicknesses exposed to 35kW/m² heat flux.

Figure 6.18: Simulated and experimental temperature profiles of top and bottom surfaces of GRE exposed to 15kW/m² heat flux.

Figure 6.19: Simulated and experimental temperature profiles of top and bottom surfaces of GRE exposed to 35kW/m² heat flux.

Figure 6.20: Simulated and experimental temperature profiles of top and bottom surfaces of GRE exposed to 50kW/m² heat flux.

Figure 6.21: Simulated and experimental temperature profiles of top and bottom surfaces of 3 mm GRE sample thickness exposed to 35 kW/m² heat flux.

Figure 6.22: Simulated and experimental temperature profiles of top and bottom surfaces of 4.5 mm GRE sample thickness exposed to 35 kW/m² heat flux.

Figure 6.23: Simulated and experimental temperature profiles of top and bottom surfaces of 6 mm GRE sample thickness exposed to 35 kW/m² heat flux.

Figure 6.24: Simulated and experimental temperature profiles of top and bottom surfaces of 7.5 mm GRE sample thickness exposed to 35 kW/m² heat flux.

Figure 6.25: Simulated top surface temperature profiles of GRE for 3, 4.5, 6 and 7.5 mm samples thicknesses exposed to 35kW/m².heat flux.

Figure 6.26: Time-to-ignition vs. sample thickness exposed to 35 kW/m² heat flux.

Figure 6.27: Effects of incident heat flux on the temperature profiles versus time of 3 mm GRE sample thickness.

Figure 6.28: Simulation of TTI vs. incident heat flux of 3 mm GRE thickness.

Figure 6.29: Effects of incident heat flux on the temperature profiles versus time of 4.5 mm GRE sample thickness.

Figure 6.30: Simulation of TTI vs. incident heat flux of 4.5 mm GRE thickness.

Figure 6.31: Effects of incident heat flux on the temperature profiles versus time of 6 mm GRE sample thickness.

Figure 6.32: Simulation of TTI vs. incident heat flux of GRE of 6 mm thickness.

Figure 6.33 Effects of incident heat flux on the temperature profiles versus time of 7.5 mm GRE sample thickness.

Figure 6.34: Simulation of TTI vs. incident heat flux of GRE of 7.5 mm thickness.

Figure 6.35: TTI vs. incident heat flux for 3, 4.5, 6 and 7.5 mm GRE sample thicknesses.

Figure 6.36: Predicted TTI and calculated TTI from Eqn 6.6 vs. incident heat flux for 3mm sample thickness.

Figure 6.37: Predicted TTI and calculated TTI from Eqn 6.6 vs. incident heat flux for 4.5 mm sample thickness.

Figure 6.38: Predicted TTI and calculated TTI from Eqn 6.6 vs. incident heat flux for 6mm sample thickness.

Figure 6.39: Predicted TTI and calculated TTI from Eqn 6.6 vs. incident heat flux for 7 mm sample thickness.

Figure 7.1: Schematic representation of heat transfer in intumescent coated GRE when the heating starts.

Figure 7.2: Schematic representation of heat transfer in intumescent coated GRE when the intumescent layer expands.

Figure 7.3: Thermal conductivity vs temperature curve fitted using Matlab.

Figure 7.4: Heat capacity vs temperature curve fitted using Matlab.

Figure 7.5: Density vs temperature curve fitted using Matlab.

Figure 7.6: Thermal conductivity vs temperature curve fitted using Matlab.

Figure 7.7: Heat capacity vs temperature curve fitted using Matlab.

Figure 7.8: Density vs temperature curve fitted using Matlab.

Figure 7.9: Thermal conductivity vs temperature curve fitted using Matlab.

Figure 7.10: Heat capacity vs temperature curve fitted using Matlab.

Figure 7.11: Density vs temperature curve fitted using Matlab.

Figure 7.12: Discretised GRE substrate protected by intumescent coating.

Figure 7.13: Simulated temperatures at the top side of the GRE coated with 1, 3 and 5mm thicknesses of EI exposed to 50 kW/m² heat flux.

Figure 7.14: Simulated temperatures at the bottom side of the GRE coated with 1, 3 and 5mm thicknesses of EI exposed to 50kW/m² heat flux.

Figure 7.15: Simulated temperatures at the top side of the GRE coated with 1, 3 and 5mm thicknesses of EDI exposed to 50kW/m² heat flux.

Figure 7.16: Simulated temperatures at the bottom side of the GRE coated with 1, 3 and 5mm thicknesses of EDI exposed to 50kW/m² heat flux.

Figure 7.17 Simulated temperatures at the top side of the GRE coated with 1, 3 and 5mm thicknesses of WI exposed to 50kW/m² heat flux.

Figure 7.18: Simulated temperatures at the bottom side of the GRE coated with 1, 3 and 5mm thicknesses of WI exposed to 50kW/m² heat flux.

Figure 7.19: Simulated and Experimental temperatures at the top side of the GRE coated with 1, 3 and 5mm thicknesses of EI exposed to 50kW/m² heat flux.

Figure 7.20: Simulated and Experimental temperatures at the bottom side of the GRE coated with 1, 3 and 5mm thicknesses of EI exposed to 50kW/m² heat flux.

Figure 7.21: Simulated and Experimental temperatures at the top side of the GRE coated with 1, 3 and 5mm thicknesses of EDI exposed to 50kW/m² heat flux.

Figure 7.22: Simulated vs. Experimental temperatures at the bottom side of the GRE coated with 1, 3 and 5mm thicknesses of EDI exposed to 50kW/m² heat flux.

Figure 7.23: Simulated and Experimental temperatures at the top side of the GRE coated with 1, 3 and 5mm thicknesses of WI exposed to 50kW/m² heat flux.

Figure 7.24: Simulated and Experimental temperatures at the bottom side of the GRE coated with 1, 3 and 5mm thicknesses of WI exposed to 50kW/m² heat flux.

LIST OF TABLES

Table 2.1: Algebraic expressions of functions of the most common reaction mechanisms operating in solid-phase reactions

Table 2.2: Summary of experimental kinetic data from selected polymers from literature

Table 3.1: Analysis of thermal behaviour (DTA-TGA) of polymers in air and nitrogen atmosphere (values reported in parenthesis) of polymers (taken from ref [197]).

Table 3.2: Furnace temperature settings for melt dripping experiments (taken from ref [197])

Table 3.3 (Taken from reference [202]): Cone calorimetric results for different intumescent coatings of varying thicknesses on GRE composite samples, exposed to 50 kW/m² heat flux.

Table 3.4: (taken from reference [202]: Char residual digital images, exposure time, char thicknesses and expansion ratio of EI, ED-I and WI with 1, 3 and 5mm intumescent coatings exposed to 50 kW/m² incident heat flux.

Table 3.5: Thermophysical parameters of GRE as a function of temperature

Table 3.6: Thermophysical parameters of EI as a function of temperature

Table 3.7: Thermophysical parameters of EDI as a function of temperature

Table 3.8: Thermophysical parameters of WI as a function of temperature

Tables 4.1 a-d: Thermophysical properties of different polymers used to build the numerical model.

Table 4.2: A comparison of measured temperatures from DSC and those simulated by FDM (Matlab)

Table 4.3: Degree of degradation in drops of the thermoplastic polymer from Figure 4.18 to 4.29.

Table 6.1: Thermophysical values embedded in designed Matlab programme.

Table 7.1: Activation energy and exponential factor for WI, EDI and EI intumescent

Table 7.2: Values of char thickness, exposure time and approximated expansion factor.

Table 7.3: Polynomial constant of $k(T)$, $C_p(T)$ and $\rho(T)$ equations.

Table 7.4: Polynomial constant of $k(T)$, $C_p(T)$ and $\rho(T)$ of equations.

Table 7.5: Polynomial constant of $k(T)$, $C_p(T)$ and $\rho(T)$ equations.

Chapter 1: Introduction

The scientific discipline of modelling the thermal response of polymeric materials under heat exposures has increased in importance in the same way that new and innovative materials are increasingly used to replace wood or metal-based structures in conventional applications across all industries. Accurate theoretical predictions are required to provide assistance during the design process of these new materials and structures. Simulating the fire performance with these models initially reduces the need for expensive and time-consuming fire testing. Additionally, such models provide the opportunity of developing and accessing innovative materials with tailor-made properties, before the prototypes are built.

Two approaches to investigate the problem are; (i) using computational software tools based upon mathematical models or (ii) performing fire experiments. Performing tests could be restricted in number because of associated high cost. Computer modelling is frequently used due to convenience and relatively low-cost. It is becoming increasingly desirable to know the thermal response of polymeric materials in different heating scenarios so as to screen new polymeric materials and additives early in the design process. This can be done using mathematical model simulation well in advance of experiments and industrial scale-up and assess as accurately as possible their inherent resistance to heat exposure and fire damage.

Such mathematical model simulation should also help engineers to better understand and control the thermal and chemical processes underlying heat damage and combustion, providing an early opportunity to reformulate where inherent weaknesses are identified. In the longer term, highly accurate predictive computer models of heat transfer within polymeric materials subjected to heat and/or fire, which has been closely validated by experimental data, offers the potential to partially or even reduce experimental testing as the principal means of confirming the fire resilience of structural polymeric materials.

To develop a computer code based on the mathematical model, theoretical thermal balance equations that are non-linear partial differential equations with no analytical solution have to be sat. To obtain a potential approximate solution using numerical method is still difficult due to the complex nature and the number of variables from occurring phenomenon such as polymeric materials degradation,, ignition criteria and combustion. Also, there are various types of polymeric materials involved; charring and non-charring polymer. Therefore, it is important to develop a model with great flexibility to predict the behaviour of these different

types of polymeric materials considering all the different aspects during their heating process.

1.1 Polymeric behaviour on exposure to heat

In general, when a polymeric material is subjected to an incident heat flux it will heat up substantially by conduction from the exposed surface. On reaching the degradation temperature it decomposes and produces non-flammable and flammable gases. The mixture of the flammable gases with the air results in the formation of a flammable gas phase [9]. Beyond a critical value of the surface temperature, the ignition can be caused either by a source (flame, incandescent particles.) or by exothermic chemical reactions which are oxidation reactions [1, 2]. The flame produces a heat flux in addition to the initial flux and, then contributes to its spread on the surface [3-4]. The region of burning material will thus continue to produce combustion gas, but mainly as a source of heat capable of causing the ignition to the remaining polymeric materials exposed to the burning region. The overall gas flux causes an acceleration of the entire phenomenon. This dynamic loop of combustion simultaneously leads to the fire growth till the complete combustion of the material. It is typically fastest in the upward direction when there is an extended area of fuel that is burning and thereby increasing the overall heat release rate [5]. Therefore, the fire-resistance and mechanical resilience of polymeric material structures to thermal attack are of crucial importance to their use and specifications in the major engineering applications such as aerospace and marine. In particular, the ability of these polymeric materials to retain structural integrity and mechanical strength for the longest possible time after ignition is a key design objective. In cases where it is not feasible to prevent ignition entirely or even delay it significantly using fire retardant additives, it is then necessary to assess the time at which a polymeric material will lose its structural integrity, the rate with which this will occur, and most importantly, the severity of this loss in strength.

Commonly used engineering polymeric materials can be ranked into two categories : i) thermoplastics and ii) thermosets. The basic difference between them is that, prior to undergoing thermal decomposition, thermoplastics melt and flow. From flammability and modelling points of view the polymers can be categorised as i) non-charring polymers and ii) charring polymers. While all thermosets are charring polymers, thermoplastics can be both non-charring and charring polymers. Polymethyl methacrylate (PMMA), polystyrene (PS), polyester (PET) and polypropylene (PP) are examples of non-charring thermoplastic polymers. Charring thermoplastics or with a tendency to char include poly vinyl chloride (PVC), polyamides (PA) and polyester (PET). In Figure 1.1 the thermal responses of different types of polymeric materials are shown.

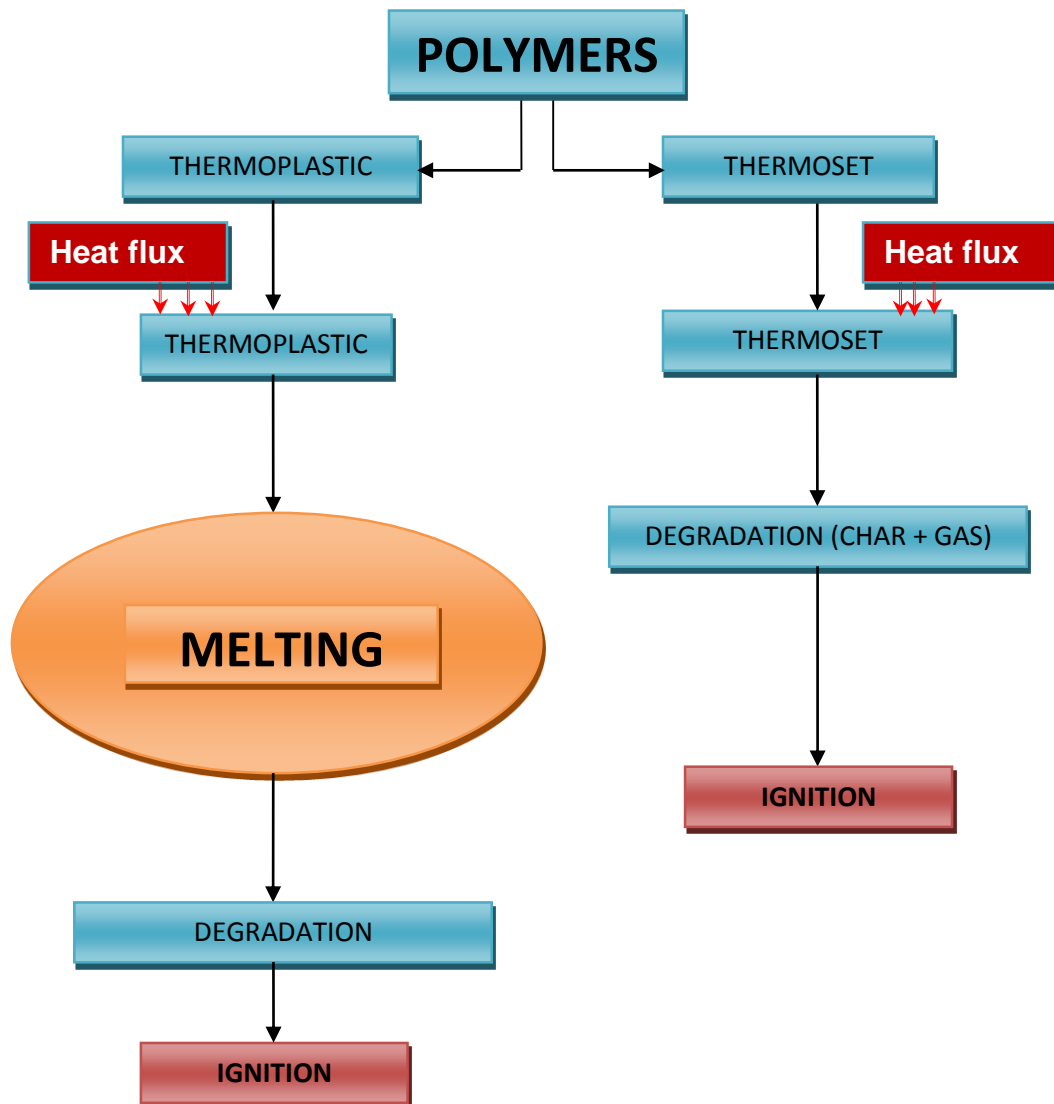


Figure 1.1: Thermal response of different polymer types

Charring and non-charring polymeric materials experience different degradation processes under external heat flux. Charring polymers such as PC and PET decompose into volatiles and a solid phase divided into char layer, degradation layer and virgin material. This creates complexity as the different solid phases are behaving differently under heat exposure. PC and PET, characteristics of shrinkage or expansion, are dependent on the material itself; for example, while PET goes through shrinkage under external heat flux, PC undergoes expansion. However non-charring polymers, such as PMMA, PS, PET and PP, can decompose entirely into gas volatiles directly at high temperature after their thermal

degradation processes [6-9] or they left with no or very little residues [10]. Both polymeric degradation processes can be expressed by a one-step reaction [11].

Another aspect of the behaviour of polymeric materials under heat and/or fire is that they tend to deform significantly as they burn. Thus, large changes in the geometric shape in burning conditions are common, specifically for thermoplastic materials. In this case, the downward flow of flaming liquid from melting and dripping polymer results in a pool fire [12]. These thermal aspects of thermoplastics are difficult to control and there is a need to understand the process in both the real life situation and through mathematical modelling simulations.

1.2 Mathematical modelling process

“A model can at best be as good as its underlying assumptions [13]”. Therefore, the problem formulation of heat transfer within material based polymer needs to start by providing first, a clear picture of which phenomena are to be taken into account and those that are not, and the errors introduced because of the model simplifications. The applications of a numerical model are limited if it only focuses on one type of polymeric materials. For each type of polymeric materials, computational domain, volume change, pyrolysis reactions, thermal properties are different. A large number of these thermophysical parameters of the polymeric materials are needed for modelling input. These input parameters may show large ranges of data in references. Therefore, it is significant to develop an optimised mathematical model that can integrate several input data for different types of polymeric materials. Moreover, a mathematical model for one type of polymeric material cannot be applied to another because their thermophysical properties differences. In most cases in real life fire situation, there is more than one type of polymeric materials, hence the modelling accuracy can be challenged. The methodology to develop a mathematical model of the thermal effects within different polymeric materials can be developed in three steps; (i) the first is to build a computational mathematical model based on balance Non-linear Partial Differential Equations able to predict the temperature profiles using specific initial conditions. These Partial Differential Equations have no analytical solution so that they be solved using Finite Difference Method expressed in a form of a programme code embedded in MatLab software, (ii) The second step is to conduct laboratory experiments to heat polymer samples with several incidents thermal fluxes in order obtain different experimental temperature profiles Finally, (iii) the third step is to validate the numerical model by comparing the predicted temperature profiles with the experimental temperature profiles. If both, experiment and predicted temperature profiles have a good agreement, the numerical model is considered to be validated. Therefore, the mathematical model is an input-output transformation capable of generating results similar to

those obtained by performing experimental tests. The nature of the problem is such that models are both space-time dependent with coupled equations.

To develop a mathematical model a description of the heat transfer mechanisms are schematically shown in Figure 1.2 where the different processes occurring are described in a polymer sample exposed to a constant incident heat flux q_{in} and insulated on the sides and the bottom to sustain the assumption of a one dimensional heat transfer model for simplicity. The heated surface of the polymeric material is involved with the heat flow of each of these following heat transfer mechanisms; radiation, convection and conduction. Also, the phenomenon of degradation occurs at a critical temperature, whereby the polymeric material progressively degrades and releases volatile products which can subsequently act as a combustible fuels.

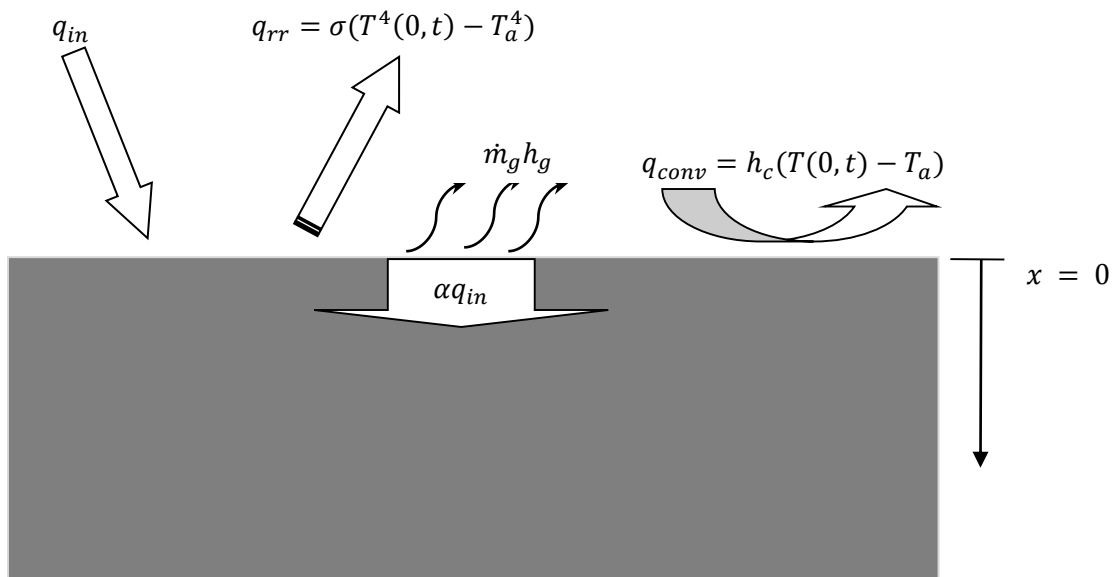


Figure 1.2: Schematic representation of the heat transfer mechanism within a polymeric sample

Where: α is the Stefan – Boltzmann constant, $T(0, t)$ is the surface temperature at time t , h_c is the convective heat transfer coefficient, T_a is the ambient temperature, \dot{m}_g is the volatile mass flux and h_g is the volatile enthalpy.

The energy going to and coming from the sample surface is the absorbed incident heat flux αq_{in} , the transferred heat by conduction q_{cond} , the emitted energy q_{rr} and the convective energy q_{conv} . The sum of αq_{in} , q_{rr} and q_{conv} is taken to be equal to q_{in} . Since the polymeric materials studied here after softening and melting, decompose and even char on heating / burning, the surface emissivity can be taken as equal to 1 with the black body assumption

[8]. However, this approximation is not always true for flame retarded polymers, for example for those which release SiO₂ on burning.

A non-linear thermal balance equation that is Partial Differential Equations which approximate solution is able to predict the 1 temperature profiles mathematical model can be developed based on the partition of the energy balance as follows [14]:

$$\alpha q_{in} = q_{cond} + q_{rr} + q_{conv} + \dot{m}_g h_g$$

The overall heat transfer processes are described as a flow of heat into, through and out of the polymeric material. An external steady-state heat flux radiates upon the top surface of the polymeric material, part of which is absorbed into the bulk of the material, and part of which is either re-radiated back into the headspace or is exchanged by convection back into the headspace fluid, (usually air). The heat transfer process is principally a function of the relative emissivity of the surface, the convective heat transfer coefficient from the surface to the headspace fluid, and the conductivity of the bulk material itself.

Due to this complex nature of the problem described above, the statement of the thermodynamical balance equations balance governing the overall thermal exchange can be approximated mathematically by a set of Non-linear Partial Differential equations. These equations have terms that incorporate melting, decomposition and ignition phenomena. The only potential theoretical solution currently usable is one utilising the Finite Difference Method to find a numerical solution to the related Partial Differential Equation (PDE).

The approach is to generate a numerical solution of the balance equations describing the physical state. The process is then to use the finite difference methodology in the form of a coded programme to compute the partial differential equations which are so complex that they cannot be solved analytically.

Many models have been developed to simulate fire behaviour of non-charring polymers [15-16] and charring polymers [17-24]. It is difficult to find in the literature a model that can describe all types of polymeric materials as modelling differences exist among them [25-30]. For example, non-charring polymers can be modelled using theory similar to flammable liquids. In contrary, the thermal response of charring polymers is the result of a complex interplay of chemistry, heat and mass transfer. Therefore, it can be modelled regarding a thermal degradation front penetrating into the polymeric materials with an increasing surface temperature and without a well-defined steady-state [25].

In literature, most of thermal models of polymeric materials show that differences still exist between modelling results and experimental data. For example, many models have

considered external heat flux, but no common agreement was found about its description or influences. Different elements used to develop a thermal mathematic model are defined as the input parameters of the model. The most sensitive input of the mathematical models are the thermal properties of the different polymeric materials changing with temperature [18, 28-29]. Therefore, these input parameters of the model constitute a very important aspect of the thermal modelling behaviour of polymeric materials. Thermal properties of wood are linearly dependent on temperature, and no transition temperature has been observed [31-32]. Thermal properties of polymeric materials will go through glass transition temperature or melting temperature as temperature rises. They show different behaviour and transition temperature that is considered at the changing point of the maximum inflexion point of an apparent glass transition or a melting peak [33-36].

Moreover, ignition is also an important aspect of combustion development as polymeric materials can ignite with the acceleration of spark plug or independent flame. Almost all previous modelling designed has focused on piloted ignition [37]. However, their applications have some limitations as almost all these models have only focused on one type of polymeric materials so that the accuracy of their results output are reduced in real life fire conditions where more than one material type is involved resulting in a lack of a certain understanding overview.

1.3 Aims and objectives

The main aim of this research is to develop mathematical models to simulate temperature changes within polymeric materials exposed to different heating scenarios and heat fluxes and predict temperature induced degradation and ignition of the polymers. To achieve this aim, the following objectives are proposed:

- 1) To develop heat transfer model to predict through-thickness temperature profiles in polymers exposed to two different heating scenarios: a) a radiant heat uniform on all sides in vertically oriented samples and b) the heat applied on the top surface of a horizontally oriented sample while the other sides of the polymer sample are insulated.
- 2) To carry out a parametric sensitivity analysis of the developed models in order to establish the parameter which has the largest influence on the various material properties.
- 3) To predict heat induced degradation and ignition of the polymers.

- 4) To validate the model by experimental data and to refine accordingly.

1.4 Thesis structure

The outlines of the thesis chapters are discussed below:

Chapter 2 presents a literature review of mathematical modelling of polymeric materials which explores and collects the necessary background material relevant to the work presented in this thesis.

Chapter 3 describes the experimental setup and the results obtained from the different heat transfer scenarios undertaken in this work to validate the associated numerical models developed. To validate the accuracy of the different numerical models developed in Chapter 4 to 7, some standard fire tests were carried out.

The work is divided into four parts based on different scenarios used to simulate and experimentally validate temperature variations during melting, decomposition, charring and ignition phases of polymers. In first two parts melting behaviour of thermoplastic polymers (polypropylene, polyester, polyamide 6, polymethyl methacrylate, polycarbonate and polystyrene) has been studied. In the first part the polymer sample is heated in a vertically oriented tubular furnace to measure the temperatures of melting drips. In the second test scenario, the sample is placed horizontally in a cone calorimeter which is the standard cone sample holder according to ISO 5660 and heat applied only on the top surface while the other sides of the polymer sample are insulated.

In the third and fourth parts decomposition, charring and ignition behaviour of glass fibre – reinforced epoxy polymeric materials and thermally insulated polymeric materials have been studied.

In **Chapter 4** the temperature profiles of thermoplastics have been modelled. The first scenario deals with the vertically oriented sample while they are melting and dripping. The sample is placed in a tubular furnace and the radiant heat is taken to be uniform on all sides of the sample. A one dimensional heat transfer model is developed. The objective is to estimate the melting temperature of the different polymer samples by predicting the temperature profile in the slab of the polymer exposed to heat in the vertical tubular furnace. Then from the predicted temperatures of the heated polymers, the degree of polymer

degradation in each case has been modelled and compared with the experimental results from Chapter 3.

Chapter 5 investigates the melting behaviour of three semi-crystalline thermoplastic polymers (Polypropylene (PP), Polyamide 6 (PA6) and Polyethylene terephthalate (PET)) and attempts to identify the melting characters of different polymers on exposure to a radiant heat on one surface only in a cone calorimeter. Also, a simulation model for polymer melting and decomposition including burning behaviour was developed. This study has focused on horizontal slabs heated by cone calorimeter radiation on the top face only and the others being insulated. The cone calorimeter experimental results obtained in Chapter 3 are used to validate the numerical model computed by MatLab software.

The focus in **Chapter 6** is on heat transfer in glass fibre - reinforced epoxy composites (GRE), exposed to the radiant heat of different heat fluxes in a cone calorimeter. On the model developed in Chapters 4 and 5, the heat transfer throughout the polymeric material sample is affected by the glass fibres which do not undergo thermal decomposition while epoxy resin matrix does. Therefore, the heat transfer model takes into account the volume fraction of the fibres and the matrix resin with the contribution of their thermophysical properties accordingly. The model incorporates the ignition and combustion condition when the ignition temperature is reached. Also, further analysis is performed to establish how the ignition time is behaving when the sample thicknesses and the incident heat fluxes are varied.

In **Chapter 7** the heat transfer in GRE composite sample coated with three different intumescent paints has been studied. Under incident heat flux, the reactive intumescent paint layer becomes viscous before a threshold temperature T_c after which it becomes a non-reactive char layer. The low thermal conductivity of that thick layered char provide a thermal protective barrier for the GRE composite. A numerical model based MatLab software capable of simulating the temperature profile inside the GFREP surface protected by a thermally insulate intumesced char structure is developed. Comparing to the chapter 6, this model includes the change in thickness when the intumescent layer expands.

Chapter 8 reviews the findings and contributions to knowledge from the work undertaken in this thesis and also makes recommendations for future research.

Chapter 2: Literature review

The theory underlying heat transfer, degradation, and combustion observed in polymeric materials subjected to heat and/or fire, encompasses many disciplines from thermodynamics to gas chemistry and fluid dynamics so that the literature on this subject is diverse.

In addition, the theory also needs to consider;

- 1) The heat transfer through the thickness of the various polymeric materials
- 2) The polymer degradation and kinetics of degradation reaction causing the gas mass transfer through the polymeric material and,
- 3) Ignition and combustion.

Over the last fifty years researchers have tackled this challenge of modelling the behaviour of polymeric materials subjected to heat and/or fire, using numerous mathematical models. While heat transfer models for metals involves only conduction, in polymers degradation kinetics leading to the ignition and combustion of the polymeric materials also need to be incorporated into the models. In this chapter, the studies taken from the relevant literature are reviewed to have a better understanding of how theories have involved throughout the history. The earlier heat transfer models were simpler due to limited computing powers, whereas recent ones can incorporate multiple components, hence are more sophisticated. The heat transfer modelling within polymeric materials is designed to predict their through the thickness temperature profiles and thermal responses as accurately as possible, when subjected to incident heat flux. Therefore, modelling the kinetics parameters of polymer degradation and the accumulation of gases evolved as well as their transport through the polymer are important parts of the mathematical modelling of the overall behaviour of polymeric materials under heat and/or fire allowing implementation of more realistic heating scenarios. These are reviewed separately and prior to heat transfer modelling. These are then followed by modelling for particular scenarios such as melt dripping in thermoplastics and heat transfer in thermally insulated surface of polymeric materials to constitute a thermally protective barrier.

2.1 Kinetics modelling

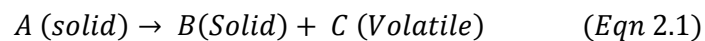
In the case of limited heat flux (less than 20 kW/m^2), the heat transfer in materials can be modelled by only using heat conduction equation. However, as soon as the heat flux becomes more intense, the material composition and its internal structure are altered as a result of chemical reactions [38]. The thermal decomposition is defined by the American Society for Testing and Materials (ASTM) as "a process of extensive chemical species

change caused by heat", and involves complex different physical and chemical processes taking place at the same time [39]. The degradation of materials is as an endothermic process in which the energy input (activation energy) must be sufficient to break chemical bonds [40-44].

Thus, the kinetics of polymer degradation is an important area in heat transfer of polymeric materials and the successful modelling of degradation to predict the rate of volatile evolution is central to heat transfer analysis. So, the determination of the material parameters is one of the key challenges of numerical thermal simulation attempting to predict the temperature profile within the polymeric material. To model the reaction mechanism of the decomposition process with Arrhenius equation, it is necessary to ascertain the values of the activation energy and the pre-exponential factor using kinetic analysis methods, such as Kissinger, Flynn-Wall-Ozawa, Friedman, Coats-Redfern and Criado method.

2.1.1 Methods of kinetic analysis.

From a simple thermogravimetric (TG) trace, meaningful values of parameters such as activation energy, pre-exponential factor rate of reaction, etc. can be obtained using Arrhenius equation. There are many proposed methods to calculate kinetic parameters and these reported values depend not only on experimental conditions but also on mathematical treatment of the data obtained. The following simple reaction scheme may represent the degradation process [45]:



All kinetic studies assume that the isothermal rate of conversion, $d\alpha/dt$, for thermogravimetric experiment at constant rate of temperature change, $\beta = dT / dt$, is a linear function of a temperature-dependent rate constant, k , and a temperature-independent function of the conversion, α , that is [45]:

$$\frac{d\alpha}{dt} = \beta \frac{d\alpha}{dT} = kf(\alpha) \quad (\text{Eqn 2.2})$$

Where: α is the degree of advance reaction, $f(\alpha)$ and $K(T)$ are functions of conversion and temperature, respectively. $K(T)$, the temperature dependence of the rate of weight loss, is often modeled successfully by the Arrhenius equation [45]:

$$K(T) = A \cdot \exp\left(-\frac{E_a}{RT}\right) \quad (\text{Eqn 2.3})$$

Where, E_a is the apparent activation energy, A the pre-exponential factor and R is the gas constant. All kinetic information can be extracted from dynamic experiments by various methods, some of which are discussed here:

(i) Coats–Redfern [46].

The coats-redfern method is called an integral method, and it involves the thermal degradation mechanism. Using an asymptotic approximation for the resolution of Eqn 2.2, $2RTE_a \ll 1$, the following equation can be obtained:

$$\ln\left(\frac{g(\alpha)}{T^2}\right) = \ln\left(\frac{AR}{\beta E_a}\right) - \frac{E_a}{RT} \quad (\text{Eqn 2.4})$$

(ii) Kissinger-Akahira-Sunose method (KAS) [47].

The standard Eqn 2.2 can be shown as follows:

$$\frac{d\alpha}{f(\alpha)} = \frac{A}{\beta} \exp\left(-\frac{E_a}{RT}\right) dT \quad (\text{Eqn 2.5})$$

Which is integrated with the initial condition of $\alpha = 0$ at $T = T_0$, to obtain the following expression:

$$g(\alpha) = \int_0^\alpha \frac{d\alpha}{f(\alpha)} = \frac{A}{\beta} \int_{T_0}^T \exp\left(-\frac{E_a}{RT}\right) dT \quad (\text{Eqn 2.6})$$

Since, essentially the technique assumes that A , $f(\alpha)$ and E are independent of T , while A and E are independent of α . The KAS method is based on the Coats-Redfern approximation [46] and Eqn 2.6:

$$\ln\left(\frac{\beta}{T^2}\right) = \ln\left(\frac{AR}{E_a g(\alpha)}\right) - \frac{E_a}{RT} \quad (\text{Eqn 2.7})$$

Thus, the plot of $\ln(\beta/T^2)$ vs. $1/T$ for a constant value of α should be a straight line whose slope can be used to evaluate the apparent activation energy.

(iii) Friedman [48].

This method is a differential isoconversional method and is directly based on Eqn 2.2 whose logarithm is:

$$\ln\left(\frac{d\alpha}{dt}\right) = \ln\left(\beta \frac{d\alpha}{dT}\right) = \ln[Af(\alpha)] - \frac{E_a}{RT} \quad (\text{Eqn 2.8})$$

From Eqn 2.8, it is easy to obtain values for E_a over a wide range of conversions by plotting $\ln(\beta d\alpha/dT)$ against $1/T$ for a constant α value.

(iv) Flynn-Wall-Ozawa [49].

This method is derived from the integral isoconversional method. Using Doyle's approximation [198] the result of the integration of Eqn 2.6, after taking the logarithms is:

$$\ln(\beta) = \ln\left(\frac{AE_a}{Rg(\alpha)}\right) - 5.331 - 1.052 \frac{E_a}{RT} \quad (\text{Eqn 2.9})$$

Thus, for $\alpha = \text{const.}$, the plot $\ln\beta$ vs. $1/T$, obtained from thermograms recorded at several heating rates, should be a straight line whose slope can be used to evaluate the apparent activation energy.

(v) Criado [50].

If the value of the apparent activation energy is known, the kinetic model of the process can be determined by this method. Combining Eqn 2.2 with Eqn 2.4 the following equation is obtained:

$$\frac{Z(\alpha)}{Z(0.5)} = \frac{f(\alpha)g(\alpha)}{f(0.5)g(0.5)} = \left(\frac{T_\alpha}{T_{0.5}}\right)^2 \cdot \frac{(d\alpha/dt)_\alpha}{(d\alpha/dt)_{0.5}} \quad (\text{Eqn 2.10})$$

Where 0.5 refers to the conversion of α .

The left side of Eqn 2.10, $(f(\alpha)g(\alpha))/(f(0.5)g(0.5))$ is a reduced theoretical curve, which is characteristic of each reaction mechanism, whereas the right side of the equation associated with the reduced rate can be obtained from experimental data. A comparison of both sides of Eqn 2.10 tells us which kinetic model describes an experimental reactive process.

Table 2.1 summarises the algebraic expressions of $f(x)$ and $g(x)$ used for various kinetic models.

Mechanism	$f(\alpha)$	$g(\alpha)$
Power law (P2)	$2\alpha^{1/2}$	$\alpha^{1/2}$
Power law (P3)	$3\alpha^{2/3}$	$\alpha^{1/3}$
Power law (P4)	$4\alpha^{3/4}$	$\alpha^{1/4}$
Avarami-Erofe'ev (A2)	$2(1-\alpha)[- \ln(1-\alpha)]^{1/2}$	$[- \ln(1-\alpha)]^{1/2}$
Avarami-Erofe'ev (A3)	$3(1-\alpha)[- \ln(1-\alpha)]^{2/3}$	$[- \ln(1-\alpha)]^{1/3}$
Avarami-Erofe'ev (A4)	$4(1-\alpha)[- \ln(1-\alpha)]^{3/4}$	$[- \ln(1-\alpha)]^{1/4}$
Contracting area (R2)	$2(1-\alpha)^{1/2}$	$[1-(1-\alpha)^{1/2}]$
Contracting volume (R3)	$3(1-\alpha)^{2/3}$	$[1-(1-\alpha)^{1/3}]$
One-dimensional diffusion (D1)	$1/2\alpha$	α^2
Two-dimensional diffusion (D2)	$[- \ln(1-\alpha)]^{-1}$	$[(1-\alpha) \ln(1-\alpha)] + \alpha$
First-order (F1)	$(1-\alpha)$	$-\ln(1-\alpha)$
Second-order (F2)	$(1-\alpha)^2$	$(1-\alpha)^{-1} - 1$
Third-order (F3)	$(1-\alpha)^3$	$[(1-x)^{-2} - 1]/2$

Table 2.1: Algebraic expressions of functions of the most common reaction mechanisms operating in solid-phase reactions [45]

The non-isothermal methods above are the most commonly used for performing the kinetic analysis of polymer degradation [51-58]. These methods were originally developed by assuming orderⁿ kinetic models and have been generalised for being used for all the kinetic models describing solid state reactions [59-61]. All the methods discussed have been developed by assuming that both the activation energy and the kinetic model do not change along the heating process. Friedman [48] and Flynn et al. [49] isoconversional methods have been the most generally used for determining the activation energy as a function of the reacted fraction without any previous assumption on the kinetic model fitted by the reaction. The use of the Ozawa method has been strongly criticised because this equation was developed by integrating the Arrhenius equation by assuming that neither the activation energy nor the kinetic model change all over the reaction, suggesting that reliable values of the activation energy would be obtained only if the activation energy remains constant [62-65]. Vyazovkin [66] has developed an iterative method for overcoming this problem.

However, the analysis of the thermal degradation of polymeric materials is of major interest since it can, in many cases; determine the upper-temperature limit of use for polymeric materials. Polymer degradation is mathematically described through a system of coupled equations. The basic equations are those of chemical kinetics, heat transfer and mass transfer. The use of the different methods described above can give different values of the activation energy and the pre-exponential factors. These values lead to the Arrhenius

equation describing the polymeric material degradation which is incorporated in the balance equation for the main heat transfer model predicting the temperature profile within the materials.

The heat transfer model determines the temperature profiles that serve as input to the kinetics model. Hence, the detail of the heat transfer model often determines the accuracy of prediction of the overall model. This then relates to the point that accurate values of the kinetic parameters are required to develop a heat transfer model. In Table 2.2, the values of the activation energy and the pre-exponential factors of degradation reactions of selected polymers expressed by the one-step kinetic equation using different methods from literature have been compiled.

References	Polymeric materials	Experiment conditions	Temperatures Range (K)	Arrhenius equations A(s ⁻¹): Pre-exponential factor E _a (kJ/mol): Activation energy
Stoliarov et al. [31]	PMMA	TGA	-	A=8.5·10 ¹² / E _a =-188
Kang et al. [32]	PMMA	TGA (5 K/min) TGA (10 K/min) TGA (15 K/min) TGA (20 K/min)	-	A= 2.15·10 ¹⁶ / E _a =-102.46 A=3.65·10 ¹⁹ . / E _a =-118.49 A=1.35·10 ¹⁷ / E _a =-103.82 A=3.82·10 ²³ / E _a =-13.5
Bockhorn et al. [33]	PS	Isothermal	633-683	A=2.08·10 ⁸ . / E _a =-95
Ciutacu et al. [34]	PE	Non-isothermal	503-653 653-823	A=1.8·10 ³ / E _a =-67 A=2.6·10 ⁶ / E _a =-122
Straus and Wall [35]	PP	-	-	A=2.51·10 ¹⁴ / E _a =-247
Kannan et al. [36]	PP	TGA	673-713	A=3.2·10 ¹⁵ / E _a =-244 A=2.2·10 ¹¹ / E _a =-188
Fuoss et al. [37]	PS	Isothermal	667	A=5.0·10 ²⁴ / E _a =-323
Kuroki et al. [38]	PS	-	583-653	A=1.8·10 ¹¹ / E _a =-152
Madorsky [39]	PS	-	608-628	A=9.0·10 ¹⁵ / E _a =-44
Sato et al. [40]	PS	-	373-873	A=3.5·10 ¹¹ / E _a =-177
Kannan et al. [36]	PS	TGA	638-673	A=3.3·10 ¹³ / E _a =-204
Grammelis et al. [41]	PP	-	-	A=3.17·10 ²⁴ / E _a =-373.5
Grammelis et al. [41]	PS	-	-	A=4.0·10 ²⁶ / E _a =-415
Ciutacu et al. [42]	PA	Non-isothermal	563-793	A=1.9·10 ⁵ / E _a =-110.5
Ciutacu et al. [42]	ABS	Non-isothermal	523-743 743-903	A=2.5·10 ³ / E _a =-84 A=1.0·10 ⁸ / E _a =-170
Grammelis et al. [41]	PA	-	-	A=2.83·10 ¹⁶ / E _a =-257
Simon [43]	PVC	-	-	A=6.61·10 ¹² / E _a =-163 A=5.88·10 ¹² / E _a =-172
Ciutacu et al. [42]	PC	Non-isothermal	503-783 783-893	A=2.8·10 ⁸ / E _a =-151.5 A=3.8·10 ⁸ . s ⁻¹ / E _a =-90.5
Grammelis et al. [41]	PC	-	-	A=9.33·10 ²⁰ / E _a =-341

Table 2.2: Summary of experimental kinetic data from selected polymers from literature [67]

2.2 Heat transfer modelling

Modelling heat transfer within polymeric materials dates back to mid-1940s, starting with the fire behaviour of wood [61-68]. These first mathematical modelling constitute the framework for the mathematical formulation of the behaviour of all different polymeric materials subjected to heat and / or fire and they have been adapted by several studies since [38-44, 68-74]. Henderson, [68], provided the first most fundamental formulation of the problem with a solution strategy which has remained the starting point for most workers. More recently workers such as Gibson & Mouritz, [69], Drysdale, [70-71], Lyon, [40, 72], Staggs, [41-44], and Galgano et. al., [73], have provided refinements of the Henderson model.

Polymeric materials can be classified into two major types according to their characteristics:

(i) Charring polymeric materials

Wood is a charring polymeric material, and It can be further divided into hardwood and softwood. Hardwood has pores or vessel elements that occur among fibre and parenchyma cells. Softwood is composed of overlapping tracheid, connected by bordered pit apertures, and parenchyma cells and, in some cases, resin canals [75]. Main chemical compositions of wood are cellulose, hemicellulose, and lignin. Hardwood and softwood have a similar percentage of cellulose. Percentage of hemicelluloses for hardwood are little higher than that of softwood, but with less percentage of lignin [76].

For charring polymers such as PC, PVC, PET, PA, etc., characteristics of shrinkage or expansion are dependent on the material itself. Polymers such as PET go through shrinkage under external heat flux, but PVC and PC undergo expansion [77-78].

(ii) Non-charring polymeric materials,

Polymers such as PMMA, PS, and PE are non-charring polymers. Non-charring polymers change into gas volatiles during degradation reactions, leaving no or very few residues [79].

2.2.1 Heat transfer modelling in non-charring polymeric materials

Non-charring polymers burn out with no or very few residue. The heat transfer within these polymers is similar to the heat transfer in wood (described in the next section), which is shown in Figure 2.1 below. The solid phase of non-charring polymers can be divided into two layers. The upper layer is degradation layer, in which degradation reactions occur. Gas volatiles and vapour are produced in this layer, which escapes to the air from degradation layer through the surface. During this process, mass flux of gas volatiles is determined by

several properties, such as permeability, porosity, internal pressure, etc. The bottom layer is a virgin polymer. Non-charring polymers leave no or very few residues, which can be modelled using theory similar to flammable liquids [80].

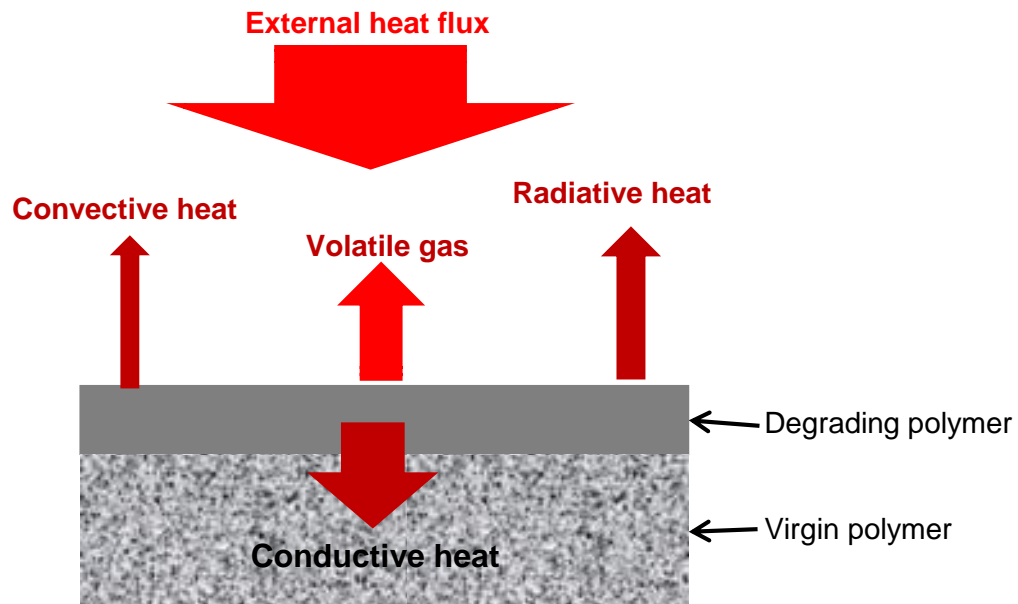


Figure 2.1: Schematic representation of heat transfer in non-charring polymeric material exposed to an external heat flux

2.2.2 Heat transfer modelling in charring polymeric materials

2.2.2.1 Heat transfer modelling in wood materials

Progress on heating behaviour modelling of decomposing materials has been made gradually over a year starting with the use of wood materials. Wood is a composite material in the sense it is a combination of the resin matrix and organic fibres which chemical compositions are cellulose, hemicellulose and lignin [75-76].

Heat conduction is the first heat transfer event that occurs as wood is exposed to heat. The simplest model considering heat conduction through the thickness of a wood material heated from the top side and insulated in the other sides to approximate a one-dimensional heat transfer by conduction from top to bottom is shown in Figure 2.2.

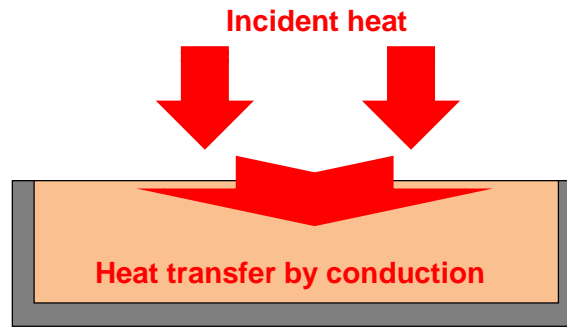


Figure 2.2: Schematic representation of 1D heat transfer by conduction through the thickness of a wood sample.

The 1D heat conduction model is described by the one-dimensional heat transfer equation as follows:

$$\frac{\partial T}{\partial t} = \alpha \frac{\partial^2 T}{\partial x^2} \quad (\text{Eqn 2.11})$$

The rate of heat conduction through the thickness of the wood depends on the incident heat flux (temperature) and the thermal diffusivity α of the material and:

$$\alpha = \frac{k}{\rho c}$$

Where: k , ρ and c are respectively the thermal conductivity, the density and the heat capacity of the wood sample.

In 1946, from the 1D heat transfer by conduction mentioned above, Bamford *et al.* [81] proposed the first mathematical model to predict the thermal response of wood as a decomposing material. They used a one-dimensional transient heat conduction equation with an additional term to include the energy associated with the thermal decomposition. Constant thermal properties and a first order decomposition reaction were used. The balance equation used by Bamford *et al.* is as following:

$$K \frac{\partial^2 T}{\partial x^2} - q \frac{\partial w}{\partial t} = c_p \frac{\partial T}{\partial t} \quad (\text{Eqn 2.12})$$

Here K is the thermal conductivity and Eqns 2.1 is modified by the addition of the term $q \frac{\partial w}{\partial t}$ taking into account the heat liberated by the decomposition of the wood, where w is the weight of volatile product of wood. It is assumed that the rate of decomposition is:

$$-\frac{\partial w}{\partial t} = kwe^{-E/RT}$$

Where k is the velocity constant, and E is the energy of activation (assumed constant).

In 1965, a one-dimensional mathematical model was developed by Tinney [82] and Hadvig et al, [83] amongst others, to simulate thermal conduction of wooden dowel heated externally. The conduction heat transfer was described by Fourier equation. And degradation was expressed by a first-order Arrhenius equation. Tinney's model has shown the progress of thermal process description in numerical modelling. The one-dimensional mathematical model he developed for cylindrical wood sample, radius r , heated externally was described by the Fourier equation for conductive heat transfer including a heat source term as follows:

$$\rho C_p \frac{\partial T}{\partial t} = k \left(\frac{\partial^2 T}{\partial r^2} + \frac{1}{r} \frac{\partial T}{\partial r} \right) - Q \frac{\partial \rho}{\partial t} \quad (\text{Eqn 2.13})$$

The surface of the wooden dowel was assumed to heat evenly, and heat penetrated from the surface to the centre. The centre was assumed as inert.

Around 1970, their work was extended by several researchers such as Munson *et al.* [84] and Panton and Rittmann [85] studying the degradation of wood in detail. The work included variable physical properties during decomposition, more accurate kinetic properties, and the effects of gas flow through the charring layer and the separation of the decomposing material into its active and residual components.

In 1972, exhausted gas volatile was considered by Kung [86]. Gas volatiles were regarded as flowing out of the sample immediately after they were produced. Kung carried out an important theoretical study of the degradation of a wood slab, one side of which is heated and the other side insulated and impervious. The physical processes contained in the model include: (1) transient conduction, (2) internal heat convection of volatiles, (3) Arrhenius decomposition of the active material into volatiles and residual char, (4) endothermic decomposition process which distinguished the active phase of wood from the residual char phase. Therefore, the model includes the charring processes present as wood degradation occurs and finally (5) variable density, specific heat, and thermal conductivity. The model

describes wood slab heated externally. Heat taken by gas volatiles and endothermicity of degradation reactions were considered. The problem formulation leads to coupled-nonlinear-parabolic partial differential equations as follows:

$$\begin{aligned}
& (\rho_a h_a + \rho_c h_c) C_p \frac{\partial T}{\partial t} \\
& = \frac{\partial}{\partial x} \left(k \frac{\partial T}{\partial x} \right) + \frac{\partial}{\partial x} (\dot{m}_g h_g) \\
& - \frac{\partial \rho}{\partial t} \left(Q_p - \frac{\rho_v}{\rho_v - \rho_f} h_a + \frac{\rho_f}{\rho_v - \rho_f} h_c - h_g \right) \quad (\text{Eqn 2.14})
\end{aligned}$$

Where ρ_v is the density of virgin wood; and ρ_f is the density of final char. The first three terms describe the effects of transient and spatial temperature changes and convection heat of gas volatiles. The last term is the source term describing the energy consumption in the degradation reactions. In numerical modelling, exposed surface is assumed to receive constant heat flux, Q_p is the endothermic energy associated with the generation of unit mass of vapours, $(\rho_a h_a + \rho_c h_c)$ is the enthalpy of the active and the char phase per unit volume, $\frac{\partial}{\partial x} \left(k \frac{\partial T}{\partial x} \right)$ is the net influx of energy due to the heat transfer by conduction, k is the total conductivity of the porous solid matrix filled with gases, $\frac{\partial}{\partial x} (\dot{m}_g h_g)$ is the net thermal energy carried out of a unit volume by the convection of the flowing volatiles, this it is assumes that these volatiles are in a good thermal contact with the solid matrix and the solid matrix does not expand or contract. (Eqns 2.4) ignores the accumulation energy of the gaseous species within the solid since so that $(\rho_a h_a + \rho_c h_c) \gg \rho_g h_g$. The conservation of mass implies that:

$$\frac{\partial \dot{m}_g}{\partial x} = \frac{\partial \rho}{\partial t}$$

Where, since the gas density is negligible compared to the solid density, the accumulated effects of vapours in the solid are neglected.

For simplicity, a single Arrhenius decomposition reaction is considered, that is:

$$\frac{\partial \rho}{\partial t} = -a_p \rho_a e^{-E_p/RT} \quad (2.15)$$

Where a_p is the pre-exponential factor, R is the universal gas constant, and E_p is the activation energy, ρ_a is the density of the solid active phase and T is the temperature in Kelvin, while the bottom was assumed inert. Boundary conditions were expressed by:

$$\text{at } x = 0, \quad -k \frac{\partial y}{\partial x} = \dot{Q}_{inc}$$

$$\text{at } x = L, \quad \frac{\partial y}{\partial x} = 0$$

Where: \dot{Q}_{inc} is the incident heat flux and L is the thickness of the sample. The results obtained show that predicted temperature of Kung's model is much higher than in practice when the surface heat losses by convection and radiation were ignored. This problem was solved later in Kansa's model in 1977 [87] as follows:

$$\text{at } x = 0, \quad -k \frac{\partial y}{\partial x} = \varepsilon \dot{Q}_{inc} - \varepsilon \sigma (T^4 - T_o^4) - h(T - T_o)$$

$$\text{at } x = L, \quad \frac{\partial y}{\partial x} = 0$$

Where σ is the Stefan-Boltzmann constant, $5.6704 \times 10^{-8} \text{ W/m}^2 \cdot \text{K}^4$, T_o is the ambient temperature and ε is the emissivity of the material. Thermal properties may change as temperature rises. In Kung's model, thermal conductivity was expressed by the rule of mixture of virgin wood and char:

$$k = \frac{\rho - \rho_c}{\rho_v - \rho_c} k_v + \frac{\rho_v - \rho}{\rho_v - \rho_c} k_c$$

In this equation, if $\rho \rightarrow \rho_v$, $\lambda = \lambda_v$; and if $\rho \rightarrow \rho_c$, $\lambda = \lambda_c$. Temperature dependent thermal properties were later used by Fan et al. in 1977 [78], which were expressed by:

$$k = k_o + p_1(T - T_o)$$

and,

$$C_p = C_{p_o} + p_2(T - T_o)$$

Where k_o and C_{p_o} are respectively the conductivity and the heat capacity at ambient temperature.

In 1977, Kansa *et al.* [87] carried out a study which is concerned with the development of a theoretical model for the degradation of porous solids and differs from previously published models primarily in the inclusion of a momentum equation for the motion of the degradation gases interior to the solid. Therefore, nonzero pressure gradients in the solid and non-uniform convective gas velocities can be accounted for. As mentioned previously, this model extends Kung's model by taking into account an internal forced convection accounting the porous structural effects of the gas flow and the overall response of the material as shown in Figure 2.3 below [87].

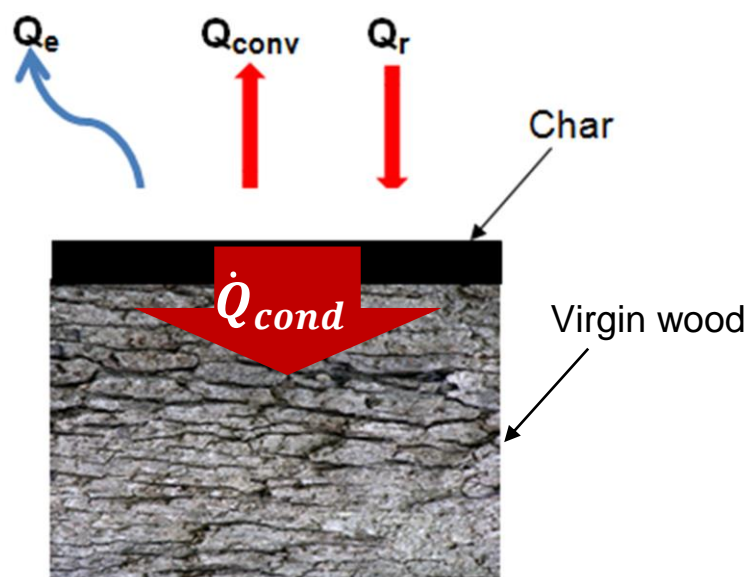


Figure 2.3: Schematic representation of 1D heat transfer by conduction through the thickness of a wood sample with char layer.

In Figure 2.3, the model described radiant (\dot{Q}_r) and convective (\dot{Q}_{conv}) heat transport to the solid surface, radiant heat emission (\dot{Q}_e) from the surface, thermal conduction (\dot{Q}_{cond}) into the solid, degradation of the wood to produce char and gases, and mass transfer with variable thermal and physical properties, a time-dependant surface radiant flux, and convective heat transport of the gas products away from the degradation zone through the char and wood (\dot{Q}_{conv}) eventually escaping from the surface.

In 1987, wood's gaseous permeability was measured and used to simulate drying process by Perre [88]. In 1990, Aerts and Ragland [89] developed a model considered gas species, consisting of O_2 , hydrocarbons, CO , CO_2 and water vapour. Subsequently, many works have

been done on one-dimensional modelling of combustible materials [90-91]. To resume theoretical studies performed since the mid-1940s on the behaviour of wood subjected to heat and/or fire developed thermochemical models that brought together the processes of heat conduction, degradation, convection flow of volatile gases, and volatile combustion at the exposed wood surface [92-93] and Kung's model established the mathematical bases adapted for the modelling, later on, of the thermal response of polymeric materials subjected to heat.

2.2.2.2 Heat transfer modelling within other polymeric materials

As commonly used in buildings, charring polymers attract much attention from researchers and engineers. The heat transfer throughout charring polymers subjected to an external heat flux is shown in Figure 2.4. Although fire processes are similar to wood, damages will be much more serious.

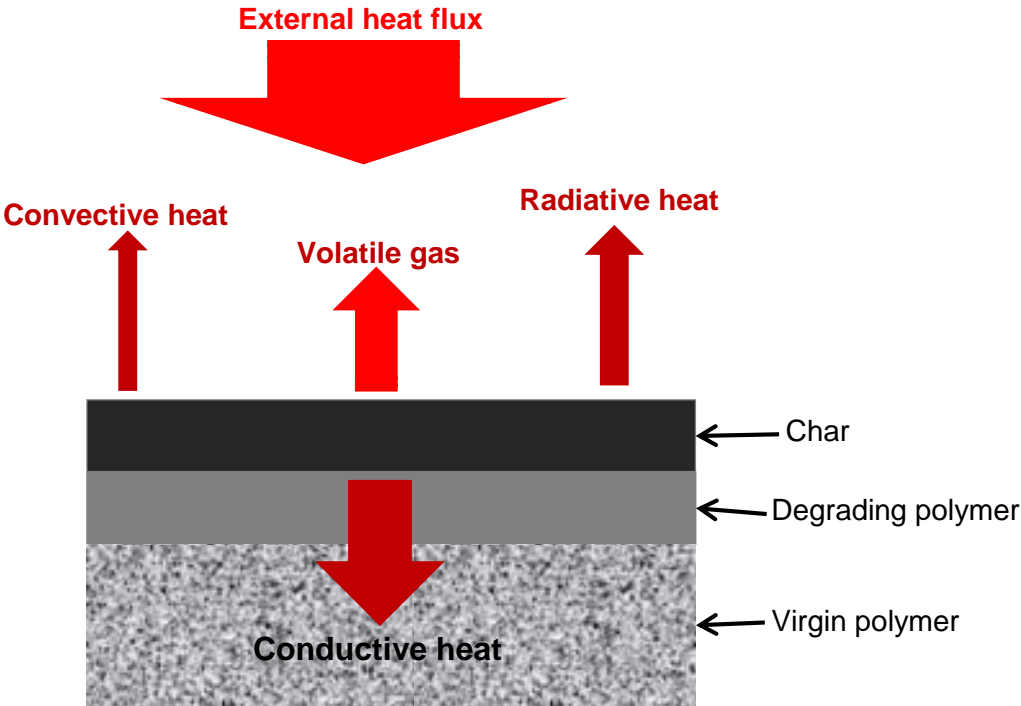


Figure 2.4: Schematic representation of heat transfer in charring polymeric material exposed to an external heat flux

The first thermal mathematical models of polymeric materials were developed with research projects conducted by NASA in 1960's to provide a practical method for protecting the

interior of spacecraft vehicle from the aerodynamic heating encountered during atmospheric re-entry. Much effort has been directed toward understanding the performance of polymeric materials used. Swann achieved analytical models for charring ablators [94-95] and estimated required weight of charring ablator base polymeric materials to provide adequate thermal protection as a function of heating conditions, and material properties have been presented. In 1962 an improved analytical model of the charring ablator was presented by Swann et al. [96] and Brooks et al. [97].

In 1965 Swann, Pitman and Smith [98] developed a mathematical model for the thermal response of ablative materials. The equations were provided for three layers of different materials, the first two of which may have moving boundaries were sustained by a metallic structure located at the back surfaces as a third layer. The analysis was developed primarily for charring ablators but is also applicable to impregnated ceramic, subliming, and heat-sink thermal protection systems. The partial differential equations governing the transient response of thermal protection systems to a hyperthermal environment were presented as follows.

$$k \frac{\partial^2 T}{\partial y^2} + \dot{m}_p c_p \frac{\partial T}{\partial y} + F = \rho c_p \frac{\partial T}{\partial t} \quad (\text{Eqn 2.16})$$

Where the first, second and third term in the left-hand-side are respectively the heat generated, the heat absorbed by degradation gases and the heat conducted within the material. The right-hand-side of Eqn 2.13 is the heat stored within the material. k , c_p , ρ and \dot{m}_p are respectively the thermal conductivity, the heat capacity, the density and the mass rate of the degradation gases, which is modelled using Arrhenius equation with a single step of decomposition similar to Eqn 2.2.

Eqns 2.13 is solved using the finite difference method to obtain an approximate solution of the temperature distribution throughout the polymeric material thickness. The principal difficulty encountered during this time in the numerical analysis of charring ablators is the extensive computer time required to obtain solutions. Therefore, a number of approximations which reduce the computer time are introduced. The conditions under which these simplifications should be used and the error involved in their use are discussed. The computer program based on the equations presented here has been found to provide a practical basis for heat-shield design studies. However the equation has been programmed for numerical solution on a digital computer. Numerical results compare favourably with available exact solutions.

In 1966 Pittman and Brewer [99] extended the work of Swann et al. [100] using Eqns 2.13 to carry out an analytical investigation of the effects of varying certain material properties on the performance of a charring ablator material which was an epoxy base material filled with phenolic. The quantities which are varied are char conductivity and, conductivity and specific heat of the uncharred material, heat of degradation, temperature of degradation, and the specific heat of the gases of degradation. The investigations on the effects of those variations on the exposed surface of the polymeric materials concerned spacecraft entering the earth's atmosphere at high velocities subjected to severe heating. Pittman and Brewer's 1D heat conduction model stated the base for successive thermal mathematical models till 1979.

In 1980 Pering et al. [101] studied graphite epoxy composite material and developed one of the first models to include the effect of mass loss caused by the thermal decomposition of organic matrices in combination with transient heat conduct. They used a simplified Pittman and Brewer's model through the assumption that the energy transfer by gas convection is negligible, as there is the immediate removal of volatile gases produced through degradation from the composite (which have no effect on temperature). Equation 2.13 now becomes;

$$\rho c_p \frac{\partial T}{\partial t} = k \frac{\partial^2 T}{\partial x^2} + \frac{\partial m}{\partial t} Q_p \quad (\text{Eqn 2.17})$$

The model considers the combined effect of the heat conduction and the degradation of the matrix causing an increase of thermal energy in the material. The heat conduction is calculated using Eqns 2.1, and the heat of degradation is calculated through theoretical analysis of the mass loss rate using Arrhenius equation and the heat of decomposition Q_p .

Griffis et al. [102], in 1981 developed the first thermal response model for Graphite epoxy composites exposed to rapid heating by fire or laser or irradiation. The one-dimensional balance equation is as follows:

$$\rho c_p \frac{\partial T}{\partial t} = k \frac{\partial^2 T}{\partial z^2} + \rho c_p V \frac{\partial T}{\partial z} \quad (\text{Eqn 2.18})$$

Where, $T(z, t)$, k , T and c_p represent the temperature, thermal conductivity, density, and heat capacity, respectively. The quantity V denotes the surface recession rate and is regarded as an unknown function of time. For this one-dimensional model the finite difference method is used to compute the temperature distribution within a composite plate considering fibre ablation, matrix decomposition, and combined radiative and convective heat flux to the

surface of the plate. Predictions of temperature distribution agreed well with experimental data, though uniform and steady-state heat flux were used for both the experiments and predicted results.

Stepped temperature-dependent effective thermal properties and uniform steady-state heat flux were used in this model. The resulting temperature profiles agreed well with measured values for graphite epoxy plates. Later, the same thermo-physical property model was used by Chen et al. [103], Griffis et al. [104], Chang [105] and Milke and Vizzini [106].

McManus and Coyne [100], in 1982 developed a thermochemical model coupled with a mechanical model in a numerical computer code named the TRAP model. Assembling similar thermo-physical property models as in reference [89], the validation of the thermo-chemical portion of the TRAP was performed on carbon and aramid fibre-reinforced epoxy composites by Fanucci [107]. The agreement between predicted and experimental results was reasonably good. Later, different temperature-dependent thermophysical property models were introduced by Henderson et al. [68, 108]. The concept of “effective material property” was once again discussed, though not used, because the various phenomena were explicitly treated in the final governing equations. The temperature-dependent properties were obtained by curve fitting based on the experimental data of the original and charred materials at different temperatures [109-110]. These material properties were assembled into a thermochemical model, and a finite difference method was used to solve the governing equations. Comparison of predicted and experimental results obtained by heating a glass fibre-reinforced phenolic composite by electrical radiant heaters revealed only small discrepancies.

In 1984 Springer [111] presented a thermochemical model in conjunction with a thermo-mechanical model. The temperature-dependent thermophysical property models were similar to the one used in Henderson’s work. Validation was performed by comparing predictions with the experimental data on graphite epoxy composites from Pering [101]. Springer’s model is a three-dimensional model predicting the temperatures to investigate the mechanical properties of composites Graphite/epoxy and wood at elevated temperature. The balance equation of the model is as follows:

$$\rho c_p \frac{\partial T}{\partial t} = k_x \frac{\partial^2 T}{\partial x^2} + k_y \frac{\partial^2 T}{\partial y^2} + k_z \frac{\partial^2 T}{\partial z^2} + \frac{\partial \rho}{\partial t} Q_p \quad (\text{Eqn 2.19})$$

In 1985, Spring's work was extended mainly by Henderson et al. [68], thereby providing the first most fundamental formulation of the problem with a solution strategy which has remained the starting point for most workers since. Henderson's model used the same methodology as the model proposed by Kansa et al. [87]. The model predicted the heat transfer using the one-dimensional transient heat conduction equation with extra terms to account the decomposition reaction and the cooling effect of the decomposition gases flowing back through the charred material. The decomposition reaction was modelled using an n^{th} order Arrhenius equation. Temperature and mass dependent thermal material properties were used. These material properties were calculated in previous works by Henderson et al. [112-114]. The decomposition term also took account of carbon-silica reactions at higher temperatures. Henderson's balance equation is a non-linear partial differential equation (Eqns 2.6) with simplifying assumptions which are; 1) no accumulation of decomposition gases in the solid material, 2) no thermochemical expansion, 3) thermal equilibrium between the decomposition gases and solid material.

$$\rho C_p \frac{\partial T}{\partial t} = \frac{\partial}{\partial x} \left(k \frac{\partial T}{\partial x} \right) - \frac{\partial}{\partial x} (\dot{m}_g h_{gas}) - \frac{\partial \rho}{\partial t} (Q_{gas} + h_c - h_G) \quad (\text{Eqn 2.20})$$

Where \dot{m}_g is the mass flux of the volatile gas; ρ, C_p and k are the density, the specific heat and the thermal conductivity respectively, of the material in the through thickness direction x ; T is the temperature; t is the time; Q , h_c and h_g are respectively the heat of decomposition, enthalpy of the solid phase and enthalpy of the volatile gas. In Eqns 2.6 $\left(\rho C_p \frac{\partial T}{\partial t} \right)$ is the rate of change of internal energy per unit volume, $\left(\frac{\partial}{\partial x} \left(k \frac{\partial T}{\partial x} \right) \right)$ is the heat flux transferred by conduction, $\left(\frac{\partial}{\partial x} (\dot{m}_g h_{gas}) \right)$ is the convection of energy resulting from the gaseous products flowing back through the char structure and $\left(\frac{\partial \rho}{\partial t} (Q_{gas} + h_c - h_G) \right)$ is the heat from solid decomposition, solid phase and gas phase.

(Eqns 2.6) was solved simultaneously with equations for the rate of decomposition and the mass flux of gas. The rate of decomposition is given by n^{th} order kinetic rate equation of the form:

$$\frac{\partial m}{\partial t} = -A_i m_o \left[\frac{(m - m_f)}{m_o} \right]^{n_i} \exp(E_i/RT)$$

Where m is the mass, m_o is the initial mass, m_f is the final mass, A_i is the pre-exponential factor, T is the temperature in Kelvin, n_i is the order of reaction, E_i is the activation energy

and R is the gas constant. The subscript i refers to either the degradation or carbon-silica reactions. The accumulation of gases being ignored, the conservation of mass is written as:

$$\frac{\partial \dot{m}_g}{\partial x} = -\frac{\partial \rho}{\partial t} \quad (\text{Eqn 2.21})$$

The mass flux, \dot{m}_g , at any spatial location and time is calculated by integrating the previous equation as follows:

$$\dot{m}_g = \int_x^L \frac{\partial \rho}{\partial t} dx$$

Where L is the material thickness and x is the thickness variable.

Henderson's equation makes an assumption by considering only two-phase material (virgin + char) while the gas phase is neglected. This approximation implies that the conservation equations are exact since the gas flow term appears without the variation in the quantity of gas is considered (Eqn 2.7). The different phases are assumed to be locally in thermal equilibrium.

Subsequently, in 1987, Henderson et al. [115] developed a second three-phase model (gas+char+virgin) taking into account the accumulation of the degradation gases. This work carried on the work done in 1985 with further considerations:

- 1) The decomposition gases are part of the balance equation, and the flow of these is described by Darcy's law.
- 2) A mechanical effect of expansion / contraction of the polymeric material is added
- 3) The surface emissivity changes as degradation occur.
- 4) The degradation gas flow is not anymore in only one boundary surface, but the build-up pressure effect in the material results in the exhaust by the two boundary surfaces (top and bottom).

The gas flow rates is more important in early decomposition because the reactions are concentrated mainly at the boundary surfaces. However, the temperature profile in the

material does not give better results than in those obtained in 1985 and therefore does not allow evaluating the relevance of the new model.

In 1991 Florio et al. [116] extended Henderson et al. work undertaken in 1987 taking into account the effects of the heat exchanged by convection between the solid phase and the gas phase. The results obtained showed that the small temperature difference between the phases has a significant effect in the polymer degradation process. Indeed, the gas flow increased significantly showing that the polymer decomposition reached the bottom surface of the sample that was not exposed to the thermal flux. Another extended Henderson et al. was presented by Milke et al. [117]. They developed a fully three-dimensional thermal response model for anisotropic composite laminates exposed to non-uniform radiative and convective heat fluxes applied to any surface of the structure. The temperatures predicted by this model are in excellent agreement with measured values. Though this model does not consider mass loss or other thermo-chemical reactions as the models developed by McManus et al., it is perhaps the most appropriate thermal response model for thick-section composite structures.

In 1992, McManus et al. [118-119] developed a model to calculate the temperature distribution within a composite plate, and the also calculates the pressure distribution due to the expansion of decomposition gases, volatile formation rates, the amount of char, and thermal stresses and strains. Though this model considers more thermochemical phenomena than the models mentioned previously and its predicted results have a good agreement with experimental results. The approach by McManus et al. was also similar to Henderson's work, though it was specifically developed for carbon fibre-reinforced phenolic composites. Furthermore, in 1992 Sullivan and Salamon [120-121] introduced a further thermochemical model in which the simulated phenomena were the same as in the McManus and Springer models [118-1119], and the material property models were similar to that of Henderson's work [115]. A model for the thermomechanical behaviour of glass epoxy composites was developed by Dimitrienko in 1997 [122] in which a similar heat capacity model was used as in Henderson's work while a more complicated thermal conductivity model was employed.

In 1995, Gibson et al. [123] developed a model similar to Henderson's model. In his work, the thermochemical model was coupled with a thermo-mechanical model. Constant material properties were used with a first order decomposition equation to model the degradation reaction. The one-dimensional balance equation has the following form:

$$\rho C_p \frac{\partial T}{\partial t} = \frac{\partial}{\partial x} \left(k \frac{\partial T}{\partial x} \right) - \frac{\partial}{\partial x} (\dot{m}_g h_{gas}) - \rho A \left[\frac{(m - m_f)}{m_o} \right]^n e^{-\frac{E}{RT}} (Q_{gas} + h_c - h_G) \quad (Eqn 2.22)$$

Equation 2.18 is a non-linear equation and incorporates the processes of conductive heat transfer through the material, endothermic decomposition of the polymer matrix, and convective mass transfer of volatile products from the reaction zone to the hot composite surface. The model was verified by comparison with furnace testing of glass/polyester panels from 10mm-22mm thick under the hydrocarbon fire curve. The hot face temperature was used as the input condition to the model and on the cold face free convection was assumed to the surrounding air. The model can predict some fire reaction properties such as time-to-ignition, mass loss rate and char formation. However, it has to be remarked that the model has not considered the fact that these char provide a significant heat isolating effect.

2.3 Modelling gas mass transport process

Modelling kinetics implies consideration of the accumulation of degradation gases as well as their transport thereof throughout the polymeric material. Numerous theoretical models have been previously proposed by Crank et al. [124], Dhingra et al. [125] and Aminabhavi et al. [126], Stern et al. [127] and Stern [128] to describe the transport mechanism of the volatile gases. Such models involve expressions of the coefficients of diffusion and permeability from statistical mechanical considerations (free volume theory) and energetic or structural considerations. Henderson and Wiecek [108] considered a porous material to calculate the mass flux of gas volatiles. The mass flux of volatile gas transportation inside the solid phase was calculated using Darcy's law which is used to describe fluid flow in porous media at low Reynolds number. Darcy's law is the equation of the conservation of momentum in which the inertial terms are neglected. At the macroscopic scale, neglecting contribution of inert gas initially presents in the pores polymeric material, velocity and pressure of gas volatiles throughout the polymeric material were expressed as follows [129]:

$$\vec{v}_g = -\frac{\beta}{\mu} (\vec{\nabla}P - \rho_g \vec{g})$$

This expression relates a superficial average gas velocity, \vec{v}_g , to the pressure gradient within the polymeric material, by means of a permeability, β , and the dynamic viscosity of the melt, μ , ρ_g is the gas density and, \vec{g} is the gravitational acceleration. In the case of polymeric material, the gravitational acceleration term is negligible so that the mass flow rate of volatile gas can be expressed as follows [130]:

$$\dot{m}_g = -\frac{\beta \rho_g}{\mu F_g} \frac{\partial P}{\partial x}$$

Where F_g is the volume fraction of the gas phase.

Later, several models used Darcy's law to describe gas transportation inside combustible materials [131-135].

Staggs, [136], provides some approaches to the mass transfer of volatile degradation gases. He used experimental data which can be easily obtained, such as the instantaneous temperature gradient through a polymer melt. He derived an expression of the gas mass flux as follows:

$$\dot{m}_v(x, t) = -\beta_T \rho (1 - f_{char}) \frac{\partial T}{\partial x}$$

Where, $\dot{m}_v(x, t)$ is the instantaneous mass flux of gas at time, t and position x within the polymeric material, β_T is the product of a thermal gas diffusivity coefficient, ρ is the density of the polymer melt, $(1 - f_{char})$ is the proportion of gas formed by degradation within the polymeric material, and $\frac{\partial T}{\partial x}$ is the temperature gradient through the polymeric material.

Physically, the basis of the equation is that the velocity of gas is proportional to the negative viscosity gradient within the polymeric material, which itself is inversely proportional to the temperature gradient, hence the negative sign on the right hand side of the equation. The result is that when this model is employed in a combustion model, an upward flow of gas through the polymeric material is simulated, consistent with the temperature gradient calculated from the heat balance [136].

2.4 Modelling ignition and combustion processes

Ignition and combustion of a polymeric material depend not only on the availability of heat but also on that of fuel and oxygen. Therefore, the degradation and the diffusion of volatile gases through the polymeric material is of greater importance for the propagation of combustion. That combustion carries on while a necessary proportion of fuel is present as gaseous volatile released by the degradation of polymeric materials combined with oxygen providing a flammable mixture [137-138].

Kanury [138] described two types of combustion when a partly degraded polymeric material is concerned, a) combustion of the volatile gaseous products of degradation, and b) the combustion of the solid, usually carbonaceous, and the residue which is also produced. The heat of combustion was determined by assuming the polymeric material as an isothermal system [139] with,

$$\dot{Q}_{comb} = \frac{hA(T_s - T_a)}{V} \quad (Eqn 2.23)$$

Here, the first term represents the heat generated by the exothermic combustion reaction and the second term represents all of that heat been withdrawn from the system through the exposed surface, A , of the polymeric material. V is the volume of the system and h , the convective heat transfer coefficient at the exposed surface of the polymeric material. Heat loss generally occurs by means of a combination of convection and radiation, where the system at temperature T_s is surrounded by an external fluid at temperature T_a .

Alternatively, Lyon et al. [137] calculated the heat of combustion considering the polymeric material in combustion in an adiabatic condition, namely the material is fully insulated system where there is no exchange of heat with the surroundings. This scenario may be used to approximate a real situation where heat of combustion is generated so rapidly outwards that the system is considered to be adiabatic:

$$\dot{Q}_{comb} = \rho c_p \frac{dT}{dt} \quad (Eqn 2.24)$$

In practice, the combustion reactions in real life situation may be considered to be hybrids of the ideal adiabatic and ideal isothermal cases, i.e. an equation may be written, which allows both for heat transfer across the system boundary to the surroundings and a temperature rise within the polymeric material:

$$\dot{Q}_{comb} = \rho c_p \frac{dT}{dt} - \frac{hA(T_s - T_a)}{V} \quad (Eqn 2.25)$$

Equation 2.225 represents the *energy conservation equation* for a combustion system. This equation forms the basis for developing mathematical criteria for ignition by Kanury [138]. These criteria normally include critical, spontaneous ignition temperature and time, as well as critical heat and gas mass fluxes.

Other models are also presented in the literature for quantities such as critical ignition temperature and critical heat and mass fluxes. Lyon et. al., [137], presented a similar analysis to that of Kanury, [138], by performing a lot of experiment using cone calorimeter in piloted ignition condition i.e. sparks are generated by the cone at random close to the exposed surface of the polymeric samples. In parallel he developed equations, beginning with the first law of thermodynamics, and deriving critical parameters, such as ignition temperature, critical heat flux and time to ignition, where ignition would be expected to happen.

To reach the ignition temperature T_{ign} , a critical heat combustion is necessary to cause the ignition of the mixture composed by volatile gas from degraded polymeric material and the air oxygen. The critical heat flux for ignition is the minimum heat flux capable of heating a material to its ignition point. It is given by Lyon et al as follows:

$$q_{cr} = \sigma(T_{ign}^4 - T_{\infty}^4) + h_c(T_{ign} - T_a) \quad (Eqn 2.26)$$

Hence q_{cr} can be written as:

$$q_{cr} = h_{ign}(T_{ign} - T_a)$$

Where h_{ign} is the total heat transfer coefficient at ignition.

Also, the ignition temperature is derived as follows:

$$T_{ign} \approx \left[\frac{T_0 \cdot \Delta H_g}{c_0} \right]^{\frac{1}{2}} \quad (Eqn 2.27)$$

Where c_0 is the heat capacity of the solid at $T_0 = 298 K$, ΔH_g is the heat of gasification per unit mass of polymeric material.

Lyon et al. [137] expressed time-to-ignition as follows:

$$t_{ign} = \frac{\pi}{4} \cdot k\rho c \frac{(T_{ign} - T_a)^2}{(q_{inc} - q_{cr})^2} \quad (Eqn 2.28)$$

Where T_a is the ambient temperature in Kelvin q_{cr} , is the critical heat flux for ignition. The heat flux q_{rr} lost due to the re-radiation from the heated composite laminates surface at T_{ign} can be expressed as:

$$q_{rr} = \varepsilon_s \sigma T_{ign}^4 = \varepsilon_s \sigma \left[\frac{T_0 h_g}{c_0} \right]^2$$

The total heat flux q_f from the flame includes both radiant and convective flame heating, respectively $q_{f,r}$ and $q_{f,c}$, is $q_f = q_{f,r} + q_{f,c}$ then:

$$q_{f,r} = \varepsilon_f \alpha_s \sigma T_f^4$$

$$q_{f,c} = h_c (T_f - T_s)$$

T_f is the flame temperature, h_c is the convective heat transfer coefficient.

Other researchers such as Babrauskas [139-140], Delichatsios et al. [141], Atreya et al. [142], Mikkola et al. [143], Carslaw et al. [144], Janssens [145] and Harada [146] developed a different formula for TTI. TTI relates to the material properties or environmental factors, such as thermal inertia, thickness, external heat flux, critical heat flux, and emissivity.

2.5 Heat transfer in polymers with thermally insulated surface

Intumescent thermal barrier protections are chemical systems applied on metallic or polymers surfaces. Intumescent systems on heating which melt, effervesce and expand, producing a porous, non-inflammable, carbonaceous char, when they are exposed to heat above a certain temperature. Gases trapped in the foamed structure are a poor conductor of heat so that the underlying structures are insulated from the heat source. With prolonged exposure to fire, the carbonaceous char decomposes at a temperature around 700°C so that its effect is not permanent.

Various phosphate-pentaerythritol systems have been developed as intumescent charring systems. Such a system require an acid source, a carbon source to be decomposed by acid attack, and a spumific agent which decomposes under the action of the heat releasing non-combustible gases that expand the carbonaceous foam while it is still in a semi-liquid state. It is important that the acid source decomposes first, followed by the carbon source, and then the spumific for the intumescent system to be effective. The complicated physical, chemical and thermal sequence that characterise intumescent behaviour in not yet completely understood, [147].

The simulation process for thermal coatings classified as moving boundary involved when active intumescent coatings are exposed to heat and/or fire. The main processes to be

accounted for in a heat transfer model for intumescent coatings are the decomposition of active coating compounds, the gas flow of the produced volatiles and the expansion of porous char and basic heat conduction [148] as shown in Figure 2.5 below:

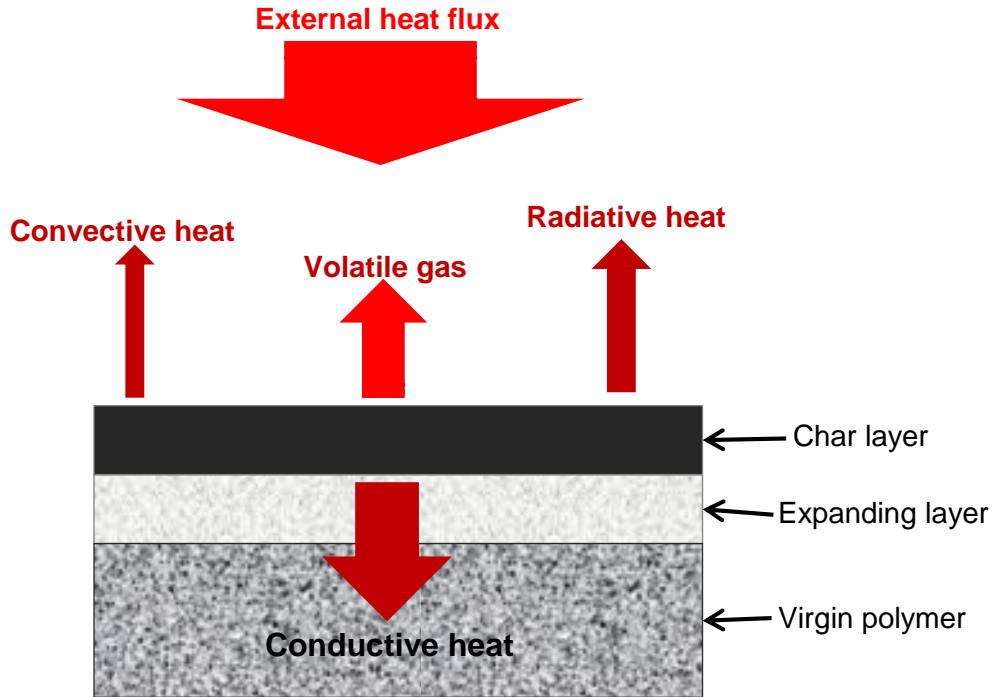


Figure 2.5: Schematic representation of heat transfer in polymeric material with intumescent coating exposed to an external heat flux.

A concise review on this subject has been published by Griffin [149] outlining the research efforts and the limitation of earlier studies [150-155]. In this study, Griffin presents a governing equation for the one-dimensional heat transfer across an intumescent coating taking into account those thermally induced effects described at the beginning of 2.4, giving, above.

$$\rho_{Int}c_{p,Int} \frac{\partial T}{\partial t} = k_{Int} \frac{\partial^2 T}{\partial x^2} - v_x \rho_{gas} c_{p,gas} \frac{\partial T}{\partial x} + \Delta h_{Int} \quad (Eqn 2.29)$$

$$\Delta h_{Int} = \rho_{0,Int} (1 - \omega) \sum_k \gamma_k r_k \Delta h_k \quad (Eqn 2.30)$$

Where, v_x is the velocity of velocity of volatiles in $x - direction$, ω is the void fraction, γ_k is the initial mass fraction of coating consumed during reaction k , r_k is the rate of reaction k , Δh_k is the specific enthalpy change for reaction k .

The first term of the right-hand side of equation (Eqn 2.19) describes the heat conduction through the coating whereas the second term denotes the energy balance arising from the cooling effect of volatile gas flow and the last term accounts for the absorbed or evolved energies during the decomposition reactions of the individual chemical compounds. Due to the physical expansion of the coating during heat exposure, the spatial dimension between neighbouring nodal points of the simulation needs to be adjusted as follows:

$$x_{i+1,j} - x_{i,j} = \alpha_{ex} \cdot m_k (x_{i+1,0} - x_{i,0}) \quad (Eqn 2.31)$$

Where $\alpha_{ex} \cdot m_k$ is a variable expansion parameter determined by the overall conversion of gas-forming components within the expanded layer. Equations 2.19, 2.20 and 2.21 are solved simultaneously using Finite Difference Method (See Appendix 1).

One of the most significant limitations of the current models, and consequently the greatest challenge to overcome, as pointed out by Griffin and later by Staggs et al. [156] is an accurate reproduction of the expansion behaviour. The introduction of an expansion faction is of widespread use either as a parameter directly determined from experimental observations [157] or coupled to the conversion of intumescent components into gaseous products [152]. It is shown in studies, e.g. Kandare et al. [158], that a reasonable correlation between calculated and experimental temperature profiles can be achieved despite acknowledging the shortcomings that are due to the consequences of using a simplified expansion factor. As the process of expansion is a complex issue due to its non-uniform and non-linear characteristics influenced by room conditions, type of heat source, the rheological properties of the char melt and coating thickness, a detailed and accurate mathematical description of intumescent swelling is yet to be established. Studies into the kinetics of the decomposition reactions, such as [159-161], can be an aid to further the understanding of the complex process involved and contribute towards the development of more sophisticated models.

Butler et al. [162-164] have developed a theoretical three-dimension mathematical model of heat transfer in an intumescent protected system to model the swelling and the heat transfer rather than input from experimental data. A heat flux applied to one side of the material raises the temperature to a critical value causing the expansion of the intumescent layer. As

the temperature of the intumescent sample rises, gasification reactions are triggered progressively further from the upper surface. Equations of mass, momentum and energy are solved under local conditions to determine the growth rate, the rate of migration and thermal effects of each bubble formed within the material. A balance equation described the collective behaviour of the system by taking into account all the phenomenon involved.

A heat transfer sub-model in the model employs an analytical solution regarding the error function for the temperature profile. Here 10000 infinitesimal bubble nucleation sites are randomly distributed through the initial geometry [165]. In the vicinity of a bubble, thermal conductivity is lower in the interior of the bubble than in the melt outside, and an endothermal heat flux due to the gasification reactions is applied at the bubble surface. Butler et al. noted that the heat of reaction is not just at the bubble surface but distributed throughout the melt [162]. However, the simplification permits an approximate analytical solution.

A hydrodynamics sub-model determines the velocity field generated by expanding bubbles. In a growth sub-model, the growth rate of bubbles depends on the chemistry of decomposition of the blowing agent, and the physical properties of the gas and the surrounding melt. An Arrhenius expression relates gasification reactions to local temperatures. As a first approximation, the bubbles are assumed to be retained by the sample [162]. Bubbles are allowed to coalesce, and the upper surface stretches to prevent bubbles bursting.

The three sub-models are coupled as the model moves forward in time. At each time step, temperature, temperature gradient, and material properties are determined for each bubble. A Runge-Kutta procedure increments the position of bubbles and nodes on a rectangular grid. The diffusion of gases affecting the growth rate of bubbles, and their migration to regions of higher temperature, is critical to swelling and heat transport.

In a further investigation of bubbling behaviour, Butler [166] has developed a one-dimensional oceanography model incorporating a turbulent layer, to give a mixed-layer pyrolysis model for polypropylene exposed to high temperature. The solid melts to produce a perfectly mixed bubble layer of uniform temperature. The incident heat flux generates turbulent motion, and bubbles grow, move and burst within the mixed layer. The rate of gasification which determines the production of bubbles is a temperature dependent Arrhenius function.

Bourbigot et al. [167] examined an approach to model fire protection using intumescent paint on a steel plate which is a typical problem of heat transfer including moving boundaries. The approach is to take into account the dynamic of the problem using Arbitrary-Lagrangian-Eulerian method (ALE) implemented in Comsol-Multiphysics software coupled with heat transfer and fluid dynamic. The relevant equations used are the heat diffusion with a heat source to model the degradation and a convective term (Eqn 2.32) and the Navier-Stokes equation (Eqn 2.33) for an incompressible flow (Eqn 2.34):

$$\rho C_p \frac{\partial T}{\partial t} + \nabla \cdot (-k \nabla T) = Q - \rho C_p \cdot u \cdot \nabla T \quad (\text{Eqn 2.32})$$

$$\rho \frac{\partial u}{\partial t} + \rho(u \cdot \nabla)u = \nabla \cdot [-\rho I + \eta(\nabla u + (\nabla u)^T)] + F \quad (\text{Eqn 2.33})$$

$$\nabla u = 0 \quad (\text{Eqn 2.34})$$

In Eqn 2.32, the heat source Q represents the energy of the degradation of the material. In Equation 2.33, the vector F is used to simulate internal forces taking place during the swelling of the material.

The results of the computation show that their approach permits to simulate the expansion (intumescence) of the paint when undergoing an external heat flux.

2.6. Modelling melt dripping of thermoplastic polymers

Modelling the heat transfer within thermoplastic polymer materials has long been recognised as a very difficult undertaking because they tend to melt and yield extra complexity when they are heated. At melting temperature, the heat transfer within the material involves changing states of matter and a boundary separating the solid and the liquid phases develops as the melting process progresses. The position of the boundary between the two phases is not known in advance but has to be determined as part of the modelling work.

In the 1900s, Stefan studied the melting of a thick plate of polar ice, where the melt is removed continuously and immediately from the surface [168]. Initially, the plate is at a temperature T_0 (below zero). The surface temperature is raised to a temperature T_s above zero degrees, and maintained at that temperature. Thus, the melting starts at the surface and a solid-liquid interface $S(t)$ at melting temperature T_m (taken to be zero) moves throughout the ice as the liquid phase is formed. This is a one-phase problem and the one-dimensional heat conduction equation is as follows:

$$C_p \rho \frac{\partial T}{\partial t} = k \frac{\partial^2 T}{\partial x^2}, \quad k \quad 0 < x < S(t), \quad t > 0$$

And,

$$-k \frac{\partial T}{\partial x} = L \rho \frac{dS(t)}{dt}, \quad x = S(t), \quad t > 0$$

The boundary condition at the exposed surface to a radiant heat \dot{q} is:

$$-k \frac{\partial T}{\partial x} = \dot{q} - h(T_s - T_a) - \epsilon \sigma (T_s^4 - T_a^4)$$

The specific heat capacity, density, heat convection and heat conductivity, C_p , ρ , h and k respectively, were constant. \dot{q} is the incident radiation heat flux on the surface which intensity is modified by heat losses by convection and re-radiation from the surface as well. The equations above are non-linear and difficult to solve analytically.

The moving boundary phenomenon implying phase change state with heat transfer by conduction within a material is referred to as Stefan problem since.

Crank [69-170] discusses a variety of both analytical and numerical methods to solve moving boundary problem. The majority of researchers have tested this methodology on ice-water test cases, although the Stefan's approach has been applied to the solidification metal castings [171], blow moulding [172] and laser welding [173].

In the 1950s and 1960s, Stefan's method was used by researchers from NASA to model polymer melt behaviour by studying thermal ablation in the aerospace industry. Work done by Landau [174], Dewey et al. [175], Lotkin [176] and Citron [177] started using numerical methods to approximate the solution of the partial differential equations involved. Because of the inherent complexity of obtaining numerical solutions to the non-linear partial differential equations they investigated the possibility to further reduce the problem by simplifying the boundary conditions before any numerical work is started. They considered a one-dimensional polymer slab with temperature-dependent thermal properties subjected to an arbitrary heat input $Q(t)$ on one face. No restrictions are placed on the boundary conditions which may be prescribed on the other face of the slab. Once melting occurs at the heated side the problem to be solved requires the determination of the temperature distribution $T(x,t)$ in the slab and the amount of material melted as a function of time $s(t)$. The molten material is taken to be immediately removed upon formation. For the determination of $T(x,t)$ and $s(t)$, the solution of the following heat conduction equation is determined numerically:

$$\frac{\partial}{\partial x} \left[k \frac{\partial T}{\partial x} \right] = c_p \rho \frac{\partial T}{\partial t}, \quad S(t) 0 < x < l, \quad t > 0$$

The equation above is subject to two initial conditions:

$$a) T(x, t^*) = T_0(x),$$

$$b) T(S, t) = T^*,$$

and three boundary conditions

$$c) Q(t) = -k(T^*) \frac{\partial T(S, t)}{\partial x} + \rho L \dot{S}$$

$$d) G \left(T, \frac{\partial T}{\partial x}, \dots \right) = g(x)$$

$$e) S^* = 0$$

The first condition gives the temperature distribution at the start of melting $t = t^*$. Condition b) requires that the melting face is maintained at the melting temperature T^* while conditioning c) specifies the division of the incident heat flux between the part entering the solid and the part going toward overcoming the latent heat of melting L . The function $G \left(T, \frac{\partial T}{\partial x}, \dots \right)$ in condition d) represents an arbitrary boundary condition on the temperature at the face $x = L$. Condition e) is an initial condition on the amount of material melted.

Since 1960 the mathematical modelling of polymer melting behaviour using Stefan Method has been used in varying degrees of complexity in accordance with the continued development of computer processing. Following experimental investigations carried out on melting behaviour of thermoplastic polymers in burning condition [178-179], Zhang et al. [180] focussed their work on the melting behaviour of both, thermoplastic and thermosetting polymers during burning. They attempted to identify the melting characters of the individual polymers under cone calorimeter fire conditions. On the base of the experimental results, a simulation model for polymer burning was developed to include the melting behaviour. A physical description of this two-phase model is shown in Figure 2.6.

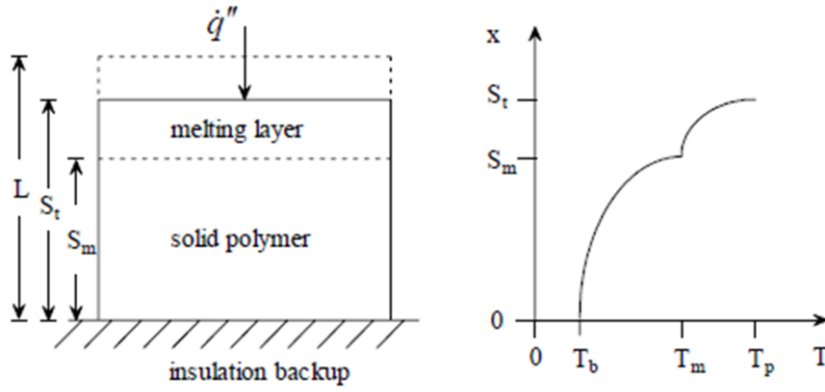


Figure 2.6: Physical model of melting polymer during burning [195].

The mathematical formulations are as follows:

Before the melting occurs, the heat conduction in the polymer is governed by:

$$\frac{\partial T}{\partial t} = \frac{k}{C_p \rho} \frac{\partial^2 T}{\partial x^2} \quad (\text{Eqn 2.35})$$

subjected to the initial conditions,

$$T|_{t=0} = T_\infty \quad (\text{Eqn 2.36})$$

And three boundary conditions

$$k \frac{\partial T}{\partial x} \Big|_{x=L} = \varepsilon \dot{q}'' - h(T_s - T_\infty) - \varepsilon \sigma (T_s^4 - T_\infty^4) \quad (\text{Eqn 2.37})$$

$$k \frac{\partial T}{\partial x} \Big|_{x=0} = 0 \quad (\text{Eqn 2.38})$$

Where T is temperature distribution in the polymer, T_s the surface temperature, T_∞ the environment temperature, k thermal conductivity, ρ density, C_p specific heat, ε emissivity, σ Stefan-Boltzmann constant, and \dot{q}'' external heat flux.

(a) After the polymer starts to melt, for the upper layer ($S_m \leq x \leq S_t$)

The heat conduction in the melt is governed by:

$$\frac{\partial T}{\partial t} = \frac{k_m}{C_m \rho} \frac{\partial^2 T}{\partial x^2} \quad (\text{Eqn 2.39})$$

subject to the initial conditions and boundary conditions as follows:

$$T|_{x=S_m} = T_m \quad (\text{Eqn 2.40})$$

When $t < t_{ig}$

$$k_m \frac{\partial T}{\partial x} \Big|_{x=S_t} = \varepsilon \dot{q} - h(T_s - T_\infty) - \varepsilon \sigma (T_s^4 - T_\infty^4) \quad (\text{Eqn 2.41})$$

When $t \geq t_{ig}$

$$T|_{x=S_t} = T_p \quad (\text{Eqn 2.29})$$

$$k_m \frac{\partial T}{\partial x} \Big|_{x=S_t} - \rho Q \frac{dS_t}{dt} = \varepsilon \dot{q} - h(T_p - T_\infty) - \varepsilon \sigma (T_p^4 - T_\infty^4) \quad (\text{Eqn 2.42})$$

(b) For the solid polymer layer ($0 \leq x \leq S_m$)

The heat conduction in the solid phase is governed by Eqn 2.39, subjected to the boundary conditions of Eqn 2.41 and 2.42.

(c) At the interface between the melt and solid phases

$$k_m \frac{\partial T}{\partial x} \Big|_{x=S_m} - k \frac{\partial T}{\partial x} = -\rho(C_m - C)T_m \frac{dS_m}{dt} \quad (\text{Eqn 2.43})$$

Using the Finite Difference Method, the above equations were solved numerically using a computer. The temperature distributions within the polymers at time t are thus obtained. The comparison between the model predictions and the experimental results was in fair good agreement provided the appropriate thermal property parameters were used.

Over the past decade, new numerical methods have been developed to solve problems involving large deformations of the polymer exposed surface [181]. In these methods, the governing equations for both fluids and solids are written using a Lagrangian description, which follows the motion of individual particles in the flow. This approach eliminates the convective term in the equations and provides many advantages in computational efficiency. In the Particle Finite Element Method (PFEM), the particles represent the nodes of a finite element mesh [182-184] while in Finite Difference Method (FDM) a delimited region is taken as a node.

Butler et al. [185] carried out the modelling of thermoplastic melt dripping by using the Particle Finite Element Method (PFEM). The modelling effort is based on the data collected from a set of experiments carried out by Ohlemiller et al. [184, 186]. A schematic of the apparatus used in the experiments is shown in Figure 2.7 below.

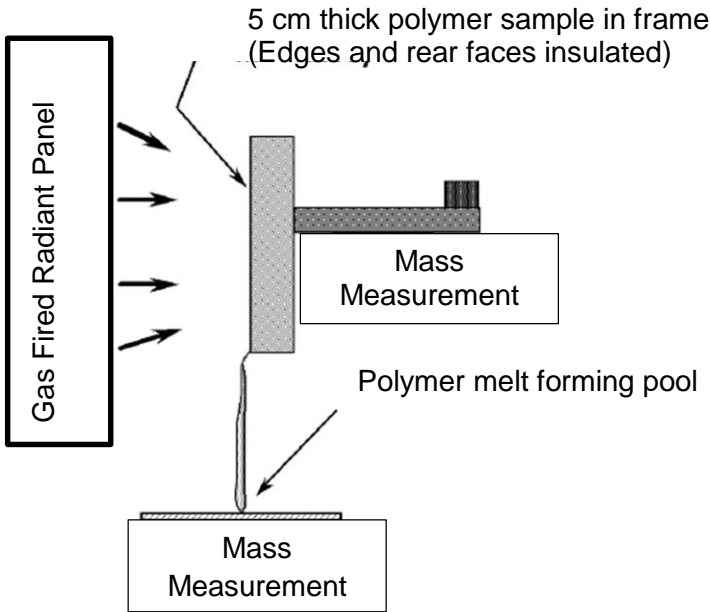


Figure 2.7: Schematic of Polymer melts apparatus [185].

A rectangular polymeric sample with dimensions, 10 cm high by 10 cm wide by 5 cm thick is mounted upright and exposed to uniform heating on one face from a radiant heater placed on its side. The sample is insulated on its lateral and rear faces. The melt flows down the heated face of the sample and drips onto a surface below. A load cell monitors the mass of polymer remaining in the sample, and a laboratory balance measures the mass of polymer falling onto the catch surface.

The Particle Finite Element Method is applied to the 1D model to solve the energy equation for a gasifying slab of material of thickness L heated at incident heat flux q_0 at $z = L$:

$$C_p \rho \left(\frac{\partial T}{\partial t} + W \frac{\partial T}{\partial z} \right) + H_v \frac{dm}{dt} = k \frac{\partial^2 T}{\partial z^2} \quad (\text{Eqn 2.44})$$

Where T is temperature, ρ is density, C_p is specific heat, k is thermal conductivity, H_v is the heat of vaporisation, and mass loss rate is given by the Arrhenius expression:

$$\frac{dm}{dt} = \rho B e^{-E/RT}$$

The velocity W at any position z within the slab is:

$$W(z, t) = \int_0^z \frac{(dm/dt)}{\rho} dz$$

And the velocity at the surface is $dL/dt = W(L, t)$. The initial conditions are $T = T_0$ and $L = L_0$ at time $t = 0$. An adiabatic boundary condition $\frac{\partial T}{\partial z} = 0$ is applied at $z = 0$, and at $z = L(t)$ the boundary condition is:

$$-k \frac{\partial T}{\partial x} = \varepsilon q_0 - h(T_s - T_a) - \varepsilon \sigma (T_s^4 - T_a^4)$$

Where q_0 is incident heat flux, ε is emissivity, σ is the Stefan-Boltzmann constant, and h is the convective heat transfer coefficient. The accuracy of the PFEM model was checked by comparison to a 1D model of gasification that solves the identical problem. Butler et al. [186-188] approached the modelling of thermoplastic melt dripping in a stepwise strategy with parallel experiments to test each model step. As a first step, the focus is on the non-burning behaviour of the polymeric material, looking just at the behaviour of a simple vertical thermoplastic slab heated uniformly on one vertical side. The slab, in general, can respond to the heating by both melting and gasifying. In the next step, it can be burned on that face. In the following step, it can be burning on its face and interacting with its own melt pool fire. In the final step, the slab is extended laterally, ignited locally and a melt pool-assisted flame can spread over and consume the entire slab. In practice, the first step has proven to be a major

challenge. Commercial computational fluid dynamics (CFD) codes applied to this problem give impractically long solution times leading to many days per case [185].

2.7 Conclusions

Various studies in the literature have shown that many physical phenomena occur when a polymeric material is subjected to a high incident heat. All these phenomena interact and are still not fully understood. Taking this into account in the models is often greatly simplified. Several thermal degradation models have been developed since the 1980s, and most have provided significant benefit to mathematical modelling purposes. However, developing a more flexible model will allow taking into account a greater number of parameters to simulate the multiple phenomena occurring and their interactions. Indeed, the number of parameters will increase the complexity of the model and these needs to be characterised each type of polymeric materials. Systematic experimental validation will better quantify the interactions of phenomena, and therefore improve the models.

According to the background work undertaken in this chapter, modelling the behaviour of polymeric material exposed to heat and fire is difficult due to the complexity of the phenomenon involved. The governing equations are Partial Differential Equation without analytical solutions. Moreover, there is no bespoke or dedicated software available to simulate the problem. Researchers working on the subject have to develop their resources for the approximate solutions. Therefore, the only way is to use a numerical methodology such Finite Difference Method embedded in appropriate software by developing a specific code to obtain an approximate solution near to real life behaviour with a reasonable computational time

In the last few years Lautenberger and Fernandez-Pello [189-192] developed a generalised model, named Gyro, for non-charring polymers, charring solids, intumescent coating, and smoulder in porous media. Also, Stoliarov et al. [193-196] developed a computer programme based upon a complex chemically model, named ThermaKin, to describe the degradation of solid materials exposed to external heat flux, such as non-charring, charring, and intumescent solids.

Chapter 3: Experimental procedures and their associated results

3.1 Introduction

In this chapter the different experimental processes are described and the results given. In order to validate the accuracy of the different numerical models developed in Chapters 4 to 7, a number of standard fire tests were carried out. While some experimental results to validate the different numerical models developed here are taken from other researchers' work at Bolton [197-202], additional sets of experiments were specifically developed for this work. The work taken from previous projects or carried out in this project has been clearly identified in this chapter. The previous work has been given to understand the conditions used while discussing the simulated and experimental results.

The work is divided in four parts based on different scenarios used to simulate and experimentally validate temperature variations during melting, decomposition, charring and ignition phases of polymers. In first two parts melting behaviour of thermoplastic polymers (polypropylene, polyester, polyamide 6, polymethyl methacrylate, polycarbonate and polystyrene) have been studied. In the first part the polymer sample is heated in a vertically oriented tubular furnace to measure the temperatures of melting drips. In the second test scenario the sample is placed horizontally in a cone calorimeter (standard cone sample holder according to ISO 5660) and heat applied only on the top surface while the other sides of the polymer sample are insulated.

In the third and fourth parts decomposition, charring and ignition behaviour of glass fibre – reinforced epoxy composites and thermally insulated composites have been studied. The experimental results obtained are from previous works at the University of Bolton [197-202], where temperature profiles through the thickness of samples were measured using thermocouples as the samples were exposed to different heat fluxes in a cone calorimeter.

3.2 Melt dripping thermoplastics

3.2.1 Polymer samples

The following six commercially available polymers were sourced in chip forms:

1) Polypropylene (PP), Moplen HP516R, Basell.

Nominal melt flow rate (ISO 1133, 230°C/2.16Kg) 25 g/10 min; softening temperature (ISO 306) 155 °C; heat deflection temperature B, (ISO 75B-1, -2; 0.45 MPa, unannealed) 90 °C [203].

2) Polyamide 6 (PA6), Technyl C 301 Natural, Rhodia, France

Melting temperature (ISO11357-1/-3, 0°C/min) 220°C; parallel and normal moulding shrinkage (ISO 294-4) 1.1%; water absorption (ISO 62) 6.5%; humidity absorption (ISO 62) 2%; density (ISO 1183) 1340 kg/m³ [204].

3) Polyethylene terephthalate (PET, polyester), from Fibre Extrusion Technology, UK.

Melting temperature >250°C; boiling point >350°C; moulding temperature 121 °C; softening point (ASTM D 1525) 82°C; refractive index 1.57–1.58; intrinsic viscosity (SABIC (IRC0041) 0.76 ± 0.02 dl/g; bulk density (ASTM D 1895) 838 ± 10 Kg/m³ [205].

4) Polycarbonate (PC), Beyer Makrolon, received as a 4 mm thick sheet.

Melting volume rate (ISO 7391, 300 °C/1.2 kg) 6.0 cm³/10 min; melt temperature 250-280 °C; softening point (ASTM D 1525, at 50 N 145) 150 °C; max. water content 0.01 %; drying temperature 120 °C; heat deflection temperature (0.45 MPa) 140 °C; [206].

5) Polystyrene (PS), Rapid electronics, in form of 2 m 457x 305 blue plastic sheet (37-3142). Blue pigment less than 1% of total mass, determined via TGA. 4 mm sheets were prepared by running a thin layer of methyl ethyl ketone (MEK) over one of the surfaces and pressing together and clamping underweight.

Softening point (ISO 306B50, 1 Kg/50°C) 87°C; moulding shrinkage 0.4 – 0.7%; heat deflection temperature (Method B, 455 KPa, and Annealed) 97°C [207].

6) Polymethyl methacrylate (PMMA), Vision polymers as 4 mm sheets.

Softening point at 50 N 107°C, ISO 306; Flash point >250°C; auto ignition temperature 304°C; moulding temperature 79 - 107 °C; moulding shrinkage (ASTM 955) 0.20 - 1.00 % [208].

From polymer chips of PP, PA6 and PET, plaques were prepared by a melt pressing process where chopped polymer chips were transformed into 150mm x 150mm x ~3mm sized plaques using high temperature (melting temperature of the polymer) and pressure (20 kg/cm²) for 3 min, followed by sudden cooling. The polymer plaques were then cut into small specimens of required sizes. PC, PS and PMMA, as mentioned above, were sourced as sheets (plaques).

The polymer plaques were then cut into small specimens of 100 mm x 6 mm x 3-4 mm sizes in order to get them easily dripping into the vertical oriented furnace of 25 mm diameter presented later in Section 3.2.3.

3.2.2 TGA and DSC analysis (Not conducted in this work)

In order to establish fundamental properties of PC, PS, PA6, PMMA, PET and PP polymer samples, part of a parallel programme of work measured these properties using thermogravimetry, performed on an SDT 2960 simultaneous DTA–TGA instrument (TA Instruments) from room temperature to 600°C with an heating rate of 10 °C/min in both air and nitrogen flowing at 100 ± 5 mL/min. Also glass transition temperatures or melting temperatures of all polymers were measured using differential scanning calorimetry (DSC) (TA Instruments) at 10 °C/min in flowing N₂ (100 mL/min). Analysed results from both studies already published [197] are presented in Table 3.1 and they will be used in this work.

Polymer	TGA analysis		Glass transition temp ^b .(°C)	Melting temp ^b . (°C)
	T _{Onset} ^a	DTG maxima (°C)		
PP	274 (415)	367 (459)	-26	172
PA6	372 (375)	434, 458 (456)	54	225
PC	464 (501)	533, 638 (541)	147	267
PET	378 (397)	429,446, 538 (439)	68	256
PS	329 (387)	412, 519 (431)	96	-
PMMA	306 (327)	317 (364)	110	-

^a T_{Onset} = Onset of decomposition temp, where 5 % mass loss occurs

^b Measured by DSC

Table 3.1: Analysis of thermal behaviour (DTA-TGA) of polymers in air and nitrogen atmosphere (values reported in parenthesis) of polymers (taken from ref [197]).

3.2.3 Tubular furnace setting for vertical melting drops' temperature measurement

3.2.3.1 Description of the test rig developed previously at Bolton for evaluating melt dripping behaviour of thermoplastics [197].

In previous work at the fire lab of Bolton an experimental set up was constructed to investigate the melt dripping behaviour of vertically oriented polymers samples. The experimental set up is shown schematically in Figure 3.1 [197].

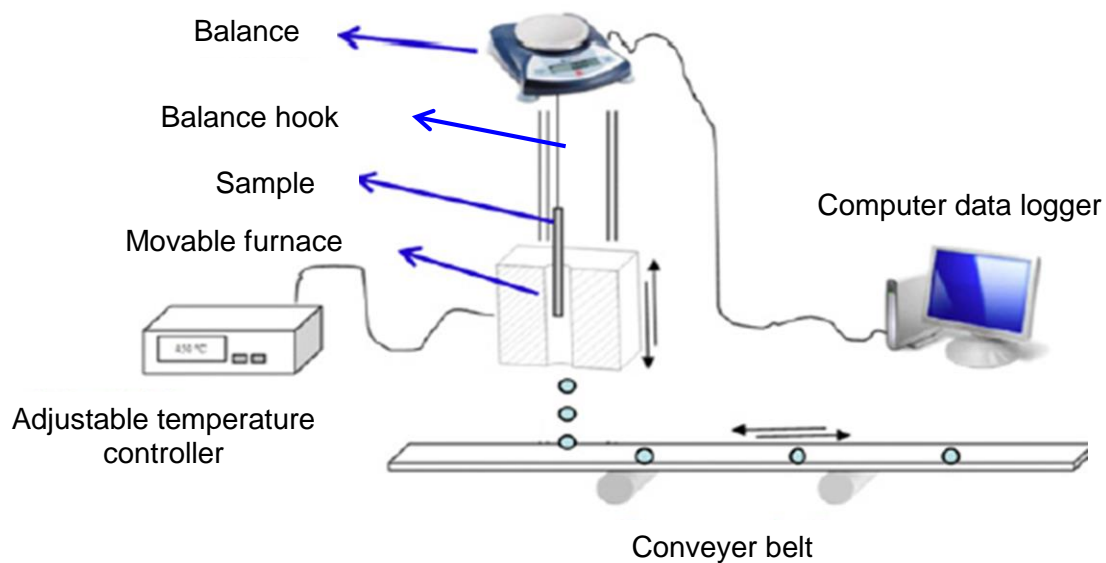


Figure 3.1: Schematic of melt dripping experiment in furnace (taken from ref [197])

A 800 W in house fabricated furnace containing a cylindrical aluminium silicate former, mounted in a casing of perforated mild steel with calcium silicate board end pieces is used as a heat source. The furnace tube had a 25 mm bore, and a length of 120 mm. The furnace is controlled by an adjustable temperature controller with a temperature limit set to 900°C. The temperature controller measures the core surface temperature in middle of the furnace via a thermocouple. Dynamic recording of the mass of the polymer sample is made by a digital mass balance (Ohaus Scout Pro) connected to a computer. The mass of the sample is shown to the nearest 0.001 g. Mass loss data is recorded in real time via the data acquisition software. The scale allows weighing of the polymer sample, located via a thin wire and built-in hook attached to the bottom of the balance. The sample is fixed and the furnace is raised on rails via a pulley arrangement until the bottom of the sample which is in the centre of the furnace.

The temperature is pre-determined and pre-fixed before the furnace is mounted. Since the thermocouple connected to the temperature controller gives the surface temperature of the furnace, it is different from the air temperature in the centre of the furnace. To measure the air temperature in the furnace, a thermocouple embedded in ceramic fibre and hung on a clamp, positioned at the centre inside the furnace. The temperature of the controller was set to a particular temperature and the furnace left to stabilise for 10 min. Then the temperature of the thermocouple was recorded. By plotting the set furnace temperature vs the temperature in the furnace, the true temperature in the furnace could be noted. According to the calibration curve shown in Figure 3.2 below it varies linearly with the temperature setting in the controller. The coefficient of proportionality 'm' between both is the tangent of the curve that is equal to 0.8748.

For example in order to set a furnace temperature of 500°C the controller has to be set at 570°C.

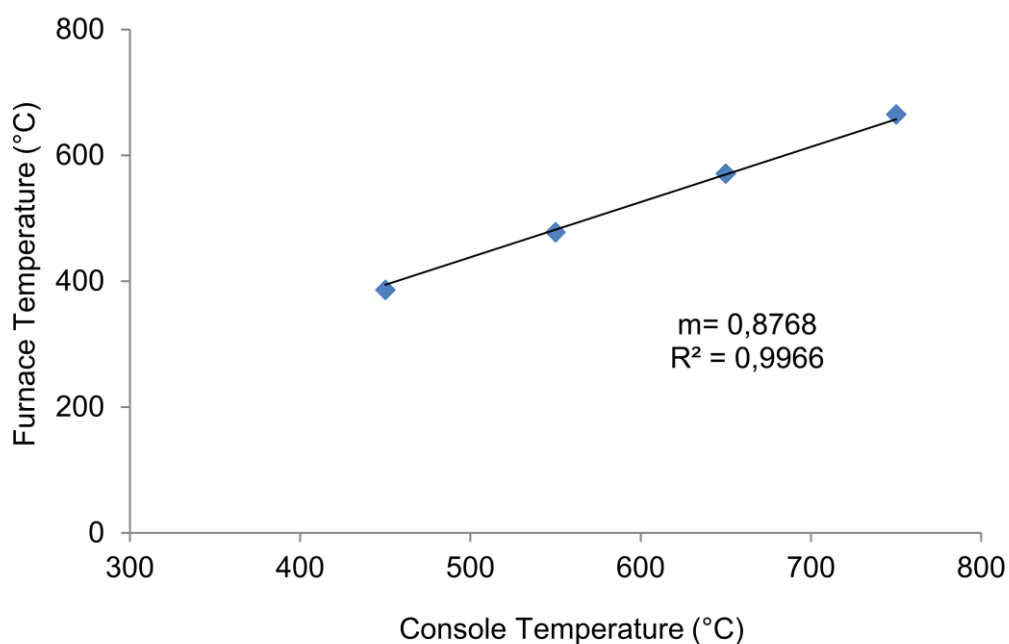


Figure 3.2: Calibration curve: Furnace Setting Temperature (FST) vs. temperature of the controller

It was also noticed that the temperature in the centre of the furnace was different from that near the top surface of the furnace bore due to air convection, amplified by the use of extractor fan above the rig. To minimise this temperature difference, a calcium silicate board sits on top of the furnace. A small hole, drilled in the centre of this board, enables a fine wire and hook bearing the sample to be connected to the balance. A long strip of aluminium foil

placed on a conveyer belt located under the bore of the furnace, collects the drops from the heated sample. The conveyer belt, 52.8 cm long and 15 cm wide, moves at a pre-determined uniform speed. Furnace set temperatures at which the measurements were taken are given in Table 3.2 below.

Polymer	Temp. when dripping starts (°C)	Temp. when sample ignites and starts burning (°C)	Selected furnace temperatures for the melt dripping test in [Ref 5] (°C)	Selected furnace temperatures for the melt drop temperature measurement (°C)
PP	617	735	625, 660*, 690, 725	350, 450, 500, 625, 660
PA6	416	639	425, 495, 560*, 630	425, 495, 560
PC	504	732	515, 585, 650*, 720	515, 585, 650
PET	407	644	415, 490, 565*, 635	415, 490, 565, 635
PS	547	622	555, 570, 595*, 615	300, 350, 400, 450, 500, 555, 570
PMMA	513	613	520, 550, 575*, 600	350, 400, 520, 550

Table 3.2: Furnace temperature settings for melt dripping experiments (taken from ref [197])

Note: * denotes furnace temperature settings of the molten drops of which TGA analyses were conducted

3.2.3.2 Experimental set up for temperature measurements of drops in melt dripping experiments

For this work the experimental rig set up described in the Section 3.2.3.1 was modified in order to be able to measure the temperature of the drops. To achieve this, the conveyer belt, previously placed beneath the furnace was replaced with an adiabatic container placed immediately beneath the furnace as shown schematically in Figures 3.3. The container was developed by drilling a hole into a block of wood, lining this with heat resistant ceramic wool and ultimately with a layer of thick aluminum foil. The polymer sample is placed on the hook and the pre-heated furnace is raised on rails via a pulley arrangement until the bottom of sample is in the centre of the tubular furnace. Due to heat transfer by radiation between the internal wall furnace at a pre-determined furnace setting temperature and the immersed sample, the polymer starts dripping when a certain temperature is reached. Five thermocouples were inserted into the collector through holes drilled in the wooden plate, the thermal insulation and aluminum foil, allowing measuring the molten polymer drops falling

directly onto the exposed tips (Figures 3.4). Temperature measurements were recorded over a period of time. From the five thermocouples used, negligible variation was observed between their temperatures. Figure 3.5 presents the maximum drop temperature peaks of number of drops in one of the PMMA experiments and is typical of the drop temperature experiments carried out during this work. Each peak represents the maximum temperature measured for a single fallen drop collected. As can be seen from Figure 3.5, the temperatures of different drops varied within a certain temperature range, the variation however, was not function of the time. Since the drop collector was placed immediately under the centre of the furnace to ensure the minimum time between the drop leaving the molten surface of the sample and its collection, hence it was assumed that heat losses between the drop falling, collection and temperature measurements can be neglected.

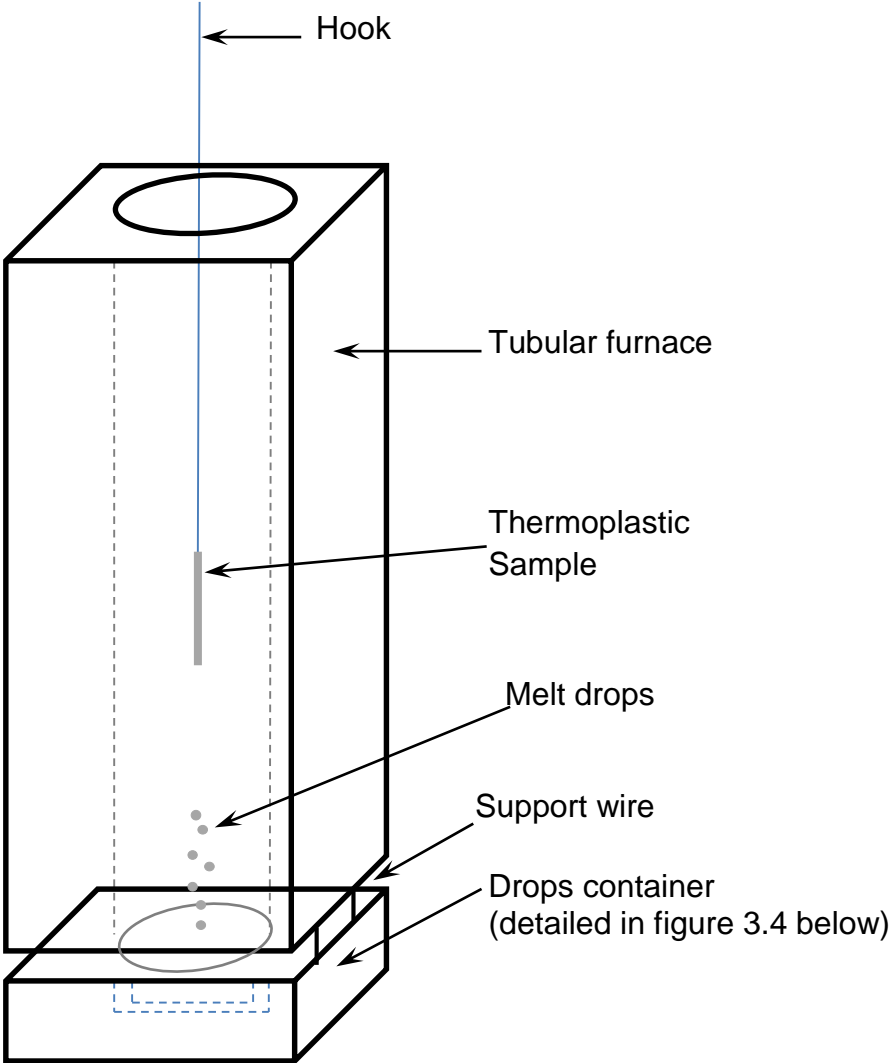


Figure 3.3: Schematical view of the tubular furnace coupled to the drops container

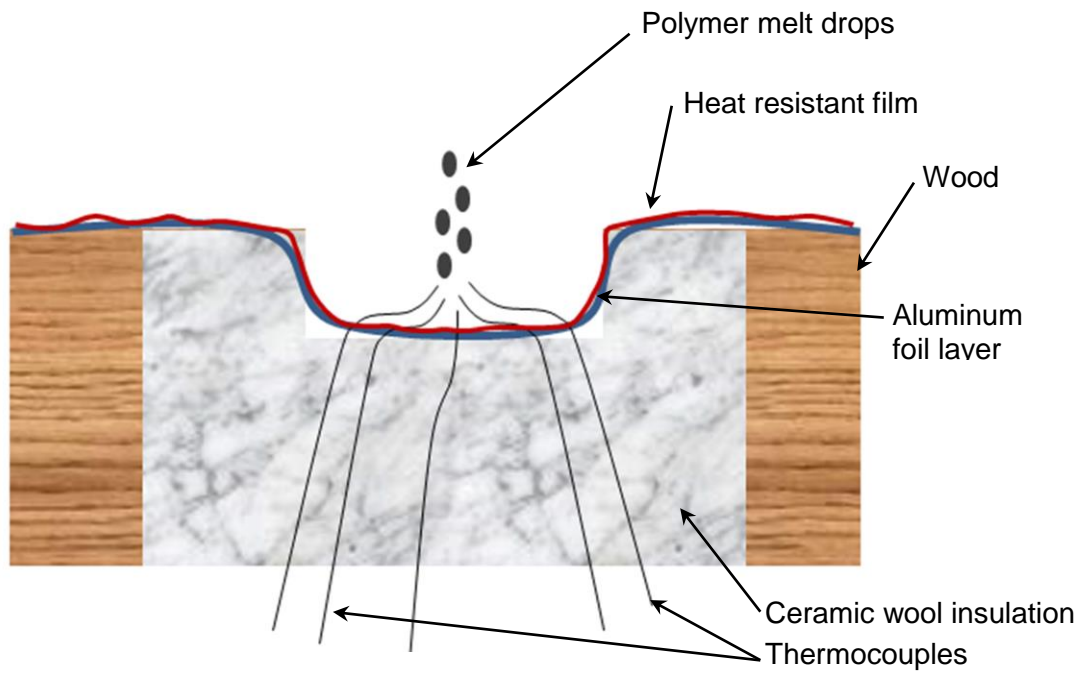


Figure 3.4: Schematic front view of the drops container.

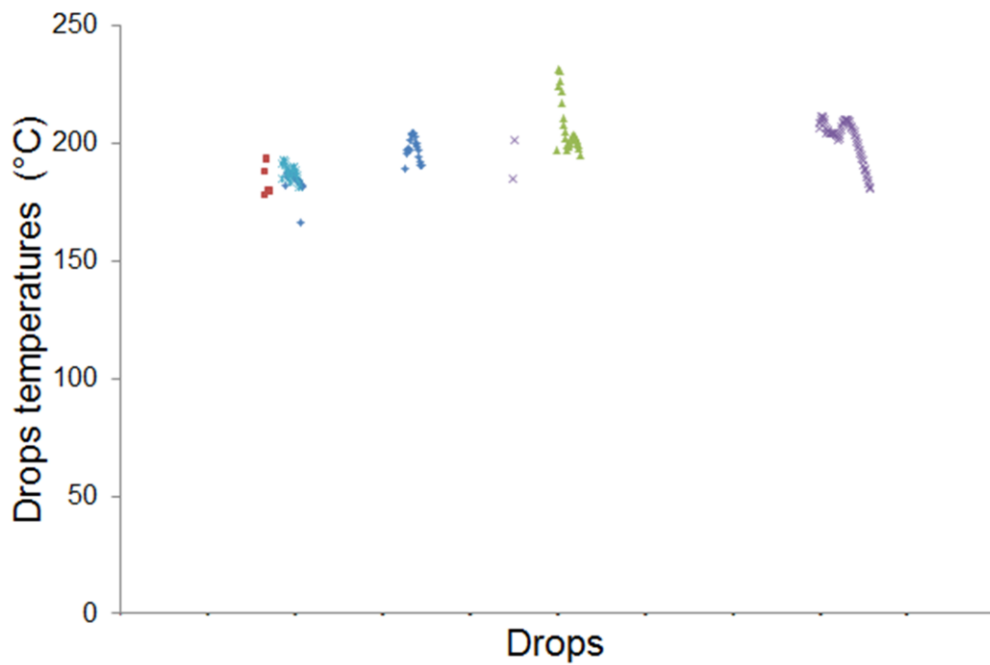


Figure 3.5: Drop temperatures measurement for PMMA at 400°C furnace setting temperature.

Furnace set temperatures at which measurements were undertaken were same as in Table 3.2.

3.2.3.3 Experimental results (temperatures of melting drops)

Experiments were carried out with PET, PA6, PMMA, PC, PS and PP thermoplastic polymer samples placed and exposed to heat in the vertical tubular furnace set at a fixed temperature (Furnace Setting Temperature (FST)) to collect melt drops with their temperatures measured. PP, PET and PA6 are semi-crystalline thermoplastic polymers. Although, most of PC are amorphous thermoplastics, some types of PC similar to the sample studied here are also semi crystalline [238-239], and their melting temperatures are available in the literature. Semi-crystalline polymers have a melting temperature T_m , which implies a supplement of energy required to achieve the phase changing up to melt state; this is the latent heat or endothermic enthalpy of melting. PMMA and PS are amorphous polymers and they do not melt but they soften and drip.

For each thermoplastic polymer at each Furnace Setting Temperature (FST), the temperatures of drops over a period of time are shown in Figures 3.6, 3.8, 3.10, 3.12, 3.14 and 3.16 while Figures 3.7, 3.9, 3.11, 3.13, 3.15 and 3.17 show the temperatures of the drops versus FST. Each temperature is average of three repeat experiments. The temperature profiles are the temperatures of falling drops of polymer samples, which in case of semi-crystalline thermoplastic polymers (PP, PET, PA6 and PC) are envisaged due to melting. But even in them at lower temperatures the drops are due to softened polymers same as for amorphous thermoplastic polymers (PMMA and PS) where at temperatures drops of PMMA and PS are envisaged due to softened polymer pieces.

a) Polymethyl Methacrylate (PMMA).

A set of experiments was performed at Furnace Setting Temperature (FST) of 350, 520 and 550°C with Polymethyl Methacrylate (PMMA) samples. Figure 3.6 and Figure 3.7 below show the experimental temperature profiles obtained.

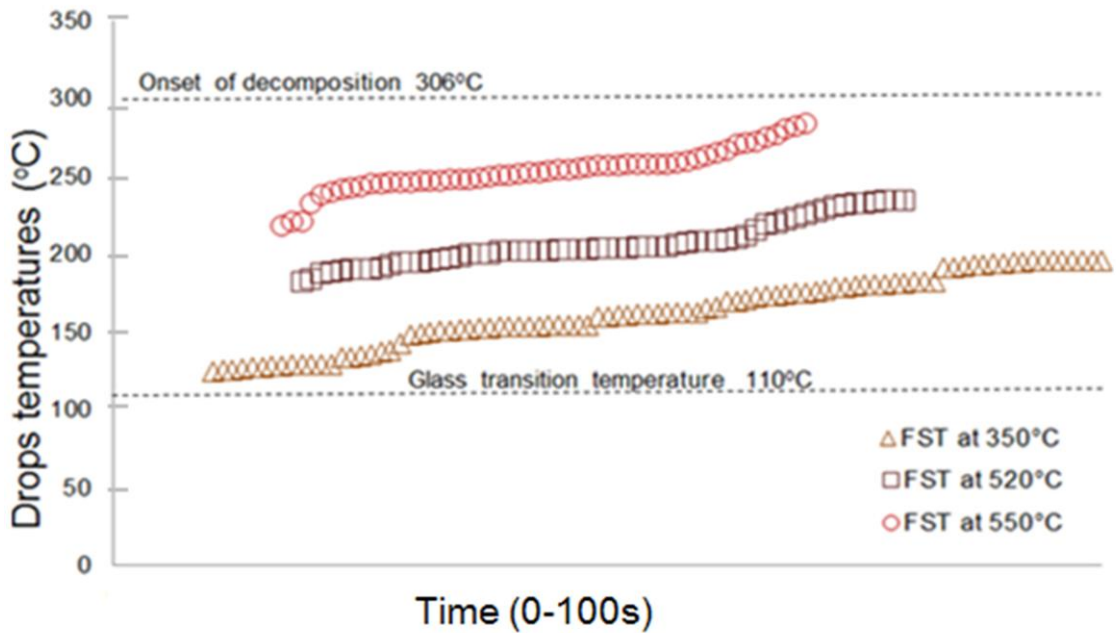


Figure 3.6: Temperatures of PMMA molten drops during a period of time.

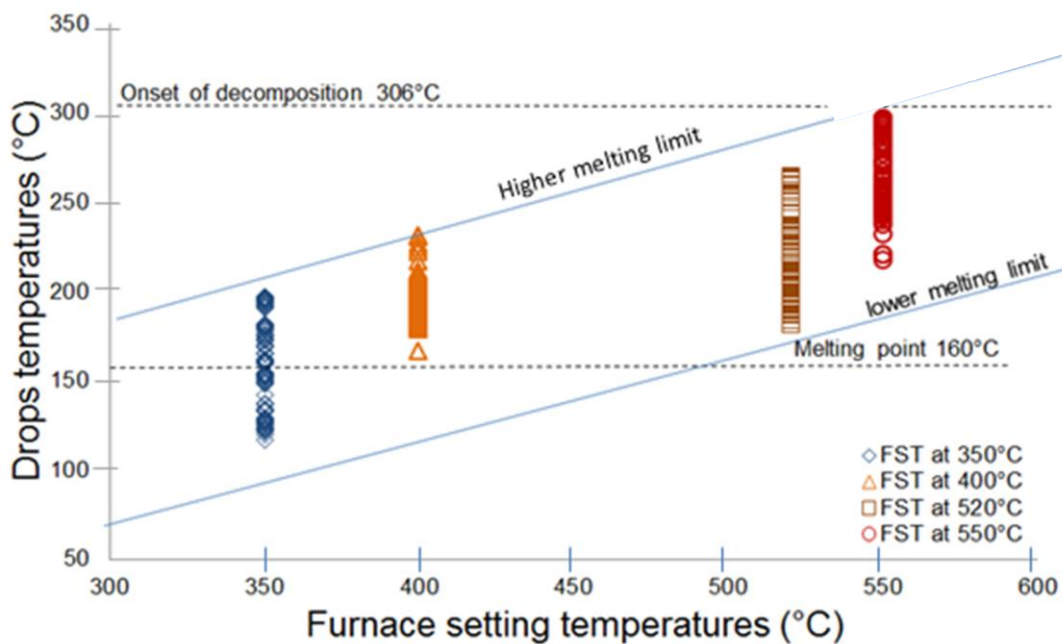


Figure 3.7: Range of temperatures of molten drops of PMMA at each FST.

The same trend is observed for all furnace setting temperatures as shown in Figure 3.7. PMMA is an amorphous thermoplastic with no melting temperature. The sample breaks down into drops falling in a discontinuous way. The onset of decomposition temperature measured from the TGA experiments [197] is 306 °C and during the experiment release of

gaseous volatiles, which is an indication of polymer degradation is observed at any setting of furnace temperature.

In Figure 3.7 the temperatures of falling drops measured by the thermocouples placed in the adiabatic container as shown in Figure 3.4 is in the range of temperatures of the interval 115°C–300°C where 115°C and 300°C are respectively the lowest and the highest drop temperature while the glass transition temperature measured by DSC is 110°C [200].

b) Polyethylene Terephthalate or Polyester (PET)

A set of experiments was performed at FST of 415, 490, 565 and 635°C with polyester (PET) samples. Figures 3.8 and 3.9 below show the experimental temperature profiles obtained.

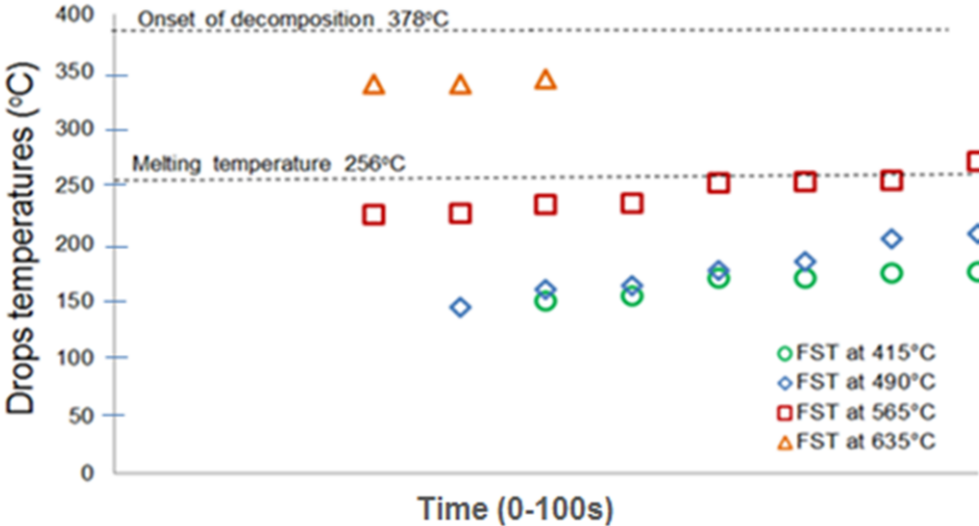


Figure 3.8: Temperatures of PET molten drops during a period of time.

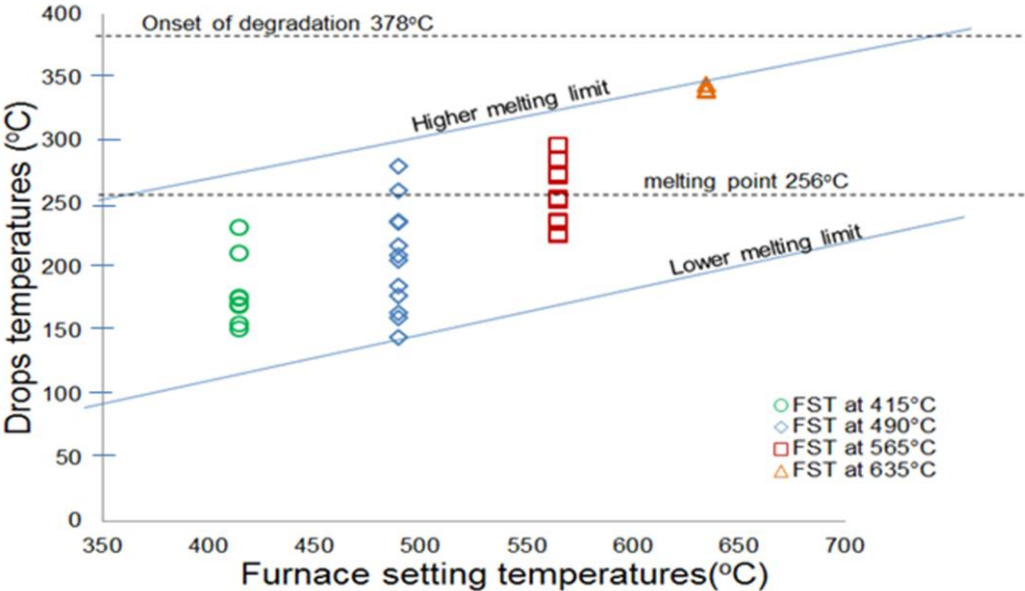


Figure 3.9: Range of temperatures of molten drops of PET at each FST.

A similar trend as seen in PMMA is observed here for all furnace setting temperature as shown in Figure 3.9. Range of molten drop temperatures obtained is below the melting point of PET at 256 °C [4]. At the furnace setting temperature of 635°C the PET molten drop temperatures remain relatively constant around 330 °C.

In Figure 3.9 molten drops' temperature measured by the thermocouples of the adiabatic container is in the range of temperatures of 150°C–350°C where 150°C and 350°C are respectively the lowest and the highest drop temperature while the melting temperature measured by DSC is 250°C [200].

c) Polypropylene (PP)

A set of experiments was performed at FST of 350, 450, 500, 625 and 660°C with PP samples. Figures 3.10 and 3.11 show the experimental temperature profiles obtained.

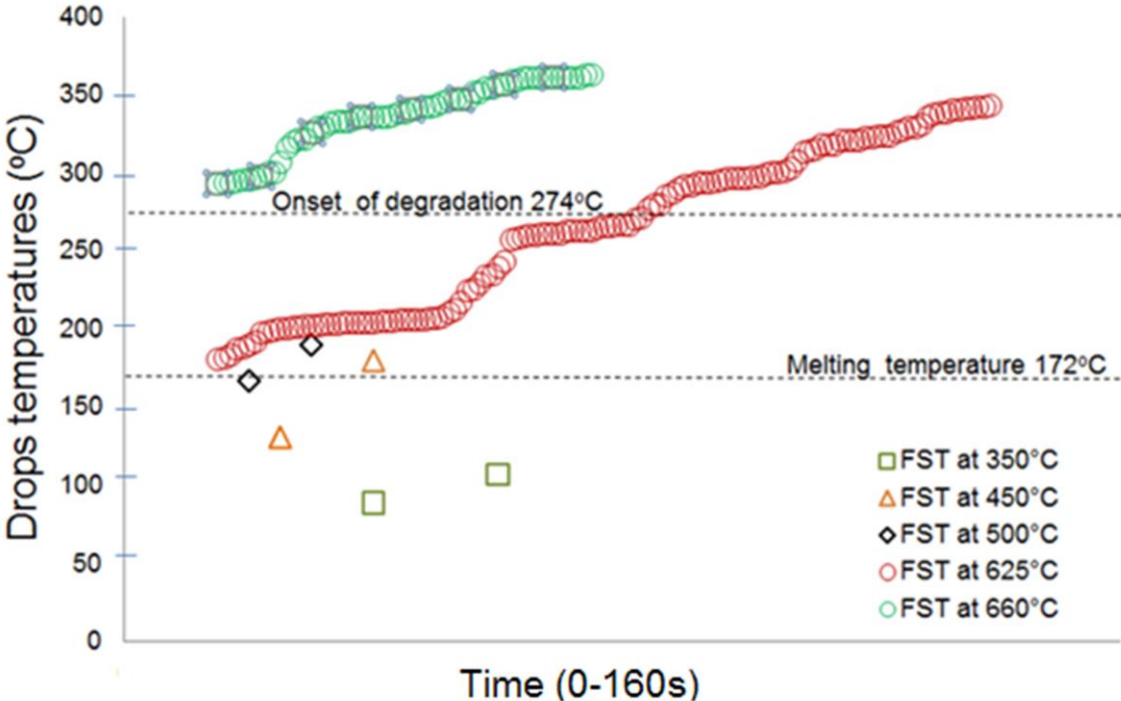


Figure 3.10: Temperatures of PP molten drops during a period of time.

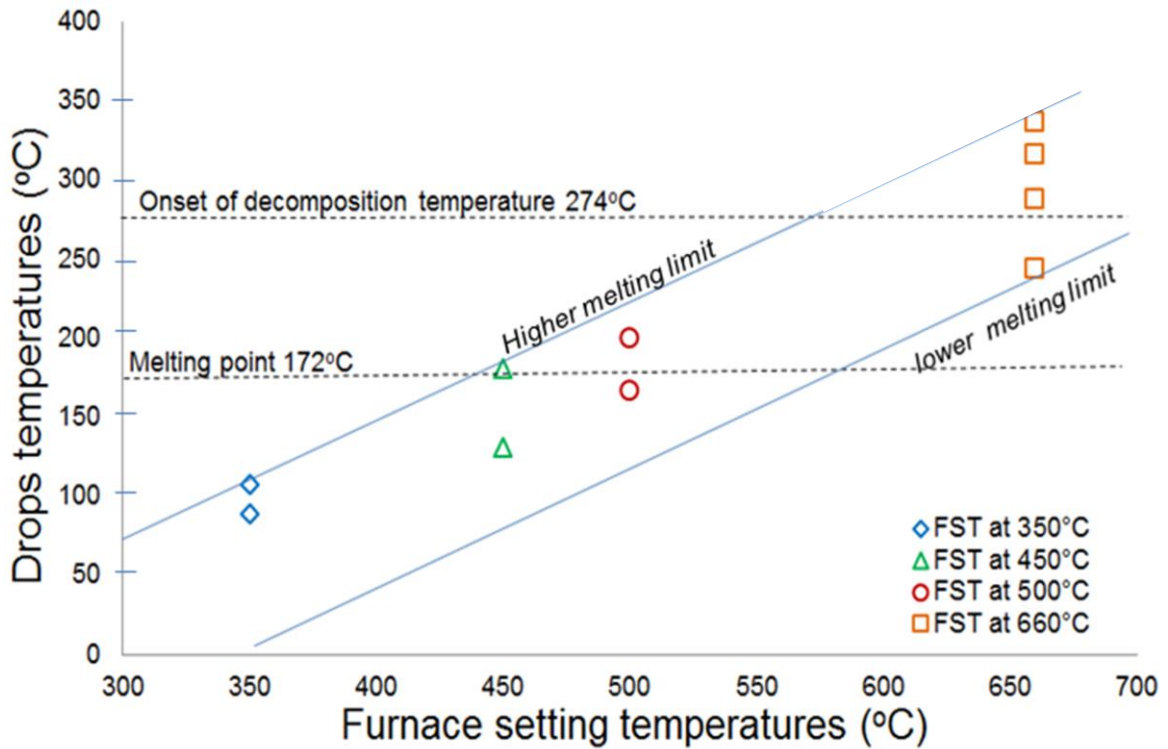


Figure 3.11: Range of temperatures of molten drops of PP at each FST.

A similar trend is observed at all furnace setting temperatures (FST) as shown in Figure 3.11. The molten drops temperature increases as the furnace's temperature increases. A higher and a lower temperature limits are visible in Figure 3.10. Most of the molten drop temperatures measured are under the onset of degradation temperature of 274 °C measured by TGA [200]. Difficulties occurred in trying to measure the temperatures of the drops were noticed because of the excessively liquid state of PP drops at high temperatures. Thermocouples did not record the temperature properly due to the lack of necessary contact with the drops when they fell.

The molten drops temperature measured by the thermocouples of the adiabatic container is in the range of temperatures of 75°C–350°C while the melting temperature measured by DSC is 172°C [200].

d) Polyamide 6 (PA6)

A set of experiments was performed at FST of 425, 495 and 560°C with PA6 samples. Figure 3.12 and Figure 3.13 show the experimental temperature profiles obtained.

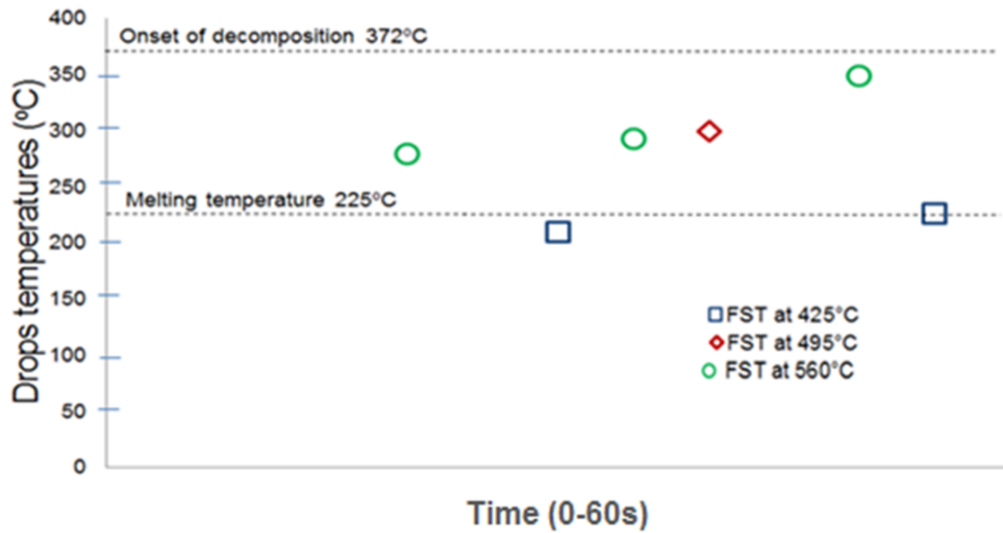


Figure 3.12: Temperatures of PA6 molten drops during a period of time.

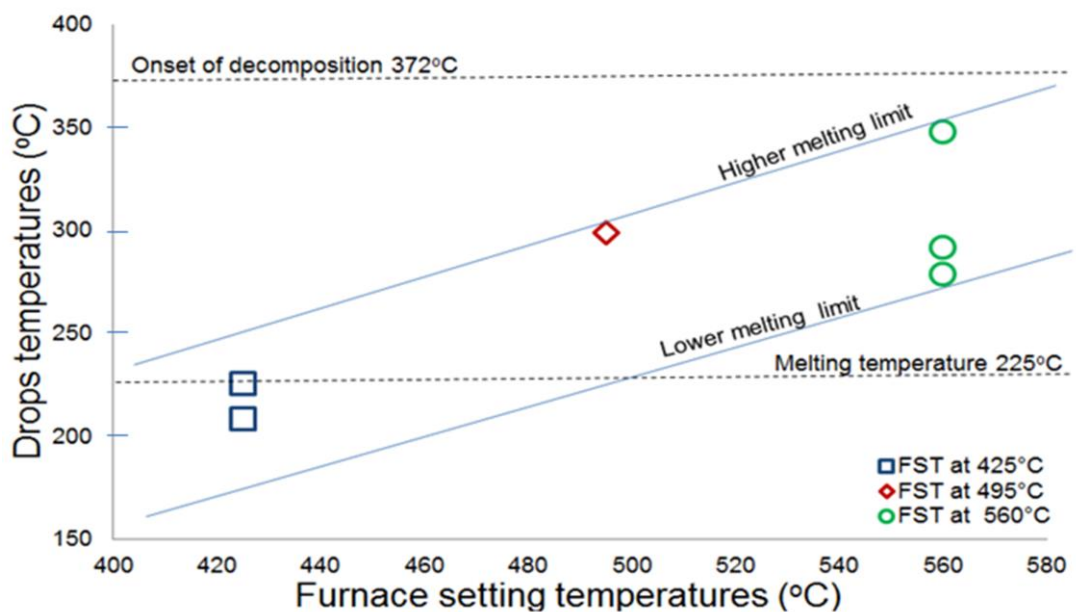


Figure 3.13: Range of temperatures of molten drops of PA6 at each FST.

As shown in Figure 3.13 most of the molten drops' temperatures measured are in the range of temperatures of 200°C– 350°C which is below the onset of decomposition temperature of 372°C measured by DSC [200].

e) Polycarbonate (PC)

A set of experiments was performed at FST of 515, 650 and 585°C with PC samples. Figures 3.14 and 3.15 show the experimental temperature profiles obtained.

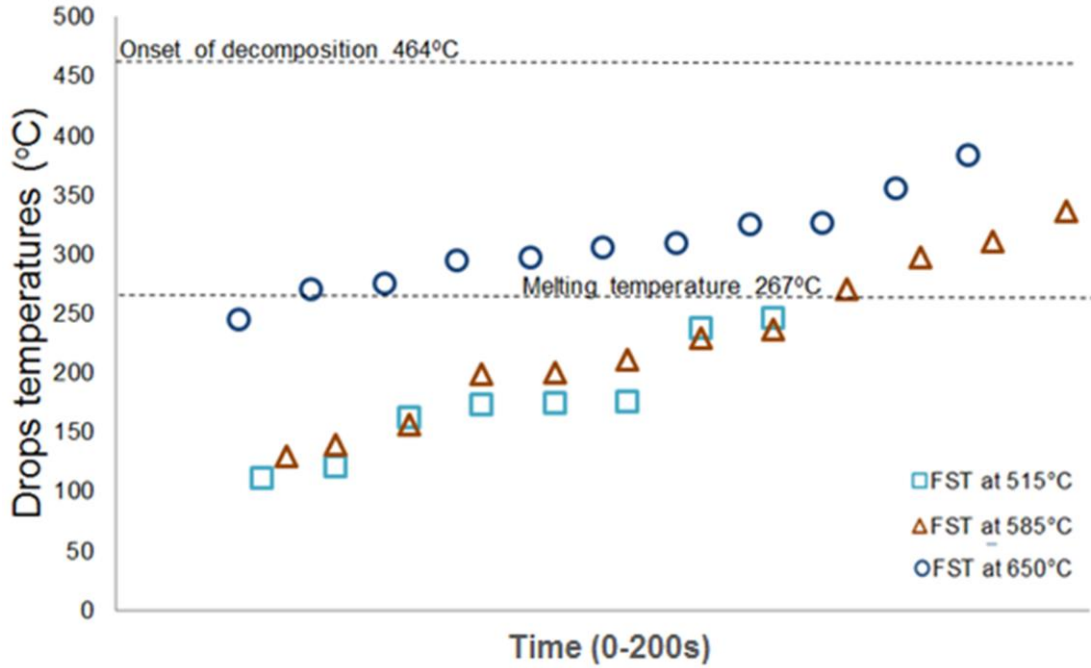


Figure 3.14: Temperatures of PC molten drops during a period of time.

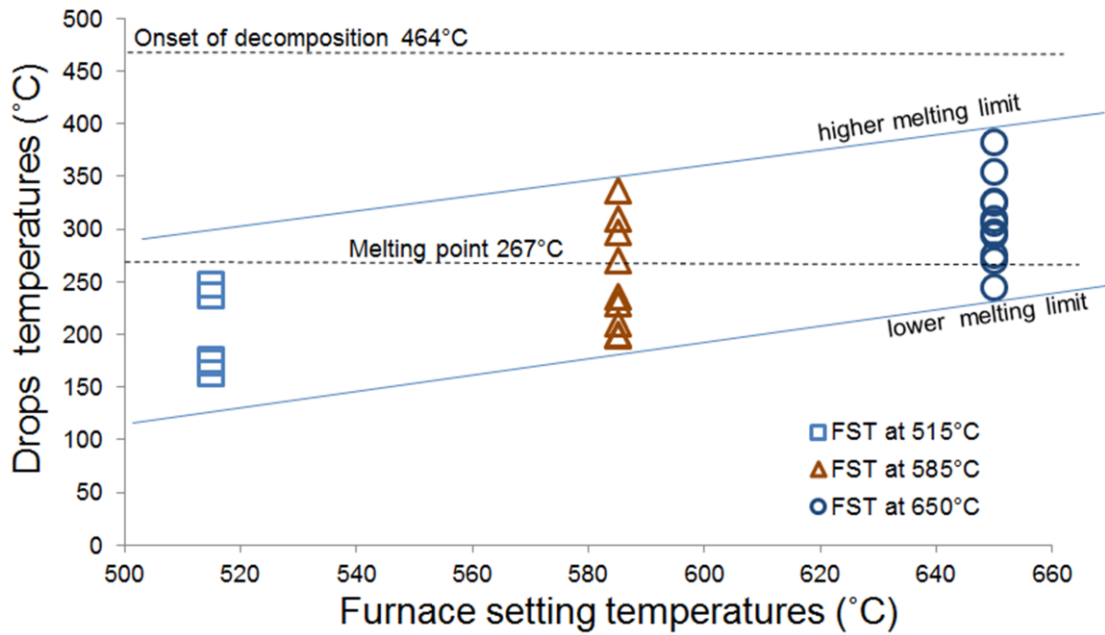


Figure 3.15: Range of temperatures of molten drops of PC at each FST.

As shown in Figure 3.15. The molten drops temperatures are increasing as the furnace setting temperature increases. The molten drops temperatures measured by the thermocouples of the adiabatic container are in the range of temperatures of 125°C – 375°C.

f) Polystyrene (PS)

A set of experiments was performed at FST of 300, 400, 555 and 570°C with PS samples. Figure 3.16 and 3.17 below show the experimental temperature profiles obtained.

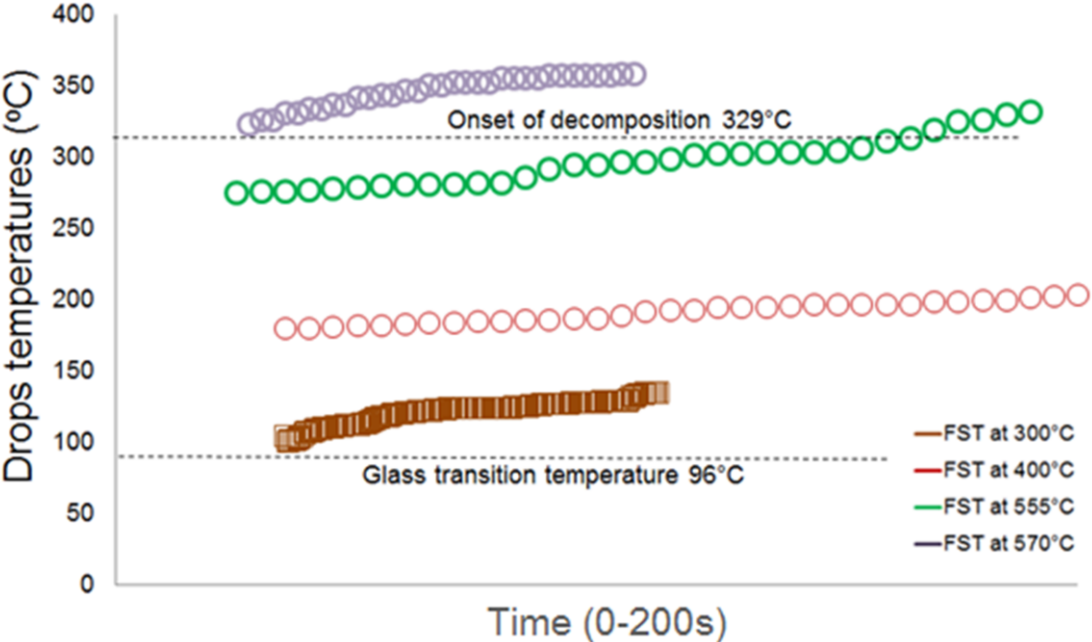


Figure 3.16: Temperatures of PS molten drops during a period of time.

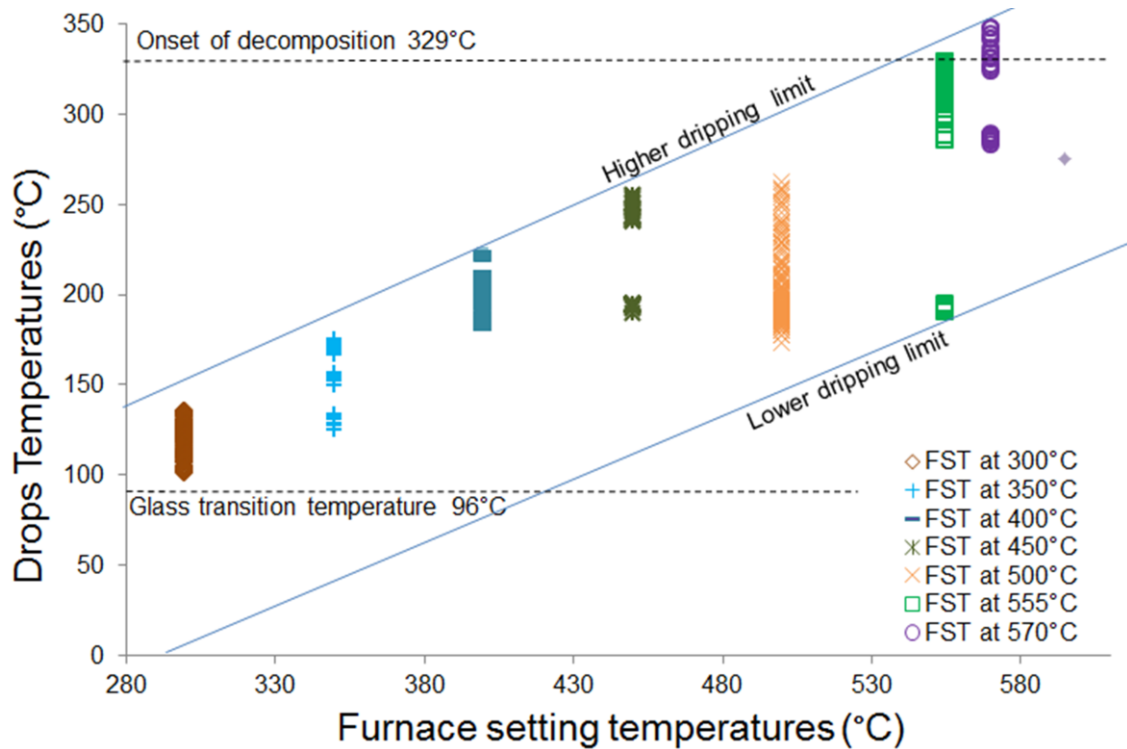


Figure 3.17: Range of temperatures of molten drops of PC at each FST.

PS is an amorphous thermoplastic, therefore, it does not have a melting temperature and when the experiments were undertaken it is interpreted that the sample breaks down into pieces falling in a discontinuous way. The onset of decomposition temperature measured by TGA is 329°C. The molten drops temperatures measured by the thermocouples of the adiabatic container are in the range of temperatures of 100°C – 350°C as shown in Figure 3.18.

3.2.3.4 Observations and analysis

Figures 3.6 to 3.17 show experimental molten drops temperatures profiles of six polymer samples placed in a tubular furnace set at different wall temperatures as discussed in Section 3.2.

The results show that the temperatures of molten drops are not constant at any particular furnace setting temperature. The graphs show a range of temperatures between lowest and highest drops' temperatures for each furnace setting temperature. The lower and higher temperatures increase with increasing furnace setting temperature. Since the diameter of the tube furnace is very small, the thermal radiations coming from the wall of the furnace penetrates the physically and thermally thin layer polymer in a short period of time rising the

temperature very quickly till the melt dripping process starts. For each polymer type three zones are delimited:

Zone 1: corresponds to the region where the temperature is under the melting temperature determined by DSC (see Section 3.2) [200]. The combination of high viscosity, thermal expansion and gravity are the principal cause of dripping by polymer stretching. Thick pieces of partially melted polymer drop down. The temperature is not high quickly enough to melt the polymer.

Zone 2: corresponds to the temperatures between the melting temperature estimated by DSC and onset of degradation temperature estimated by TGA (see Section 3.2.) [200]. The heat is absorbed during melting, while during melting the temperature remains almost constant until the whole polymer melts. As the temperature of the polymer rises, the viscosity decreases, reaching minimum enough at the melting temperature to fluidise the polymer. The combination of low viscosity, thermal expansion and gravity is the principal cause of dripping.

Zone 3: corresponds to the temperatures of polymers above degradation temperature, obtained at onset of degradation where 5% mass loss occurs in the TGA experiment. At higher FST the heat in the furnace is high enough to break up the bonds causing the polymer to degrade. The polymer sample reaches the decomposition (pyrolysis) temperature while the viscosity drops down dramatically. The combination of decomposition (pyrolysis), decrease of polymer viscosity while temperature increases, thermal expansion and gravity can be the principal cause of dripping. As the drops are highly fluidised their temperatures are important because of the close dependency between viscosity and temperature.

Furthermore comparing the behaviour of the different polymers in the furnace experiment it can be seen that mostly the measured temperatures of the drops from the adiabatic container are not above the decomposition temperature measured by DSC. Therefore there is no indication of polymer decomposition in drops except in the case of PP and PS where the temperature measured is above the temperatures of decomposition.

3.2.4 Measurement of temperatures of horizontally oriented samples exposed to radiant heat in a cone calorimeter

A cone calorimeter apparatus has been used to investigate the melting dripping behaviour of horizontally oriented polymer slabs. A schematic description of a cone calorimeter and its temperatures measurement setup is shown in Figure 3.18 below.

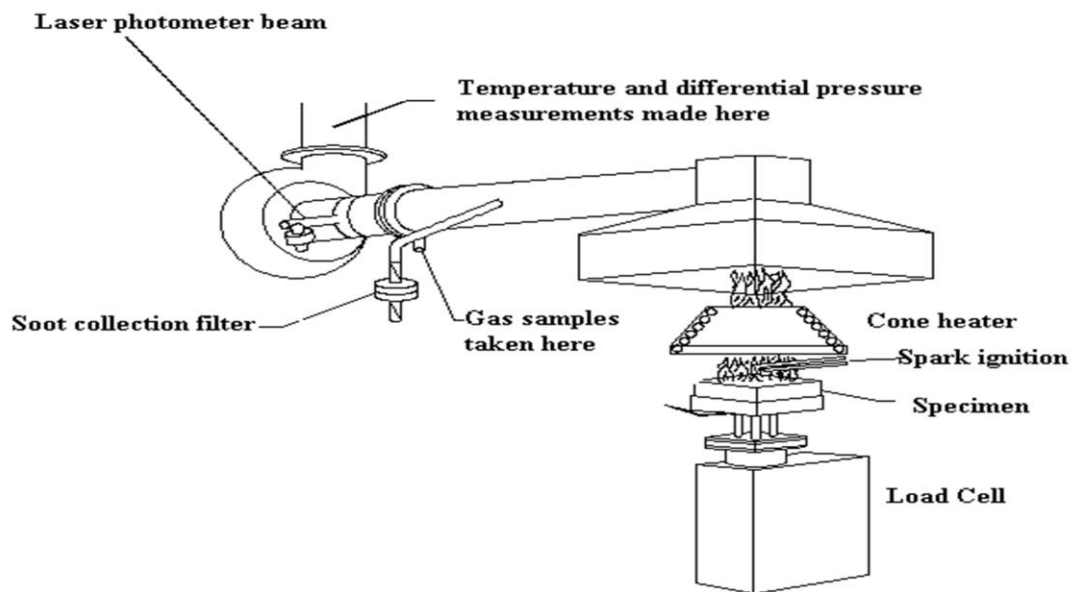


Figure 3.18: Schematic description of the assemblies of a cone calorimeter [203].

Each thermoplastic sample is subjected to the heater of the cone calorimeter (Fire Testing technology, UK) at 50 kW/m^2 heat flux in horizontal orientation at a distance of 25 mm as specified in ISO 5660 [9]. However, in this work spark ignition was not used and heat fluxes were kept low enough to measure temperature changes during melting stages of the polymers. The constant incident heat flux is applied only on the top surface of the polymeric samples, the other sides being insulated by a ceramic woven so that it is assumed one dimensional heat transfer-1D occurs. Two K-type thermocouples were inserted in each sample, one on top of the surface another one on the back surface of samples. The setup is shown in Figure 3.19 [198].

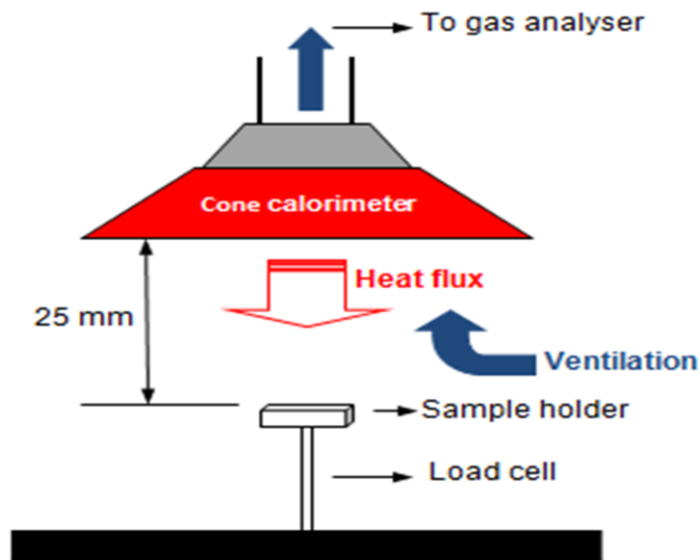


Figure 3.19: Experimental setup for temperature measurements.

In this scenario the experiments were focused on three semi-crystalline thermoplastics polymers:

- Polypropylene (PP),
- Polyamide 6 (PA6),
- Polyethylene terephthalate (PET).

For the experimental process the cone calorimeter was set at three different incident heat flux; 15, 25 and 35 kW/m^2 in order to cover the phenomenon occurring in the three zones identified in Section 3.2.3.4. Four thermocouples are placed on the sample top surface to measure the temperature of the polymer. The average temperature is used based upon four recorded temperatures and plotted.

3.2.4.1 Experimental results

The experimental measurement of the temperatures throughout the three semi-crystalline thermoplastics PP, PA6 and PET horizontally oriented and exposed to radiant heat in a cone calorimeter were undertaken. The results are shown below in Figures 3.20, 3.21 and 3.22.

a) Polypropylene (PP)

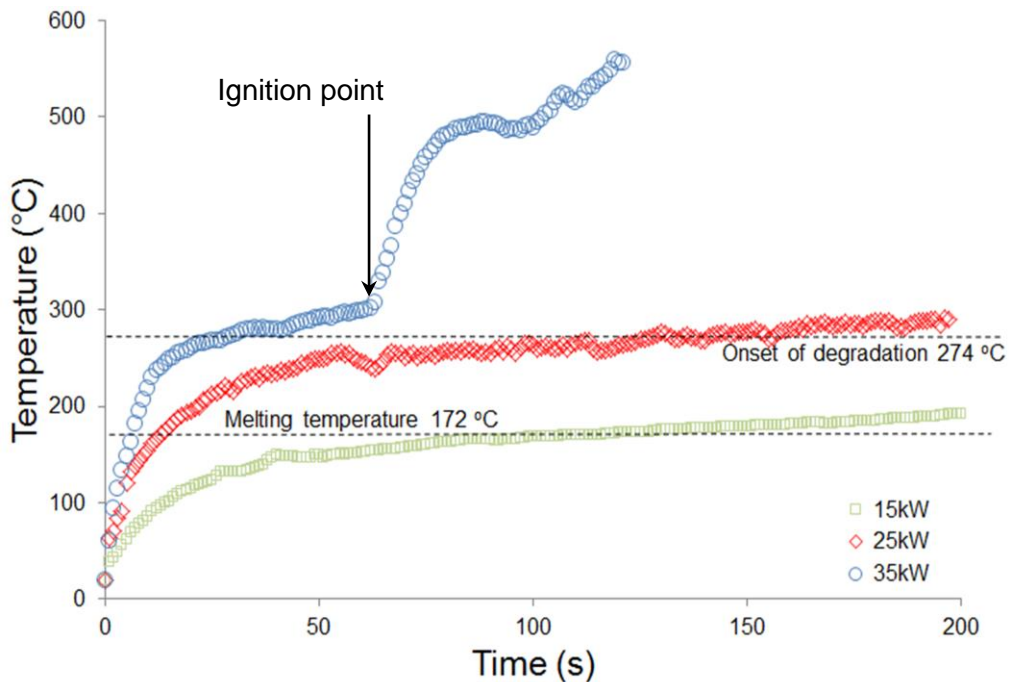


Figure 3.20: PP- Surface temperature profiles of sample exposed to 15, 25 and 35kW/m² heat fluxes.

b) Polyamide 6 (PA6),

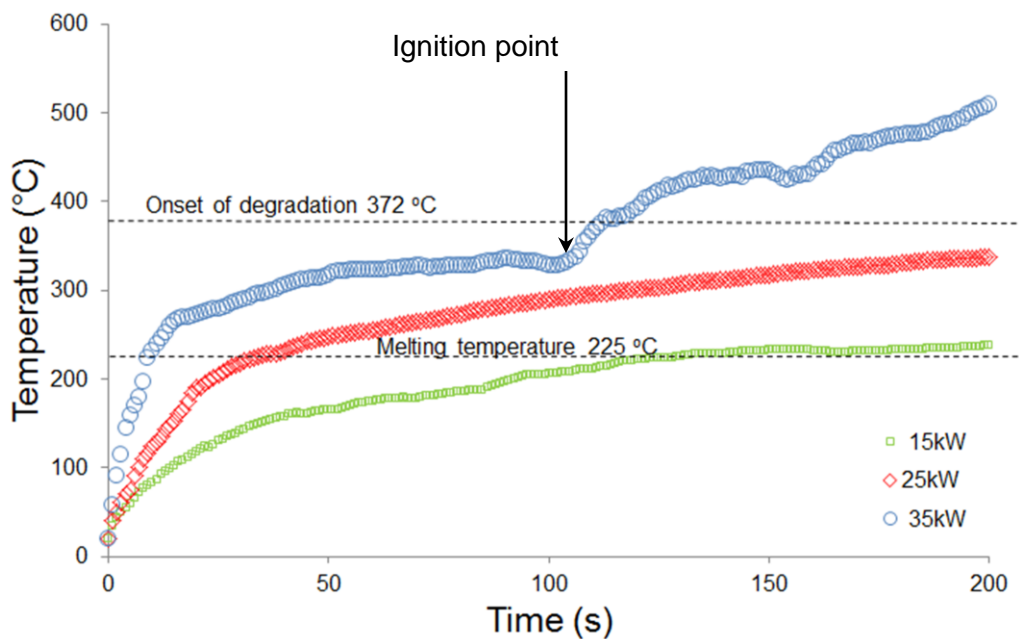


Figure 3.21: PA6- Surface temperature profiles of sample exposed to 15, 25 and 35kW/m² heat fluxes.

c) Polyethylene terephthalate (PET),

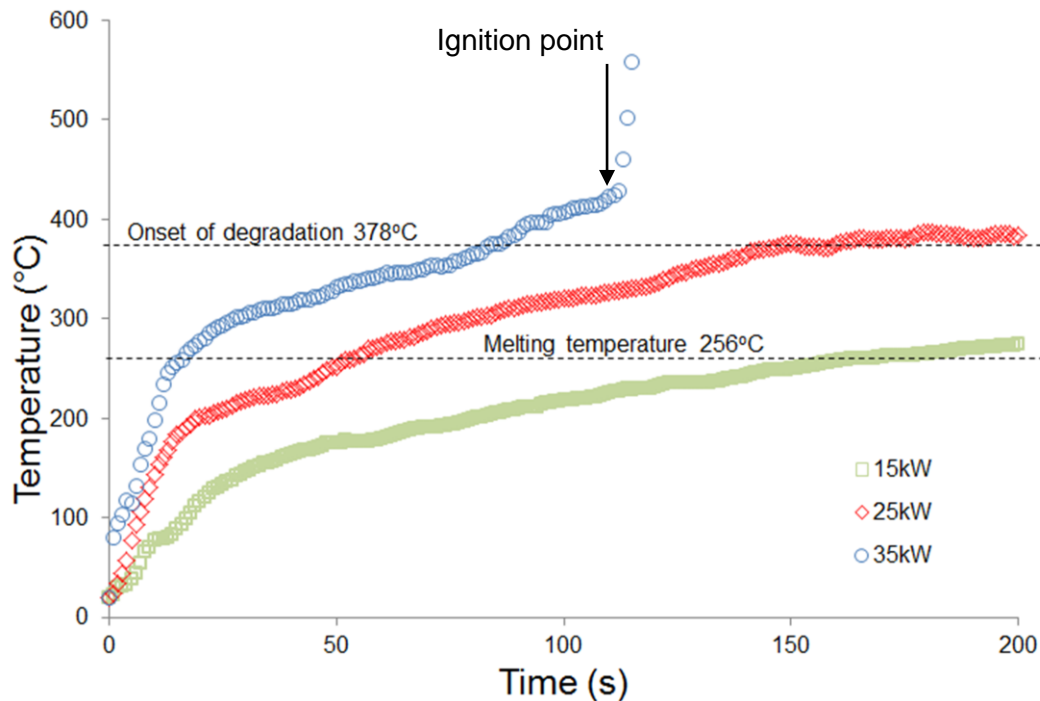


Figure 3.22: PET- Surface temperature profiles of sample exposed to 15, 25 and 35kW/m² heat fluxes.

3.2.4.2 Observations

The experiments above have been undertaken in order to obtain and to validate the simulated temperatures during melting of thermoplastic polymers while exposed to different heat fluxes in a cone calorimeter in horizontal sample orientation. Three different heat fluxes have been used: 15, 25 and 35 kW/m². For each sample type (PP, PA6 and PET) the melting temperature measured by DSC and the onset of degradation temperature measured by TGA have been used as reference in Figures 3.20 to 3.22 for the analysis of the graphs. As can be seen in all Figures, surface temperatures of all three polymers (PP, PA6 and PET) at incident heat flux of 15kW/m² are lower than the theoretical melting point, hence, only melting occurs. At 35 kW/m² in PP and PA6 temperature is below onset of degradation, hence may not be decomposing. In PET it reaches decomposition temperature.

3.3 Temperature profiles of glass fibre reinforced resin composite laminates (GRE) exposed to a cone calorimeter.

The experimental work is taken from reference [198].

3.3.1 Composite sample

Fibre reinforced resin composites of varying thicknesses ranging from 8, 12, 16 or 20 glass fibre layers impregnated with an epoxy resin were prepared, cut and used. The thicknesses of the samples depended on the number of layers therefore composites samples with 8, 12, 16 or 20 have respectively thicknesses of 3, 4.5, 6 or 7.5 mm.

3.3.2 Cone calorimeter test

Samples of 7.5 x 7.5 cm were exposed to a cone calorimeter at Incident heat flux of 15, 35 and 50 kW/m². For incident heat flux of 15 and 50 Kw/m² sample of 3 mm thickness was used while samples of 3, 4.5, 6 or 7.5 mm were used for the incident heat flux of 35 kW/m². For temperature measurements a K-thermocouple was placed at the top surface of the sample and another one at the bottom.

3.3.3 Experimental results

The experimental temperature versus time profiles for top and bottom surfaces of GRE of 3 mm thickness exposed to 15, 35 and 50kW/m² are shown in Figure 3.23, 3.24 and 3.25.

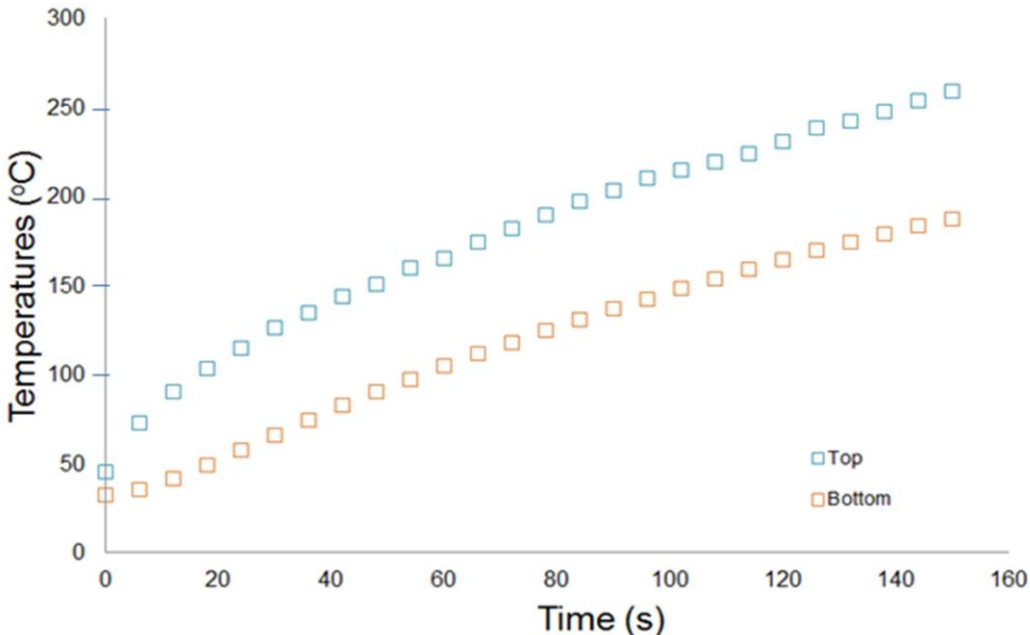


Figure 3.23: Temperature profiles at the top and bottom surface of 3 mm GRE thickness exposed to 15 kW/m² heat flux.

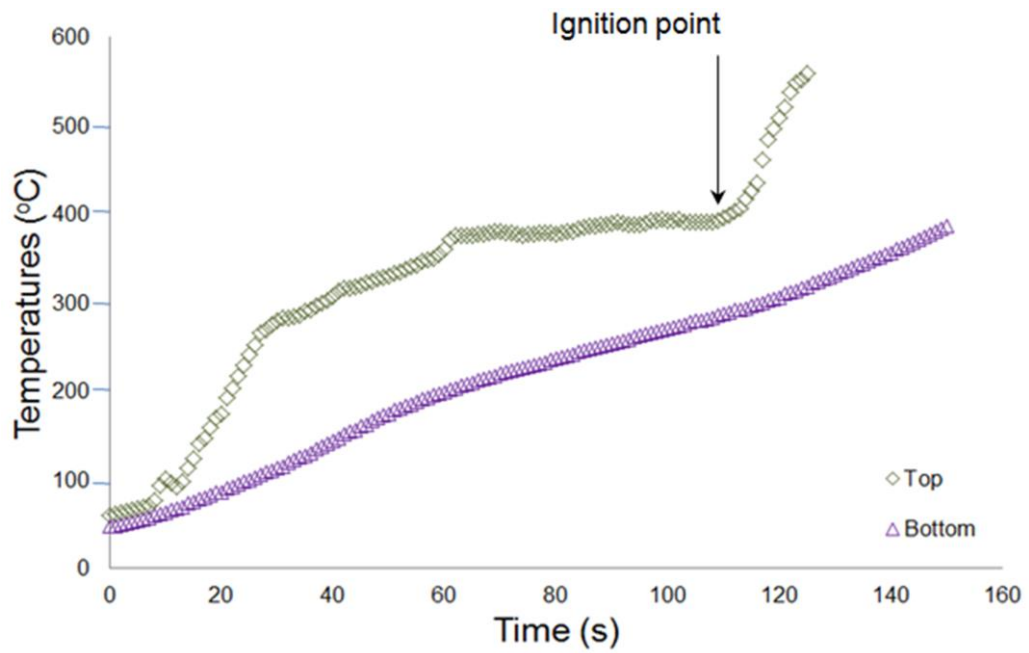


Figure 3.24: Temperature profiles at the top and bottom surface of 3mm GRE thickness exposed to 35kW/m² heat flux.

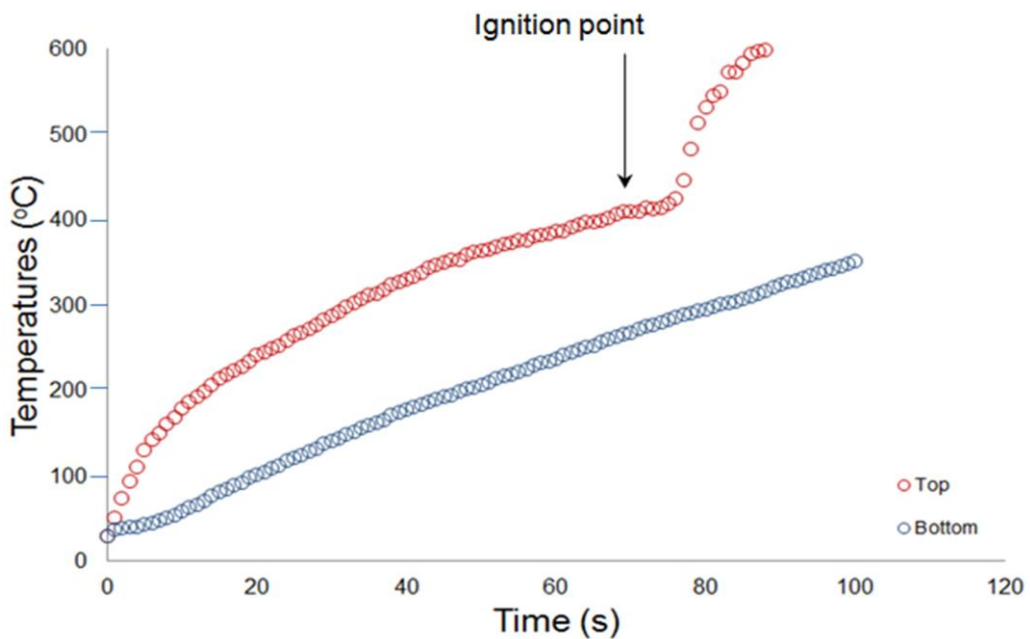


Figure 3.25: Temperature profiles at the top and bottom surface of 3 mm GRE thickness exposed to 50 kW/m² heat flux.

In Figure 3.23 the temperatures at the top and the bottom surface of the GRE go up the longer the heating continues whereas, Figures 3.24 and 3.25 show that ignition occurs, causing a sudden increase of the temperature profiles at the ignition point.

Moreover, the temperatures versus time curves of top and bottom surfaces of 3, 4.5, 6 and 7.5 mm thick samples, prepared using respectively 8, 12, 16 and 20 glass fibre layers at 35 kw/m² are shown in Figures 3.26 and 3.27 below. These Figures will be used in Chapter 5 to study the consistency of the numerical model developed. This is performed by validating the simulation results with the experimental temperatures. Also, the effect of thickness changes on the temperatures profiles of the GRE sample is analysed

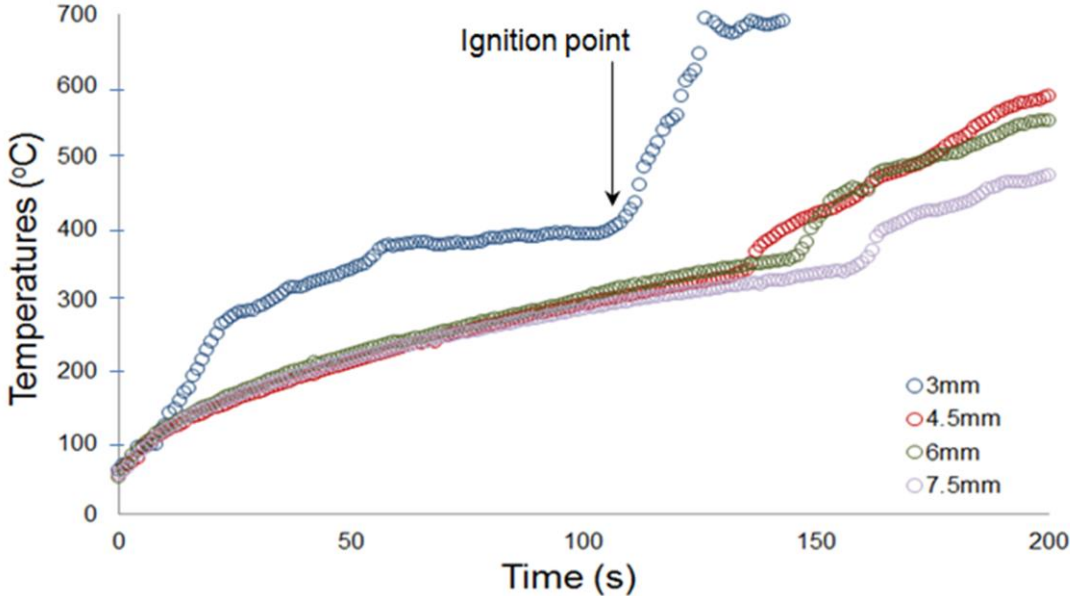


Figure 3.26: Temperature profiles at the top surface of 3, 4.5, 6 and 7.5mm GRE thicknesses exposed to 35kW/m² heat flux.

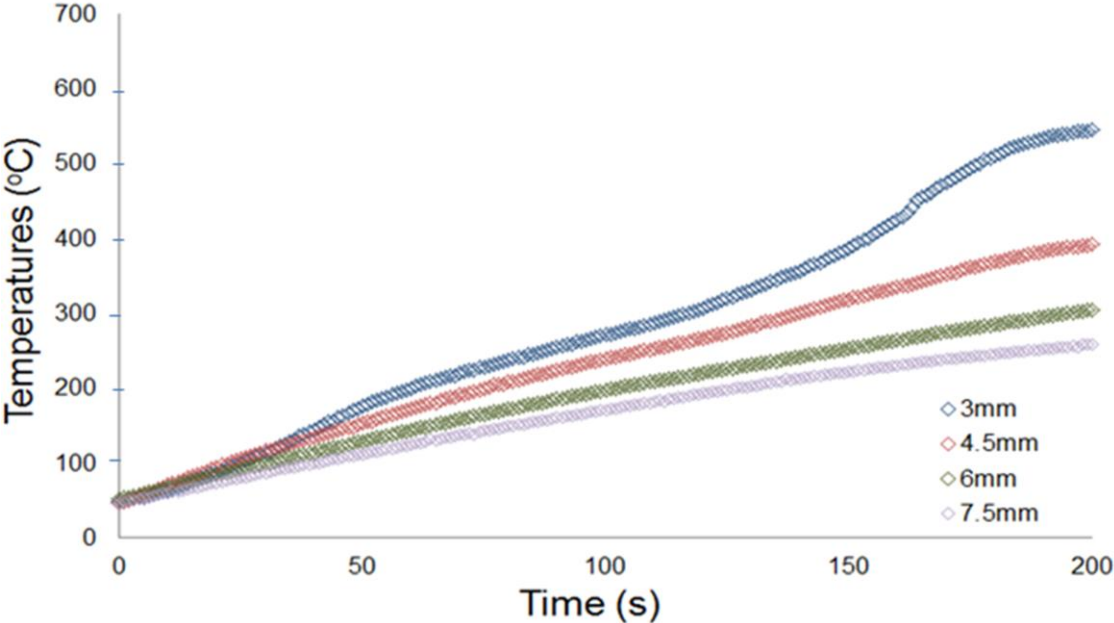


Figure 3.27: Temperature profiles at the bottom surface of 3, 4.5, 6 and 7.5mm GRE thicknesses exposed to 35kW/m² heat flux.

In Figures 3.26 and 3.27 it is shown that the temperature profiles decrease as the thickness of the composite sample increases. The jump in temperature at the ignition point is only observed for the 3mm sample thickness.

3.4 GRE with intumescent coatings for thermal barrier protection

The experimental work discussed in this section is part of the work performed by Dr Luangtriratana within a cooperation programme in the Fire Materials Laboratories of Universities of Bolton (United Kingdom) and Lille (France) and published elsewhere [202, 209-210].

3.4.1 Intumescent coated glass fibre reinforced epoxy resin composite (GRE) samples.

The glass fibre composite samples used for this work are similar to those used in above Section 3.3 and the sample thickness was also kept to be 3 mm.

Three types of commercial intumescent coatings supplied by Sherwin-Williams (formerly Leigh Paints), UK were used. These coatings being commercial products, their intumescent components are not discussed. These are named here based on the types of binders used:

(i) Epoxy based intumescent coating (EI).

The base resin contains an epoxy resin, ethyl hexyl glycidyl ether and bisphenol F-epichlorohydrin with a hardener containing 2,4,6-tris(dimethylaminomethyl)phenol and triethylenetetramine.

(ii) Flame retarded epoxy based intumescent coating (EDI).

Here, the base resin contains an epoxy resin, DOPO (9,10-Dihydro-9-oxa-10-phosphaphenanthrene-10-oxide) modified epoxy resin complex, 1,4-bis(2,3epoxypropoxy)butane and triphenyl phosphate with a hardener containing, zinc borate, tetraethylpentamine and 3-aminopropyltriethoxysilane.

(iii) Water based intumescent coating (WI).

WI is a single component material, containing vinyl acetate/vinyl ester copolymer system, thermally active pigments and water plus butyl diglycol acetate.

In order to carry out experimental testing, EI, EDI and WI were applied on the surfaces of GRE samples, the details have been discussed minutely elsewhere [202, 209-210]. In

summary, a glass fibre reinforced resin laminate plate (300mm x 300mm x 3mm) was prepared by impregnating 8 layers of glass fabrics with an epoxy resin by hand layup process and cured by vacuum bagging technique at room temperature for 24 h, and then post-cured at 80°C for 6 h. Samples of 75 mm x 75 mm sizes were cut and individually coated with three intumescent coatings to obtain 1mm thick coatings. The coated laminates were then cured at room temperature for 24 h, and then post-cured for 4 h in an oven according to manufacturers' instructions.

3.4.2 Temperature profile measurement of intumescent coated GRE exposed to a cone calorimeter.

The cone calorimetric testing was performed according to ISO 5660 standard as discussed in Section 3.2.4. In these experiments the spark igniter was used.

The cone calorimetric results of all surface coated GFREP laminates at 50 kW/m² analysed in terms of time-to-ignition (TTI), peak heat release (PHRR), time-to-PHRR / (T_{PHRR}) are given in Table 3.3 taken from reference [202]. As discussed further on, in the intumescent coated samples the resin binder of the coating ignites even before the intumescence occurs, giving a very small PHRR. The main peak due to burning (if any) of the laminate occurs at a much later stage. [202].

Sample	Coating thickness (mm)	Cone calorimetric results*			
		TTI (s)	1 st Peak	2 nd Peak	THR (MJ/m ²)
			PHRR (kW/m ²) / T _{PHRR} (s)	PHRR (kW/m ²) / T _{PHRR} (s)	
Control	-	49	733/91	-	38.8
GRE-EI1	1.27 ±0.01	44	131/74	321/205	50.8
GRE-ED-I-1	1.35 ±0.02	35	113/57	176/262	42.9
GRE-WI-1	0.94 ±0.03	17	126/47	55/134	26.6

Note: *The results presented are reproducible to within ±10%;

Table 3.3 (Taken from reference [202]): Cone calorimetric results for different intumescent coatings of varying thicknesses on GRE composite samples, exposed to 50 kW/m² heat flux.

The char expansion of EI, EDI and WI with 1, 3 and 5mm intumescent coatings was measured at the end of cone calorimetric experiments. The results; char residual digital images, exposure time, char thicknesses and expansion ratio are shown in Table 3.4 below.

The details of the experiment for char thickness measurement are explained elsewhere [202-204].







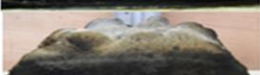



Sample	Char residual images	Exposure time (s)	Char thickness (mm)	Expansion ratio
Control		200	-	-
GRE-EI-1mm		500	6.8 ± 2.2	5.3 ± 1.8
GRE-EI-3mm		900	10.0 ± 2.0	3.4 ± 0.4
GRE-EI-5mm		1400	15.8 ± 0.9	3.0 ± 0.4
GRE-EDI-1mm		500	9.8 ± 2.8	7.2 ± 2.2
GRE-EDI-3mm		900	20.7 ± 1.3	7.0 ± 0.1
GRE-EDI-5mm		1600	27.2 ± 2.7	4.8 ± 0.4
GRE-WI-1mm		800	24.1 ± 2.6	25.6 ± 1.5
GRE-WI-3mm		800	41.7 ± 2.4	14.3 ± 0.8
GRE-WI-5mm		1200	36.3 ± 4.5	6.9 ± 0.7

Table 3.4: (taken from reference [202]: Char residual digital images, exposure time, char thicknesses and expansion ratios of EI, ED-I and WI with 1, 3 and 5mm intumescent coatings exposed to 50 kW/m² incident heat flux.

To measure the temperature profiles at the surface (TS) and the bottom (TB) of the samples, two K-type thermocouples were inserted in each coated laminates sample. Hence, the temperature measured was underneath the coating that represents the temperature at the interface of the laminate and the coating and, the temperature at the back surface of the coated laminates sample. The thermocouples recorded temperature as function of time to get the temperature profiles of each coated sample. Two specimens were tested and the average temperature-time profiles are reported in the following section.

3.4.2.1 Experimental temperature profiles.

The experimental results in the Figure 3.28, 3.30 and 3.32 below show the temperature profiles measured at the top of the glass fibre reinforced resin laminate sample whereas, Figure 3.29, 3.31 and 3.33 show the temperatures measured at the bottom. The glass fibre reinforced resin laminate samples with 1, 3 and 5mm thicknesses are coated respectively with EI, ED-I and WI that are different intumescent coating type.

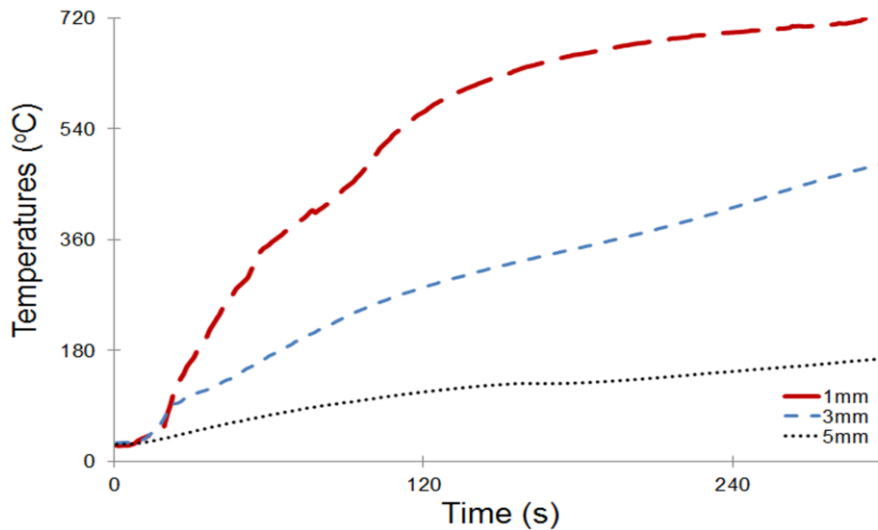


Figure 3.28: Temperature profiles at the top side of the GRE coated with 1, 3 and 5mm thicknesses of EI exposed to 50 kW/m² heat flux.

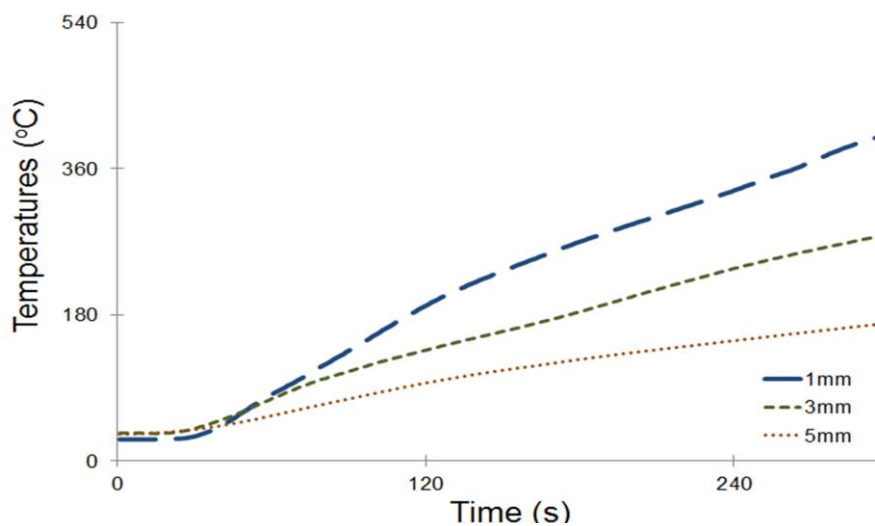


Figure 3.29: Temperature profiles at the bottom side of the GRE coated with 1, 3 and 5mm thicknesses of EI exposed to 50 kW/m² heat flux.

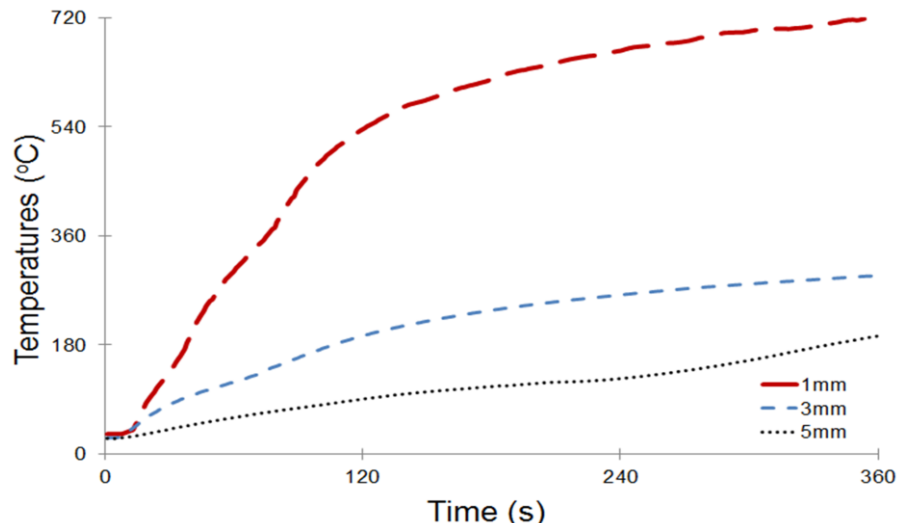


Figure 3.30: Temperature profiles at the top side of the GRE coated with 1, 3 and 5mm thicknesses of EDI exposed to 50 kW/m² heat flux.

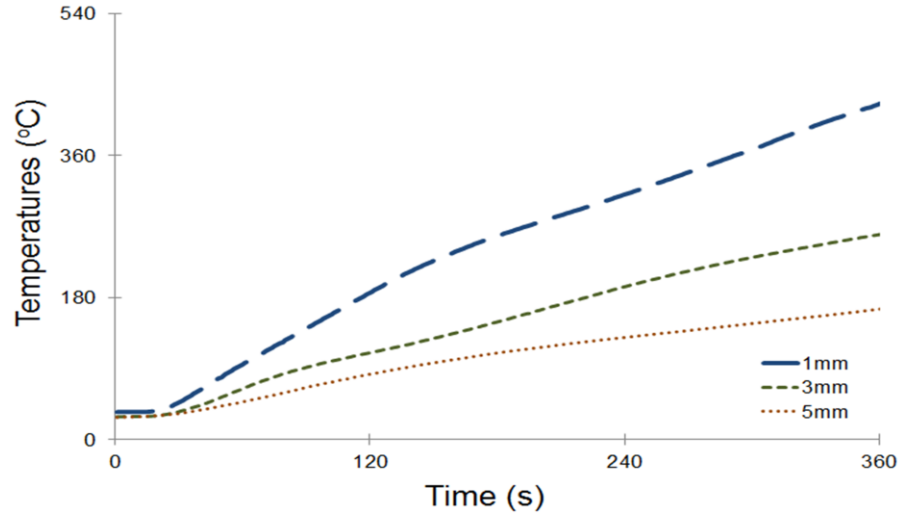


Figure 3.31: Temperature profiles at the bottom side of the GRE coated with 1, 3 and 5mm thicknesses of EDI exposed to 50 kW/m² heat flux.

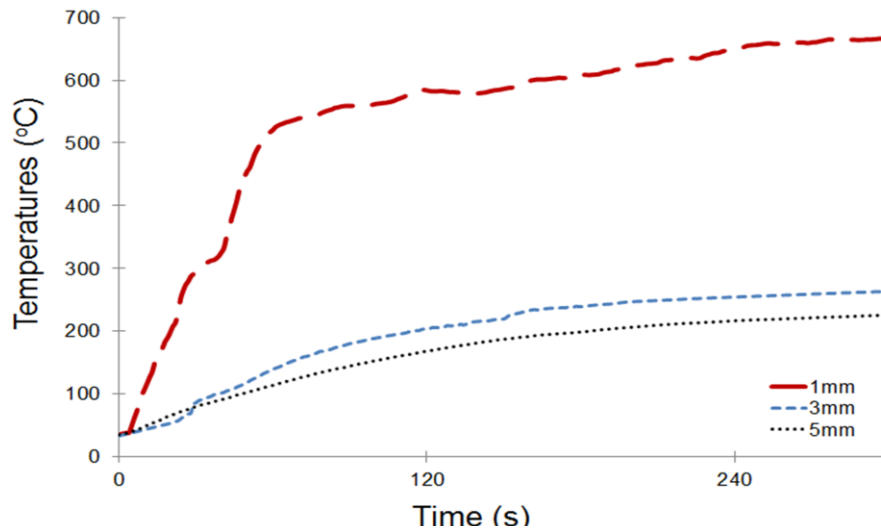


Figure 3.32: Temperature profiles at the top side of the GRE coated with 1, 3 and 5mm thicknesses of WI exposed to 50 kW/m² heat flux.

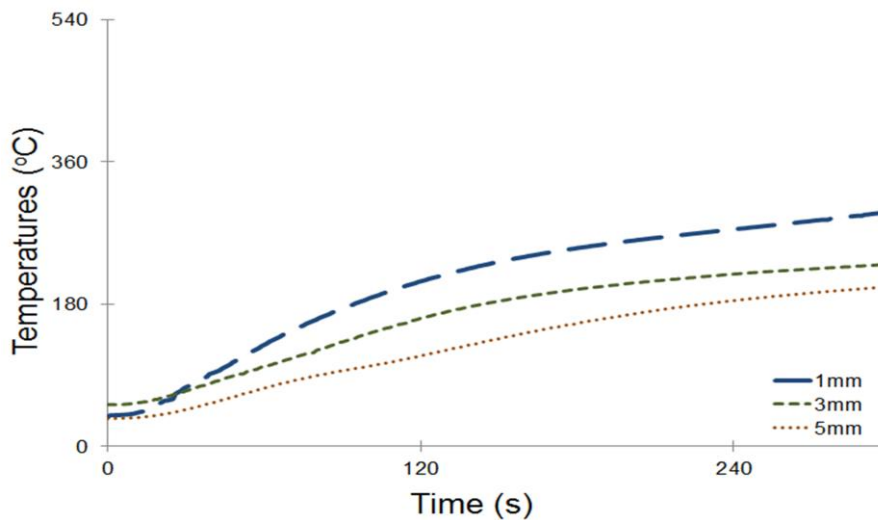


Figure 3.33: Temperature profiles at the bottom side of the GRE coated with 1, 3 and 5mm thicknesses of WI exposed to 50 kW/m² heat flux.

Figures 3.28 to 3.33 show that, independently to the type of coating paint, as the thickness of the coating increases, the temperature profiles at the top and the bottom of the glass fibre reinforced resin laminate sample decrease due to the thermal barrier insulation effect.

3.4.3 Thermophysical properties measurements of GRE, EI, EDI and WI.

The fire resistance of a commercial coating is measured using standard tests for rating the materials, e.g., ISO 834 [15] or ASTM E119 [211]. Such tests are expensive and time-consuming to conduct. This could be significantly reduced if mathematical modelling of the thermal resistance of the coating provides a computer programme that accurately describes

the developing thermal resistance of a coating subjected to the various heat sources to simulate the standardised tests. To carry out such a mathematical modelling performed in Chapter 7 the thermophysical properties such as the effective thermal conductivity, the effective heat capacity and the effective density of the coating materials (EI, EDI and WI) and the GRE are needed in order to incorporate their values in the general mathematical modelling algorithm.

The thermal conductivity, the thermal capacity and the thermal diffusivity of three intumescent coatings (EI, EDI and WI) and the composite GRE were measured by the hot disk method using a hot disk thermal constant analyser (Hot Disk TPS 2500 S, Thermo-concept, Bordeaux, France) and the experimental setup is described in details elsewhere [7]. In summary, at room temperature measurement only the hot disk sensor is placed between two sample pieces (50 mm diameter, 5 mm thickness) and installed in the guarding cylinder. The sensor is directly connected to the thermal constant analyser in order to measure the thermophysical parameters of the sample. Whereas for the thermophysical parameters measurements at different temperatures ranging from 20°C to 700°C, sample preparation involved gluing two samples together (25 mm diameter and 1 mm thickness) on each side of the hot disk sensor. The experimental set up is shown in Figure 3.34 taken from reference [202].

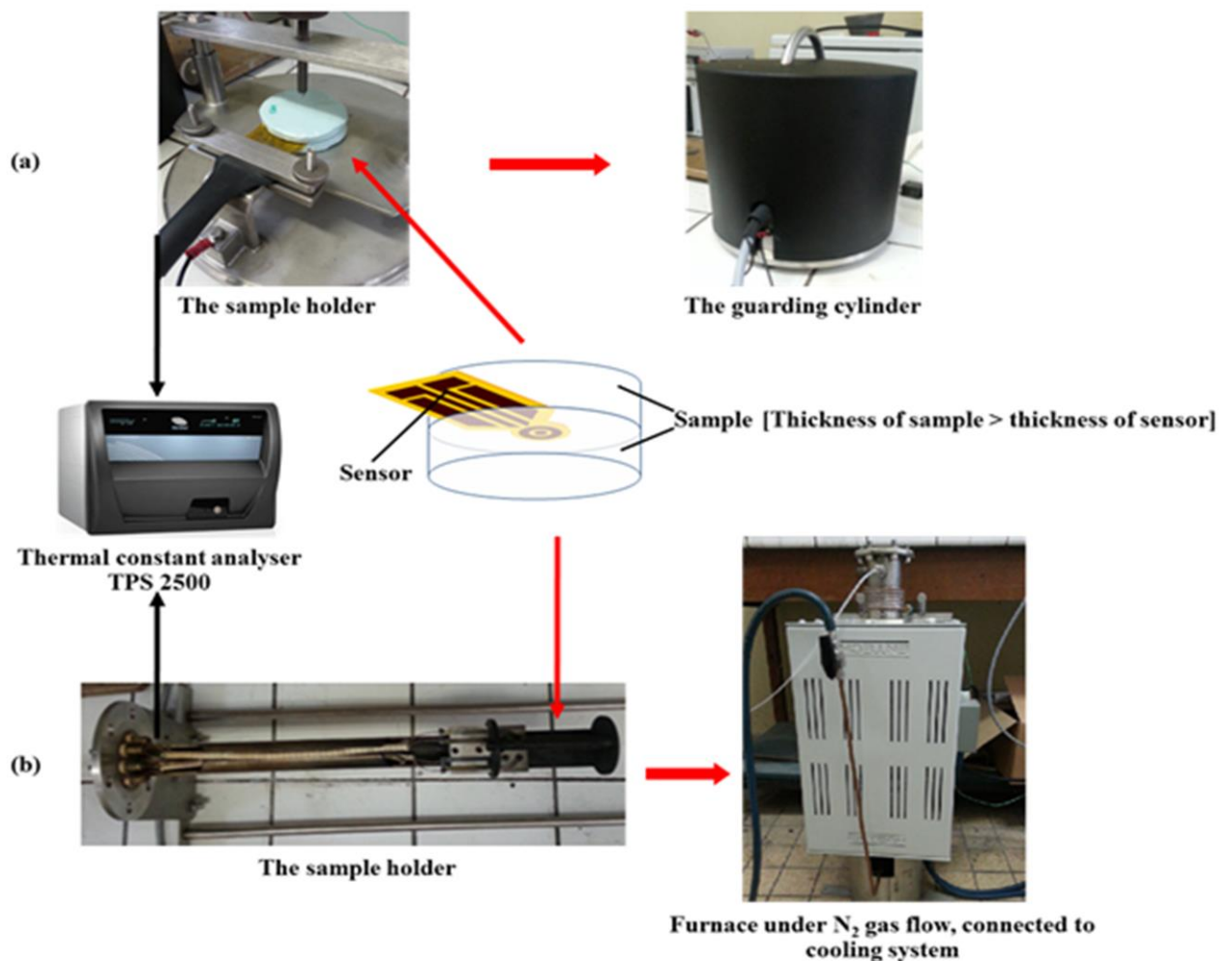


Figure 3.34 (Taken from reference [202]: Experimental setup for thermal conductivity measurement at a) room temperature and b) elevated temperatures.

The thermophysical properties values at all temperatures are average values of three measurements taken at a particular temperature. They are reported in Tables 3.35, 3.36, 3.37 and 3.38 and, will be used later to build up the numerical model developed in chapter 7.

Temperatures (°C)	Thermal conductivity (W·m/°C)	Thermal capacity (kJ/Kg)	Density (10 ³ kg/m ³)	Thermal diffusivity (10 ⁻⁶ m ² /s)
25	0.46	1.78	1.543	0.17
50	0.44	1.36	1.9	0.17
100	0.44	1.67	1.757	0.15
150	0.50	2.08	1.851	0.13
200	0.50	4.19	1.99	0.06
250	0.48	2.09	1.918	0.12
300	0.46	2.28	1.819	0.11
350	0.18	0.50	2.113	0.17
400	0.13	0.10	1.658	0.8

Table 3.35: Thermophysical parameters of GRE as a function of temperature

Temperatures (°C)	Thermal conductivity (W /m °C)	Thermal capacity (kJ/Kg)	Density (10 ³ Kg/m ³)	Thermal diffusivity (10 ⁻⁶ m ² /s)
18	0,32	0,17	1,86	1,00
200	0,20	0,05	3,79	0,98
300	0,21	0,16	1,56	0,82
400	0,14	0,62	0,23	0,98
500	0,19	0,71	0,29	0,95
600	0,25	0,91	0,29	0,94
700	0,30	0,67	0,44	1,00

Table 3.36: Thermophysical parameters of EI as a function of temperature

Temperatures (°C)	Thermal conductivity (W /m °C)	Thermal capacity (kJ/Kg)	Density (10 ³ Kg/m ³)	Thermal diffusivity (10 ⁻⁶ m ² /s)
18	0,28	0,16	1,72	1,02
200	0,18	0,06	2,93	0,99
300	0,19	0,19	1,20	0,83
400	0,15	0,57	0,26	0,99
500	0,21	0,63	0,34	1,00
600	0,26	0,71	0,36	1,00
700	0,34	1,29	0,29	0,91

Table 3.37: Thermophysical parameters of EDI as a function of temperature

Temperatures (°C)	Thermal conductivity (W /m °C)	Thermal capacity (kJ/Kg)	Density (10 ³ kg/m ³)	Thermal diffusivity (10 ⁻⁶ m ² /s)
18	0,53	0,31	1,78	0,96
200	0,20	0,10	2,12	0,98
300	0,19	0,23	0,88	0,97
400	0,10	0,99	0,11	0,89
500	0,17	0,44	0,40	0,97

Table 3.38: Thermophysical parameters of WI as a function of temperature

The thermal conductivity $k(T)$ values of EI, EDI and WI coatings with 1 mm thickness were determined at both room temperature and elevated temperatures by using Hot disk method. The observed thermal conductivity values at every 100 °C from room temperature up to 700 °C are reported in Tables 3.36 to 3.38. In literature, the thermal conductivity values of intumescent char materials are reported to be varying from 0.1W/mK to 0.4 W/mK from room temperature to 600°C [202, 210]. As can be seen from the results the obtained thermal conductivity values for these three coatings are in the within the range as reported in the literature. At room temperature, the WI coating of 1 mm thickness has the highest thermal

conductivity value of 0.53 W/mK compared to that of EI (0.32 W/mK) and EDI (0.28 W/mK). The thermal conductivity of these three coatings first decreased and then increased with increasing in temperature. The first significant drop in thermal conductivity values of these EI, EDI and WI intumescent coatings was observed at 200 °C (0.20 for EI, 0.18 for EDI and 0.20 W/mK for WI). These values remained constant until 300 °C and then decreased again, the minimum being at 400 °C, after which the values increased and kept increasing until 700°C. This behaviour is characteristic of an intumescent material, when exposed to high temperature. EI, EDI and WI expand and form a porous char structure containing voids (bubbles) up to 400°C. The volume of the char layer being at maxima, the density is then minimal; 230, 260 and 110 kg/m³ for EI, EDI and WI respectively. At this stage the expanded layer structure composed by carbonised char and, a significant number of voids and bubbles produces the lowest thermal conductivity; 0.14, 0.15 and 0.10 W /m °C for EI, EDI and WI respectively. Due to the low thermal conductivity lowering the heat diffusivity as well, the heat transfer by conduction is low. Hence, the heat capacity starts increasing consequently to the heat energy stored and not being exchanged. Above 400°C, the expanding layer loses the voids and bubbles while its volume is decreasing leading to the increase of the density, the layer being more compact. At this second stage, the thermal conductivity increases as function of temperature [202] due to the carbonised char being the main constituent of the expanded layer. Therefore, the heat diffusivity within the materials increases while their heat capacities decrease.

The values of the density of the different materials mentioned in the above tables are not measured by experiments, but they have been calculated from the effective thermal diffusivity formula α as:

$$\alpha = \frac{k}{\rho c_p}$$

Where: k is the effective thermal conductivity, c_p is the effective thermal capacity and ρ is the effective density.

3.5 Conclusions

In this chapter, experimental set up leading to experimental results used for the work in this thesis have been described. Some results for melting and dripping of thermoplastics in vertical orientation have been taken from previous researcher's work, however experiment methodology to measure temperatures of molten drops has been developed in this work. The samples have also been subjected to radiant heating on one surface in horizontal orientation

using cone calorimeter. These results will be used to validate the moving boundary model developed in Chapter 4 and the phase changed model developed in Chapter 5. For the heat transfer models designed in Chapters 6 and 7 the experimental results for temperatures measurements through the thicknesses of GRE and intumescent coated GRE samples during cone calorimetric testing and determination of temperature dependent parameters required for modelling work have been taken from previous work reported by other researchers.

Chapter 4: Modelling temperature profiles during melting of vertically oriented thermoplastic polymers

4.1 Introduction

In this Chapter 4 temperature profiles of vertically oriented thermoplastics have been modelled while they are melting and dripping. In this first scenario the sample is placed in a tubular furnace and the radiant heat is taken to be uniform on all sides of the sample. This configuration is based on the experiment process discussed in Chapter 3, Section 3.2 where the temperatures of the polymers are measured. Comparison between experimental temperatures and simulated temperatures is undertaken to validate the developed numerical model. The objective is to estimate the temperature profile in the slab of the polymer exposed to heat in a vertical tubular furnace. Then from these temperatures of the heated polymers, the degree of polymer degradation in each case has been predicted and compared with the experimental results from Chapter 3.

4.2 Modelling for surface temperature estimation

4.2.1 Model description

In this one-dimensional heat transfer model both the latent heat of melting and polymer degradation are included. The sample shape is considered as a rectangular polymer slab immersed in the furnace, preheated to a number of controlled set temperatures. The heat flux q_{inc} emitted from the internal walls of the furnace, acts on all the polymer faces as shown in Figures 4.1. It is assumed that the heat exchange by convection between the furnace and the sample is negligible compared to the exchange by radiation. It is also assumed that the surface temperature is uniform on each face of the sample, despite the fact that a rectangular slab of sample is in a cylindrical furnace. Due to the small sample size (6 mm in length x width ranging approximately from 3 to 4 mm) in comparison with the diameter of the furnace (25 mm) this approximation can be justified and hence, a one-dimensional (1D) model can be applied. The molten material is taken to be immediately removed upon formation, thus the boundary condition is moving. The heat transfer describing the model is the general balance equation, *Eqns 4.2* [185], which takes into account melting as well as gasification of thermoplastic polymer due to pyrolysis. This 1D energy equation describes a heated slab of thermoplastic polymer material of thickness L heated by an incident flux q_{inc} radiated by the internal wall furnace.

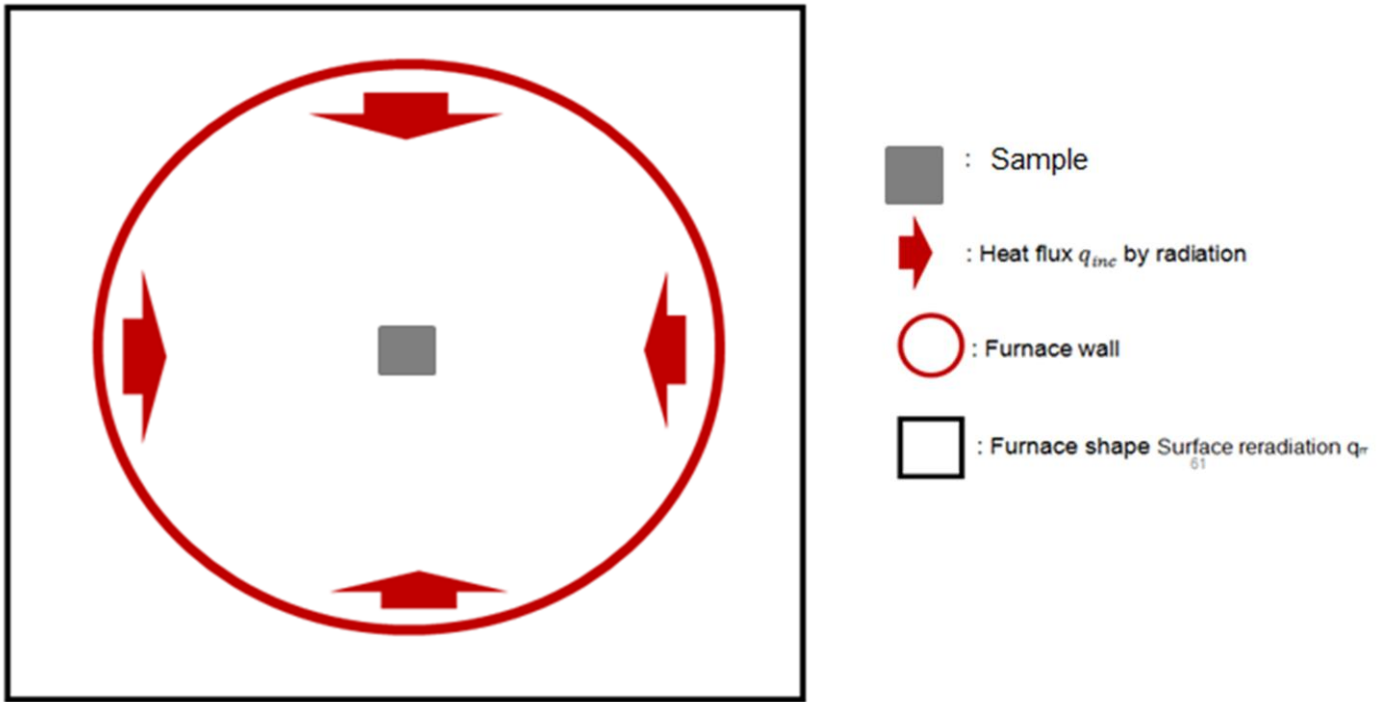


Figure 4.1: Schematic top view of furnace and heated polymer slab

4.2.2 Formulation and balance equation

4.2.2.1 Pure melting

The schematic representation of the one-dimensional (1D) pure melting slab heat transfer is shown in Figure 4.2.

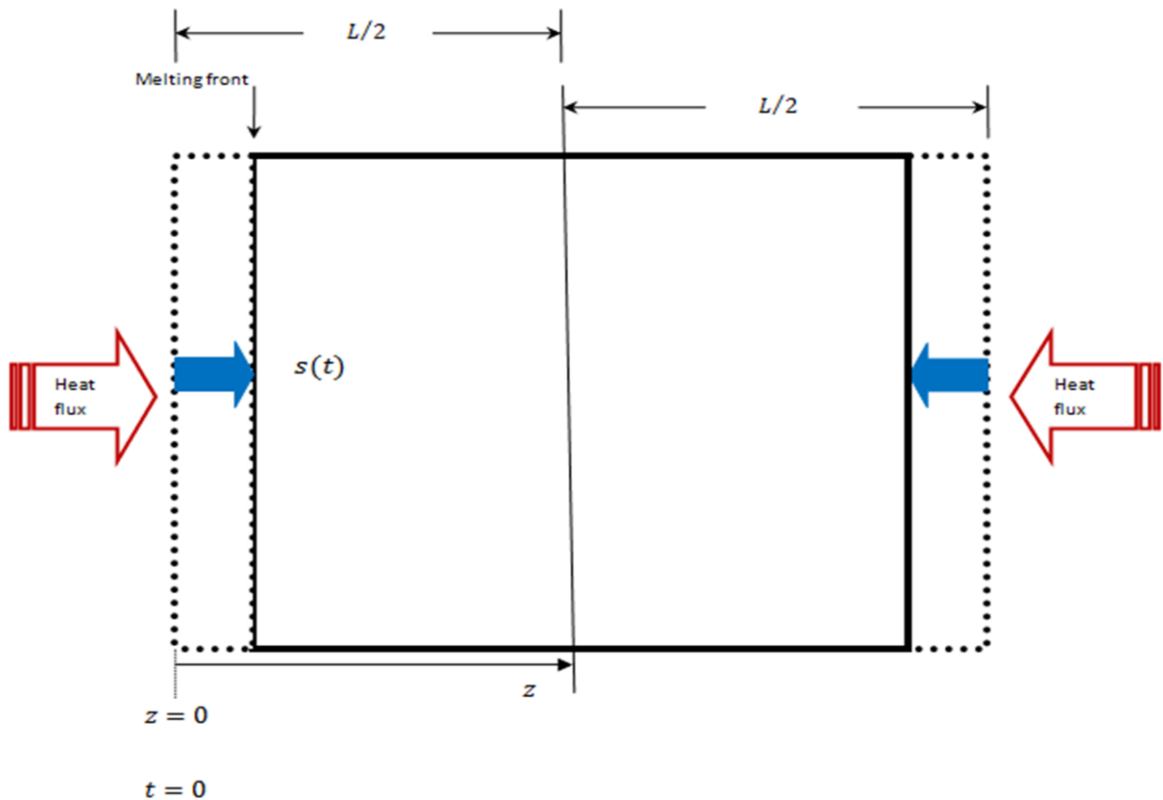


Figure 4.2: Schematic representation of pure melting slab

With, $s(t)$ the melting front as a function of time and L is the thickness of the polymer slab. So, the one-dimensional (1D) [212-215] heat transfer balance equation is given by Eqn 4.1 below;

$$\rho(T)c_p(T) \frac{\partial T}{\partial t} = k(T) \frac{\partial^2 T}{\partial z^2} + \rho(T) \frac{ds}{dt} H_L \quad \text{Eqn 4.1}$$

Where: $\rho(T)$ is the density, $c_p(T)$ is the heat capacity and $k(T)$ is the conductivity of the polymeric material. H_L is the latent heat of melting, $\frac{ds}{dt}$ is the melting rate.

The left hand side of Eqn 4.1 represents the variation of the internal energy while the right hand side is the heat transfer by conduction within the thermoplastic polymer and the necessary energy for the polymer to reach its melting point. This equation Eqn 4.1, has to be solved for $T(z, t)$ in molten and solid (virgin) polymer phase respectively [185, 200]:

The Boundary conditions for this problem are:

$$T(z, 0) = T_a < T_m \quad \text{for } 0 \leq z \leq L/2 \quad \text{and } t = 0$$

$$s(0) = 0 \quad (\text{virgin polymer initially solid})$$

Where T_m and T_a are melting and ambient temperatures respectively and L is the sample thickness.

$$T(s(t), t) = T_m \quad \text{for } t > 0$$

$$q_{net} - \rho(T) \frac{ds}{dt} H_L = -k(T) \frac{\partial T(s(t), t)}{\partial z} \quad \text{for } t > 0$$

$$\frac{ds}{dt} = \frac{1}{\rho(T)H_L} \left(q_{net} + k(T) \frac{\partial T(s(t), t)}{\partial z} \right) \quad , \text{melting rate, } \quad \text{for } t > 0$$

$$-k(T) \frac{\partial T(L/2, t)}{\partial z} = 0 \quad \text{for } t > 0$$

Where: $q_{net} = \alpha \sigma \varepsilon (T_{fce}^4 - T_s^4)$, T_m polymer melting temperature, T_s is polymer the face temperature, $q_{net} = \alpha q_{inc}$, q_{inc} is the incident heat flux. Where q_{net} is the heat exchange by radiation between the sample and the furnace absorbed by the sample, the emissivity ε of the wall furnace is taken to be 1, the polymers absorption coefficient α is 0.96 [72, 216], σ is

the Stefan Boltzmann constant, T_{fce} is the furnace wall temperature, T_s is the polymer temperature, T_a is the ambient temperature and t is the time.

4.2.2.2 Melting and decomposition

The schematic representation of the one-dimensional (1D) melting and heat transfer within slab is shown in the following Figure 4.3.

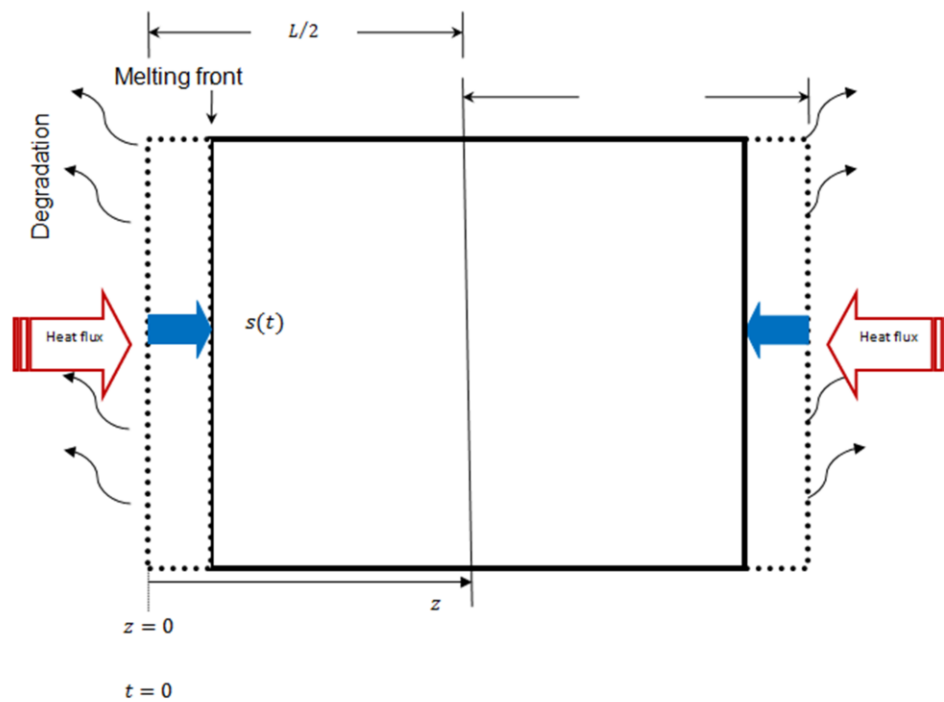


Figure 4.3: Schematic representation of melting and degradation of slab

Eqn 4.2 below is the one-dimensional heat transfer balance equation describing a gasifying slab of thermoplastic polymer material of thickness L heated at incident flux $q(t)$ at $z = L$ [185, 217-218].

$$\rho(T)c_p(T) \left(\frac{\partial T}{\partial t} \right) = k(T) \frac{\partial^2 T}{\partial z^2} + \rho(T) \frac{ds}{dt} H_L + \frac{dm}{dt} H_v - \rho(T)c_p(T)W \frac{\partial T}{\partial z} \quad \text{Eqn 4.2}$$

The left hand side of Eqn 4.2 represents the variation of the internal energy while the first term of the right hand side is the heat transfer by conduction within the thermoplastic polymer, the second term is the energy loss by pyrolysis and the third term is the moving boundary energy loss. This equation (Eqn 4.2) also has to be solved for $T(z, t)$.

Where T is the temperature, ρ is the density, c_p is the heat capacity, k is the thermal conductivity, H_v is the heat of gasification and mass loss rate is given by the Arrhenius expression:

$$\frac{dm}{dt} = \rho(T)Ae^{-E_a/RT} \quad \text{Eqn 4.3}$$

Where: A is the pre-exponential factor, E_a is the activation energy and R is the constant of perfect gas.

Due to the need to model the velocity addition boundary conditions are needed to supplement those stated in the previous Section 4.2.2.1.

Initial conditions

At $t = 0$, $T_{fce} = T_a$

While the furnace wall temperature, T_{fce} , is the set temperature for each experiment.

Boundary conditions

Gradually as the boundary layer moves with the displacement $s(t)$ as the melting of the polymer occurs, its velocity is determined by $W(x, t)$ at any position z at time t :

$$W(z, t) = - \int_0^z \frac{dm/dt}{\rho(T)} dz \quad \text{Eqn 4.4}$$

At $z = \frac{L}{2}$, $\frac{dT}{dz} = 0$.

At $z = 0$, $-k(T)\frac{dT}{dx} = q_{net} - \rho(T)\frac{ds}{dt}H_L - \frac{dm}{dt}H_v$

4.2.3 Numerical approach

The one-dimensional (1D) numerical approximation using the finite difference equation of equation Eqn 4.2 is shown below as Eqn 4.5 and Eqn 4.6.

$$\rho c_p \left(\frac{T_i^{n+1} - T_i^n}{\Delta t} \right) = k \left(\frac{T_{i+1}^n - 2T_i^n + T_{i-1}^n}{(\Delta z)^2} \right) - H_v \rho A e^{-E/RT_i^n} - \rho c_p W_i^n \left(\frac{T_i^{n+1} - T_i^n}{\Delta z} \right) \quad Eqn 4.5$$

$$T_i^{n+1} (1 + s_1) = s_2 T_{i+1}^n + T_i^n (1 + s_1 - 2s_2) - s_3 e^{-E/RT_i^n} + s_2 T_{i-1}^n \quad Eqn 4.6$$

with:

$$s_1 = \frac{W_i^n \Delta t}{\Delta z} \quad s_2 = \frac{k \Delta t}{\rho c_p (\Delta z)^2} \quad s_3 = \frac{H_v A \Delta t}{c_p}$$

'n' and 'i' are indicating respectively, the time incremented and the temperature localised within the thermoplastic sample. Eqn 4.2b and Eqn 4.2c result in algebraic equations describing the temperature profile and will be solved by writing the appropriate code in Matlab. Two key parameters of the mesh are Δz , the local distance between adjacent points in space, and Δt , the local time between adjacent time steps. The key idea of the finite difference method is to replace continuous derivatives with numerical derivatives called difference formulae that involve only the discrete values associated with positions on the mesh. Therefore applying the finite difference method to an analytical differential equation involves replacing all derivatives with difference formulae.

Moreover, for thermal mathematical modelling, properties such as thermal conductivity $k(T)$, heat capacity $c_p(T)$, density $\rho(T)$, degree of degradation reaction, energy of activation, pre-exponential factor, etc. are required. Thermal conductivity, specific heat capacity and specific density of different polymers were taken from literature. Kinetic parameters (pre-exponential factor "A" and the energy of activation, E_a) have been obtained by running TGA experiments at different heating rates in both air and nitrogen atmosphere and applying the Flynn-Wall-Ozawa method on the data [219]. Although the decomposition steps in different polymers vary from one to two, for simplifying the modelling works, in this thesis only one main decomposition step is assumed for all polymers. In future modelling work, kinetic parameters for all degradation steps will be taken into account in order to improve the accuracy of the heat transfer model. Moreover in this work, values of thermal conductivity, specific heat capacity and specific density were not obtained at all temperatures, which could be recommendation for the future work. All the thermophysical values at different temperatures available are reported in Tables 4.1a to 4.1d and used for simulations; hence due to lack of comprehensive data some differences in simulated and experimental values are expected.

The following assumptions are taken in the model:

- The radiation view factor is taken to be equal to 1. Hence, all the flux emitted by the wall furnace is entirely received by the polymer sample.
- Melting temperatures have been taken from DSC curves.

All kinetic degradation parameters are reported in Table 4.1a. In addition material properties such as thermal conductivity, heat capacity, density required to be included in the computer model have been taken from literature and reported in Table 4.1b, 4.1c, and 4.1d showing the different equations of the parameters varying with the temperature in the corresponding interval [220].

All kinetic degradation parameters are reported in Table 4.1a. In addition material properties such as thermal conductivity, heat capacity, density required to be included in the computer model have been taken from literature and reported in Table 4.1b, 4.1c, and 4.1d showing the different equations of the parameters varying with the temperature in the corresponding interval [220].

4.1a)

Arrhenius equation parameters and Pyrolysis					
Polymers	Pyrolysis energy (MJ/kg)	Activation energy (kJ/mol)		Pre-exponential factor (s ⁻¹)	
		Nitrogen	Air	Nitrogen	Air
PA6	1.4	217	75.5	10 ¹³	10 ⁷
PET	1.3	77	387	1.65 x 10 ¹¹	2.06 x 10 ²³
PMMA	1.7	78	119	7.34 x 10 ¹¹	6 x 10 ⁹
PS	1.8	238	142	3 x 10 ¹⁷	4 x 10 ¹⁰
PC	1.8	48	166	3 x 10 ²	10 ¹²
PP	1.9		122	1.2 x 10 ⁸	10 ¹⁴

4.1b)

Densities as a function of temperature		
Polymers	Density (g/cm ³) , Temperature (T) in °C	Temperature range (°C)
PA6	1.177	25
	$1.316 \exp(-4.70 \times 10^{-4} T)$	236 – 295
PET	1.350	25
	$1.39 - 7.82 \times 10^{-4} T$	274 – 342
PMMA	1.190	25
	$1.188 - 1.34 \times 10^{-4} T - 0.91 \times 10^{-6} T^2$	30 – 100
	$1.211 - 5.96 \times 10^{-4} T$	105 – 150
PS	$1.223 - 5.29 \times 10^{-4} T - 0.0507 \times 10^{-6} T^2$	120 – 270
	1.050	25
	$1.052 \exp(-2.86 \times 10^{-4} T)$	30 – 79
PC	$1.067 - 5.02 \times 10^{-4} T - 0.135 \times 10^{-6} T^2$	79– 320
	1.200	25
PP	$1.254 - 6.35 \times 10^{-4} T - 0.116 \times 10^{-6} T^2$	151 – 340
	0.910	25
PP	$0.848 - 0.19 \times 10^{-4} T - 3.05 \times 10^{-6} T^2$	80 – 120
	$0.862 \exp(-6.70 \times 10^{-4} T)$	170 – 300

4.1c)

Thermal conductivity k as a function of temperature		
Polymers	k (w/m. °C)	Temperature range (°C)
PA6	0.24	20
	0.43	30
	0.15	250
PET	0.15	20
PMMA	0.21	20
PS	0.105	20
	0.128	100
	0.13	200
	0.14	300
	0.16	400
PC	0.2	20
PP	0.12	20

4.1d)

Specific heat capacity c_p as a function of temperature		
Polymers	c_p (kJ/kg. °C)	Temperature range (°C)
PA6	1.5023	27
	2.5186	127
	2.7881	327
PET	1.172	27
	1.8203	127
	2.1136	327
PMMA	1.3755	27
	2.0766	127
	2.4323	277
PS	1.2730	27
PC	1.207	27
	1.957	177
	2.207	287
PP	1.622	27

Tables 4.1 a-d: Thermophysical properties of different polymers used to build the numerical model [220].

4.2.3.1 Simulation results

A set of simulations was performed by running the computer programme developed in Matlab software according to the Finite Difference Method applied to solve the nonlinear Partial Differential equations *Eqn 4.1* and *4.2* computing the temperature profiles of thermoplastic samples heated in vertical electrical furnace. The samples used for the simulation are PP, PET, PA6, PC, PMMA and PS.

A set of simulations was performed by running the computer programme developed in Matlab software according to the Finite Difference Method applied to solve the nonlinear Partial Differential equations *Eqn 4.1* and *4.2* computing the temperature profiles of

thermoplastic samples heated in vertical electrical furnace. The samples used for the simulation are PP, PET, PA6, PC, PMMA and PS.

PP, PET, and PA6 are semi-crystalline thermoplastic polymers. As mentioned previously in Chapter 3, Section 3.2.3.3, some types of PC are also semi crystalline [221-222], and their melting temperatures are available in the literature. Semi-crystalline polymers have a melting temperature T_m , which implies a supplement of energy required to achieve the phase changing up to melt state; this is the latent heat or endothermic enthalpy of melting. When the melting temperature is reached, an endothermic thermal energy corresponding to the latent heat of melting is stored within the thermoplastic polymer while the sample continues being heated. This energy allows the melting process to happen at a uniform rate of change of temperature or at constant temperature. Furthermore, PMMA, PS and some types of PC are amorphous polymers and they do not melt but they soften and drip. Indeed when they are heated their temperatures increase causing an increase of the heat capacity value. This addition of heat energy corresponds to a stored endothermic enthalpy similar to the case of a latent heat of melting. Therefore it will be assumed for both semi-crystalline polymer and amorphous polymer that the melting temperature or the soften temperature calculated by the simulation is effective when the temperature profile is in a steady state when the temperature gradient is negligible between two successive points.

The simulations are performed using the same conditions and configurations (e.g. sample dimensions, incident heat flux from wall furnace etc.) as those taken with the experiment described in Chapter 3. A set of computational simulations was performed. The results obtained for a set of Furnace Setting Temperatures (FST) indicated in the title of each graph for each thermoplastic polymer sample are shown in the following section.

a) Polypropylene (PP)

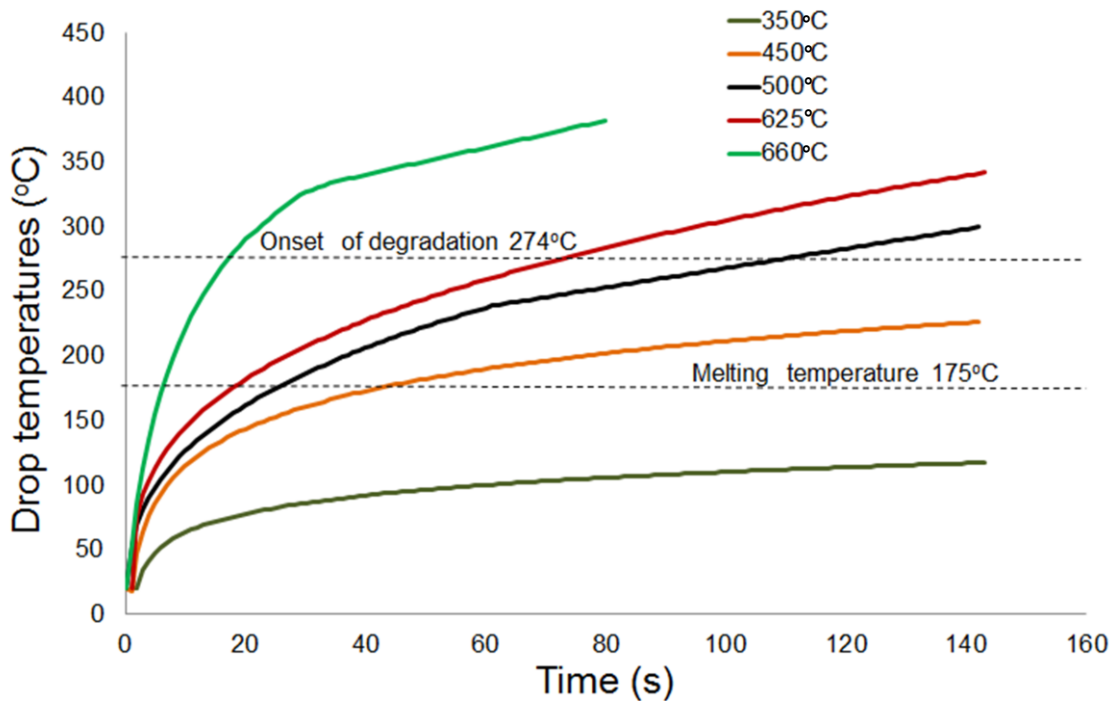


Figure 4.4: PP-Temperatures profiles simulation at FST of 660, 625, 500, 450 and 350°C.

b) Polymethyl Methacrylate (PMMA)

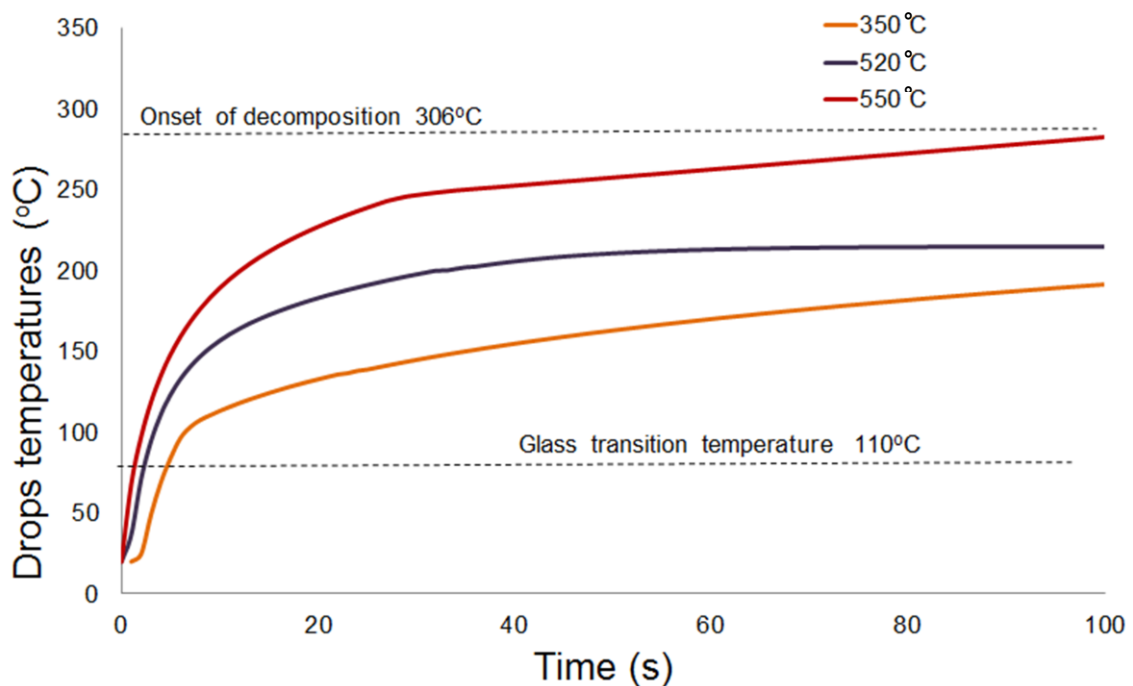


Figure 4.5: PMMA-Temperatures profiles simulation at FST of 550, 525 and 350°C.

c) Polyethylene Terephthalate (PET)

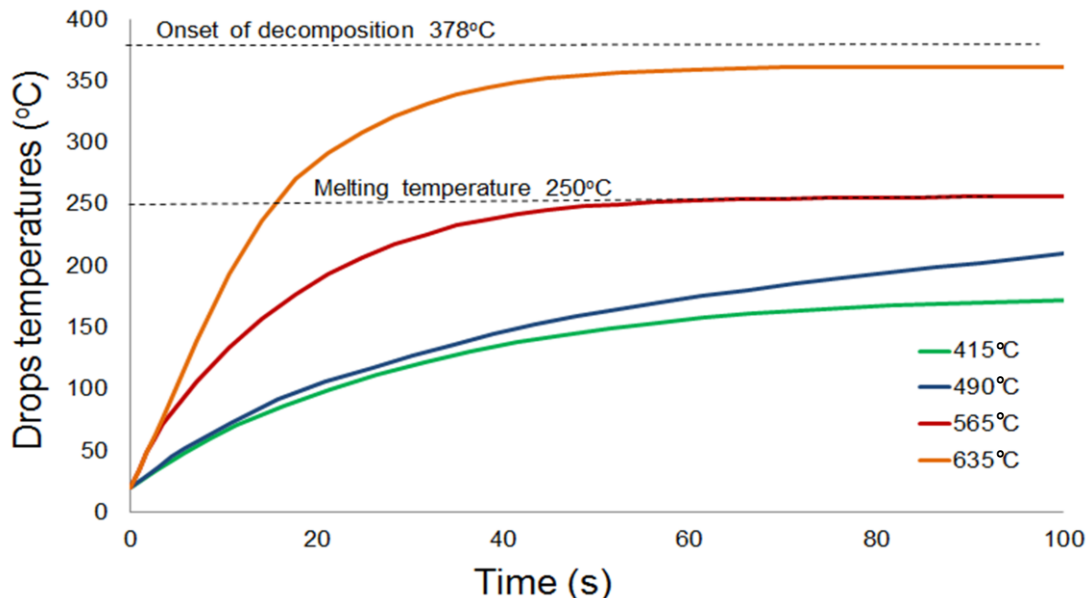


Figure 4.6: PET-Temperatures profiles simulation at FST of 635, 565, 490 and 415°C.

d) Polyamide 6 (PA6)

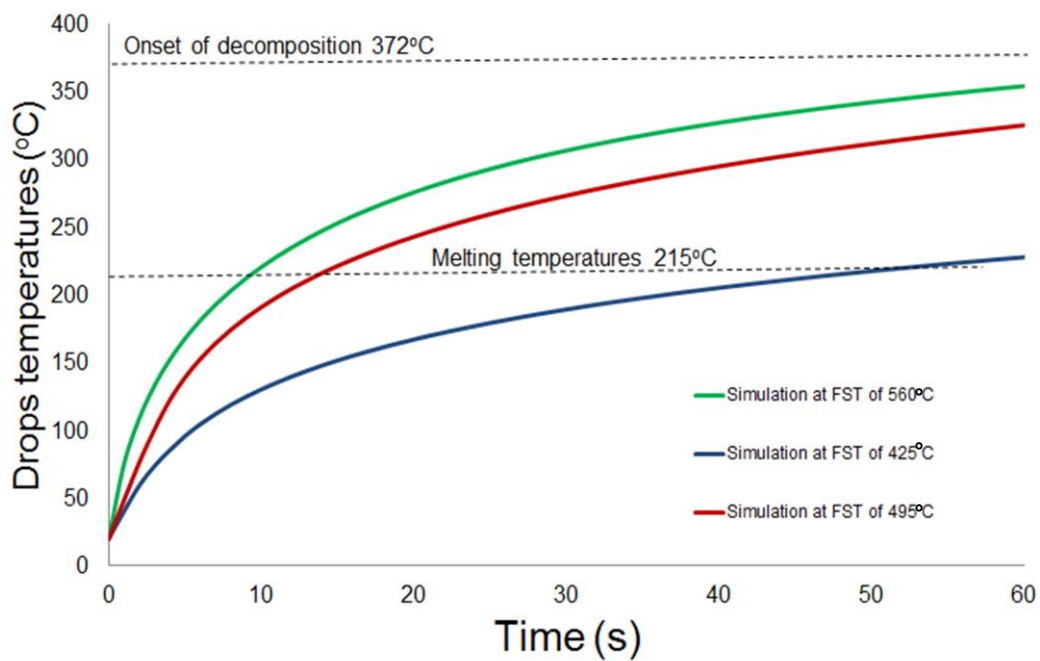


Figure 4.7: PA6-Temperatures profiles simulation at FST of 560, 495 and 425°C

e) Polycarbonate (PC)

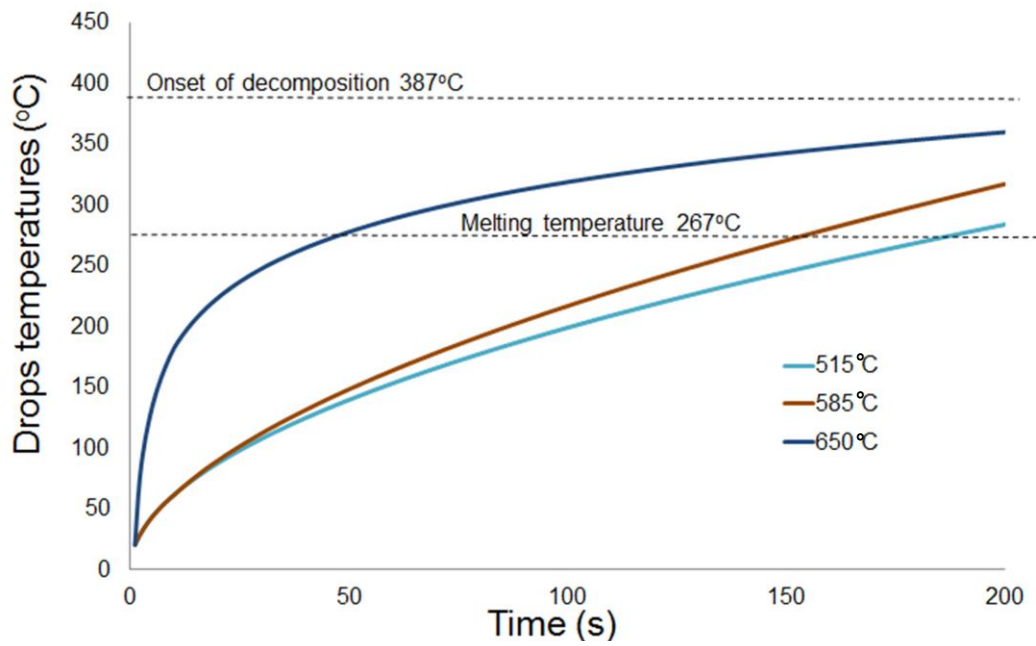


Figure 4.8: PC-Temperatures profiles simulation at FST of 650, 585 and 415°C.

f) Polystyrene (PS)

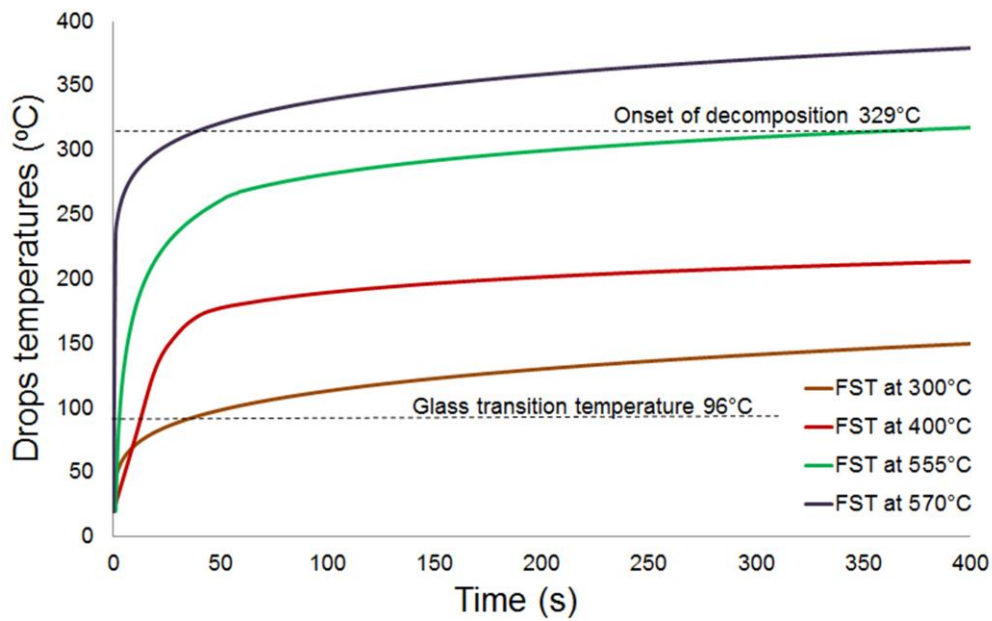


Figure 4.9: PS-Temperatures profiles simulation at FST of 595, 570, 400 and 300°C.

4.2.3.2 Analysis and comments

Experimental set up and the methodology used to measure temperatures of the thermoplastic melt dripping drops have been already explained in Section 3.2.3.2. Figures 4.4 to 4.9 show simulations of temperature profiles obtained from the modelling of the six polymer samples subjected to heat in the furnace. The simulated temperature is the surface temperatures of the sample as a function of time within the modelling conditions specified in Section 4.2.2.

The input data to fill the numerical model such as wall furnace temperatures setting and, sample types and dimensions are similar to those used to carry out the experiments according to the configuration described in Chapter 3.

The emissivity and absorptivity coefficient of the furnace are taken to be equal to 1 because the furnace wall is assumed to be a black body [72-185]. Simulated temperature profiles all show initial exponential rise. From thermodynamical point of view the melting process starts at constant temperature when the latent heat (namely 'enthalpy of fusion' for semi-crystalline thermoplastic or 'enthalpy of degradation' for amorphous thermoplastics) compensates the increase in temperature within the heated polymer slab. Then it is assumed that a temperature step is reached when the curves begin to stabilise around a steady step for each thermoplastic polymer. This phenomenon is also observed in the experimental work described in Chapter 3 and appears to justify the assumptions described above.

4.2.4. Model validation

A consistent mathematical model is expected to produce results similar to those obtained by experimental tests in identical conditions. Therefore the validation process here consists of comparing both results, simulated and experimental, explained in details in Chapter 3, Section 3.2.3.1. In Figures 4.10 to 4.15 for the experimental values the drop temperatures are not function of time, but in simulations it is to get the steady state and to determine in which part of the curve the melting process is taking place. The results for each polymer at every Furnace Setting Temperatures (FST) mentioned in the title of each graph are as following:

a) Polypropylene (PP)

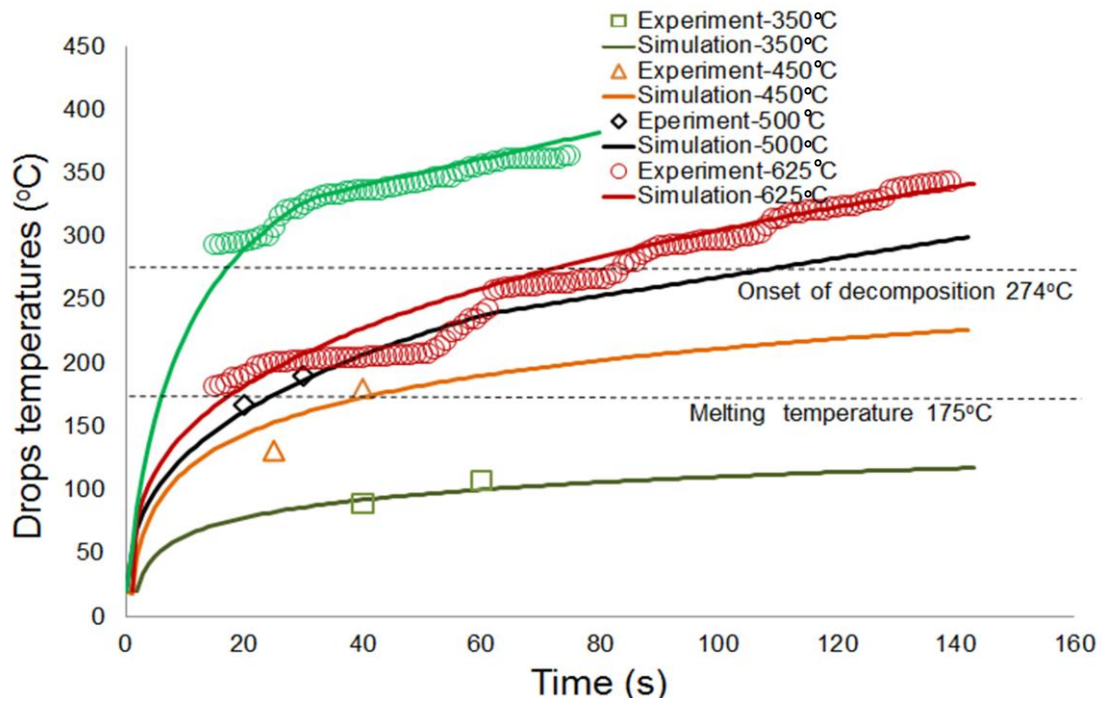


Figure 4.10: PP- Experimental vs. simulated temperatures at FST of 660, 625, 500, 450 and 350°C.

b) Polymethyl Methacrylate (PMMA),

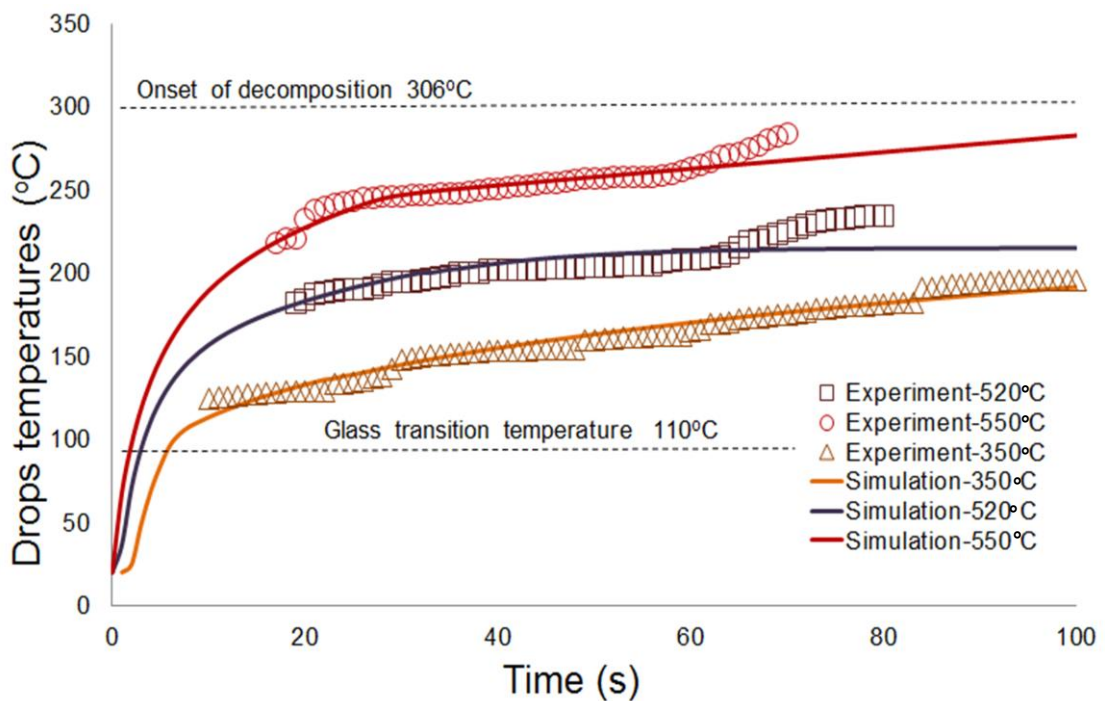


Figure 4.11: PMMA - Experimental vs. simulated temperatures at FST of 550, 520, 500 and 350°C.

c) Polyethylene Terephthalate (PET)

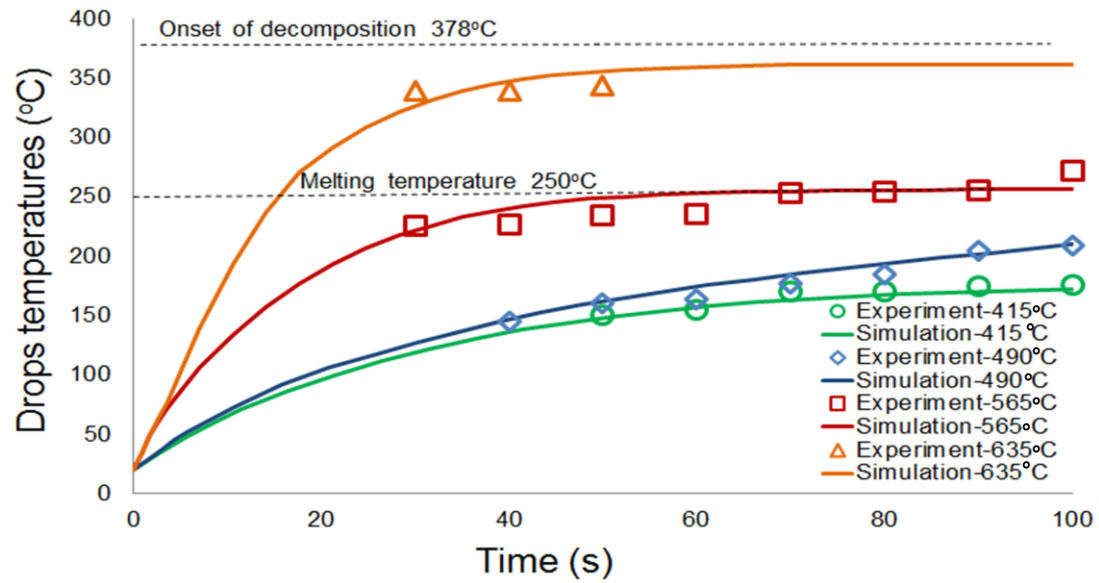


Figure 4.12: PET- Experimental vs. simulated temperatures at FST of 635, 565, 490 and 415°C.

d) Polyamide 6 (PA6)

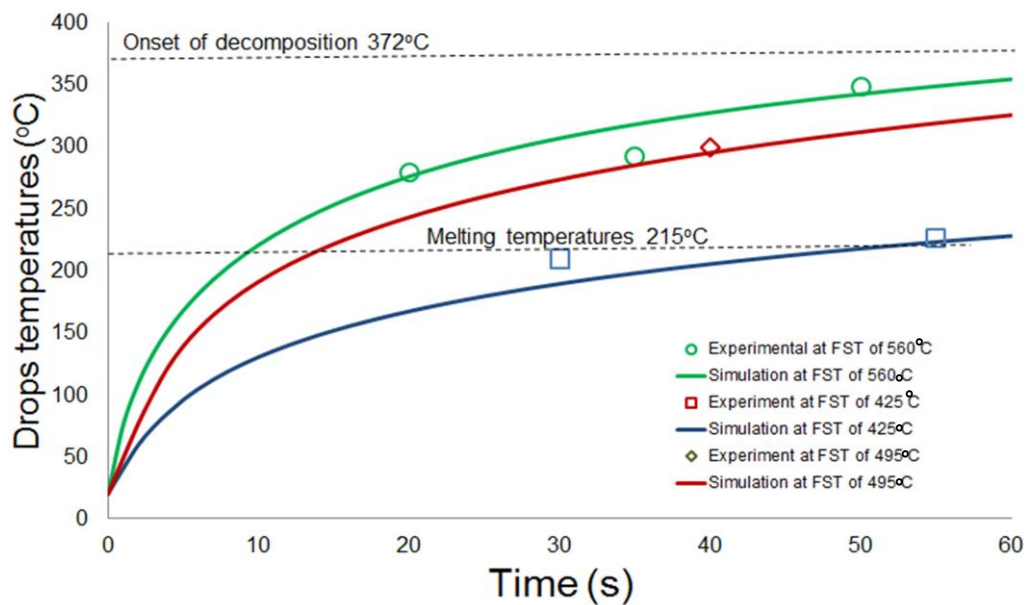


Figure 4.13: PA6 - Experimental vs. simulated temperatures at FST of 560, 595 and 425°C.

e) Polycarbonate (PC)

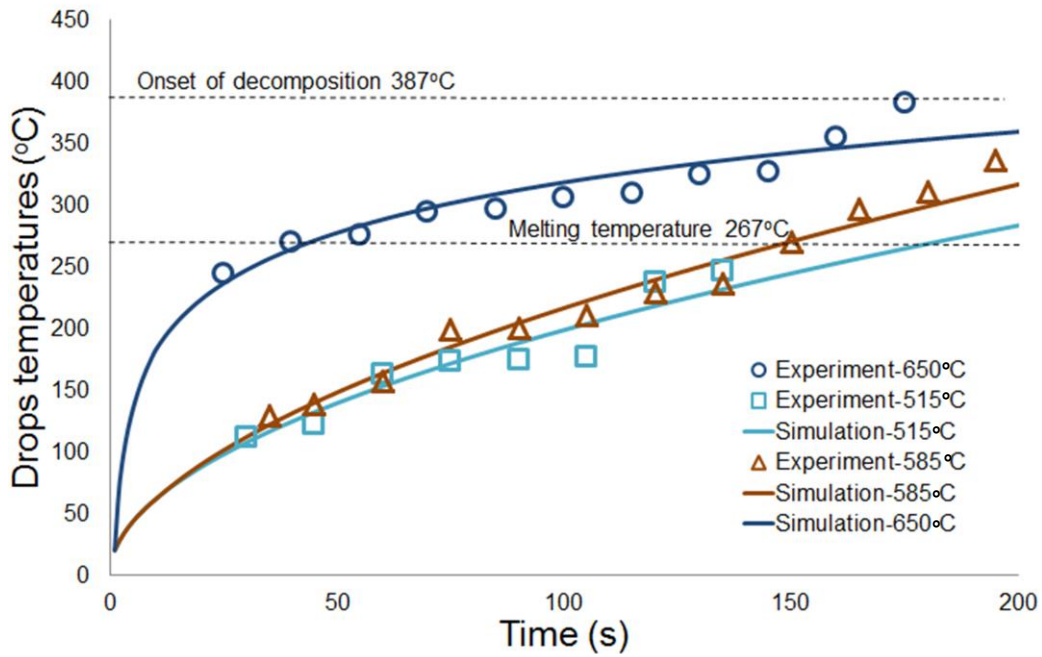


Figure 4.14: PC - Experimental vs. simulated temperatures at FST of 650, 585 and 515°C.

d) Polystyrene (PS)

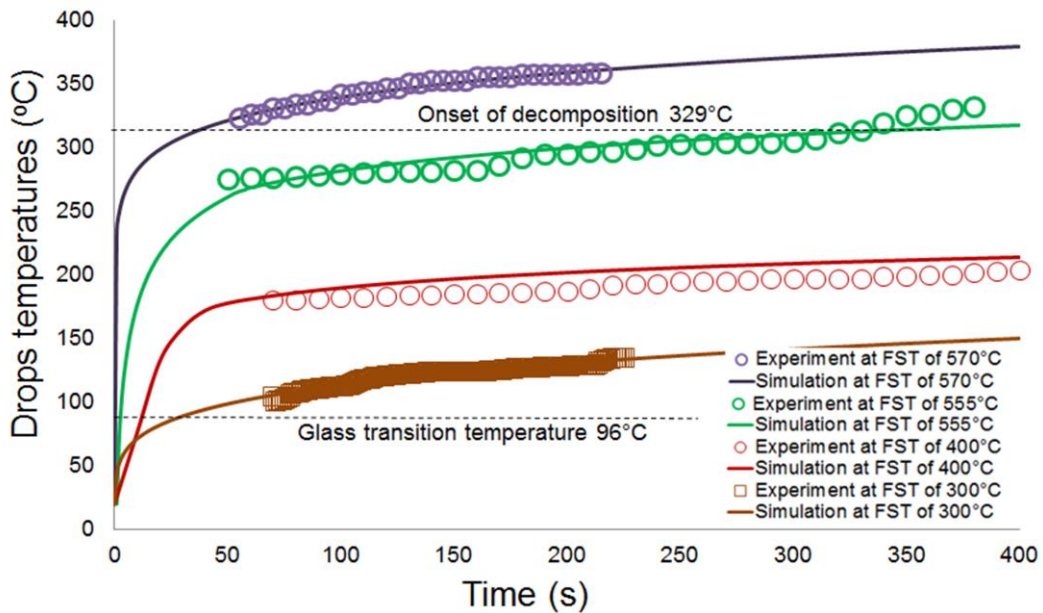


Figure 4.15: PS - Experimental vs. simulated temperatures at FST of 595, 570, 400 and 300°C.

4.2.5. Analysis and comments

The simulated results for the selected polymers at various associated furnace temperatures together with the experimental plots are shown in Figures 4.10 to 4.15 inclusive. In general most of the simulated temperature profiles show good agreement with the experimental temperature profiles. The small differences between simulation and experimental temperatures can be attributed to a combination of errors from the experiment process and from the values of thermophysical properties (conductivity, heat capacity and density) used to run the numerical model.

All samples show a rapid increase of temperatures at the beginning before having a low temperature gradient. It is well known from thermodynamical point of view that the melting process for many materials (metals such as copper, aluminium etc.) starts at constant temperature when the latent heat (namely 'enthalpy of fusion' for semi-crystalline thermoplastic or 'enthalpy of degradation' for amorphous thermoplastics) compensates the increase in temperature. Therefore, for thermoplastic polymer slab it can be assumed that this temperature step is reached at the inflection of high to low gradient point when a curve begins to stabilise around a steady step for each thermoplastic polymer. The temperature from the inflection point to the maximum temperature of the steady state curves are given in Table 4.2. Temperatures range from melting point to onset of degradation obtained from DSC and TGA, respectively are also given in Table 4.2.

Semi-crystalline thermoplastics	Temperature range (°C)	
	Melting temp – onset of decomposition	Simulation results
Polypropylene (PP)	172 – 274	75 – 350
Polyamide 6 (PA6)	215 – 372	200 – 350
Polyethylene Terephthalate (PET)	250 – 378	150 – 350
Polycarbonate (PC)	267 – 387	125 – 375
Amorphous thermoplastics		
Polymethyl Methacrylate (PMMA)	110 – 306	110 – 300
Polystyrene (PS)	160 – 329	125– 400

Table 4.2: A comparison of measured temperatures from DSC and those simulated by FDM (Matlab)

According to Table 4.2 the limits of the intervals, respectively the lowest temperature (melting temperature) and the highest temperature (onset of decomposition), measured or predicted from the melt drop polymers cannot be considered as definite or unique valuable temperature for any cases.

4.3. Prediction of degree of polymer degradation from predicted temperatures.

4.3.1 Introduction

In the above section the temperatures of the molten drops dripping from the melting surface have been computed. Here these temperatures of the molten drops have been used to predict the degree of degradation in a polymer during melt dripping. In a previously published work [200], by conducting thermogravimetric analysis of both the polymers and their molten drops, the degree of degradation of different polymers at different temperatures of exposure were calculated and reported. The values obtained from those experiments have been used to validate the models.

4.3.2 Modelling and calculating degree of degradation of thermoplastic polymers

From thermogravimetric studies, assuming the polymer decomposition is a first order process, the reaction rate can be expressed [45-50]:

$$f(\alpha) = (1 - \alpha) \quad (\text{Eqn 4.5})$$

The extent of reaction, defined by the reaction mechanism, and α is equal to:

$$\alpha = \frac{m_0 - m}{m_0 - m_\infty} \quad (\text{Eqn 4.6})$$

Where: m_0 , m and m_∞ are, respectively, the initial mass, the mass at any experimental time and the residual mass at the end of reaction process. Thus the rate of decomposition is given by:

$$\frac{d\alpha}{dt} = k(T)f(\alpha) \quad (\text{Eqn 4.7})$$

$k(T)$ is the Arrhenius rate constant and t time, A is the Arrhenius pre-exponential factor and β the heating rate. Under non-isothermal conditions, integration of this equation may be written as [49]:

$$\int_0^\alpha \frac{d\alpha}{(1-\alpha)} = \frac{A}{\beta} \int_0^T e^{\left(\frac{-E}{RT}\right)} dT \quad (\text{Eqn 4.8})$$

Solving this integration α is finally expressed theoretically by:

$$\alpha = 1 - e^{\left(\frac{-A}{\beta} \left(\frac{-E}{RT}\right) \text{Ei}\left(\frac{-E}{RT}\right) + T \cdot e^{-E/RT}\right)} \quad (\text{Eqn 4.9})$$

Where Ei is an exponential integral which standard definition is as follows [223-224]:

$$E_n(x) = \int_1^\infty \frac{e^{-xt}}{t^n} dt, \quad x > 0, \quad n = 0, 1, \dots \quad (\text{Eqn 4.10})$$

The function $E_i(x)$, defined by the principal value of the integral $E_n(x)$, is also called an exponential integral:

$$E_i(x) = \int_{-\infty}^x \frac{e^t}{t} dt, \quad x > 0 \quad (\text{Eqn 4.11})$$

Note that $E_i(-x)$ is related to $-E_1(x)$ by analytic continuation [223-224].

Thus a value for α can be calculated for any defined temperature T (degrees Kelvin) in air or in nitrogen by using kinetic parameters from TGA in air or nitrogen, and so the extent of decomposition at any estimated drop temperature can be compared to the degree of decomposition calculated from the experimental method explained elsewhere [200-214] using Eqn 4.6. It should be noted that here the predicted surface temperatures (using furnace dynamics in section 4.5) have only been used to simulate the degree of degradation using Eqn 4.9. The simulated results have then been compared with experimental results from TGA experiments. The simulations in air or nitrogen atmospheres have been carried out using kinetic parameters from respective TGA experiments in air or nitrogen atmospheres. In Figure 4.18 to Figure 4.29, the primary y-axis (left hand side) represents the furnace setting temperature during the experiments and simulations for each polymer type while the secondary y-axis (right hand side) represents the degree of degradation.

4.3.2.1 Results and analysis.

The degrees of degradation of different thermoplastic polymers as a function of temperature are calculated and modelled in air and nitrogen atmospheres. The results are shown in Figures 4.18 to 4.29 where drops temperatures range is also represented with the corresponding furnace setting temperatures (FST) mentioned in each graphs. The drops temperatures range and the FST are taken from Figure 4.10 to 4.15. The degrees of degradation (DOD) of the thermoplastic polymers estimated from these by reading the secondary axis of each graph in Figure 4.16 to 4.27. The results are also given in Tables 4.3.

a) Polypropylene (PP)

(i) In air atmosphere

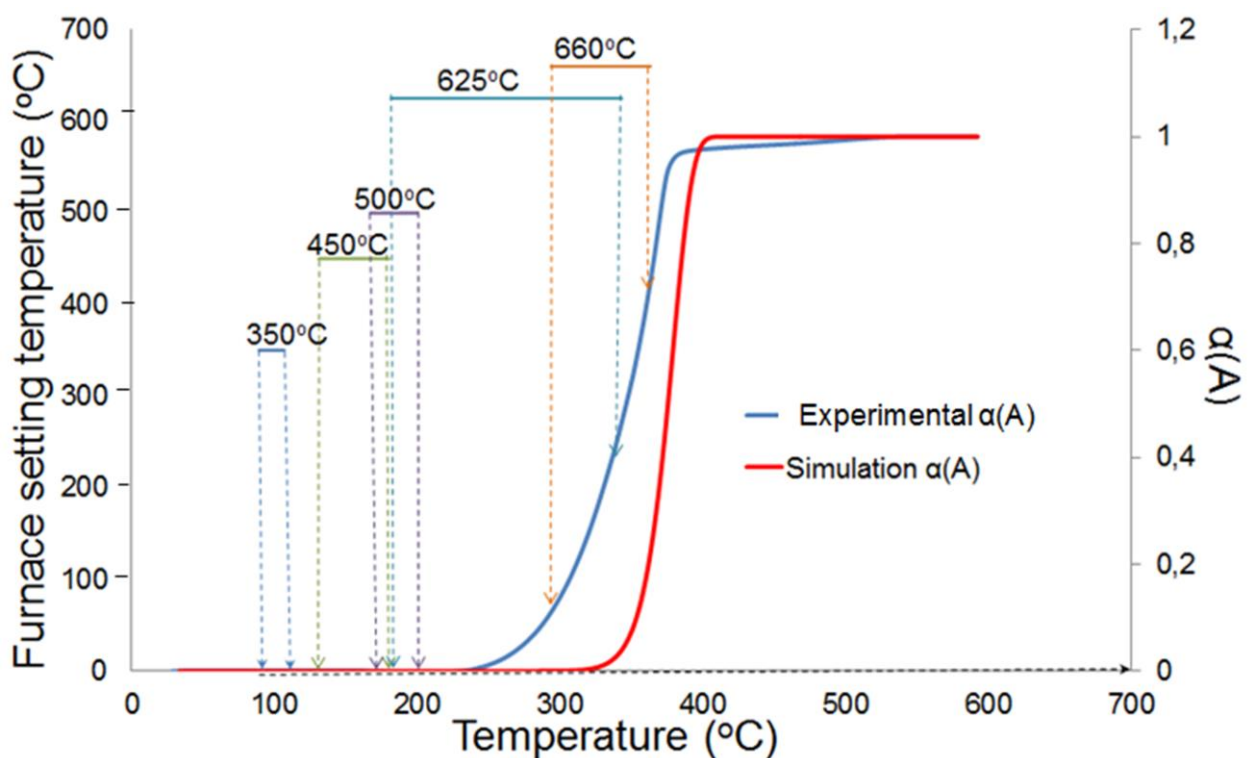


Figure 4.16: Experimental vs. simulation of degree of degradation in air atmosphere.

(ii) In nitrogen atmosphere

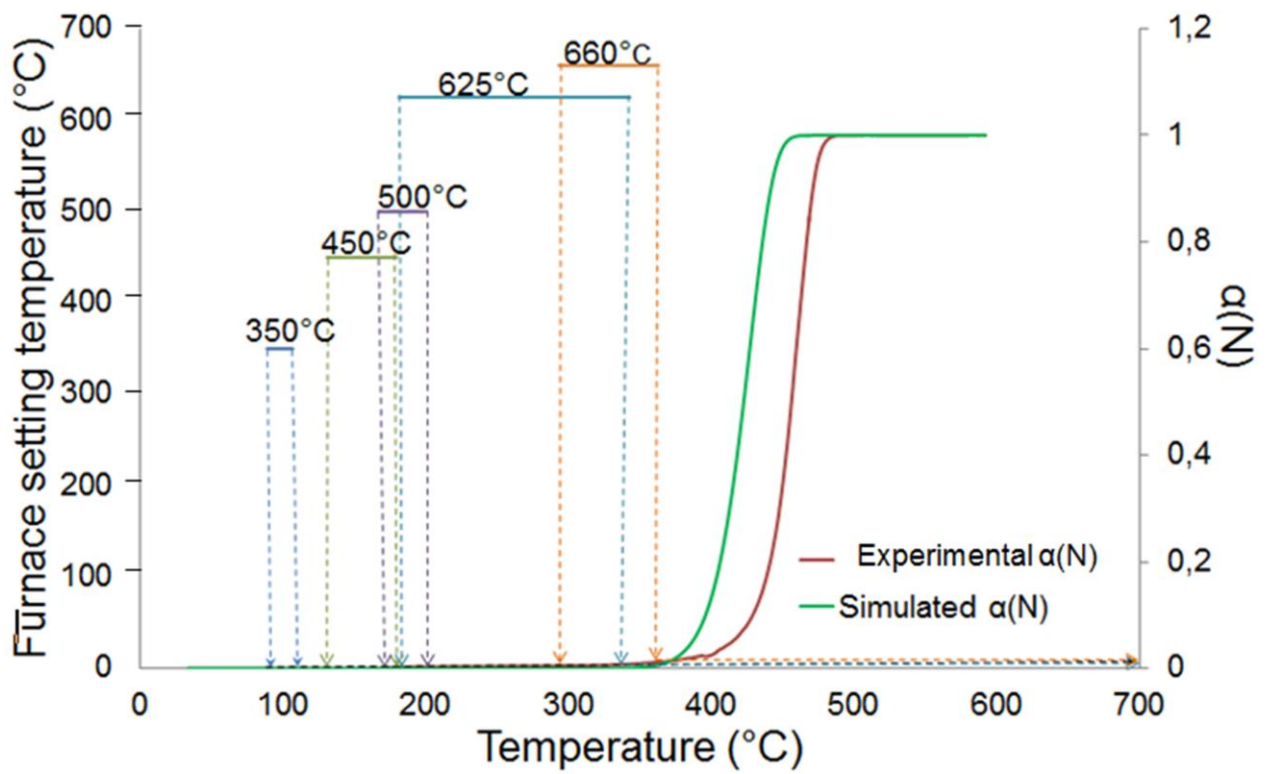


Figure 4.17: Experimental vs. simulation of degree of degradation in nitrogen atmosphere

b) Polymethyl Methacrylate (PMMA)

(i) In air atmosphere

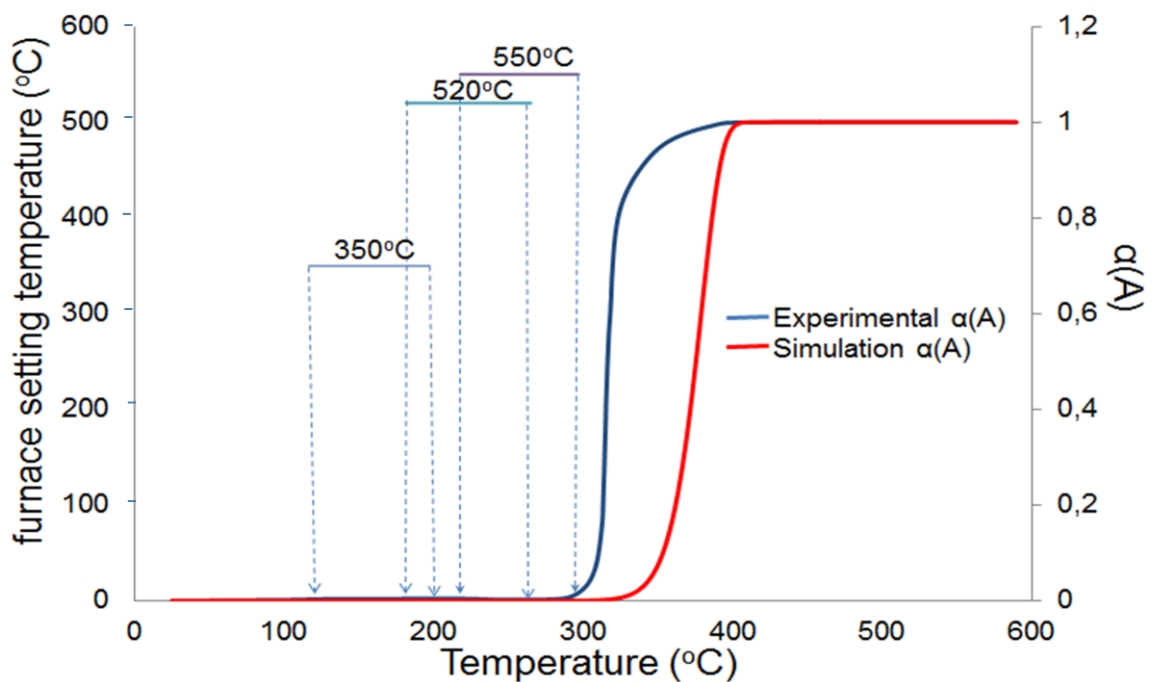


Figure 4.18: Experimental vs. simulation of degree of degradation in air atmosphere

(ii) In nitrogen atmosphere

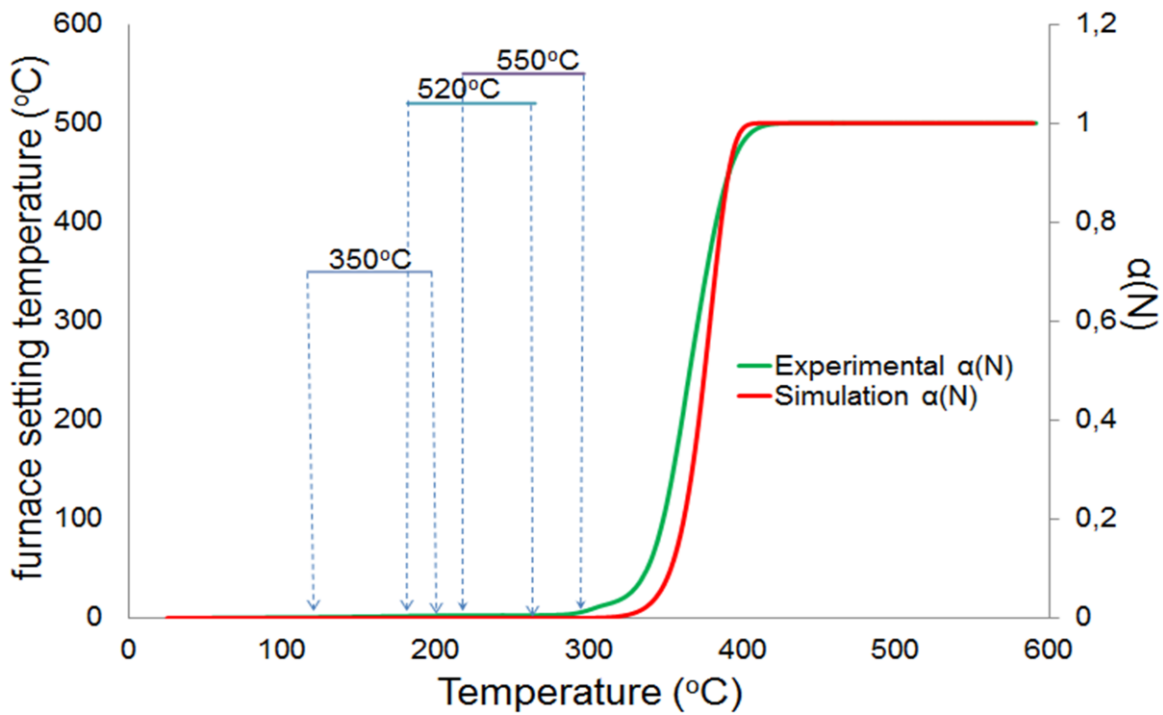


Figure 4.19: Experimental vs. simulation of degree of degradation in nitrogen atmosphere

c) Polyethylene Terephthalate (PET)

(i) In air atmosphere

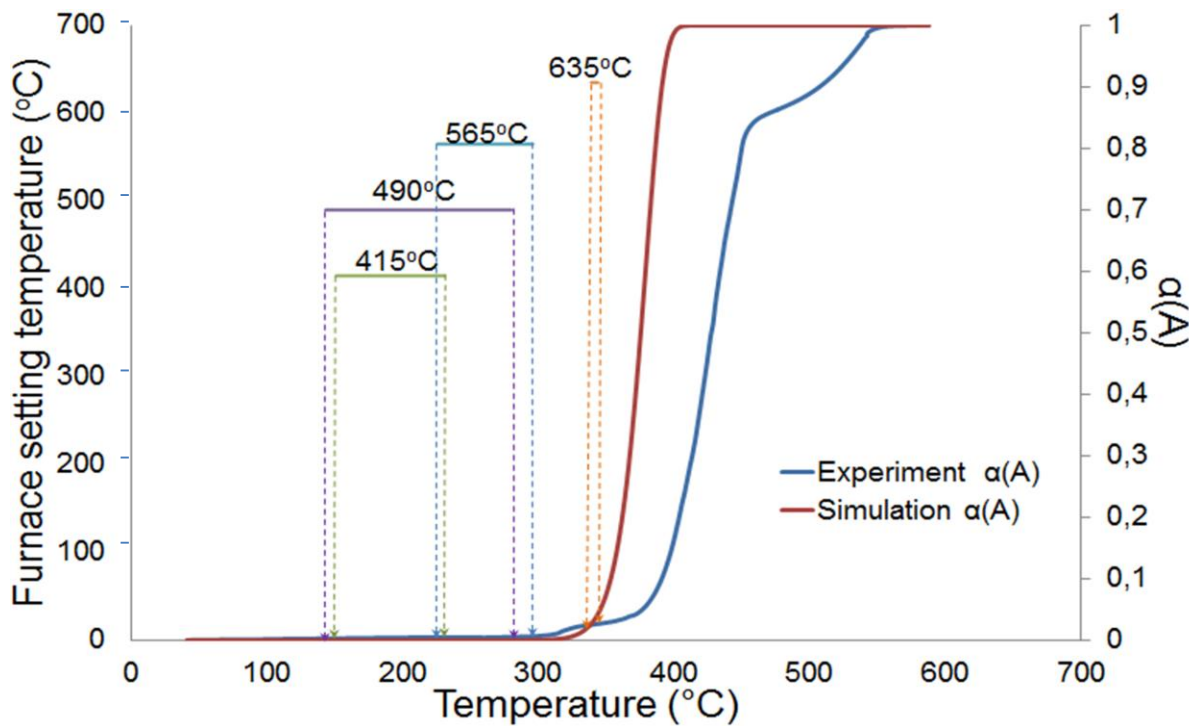


Figure 4.20: Experimental vs. simulation of degree of degradation in air atmosphere

(ii) In nitrogen atmosphere

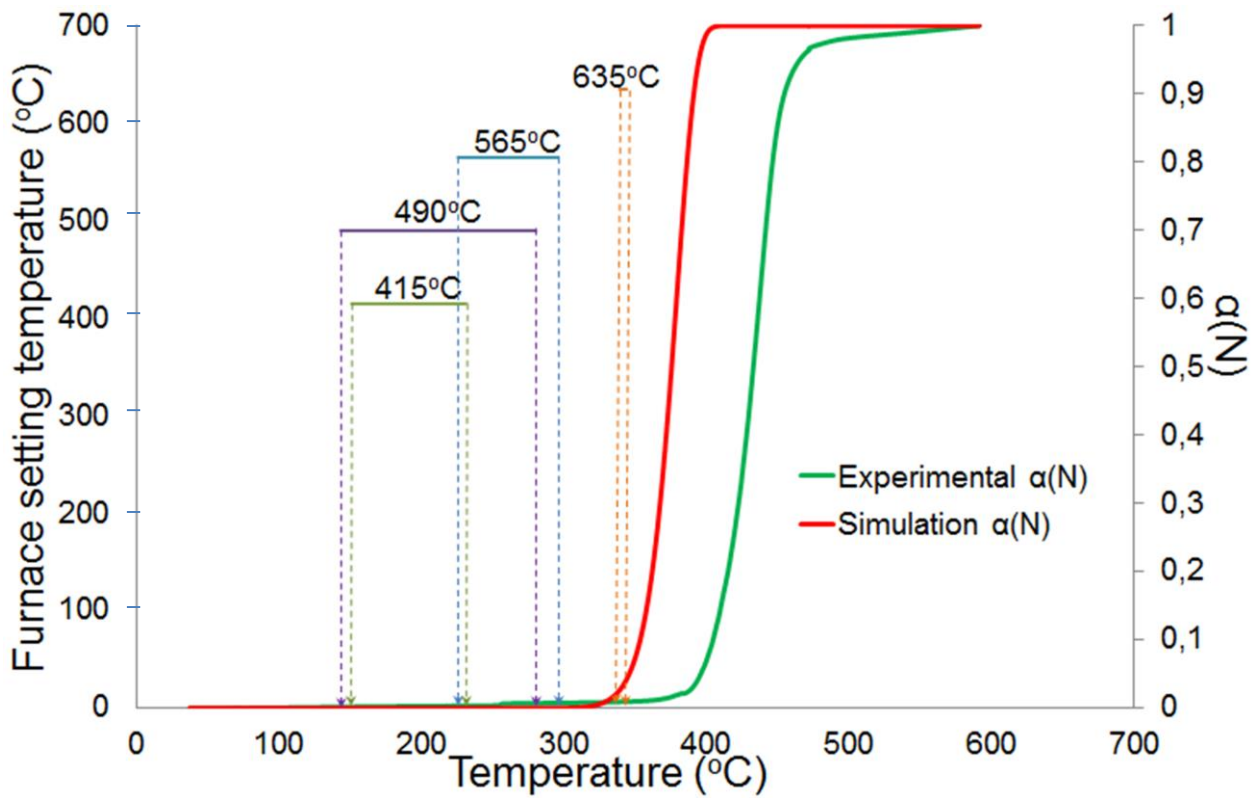


Figure 4.21: Experimental vs. simulation of degree of degradation in nitrogen atmosphere.

d) Nylon 6 (PA6)

(i) In air atmosphere

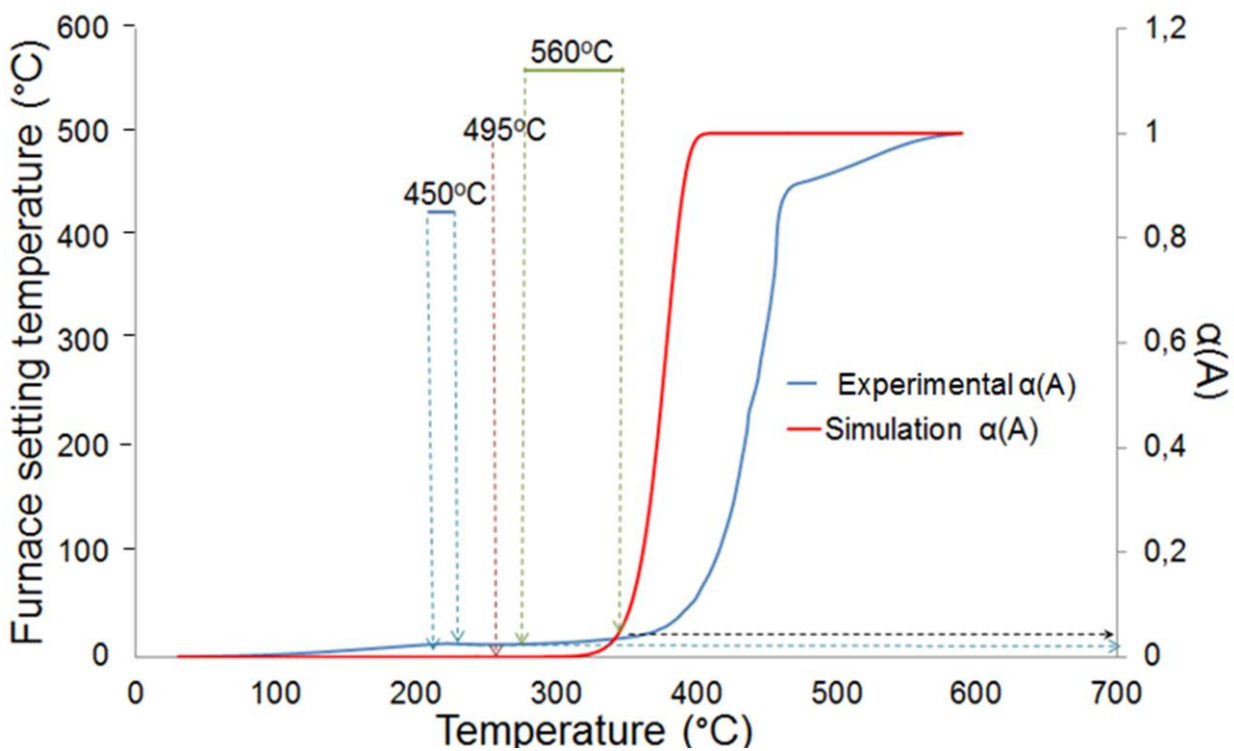


Figure 4.22: Experimental vs. simulation of degree of degradation in air atmosphere

(ii) In nitrogen atmosphere

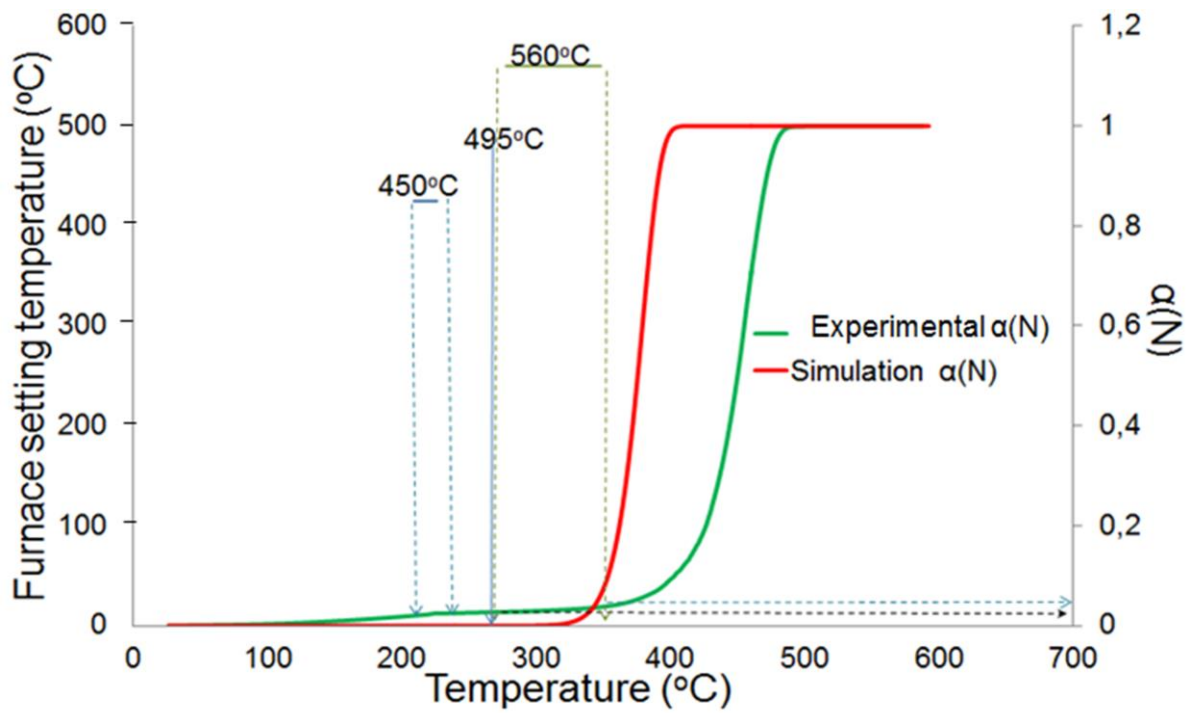


Figure 4.23: Experimental vs. simulation of degree of degradation in nitrogen atmosphere

e) Polycarbonate (PC)

(i) In air atmosphere

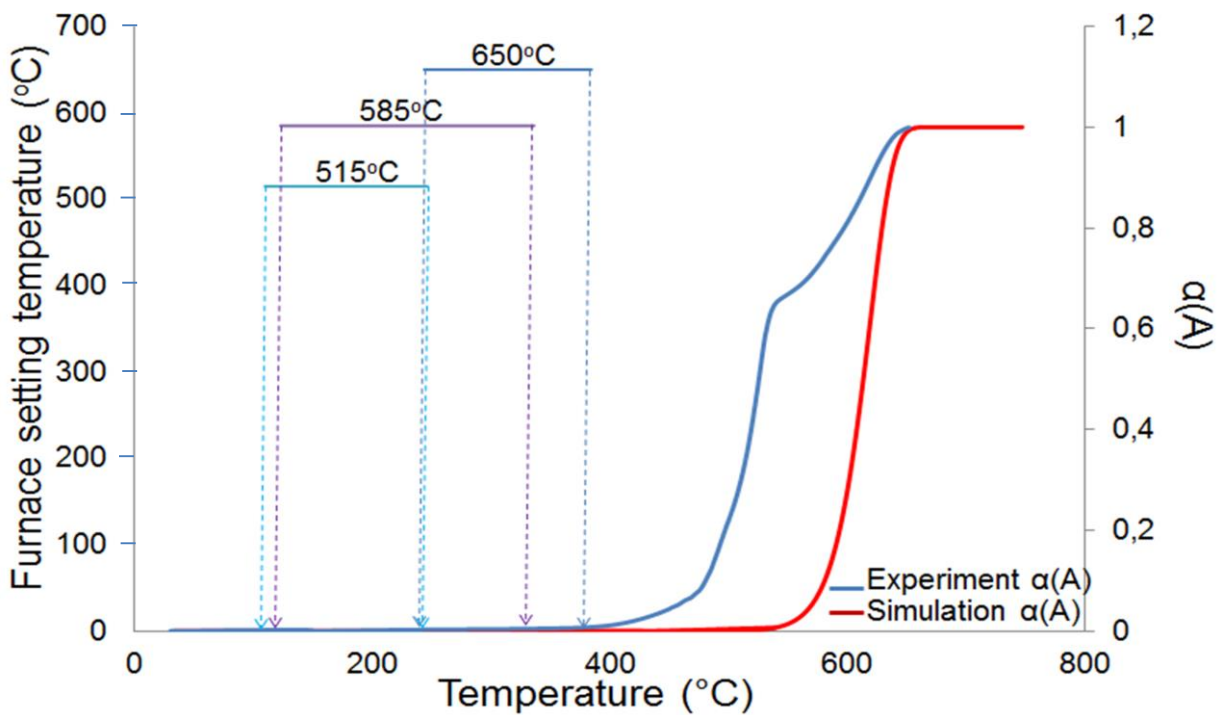


Figure 4.24: Experimental vs. simulation of degree of degradation in air atmosphere

(ii) In nitrogen atmosphere

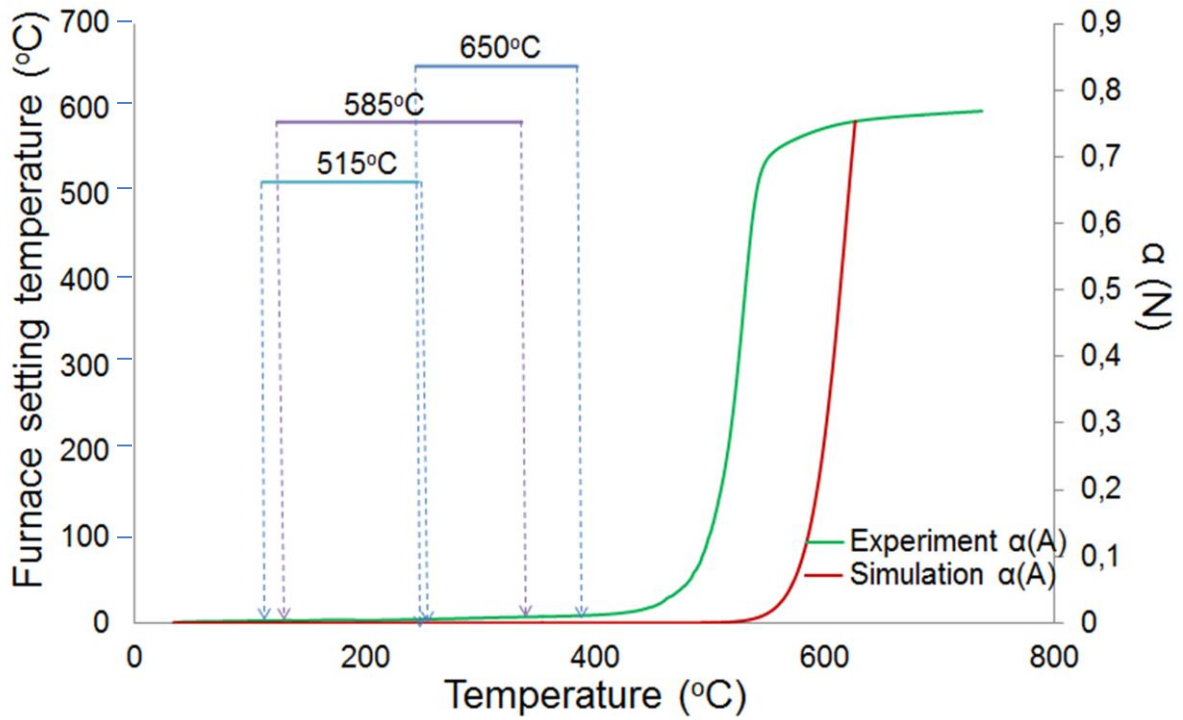


Figure 4.25: Experimental vs. simulation of degree of degradation in nitrogen atmosphere

f) Polystyrene (PS)

(i) In air atmosphere

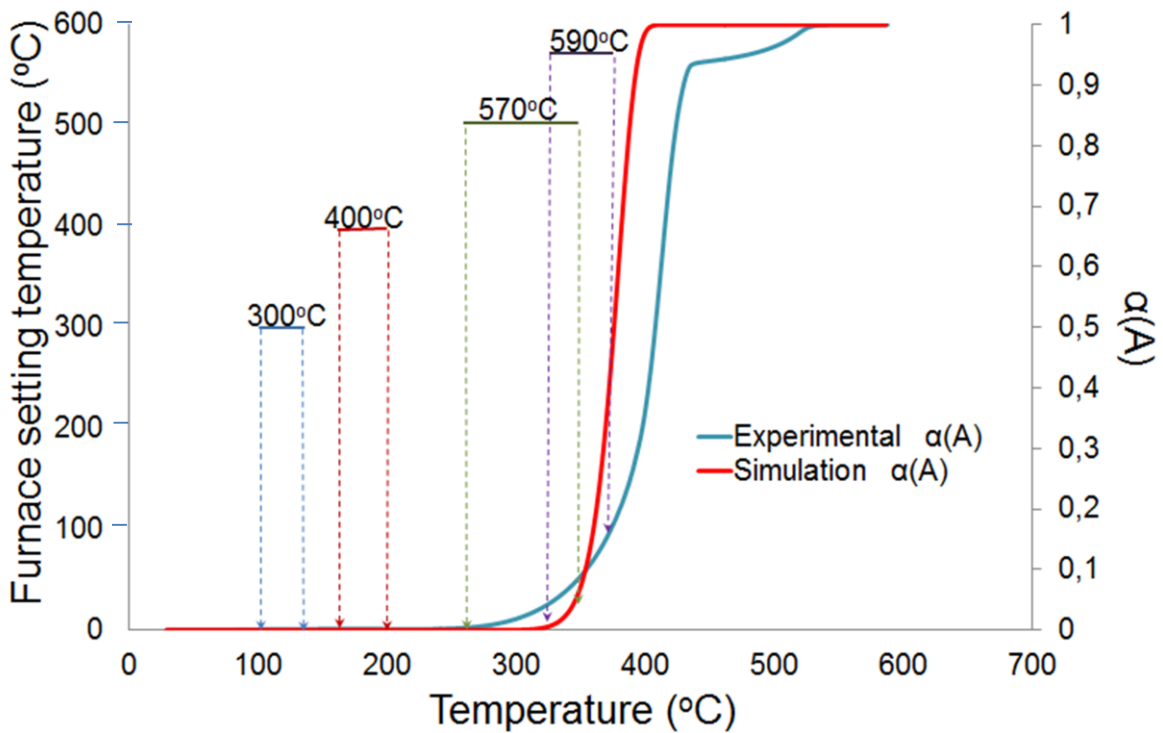


Figure 4.26: Experimental vs. simulation of degree of degradation in air atmosphere

(ii) In nitrogen atmosphere

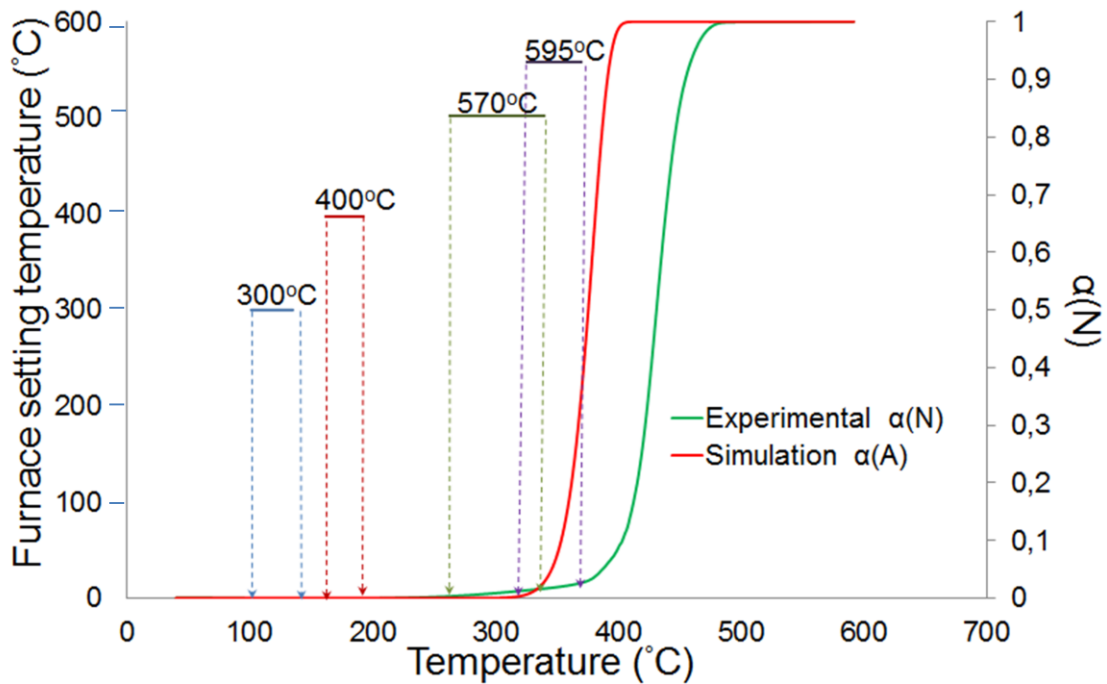


Figure 4.27: Experimental vs. simulation of degree of degradation in nitrogen atmosphere

For the six polymers considered (Figure 4.16 to 4.27) here, simulated values in both air and nitrogen are similar in shape and magnitude with those conducted experimentally; however, they are not in total agreement and there are some differences as expected due to the assumptions currently used. In the cases of PP in air and PC, PMMA in both air and nitrogen, the experimental curves preceded the theoretical curves by a gap of about 10-100°C, depending upon the polymer type. In case of PP in nitrogen and PA6, PET, PS in both air and nitrogen the predicted curves preceded the experimental ones. These discrepancies can be explained due to lack of accurate parameters at each temperature (Table 4.1a-d). In addition, differences between the two results are also related to the oxidation stage which takes place in air atmosphere as opposed to that when conducted in a nitrogen atmosphere. One-step decomposition of the thermoplastic samples is assumed in air as well for kinetic modelling, while in reality there are two stages, i.e., oxidation stage has been ignored for simplicity of modelling.

However, these observations, indicate that, although not precise, the estimation of 'α' the degree of decomposition using the temperatures predicted via the model can provide a good indication of the temperature of the molten drops and 'α' the degree of decomposition at the predicted molten drop temperature.

The summary of the analysed results of Figure 4.16 to 4.27 are given in Table 4.3 below, this shows that degradation occurs only for some furnace setting temperatures. The higher the furnace temperature for each polymer tested gives the larger degree of degradation. The difference between the experimental and the predicted values could be due to the degree of degradation being sensitive to small changes between the experimental and simulated values. It is worth noting however those both experimental and simulated curves follow the same trend as indicated in Figure 4.16 to 4.27 inclusive.

Polymers	Atmosphere	FST (°C)	Drops temperatures range (°C)	Degree of degradation range (%)	
				Experimental	Predicted
PP	Air	625	175-325	0-40	0-10
		660	300-350	0-70	0-40
	Nitrogen	N/A	N/A	N/A	N/A
PMMA	Air	550	175-200	0-2	0
	Nitrogen	N/A	N/A	N/A	N/A
PET	Air	635	350	0-5	0-5
	Nitrogen	N/A	N/A	N/A	N/A
PA6	Air	425	200-225	2	0
		495	275	2	0
		560	275-350	2-5	0-5
	Nitrogen	425	200-225	2-3	0
		495	275	3	0
		560	275-350	2-6	0-3
PC	Air	515	100-250	0	0
		585	125-350	0-0.5	0
		650	250-387	0-1	0
	Nitrogen	585	125-350	0-1	0
		650	250-387	0-2	0
PS	Air	570	275-350	0-10	0-5
		590	329-375	5-15	1-35
	Nitrogen	570	275-350	0-2	0-2
		590	329-375	1-3	0-35

Table 4.3: Degree of degradation in drops of the thermoplastic polymer from Figure 4.18 to 4.29.

4.3.2.2 Comments

In general Figures 4.16 to 4.27 above show results comparable in trend for predicted and measured degrees of degradation. However there are some differences between simulations and experimental values.

For PP in air and for PC and PMMA both in air and nitrogen atmosphere the experimental curves preceded the theoretical curves by a lag of about 10 to 50°C, the true value depending upon the polymer type. For PP in nitrogen atmosphere and for PA6, PET and PS both in air and nitrogen atmosphere the predicted curves preceded the experimental curves. These discrepancies can be explained due to lack of accurate parameters (Table 4.1a). These observations however, indicate that, although not precise, the estimation of ' α ' the degree of decomposition using the temperatures predicted via the model can provide a good indication of the temperature of the molten drops and ' α ' the degree of decomposition at the predicted molten drop temperature.

4.4. Conclusions

In this Chapter 4 a previously reported experiment for studying the melt dripping of polymers in the absence of a flame has been modified to also measure the temperature of the drops immediately after they fall from the heated polymer surface. The degree of any decomposition within the collected fallen drops was determined via TGA experiments. The temperature of the polymer surface has been estimated via a simple heat transfer model which thus provides an estimation of the molten drop temperature as it leaves the heated polymer surface. Estimation of the extent of the decomposition at the estimated temperatures can be compared to the equivalent experimental values obtained from TGA experiments on the collected molten drops. Discrepancies exist between the α vs temperature curves obtained via TGA with those calculated analytically. This is probably due to thermophysical parameters used, including only one step decomposition as opposed to multi steps obtained experimentally.

Chapter 5: Modelling melting, decomposition and combustion of horizontally oriented thermoplastic polymers

5.1 Introduction

In this chapter the study investigates the melting behaviour of three semi-crystalline thermoplastic polymers (polypropylene (PP), polyamide 6 (PA6) and polyethylene terephthalate (PET)) and attempts to identify the melting characters of different polymers on exposure to a radiant heat on one surface only in a cone calorimeter. Pure melting and melting plus partial decomposition may occur and the thermoplastic polymers can catch fire depending upon the degree of decomposition. Also a simulation model for polymer melting and decomposition including burning behaviour was developed to determine the melting point temperature and to estimate the temperature profile within the polymer slab. In this scenario the sample is contained in a horizontally oriented holder in order that the mass will not escape from the containment region. This typical problem is called the Stefan problem involving phase change solid-liquid, with reference to the early work of Wisniak and Stefan [225].

While most thermoplastic materials in consumer products are in the form of thin-walled shaped objects, this study has focused on thermally thick horizontal slabs heated by cone calorimeter radiation on one face only and the others being insulated so that it can be assumed a one-dimensional heat transfer within the sample from the top to the bottom. Also a sensitivity analysis [226] was performed to determine the thermophysical properties that have the greatest influence on the melting process of the studied thermoplastic polymers. The cone calorimeter experimental results obtained in Chapter 3 Section 3.2.4 are used to validate the numerical model results computed by Matlab software. Based on the good agreement between experimental and predicted temperature profiles, the validated numerical model could be potentially used to substitute expensive lab experiments. Thus any set of simulations can be completed easily to obtain a better understanding of the physical process of thermoplastic melting.

5.2 Mathematical modelling

5.2.1 Model description

The schematical model description of horizontal thermoplastic polymer slab is shown in Figure 5.1 below. For one-dimensional modelling purposes, the sample is subjected to an incident heat flux $q(t)$ on the top face only. Gradually the surface begins to melt and the interface (boundary region) with the solid polymer is moving. This moving boundary condition

is typical to Stefan phase change problem. Due to the number of parameters and the complexity of the boundary conditions to take into account the balance equation describing the situation is solved numerically to find an approximate solution of the temperature distribution $T(x, t)$ within the slab. The numerical method used to approximate the differential equations is the Finite Difference Method (FDM) computed in Matlab software by writing the appropriate programme code. The molten-solid interface temperature is assumed to be the temperature T_m of pure melting or melting plus partial decomposition or the ignition temperature when the thermoplastic sample catches fire.

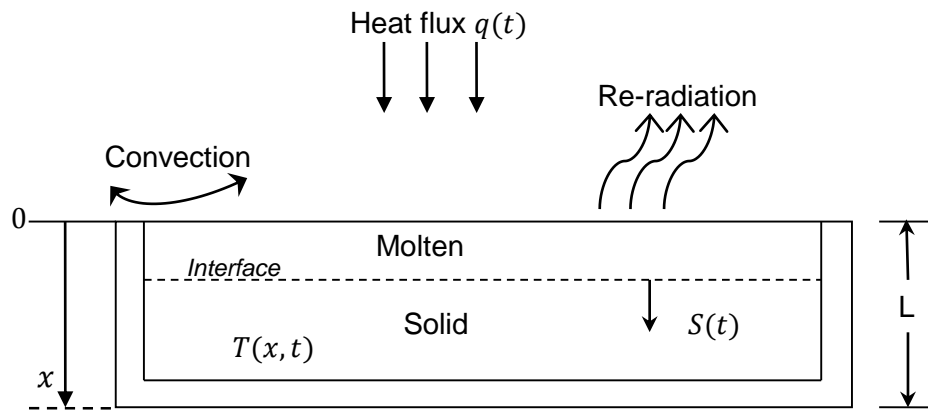


Figure 5.1: Horizontal thermoplastic slab insulated at the sides

In order to set up a mathematical model some assumptions have to be taken: (1) once the surface temperature reaches the decomposition temperature T_p , the resultant products will immediately volatilise and be ignited by the ignition source, i.e., the ignition temperature T_{ign} is assumed to be same as the decomposition temperature T_p ; (2) the decomposition process only takes place at the upper layer and there will be no mass transportation within the polymer; (3) the thickness of the interface layer between the melt and the solid phases is zero while in each phase polymers specific heat and thermal conductivity increase with increasing temperatures [227-228]. Thus, the thermal properties in the two different phases are assumed to be different and the temperature gradient in the melt phase would be lower than that in the solid layer; (4) only one dimensional heat transfer is considered therefore except for the upper surface the other sides are treated as insulated.

Since this study concerns a phase change processes, the phase change material has a constant melting temperature T_m and latent heat H_L . Each phase has thermal conductivity k_L or k_S and specific capacity c_{pL} or c_{pS} which are phase-wise constant but with $k_L \neq k_S$; and

$c_{pL} \neq c_{pS}$. The subscript 'l' and 's' denote the liquid and the solid phase. Furthermore it is assumed that heat is transferred isotropically (i.e. equal in all directions). The interface separating each phase is assumed to be sharp, planar, without surface tension and of zero thickness [168-172].

5.2.2 Model formulation

The heat transfer by conduction of the model shown schematically in Figure 5.1 above is described mathematically by the balance equation Eqn 5.1 to be solved for $T(x, t)$ [229-230]:

$$\rho(T)c_p(T) \frac{\partial T(x, t)}{\partial t} = k(T) \frac{\partial^2 T(x, t)}{\partial x^2} + \dot{m} (H_c - H_L - H_g) \quad (\text{Eqn 5.1})$$

Where: $\rho(T)$ is the polymer density, $c_p(T)$ is the polymer specific heat capacity, $k(T)$ is the polymer specific conductivity, \dot{m} is the rate of mass phase change, H_L is the latent heat of melting, H_g is the enthalpy of pyrolysis and H_c is the enthalpy of combustion.

The boundary condition is for an imposed flux $q(t)$:

$$-k(T) \frac{\partial T(0, t)}{\partial x} = q(t), \quad -k(T) \frac{\partial T(L, t)}{\partial x} = 0$$

The thermoplastic polymer sample is composed of two phases: liquid and solid phase separated by an interface $S(t)$, see Figure 5.1, which illustrates the model description. The polymer slab is isolated on its sides to have a one-dimensional slab with a thickness L where phase change process, decomposition and ignition are undergoing. For liquid phase and solid phase Eqns 5.1 becomes respectively [200, 213, 231]:

$$\frac{\partial T(x, t)}{\partial t} = \alpha_l \frac{\partial^2 T(x, t)}{\partial x^2} + \dot{m} (H_c - H_L - H_g) \quad , \quad 0 < x < S(t) \quad (\text{liquid phase})$$

$$\frac{\partial T(x, t)}{\partial t} = \alpha_s \frac{\partial^2 T(x, t)}{\partial x^2} - \dot{m} (H_L + H_g) \quad , \quad S(t) < x < L \quad (\text{solid phase})$$

Where:

$$\alpha_l = \frac{k_l}{\rho c_l} \quad \text{and} \quad \alpha_s = \frac{k_s}{\rho c_s}$$

The subscript 'l' and 's' denoting the liquid or the solid phase, α_l and α_s are the diffusivity in liquid phase and solid phase. The expression of the velocity \dot{S} of the interface $S(t)$ is proportional to the jump of the heat flux across the interface liquid/solid and it is given by:

$$\rho\dot{S}(t)H_L = k_s(T) \frac{\partial T(S(x), t)}{\partial x} - k_l(T) \frac{\partial T(S(x), t)}{\partial x}, \quad S(t) < x < L$$

Where L is the sample thickness and $\dot{S}(t)$ is the velocity of the moving interface. The material is initially solid at an ambient temperature T_a . Since an incident flux $q(t)$ is applied at $x = 0$, melting occurs when $T = T_m$, T_m being the melting temperature. At the insulated side $x = L$ the heat transfer by conduction is equal to zero where the temperature is assumed to be at ambient temperature T_a . When $t > 0$, the liquid state of the polymer occupies the space $[0; S(t))$ if $T = T_m$ while the solid state occupies $(S(t); L]$ if $T < T_m$. This leads to the two-phase Stefan problem. The initial, the interface and the boundary conditions are:

Initial conditions:

$$S(0) = 0 \quad (\text{material initially solid})$$

and,

$$T(x, 0) = T_a, \quad \text{for } 0 < x < L.$$

Interface conditions:

$$T(S(t), t) = T_m \quad \text{for } t > 0$$

and,

$$\rho\dot{S}H_L = k_s(T) \frac{\partial T(S(x), t)}{\partial x} - k_l(T) \frac{\partial T(S(x), t)}{\partial x}, \quad \text{for } t > 0.$$

where:

$$\dot{S} = -\beta \frac{\partial T(S(x), t)}{\partial x} \quad (\text{Eqn 5.2})$$

and:

$$\beta = \frac{k_s - k_l}{\rho H_L}$$

Boundary conditions:

$$T(0 < x < S(t), t) = T_m \text{ or } T_{ign}, \quad \text{for } t > 0,$$

and,

$$T(l, t) = T_a$$

5.2.3 Numerical methodology for temperature prediction.

The following algorithm solves numerically the heat equation associated with the moving boundary due to a phase change by melting. For each time step [7]:

Update the temperature distribution using an explicit scheme of the Finite Difference Method (FDM) in heat equation, *Eqns 5.1*:

$$\frac{T_i^{t+\Delta t} - T_i^t}{\Delta t} = \alpha \frac{T_{i-1}^t - 2T_i^t + T_{i+1}^t}{(\Delta x)^2} \quad (\text{Eqn 5.3})$$

Denote the space discretisation is $(0, \Delta x, 2\Delta x, \dots, n\Delta x)$ and at time t let $L = n\Delta x$ be the greatest discretisation point below $S(t)$ and the vector $T(t) = [T_1(t) \cdots T_n(t)]^T$ as the temperature vector in discretisation points: $T(t) = [T(0, t) \cdots T(n\Delta x, t)]^T$. Now *Eqns 5.3* becomes:

$$\begin{bmatrix} T_1^{t+\Delta t} \\ T_2^{t+\Delta t} \\ \vdots \\ \vdots \\ T_i^{t+\Delta t} \\ \vdots \\ \vdots \\ T_n^{t+\Delta t} \end{bmatrix} = \begin{bmatrix} T_1^t + \frac{\alpha\Delta t}{(\Delta x)^2}(-T_1^t + T_2^t) + \frac{\dot{m}\Delta t}{\rho_l c_l}(H_c - H_L - H_g) \\ T_2^t + \frac{\alpha\Delta t}{(\Delta x)^2}(T_1^t - 2T_2^t + T_3^t) - \frac{\dot{m}\Delta t}{\rho_l c_l}(H_L + H_g) \\ \vdots \\ \vdots \\ T_i^t + \frac{\alpha\Delta t}{(\Delta x)^2}(T_{i-1}^t - 2T_i^t + T_{i+1}^t) - \frac{\dot{m}\Delta t}{\rho_l c_l}(H_L + H_g) \\ \vdots \\ \vdots \\ T_n^t + \frac{\alpha\Delta t}{(\Delta x)^2}(T_{n-1}^t - T_n^t) - \frac{\dot{m}\Delta t}{\rho_l c_l}(H_L + H_g) \end{bmatrix}$$

By separating terms with $T(t)$ from terms with $T(t + \Delta t)$ Eqns 5.3 can now be solved for $T(t + \Delta t)$.

Update the boundary state using an explicit scheme of the Finite Difference Method (FDM) in eqn5.2:

$$\frac{S_x^{t+\Delta t} - S_x^t}{\Delta t} = -\beta \frac{T_x^t - T_{x-\Delta x}^t}{\Delta x}$$

Denote the space discretisation is $(0, \Delta x, 2\Delta x, \dots, n\Delta x)$ and at time t let x_0 be the discretisation point below $S(t)$. The finite difference approximation of the derivative of $T(S(t), t)$ between $(x_0 - \Delta x)$ and x_0 is:

$$\frac{\partial T(S(x), t)}{\partial x} \approx \frac{T(x_0, t) - T(x_0 - \Delta x, t)}{\Delta x} = \frac{T_{x_0}^t - T_{x_0-\Delta x}^t}{\Delta x} \quad (\text{Eqn 5.4})$$

The choice of discretisation points in the calculation of the finite difference in the boundary moving step is crucial for stability issues. The most natural choice for the space discretization points would be the boundary value and the one before the boundary, but this choice leads to unstable values of the derivative of the temperature T with respect to x . Therefore the two last discretisation points before the boundary have to be used to better approximate the derivative. Eqns 5.1 is solved by writing the appropriate code using Matlab software according to the Finite Difference Method mentioned above and the pre-set Matlab programme algorithm is as following:

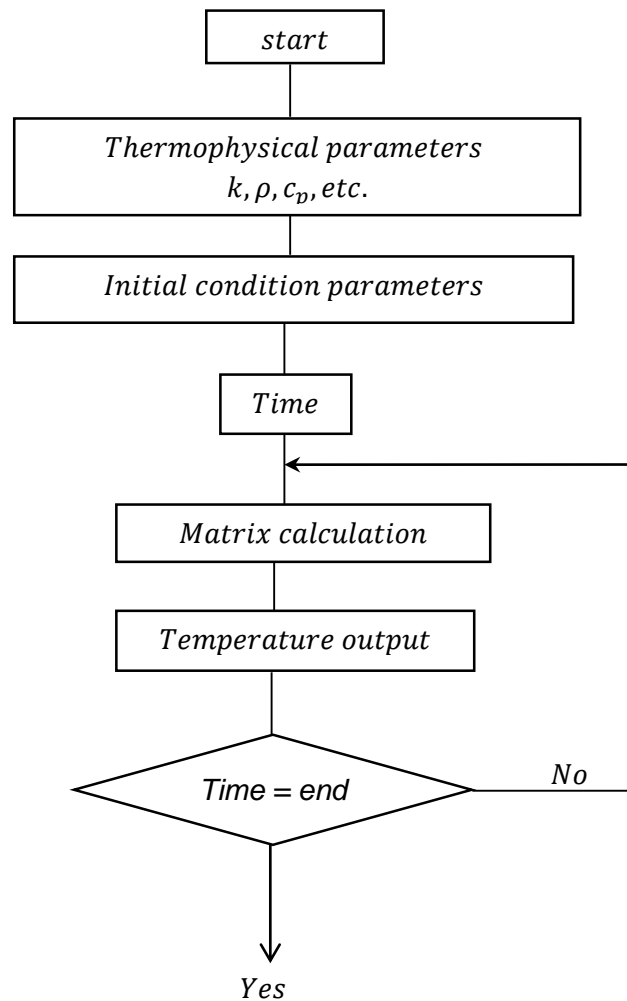


Figure 5.2: Matlab programme algorithm

5.3 Simulations and sensitivity analysis

The model was run using different values of thermal conductivity k and heat capacity C_p to obtain temperature profiles at the surface of PP, subjected to 35kW/m^2 external heat flux on the surface of the polymer slab.

It is well known that the specific thermal conductivity k and the specific heat capacity C_p vary with temperature as shown in Table 4.1 in Chapter 4 at Section 4.2.3. The values of k ($0.12\text{ W/m}\cdot^\circ\text{C}$) and C_p ($1.622\text{ kJ/kg}\cdot^\circ\text{C}$) in Table 4.1 for PP are considered in the process of performing the sensitivity analysis. The first step is to vary by $\pm 10\%$ these values of k and C_p up to $\pm 30\%$ and to look at the impact in the temperatures output in function of time. The simulated result as temperature versus time curves is shown in Figure 5.3 and 5.4 below:

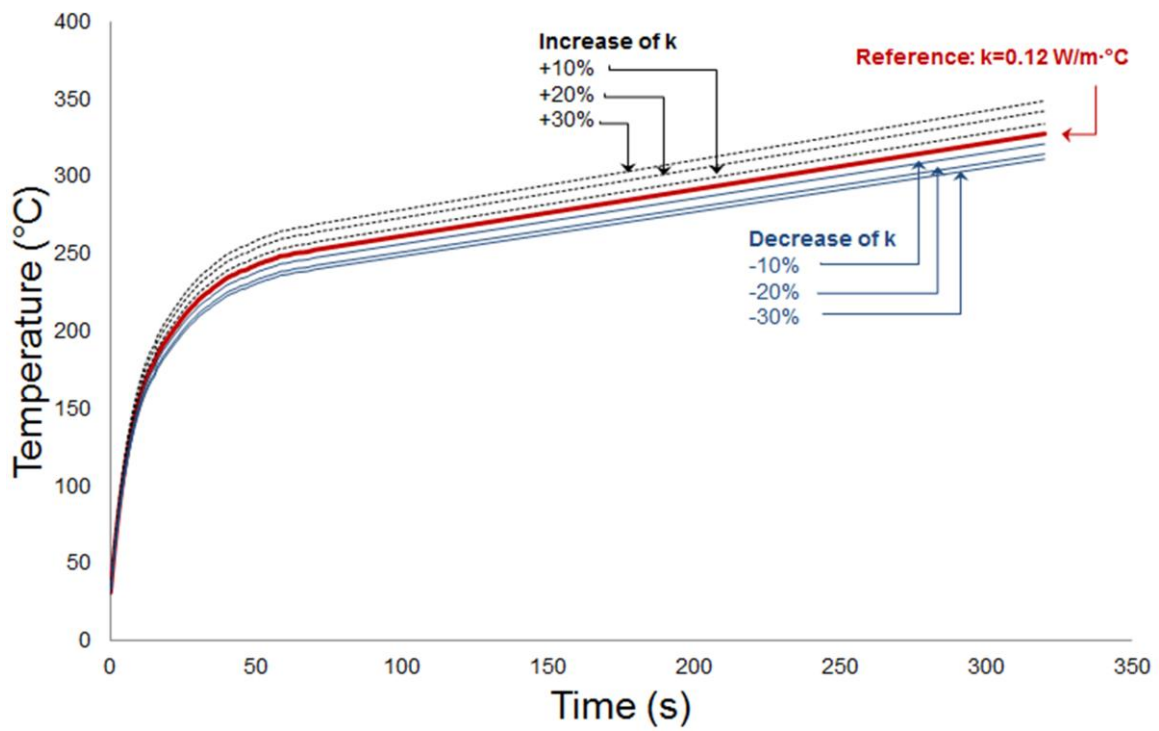


Figure 5.3: PP- Change of surface temperature versus time when the thermal conductivity is increased or decreased by 10% up to 30%.

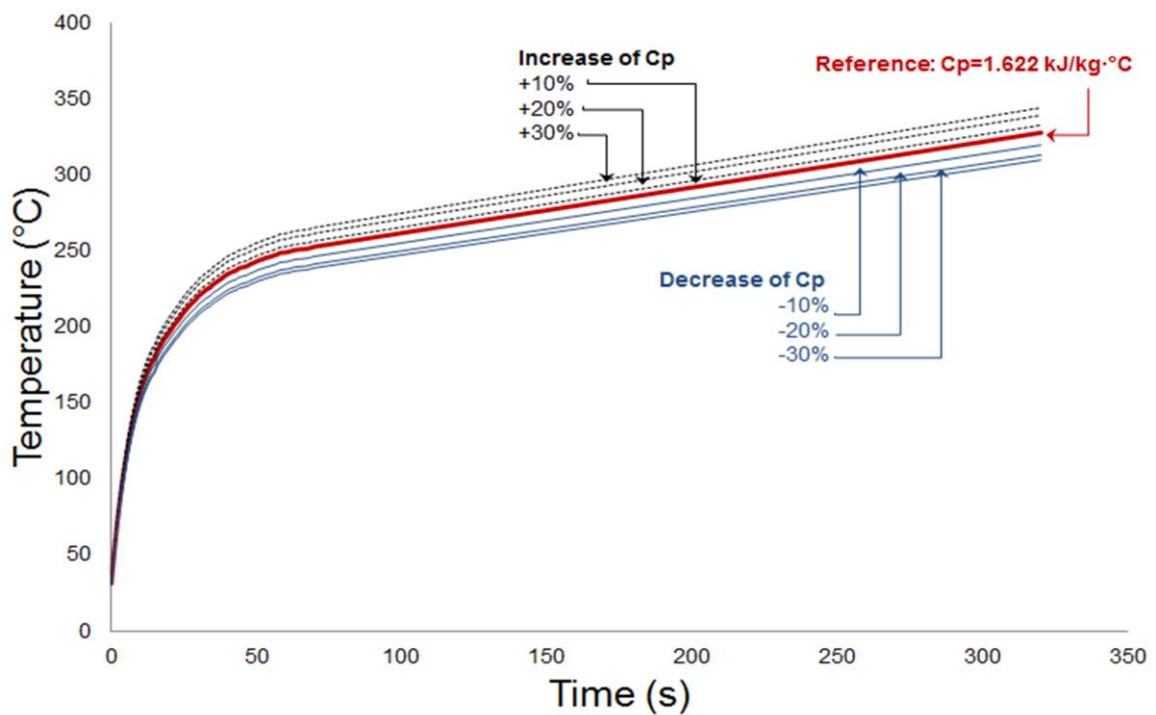


Figure 5.4: PP- Change of surface temperature versus time when the heat capacity is increased or decreased by 10% up to 30%.

The second step is to carry out a sensitivity analysis based on the 'normalised sensitivity function' which indicates the ratio between the change in percentage of k or Cp as an input and the change in percentage of the temperature profile as an output. The sensitivity function is defined as [226]:

$$S(T, k) = \frac{dT}{dk} \cdot \frac{k}{T}$$

And,

$$S(T, C_p) = \frac{dT}{dC_p} \cdot \frac{C_p}{T}$$

Where k, Cp, $\frac{dT}{dk}$ and $\frac{dT}{dC_p}$ are respectively the heat conductivity, the heat capacity, the temperature gradient related to the conductivity and the temperature gradient related to the heat capacity.

The results obtained after carried out the sensitivity analysis are shown in Figures 5.5 and 5.6 below that indicate respectively the changes of temperatures profile when the thermal conductivity or the heat capacity is increased or decreased by 10% up to 30% from their reference values; k=0.12 W/m·°C) and Cp=1.622 kJ/kg·°C.

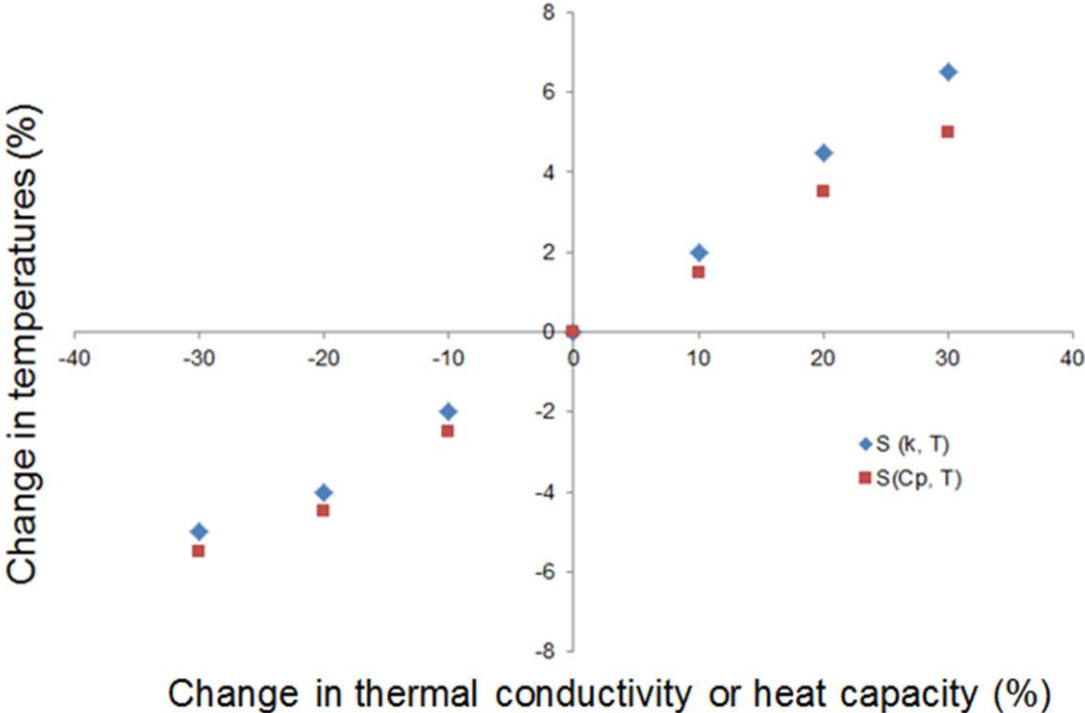


Figure 5.5: Change in temperatures (%) when the thermal conductivity (k) or the heat capacity (Cp) changes by +/- 10% up to 30%.

5.3.3 Analysis and comments

From the foregoing results shown in Figures 5.3, 5.4 and 5.5 the following observations are noticed:

The surface temperature of the polymer increases or decreases when thermophysical parameters, specific thermal conductivity (k) and specific heat capacity (C_p), increase or decrease.

The specific thermal conductivity (k) influences the output temperature profile more than the specific heat capacity. Figure 5.5 shows that the ratio given by the sensitivity analysis is around 0.2 for k and C_p which means for example the change of 10% of k or C_p induces a change of approximately 2% in the temperature profile. Therefore in order to obtain accurate temperature profiles, accurate parameters are required.

5.3.4 Simulation results

Using the generating Matlab code and the thermophysical properties in Table 4.1 all predicted temperature profiles are shown below in Figures 5.6 to 5.11.

Figure 5.6, 5.8 and 5.10 show the simulated profile temperatures using a Matlab without the implementation of the condition of ignition while Figure 5.7, 5.9 and 5.11 show the predicted profile temperatures with the ignition condition based on ignition temperature defined as following [72-232]:

$$T_{ign} \approx \left[\frac{T_0 h_g}{c_0} \right]^{\frac{1}{2}}$$

Where c_0 is the heat capacity of the solid at $T_0 = 298$ K and h_g is related to the heat of gasification per unit mass of volatile.

Also shown in the same Figures are the melting temperatures measured by DSC and the decomposition temperature (when 5% of the polymer degradation is observed) measured by TGA as mentioned in Chapter 3 Table 3.1.

a) Polypropylene (PP)

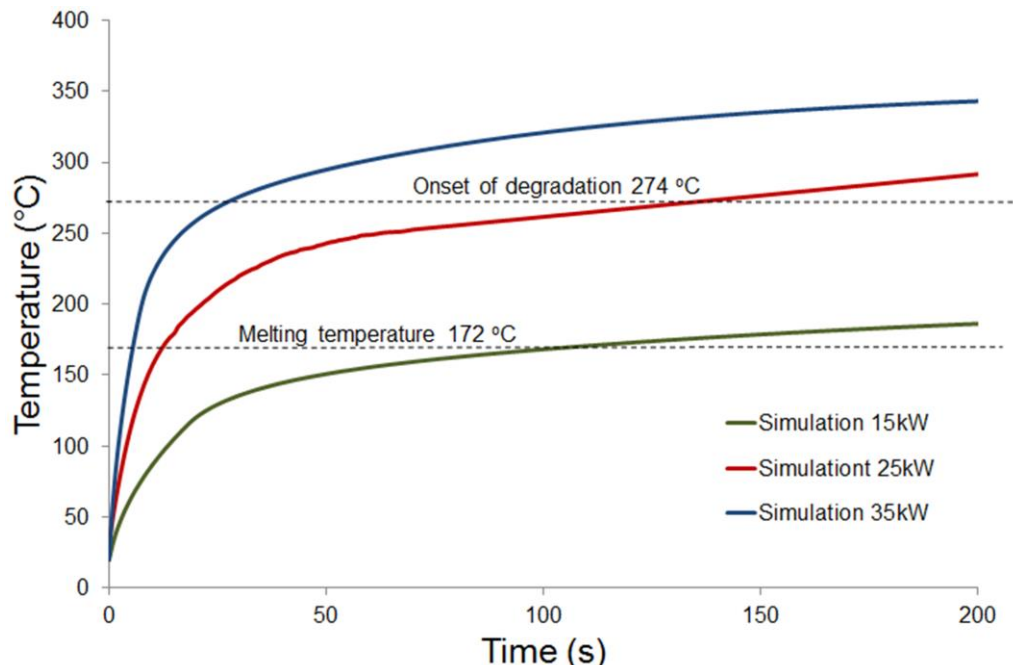


Figure 5.6: PP-Simulated surface temperature exposed to 15, 25 and 35kW/m² heat fluxes (ignition is not predicted).

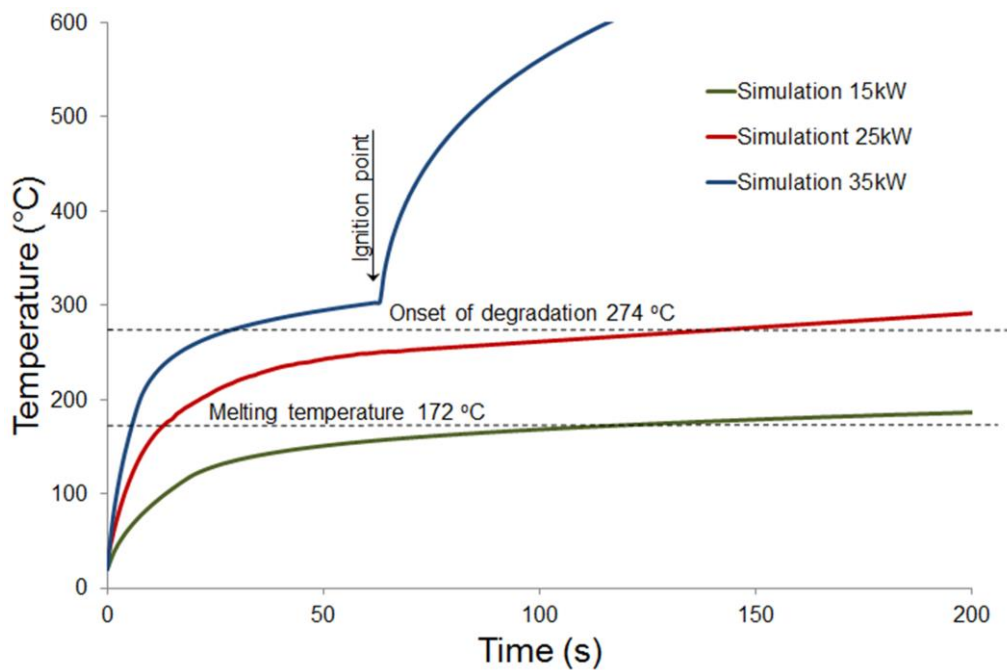


Figure 5.7: PP-Simulated surface temperature exposed to 15, 25 and 35kW/m² heat fluxes (ignition is predicted).

b) Polyamide 6 (PA6),

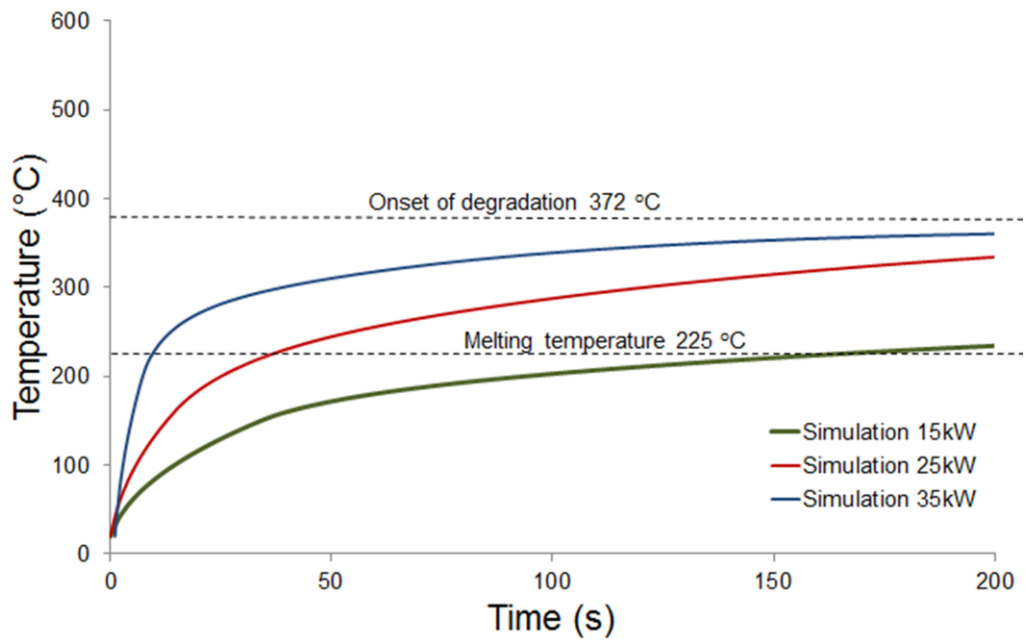


Figure 5.8: PA6- Simulated surface temperature exposed to 15, 25 and 35kW/m² heat fluxes (ignition is not predicted).

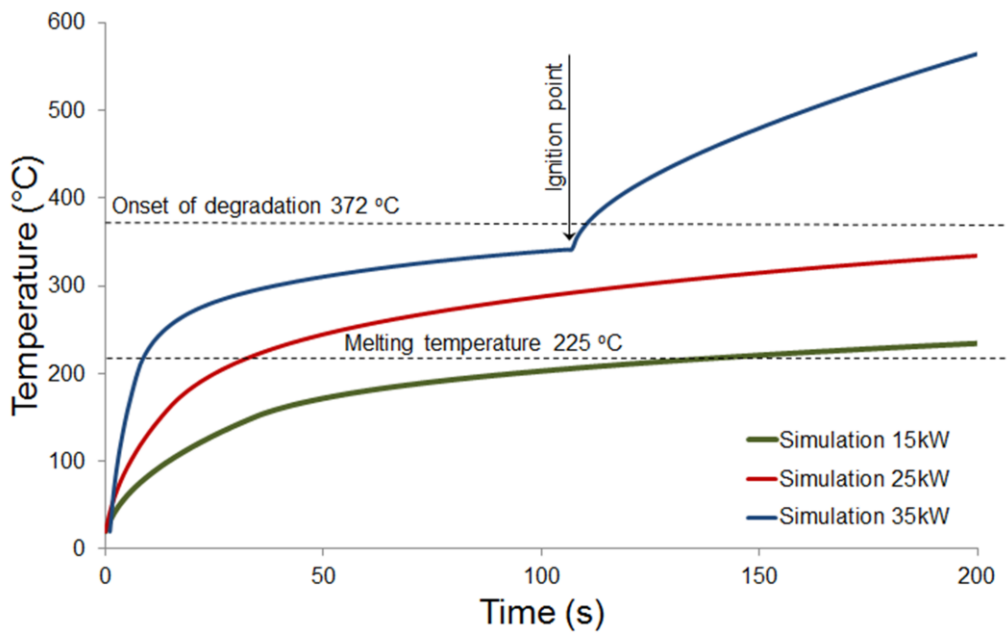


Figure 5.9: PA6- Simulated surface temperature exposed to 15, 25 and 35kW/m² heat fluxes (ignition is predicted).

c) Polyethylene terephthalate (PET),

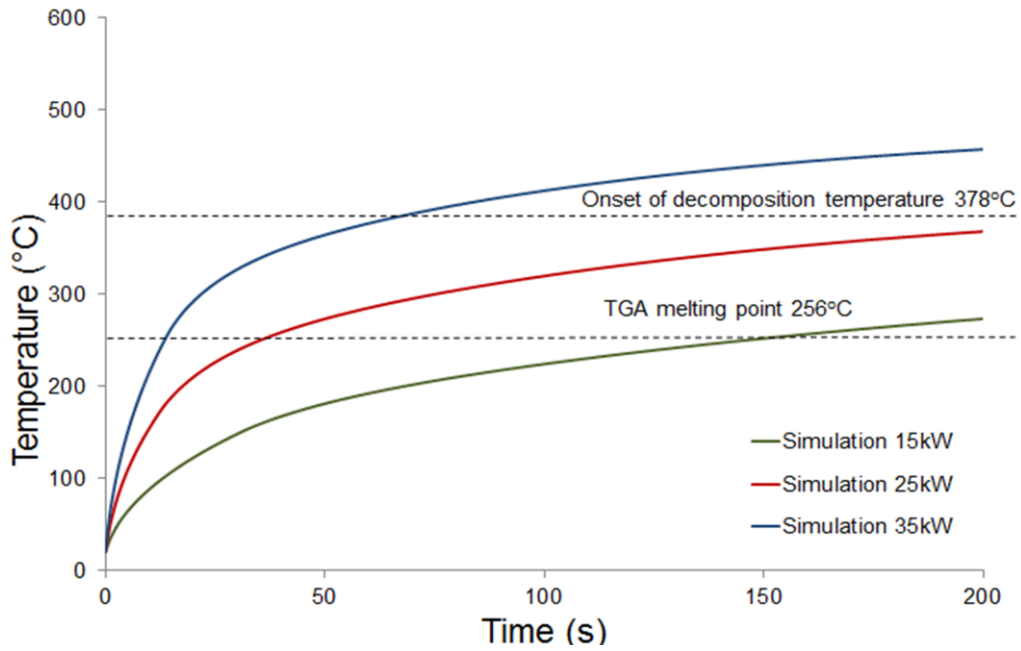


Figure 5.10: PET-Simulated surface temperature exposed to 15, 25 and 35kW/m² heat fluxes (ignition is not predicted).

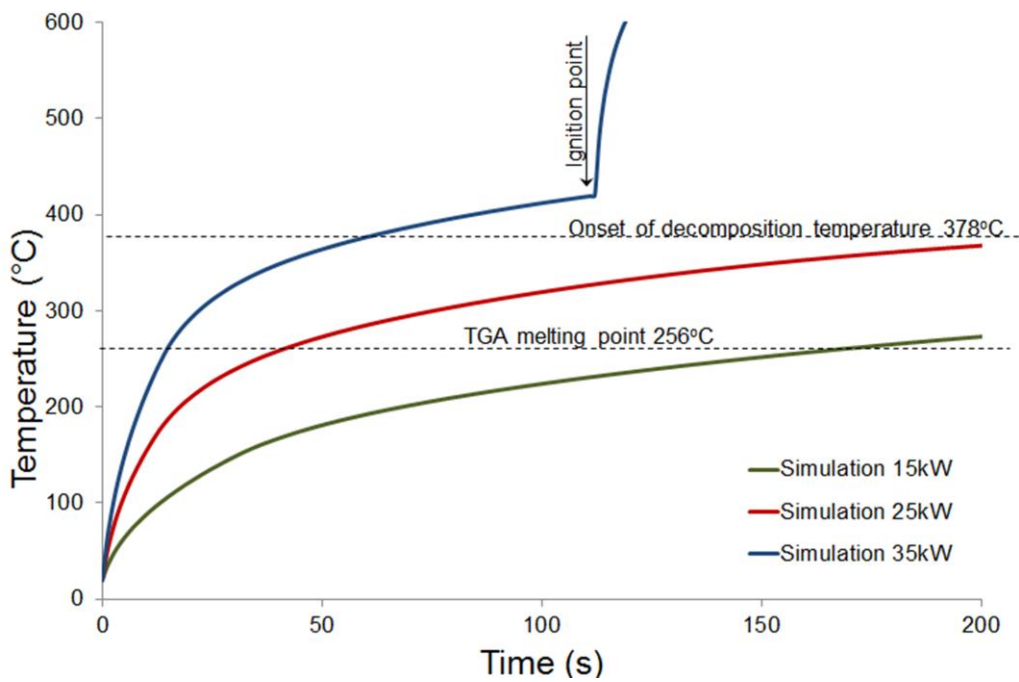


Figure 5.11: PET- Simulated surface temperature exposed to 15, 25 and 35kW/m² heat fluxes (ignition is predicted).

5.3.5 Analysis and comments

All Figures show that temperature of each polymer is not higher than the theoretical melting temperature of the polymer at an incident heat flux of 15kW/m^2 . When the heat flux is increased to 25kW/m^2 ; PP temperature is higher than the theoretical melting temperature after 150s while PA6 and PET temperature are between theoretical melting temperature and decomposition temperature. For an incident heat flux of 35kW/m^2 , PP temperature goes up to the theoretical decomposition temperature after 30s and PET temperature after 60s. But PA6 will not reach the theoretical decomposition temperature even if the polymer ignites after 100s. PP and PET start burning respectively after 60s and 110s.

5.4 Model validation

5.4.1 Comparison between experiment and simulation

A reliable and successful mathematical model is considered to be an input-output system capable of generating similar results to those obtained by carrying out lab experiments. The model validation test consist on comparing predicted results obtained from the mathematical model based Matlab program with experimental results using for the model the same materials and boundary conditions as when the experimental tests were performed.

Figures 5.12, 5.14 and 5.16 show the simulated versus experimental temperature profiles if the model is not predicting the polymer ignition. Figures 5.13, 5.15 and 5.17 show the comparison between experimental and simulated temperature profiles for each thermoplastic when the model is not predicting ignition.

a) Polypropylene (PP).

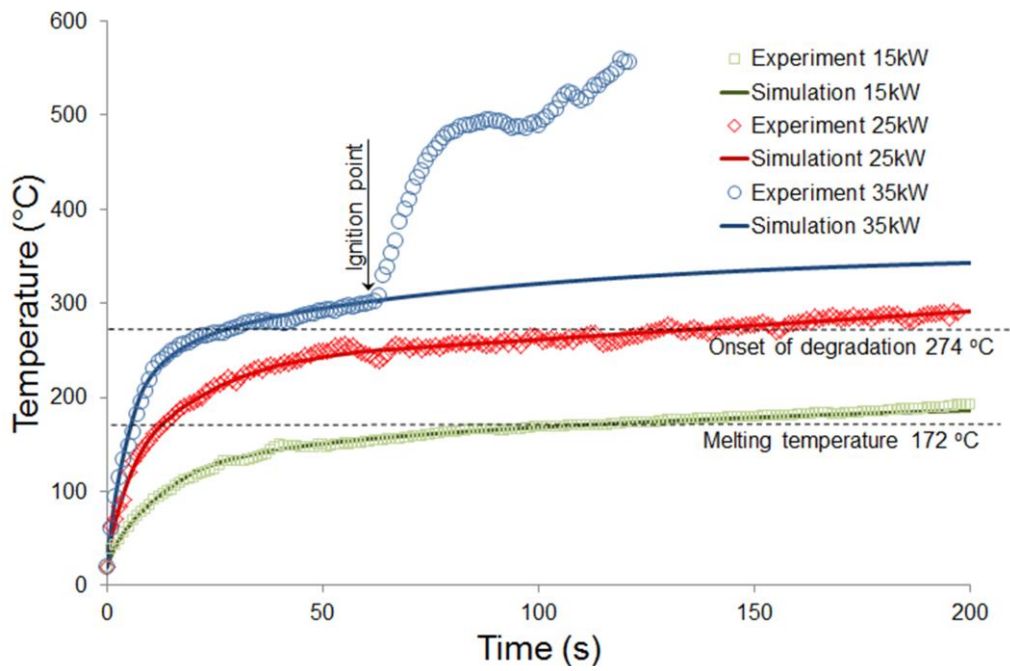


Figure 5.12: PP- Experimental vs. simulated surface temperature exposed to 15, 25 and 35kW/m² heat fluxes (ignition is not predicted).

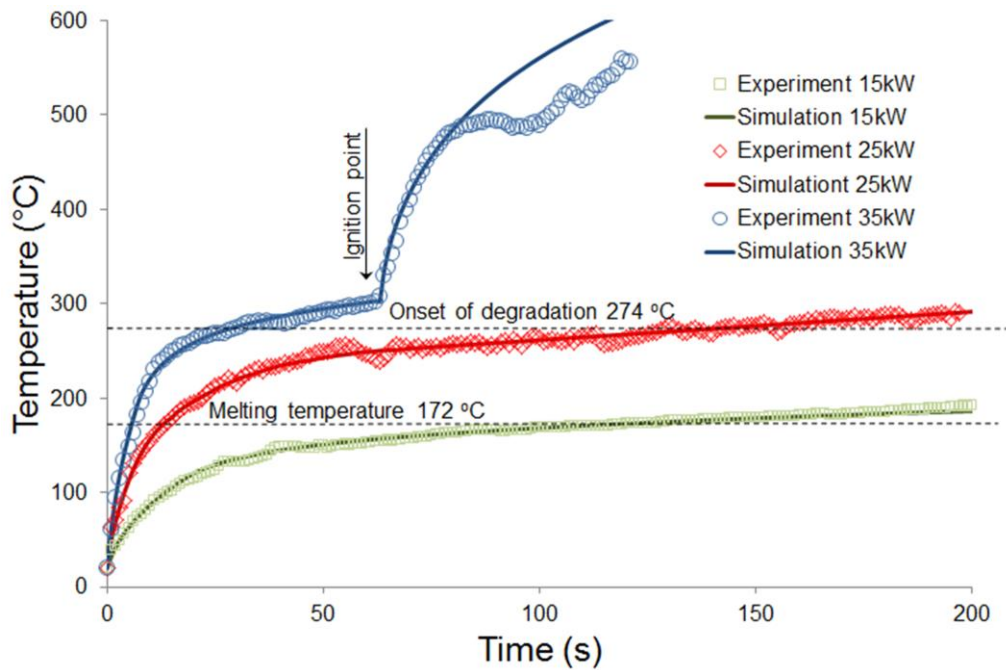


Figure 5.13: PP- Experimental vs. simulated surface temperature exposed to 15, 25 and 35kW/m² heat fluxes (ignition is predicted).

b) Polyamide 6 (PA6).

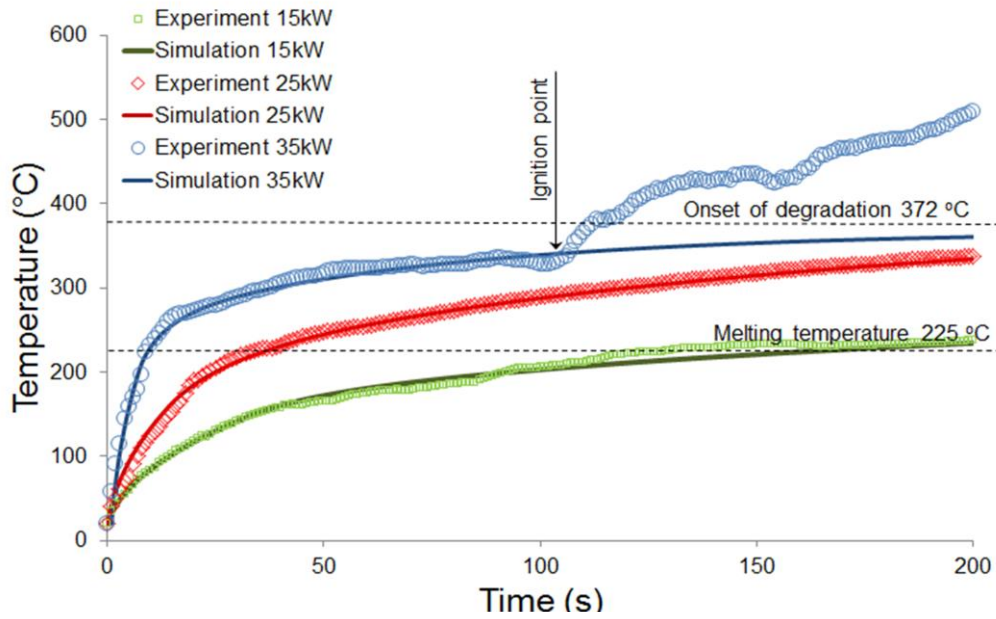


Figure 5.14: PA6-Experimental vs. simulated surface temperature exposed to 15, 25 and 35kW/m² heat fluxes (ignition is not predicted).

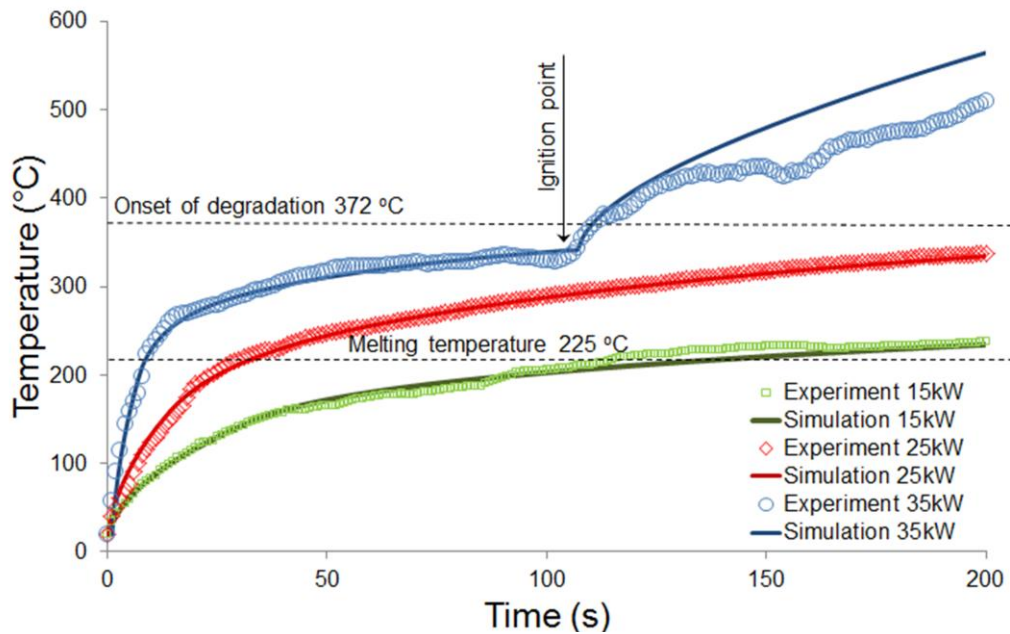


Figure 5.15: PA6-Experimental vs. simulated surface temperature exposed to 15, 25 and 35kW/m² heat fluxes (ignition is predicted).

c) Polyethylene terephthalate (PET).

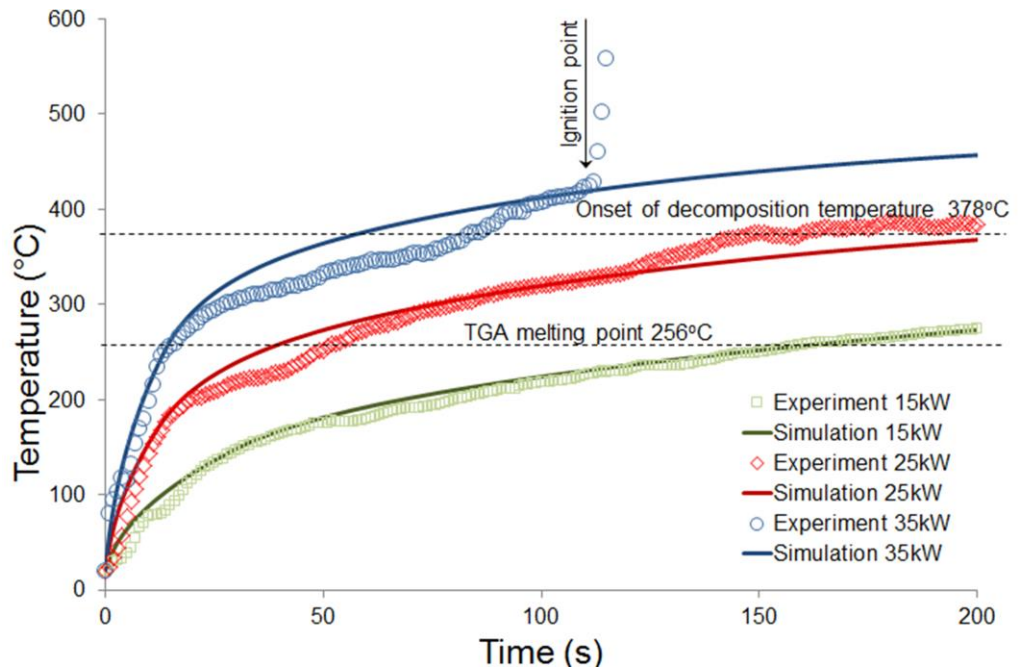


Figure 5.16: PET-Experimental vs. simulated surface temperature exposed to 15, 25 and 35kW/m² heat fluxes (ignition is not predicted).

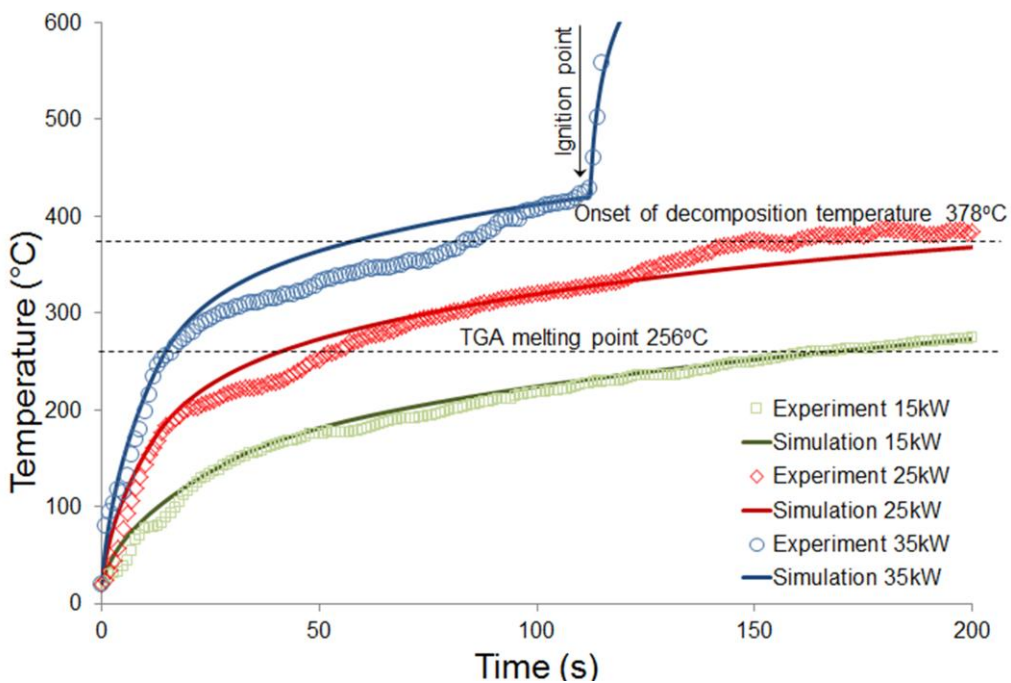


Figure 5.17: PET-Experimental vs. simulated surface temperature exposed to 15, 25 and 35kW/m² heat fluxes (ignition is predicted).

5.4.2 Analysis and comments

Comparison between predicted and experimental temperature profiles show good agreement for the three types of semi-crystalline thermoplastic polymers studied in horizontal position exposed to a cone calorimeter. The thermophysical parameters used to build the numerical model are taken from experiment as in Chapter 3 and despite the fact that they vary with temperature their accuracy is difficult to establish [8]. Experimentally the surface temperature of the sample was relatively easy to be measured compared of the temperature of the unexposed surface of the sample because thermocouples cannot be kept stable at that level as they move easily into the molten thermoplastic samples. It is shown how fast these materials can melt providing indication on the development of pool molten thermoplastic polymer formation which often leads to polymer degradation and fire when the incident heat flux is high enough [200, 233-234].

5.5 Conclusions

In this chapter a mathematical model of heat transfer by conduction throughout three semi-crystalline thermoplastic polymers (PP, PA6 and PET) has been developed. The model is based on the one-dimensional (1D) representation of static melting phenomena in horizontal position and it takes into account melting aspects as well as degradation and ignition. All these phenomena are described by a balance equation which is a nonlinear Partial Differential Equation (PDE). Approximated numerical solutions are obtained using Finite Difference Method (FDM) for the one-dimensional (1D) domain and Stefan phase change and moving boundary problem statement. Key parameters such as specific thermal conductivity and heat capacity, density and latent heat are taken from literature so that their precision will sure affect the consistency of the model therefore a sensitivity analysis is undertaken to find out which parameter influences most the model.

The temperature profiles of the thermoplastic materials in a cone calorimeter using three different heat fluxes (15, 25 and 35kW/m²) were studied and the predicted temperature profiles are presented and compared with experimental temperatures obtained in the corresponding conditions for model validation. It was noticed these comparisons show that the temperature profiles predicted by the model are consistent. Also for each sample the melting temperature measured by DSC and the onset temperature of degradation measured by TGA were used as reference. Such numerical model can be used to replace an amount of expensive laboratory experiments.

Chapter 6: Heat transfer in Glass Reinforced Epoxy (GRE)

6.1 Introduction

The focus in this Chapter 6 is on heat transfer in Glass Reinforced Epoxy (GRE), exposed to radiant heat of different heat fluxes in a cone calorimeter. GRE is a combination of two types of materials: the matrix and the fibres. In this case an epoxy resin is used as a matrix and glass fibres as reinforcement as shown in Figure 6.1 below:

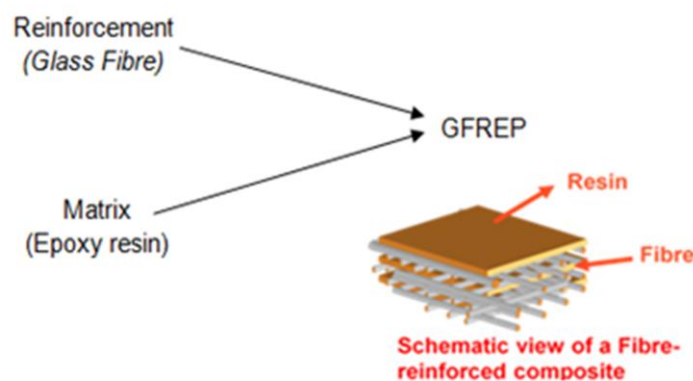


Figure 6.1: Schematic representation of Glass Reinforced Epoxy (GRE)

The reinforcement (glass fibre) and matrix (epoxy resin) behave differently on exposure to heat and/or fire. While glass fibre is non-flammable and softens above 800° [235-236], the resin softens at its glass transition temperature, degrades on reaching its decomposition temperature, producing flammable volatiles which may then ignite with external ignition source or reaching a critical mass flux [237]. Accurate knowledge of the thermal response of GRE at high temperature is therefore essential for the reliable and economical design of these structures. Suitable mathematical modelling of relevant heat transfer processes within polymer composites allows saving money by substituting large out lay of expensive testing experiments prerequisites for design and manufacturing process. Hence, a heat transfer model is here developed to simulate the temperature profiles through the thickness of a glass fibre reinforced epoxy resin composite exposed to different heat fluxes in a cone calorimeter and a further analysis performed to establish how the ignition is delayed when the sample thicknesses and the incident heat fluxes are varied.

6.2 Model description

A one-dimensional heat and mass transfer model through a composite laminates sample is schematically represented in the Figure 6.2. In this case only the top surface is heated while the other sides are insulated.

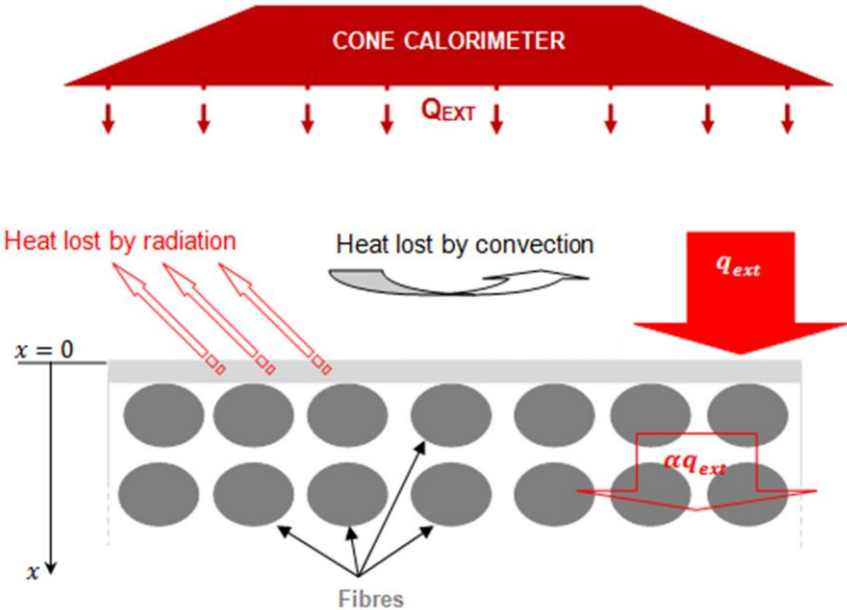


Figure 6.2: Schematic representation of the heat transfer in GRE, exposed to one sided external heat

A one-dimensional heat and mass transfer model through a composite laminates sample is schematically represented in the Figure 6.3. In this case only the top surface is heated while the other sides are insulated.

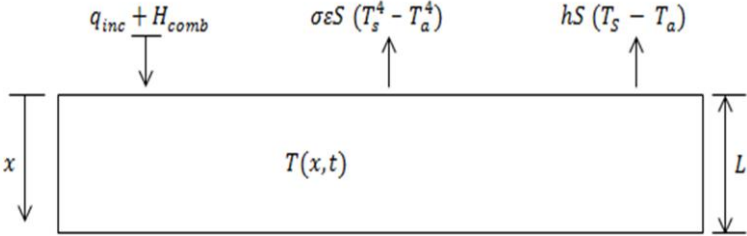


Figure 6.3: Schematic representation of heat transfer model in GRE.

The one-dimensional balance equation of heat and mass transfer, in a unit volume of fibre reinforced composite polymer undergoing thermal decomposition and leading to ignition and combustion is given by the following nonlinear partial differential equation derived from Henderson's equation [68] and applied for a heat flux provided by cone calorimeter.

$$\rho(T)c_p(T) \frac{\partial T}{\partial t} = k(T) \frac{\partial^2 T}{\partial x^2} - \frac{\partial}{\partial x}(\dot{m}_g H_g) + \sum_1^N \frac{\partial \rho_i}{\partial t} H_{r,i} \quad (Eqn 6.1)$$

Where i is the reaction involved, $H_{r,i}$ is the enthalpy of the different reactions (enthalpy of combustion H_{comb} and enthalpy of degradation H_g), $C_p(T)$ is the specific heat capacity, $k(T)$ is the specific thermal conductivity, $\rho_i(T)$ is the density of each constituent of each reaction and \dot{m}_g is the mass flux of volatile gas. Equation Eqn 6.1 means that under incident heat/fire the variation of internal energy in the composite which is the left hand side of the equation is caused by:

- The first term on the right hand side of Eqn 6.1 which represents the heat transfer by conduction within the composite material.
- The second term takes into account the energy from the flow of decomposition gases through the char structure causing internal heat transfer by convection.
- The final term represents the rate of heat generation or absorption relating to the matrix decomposition (endothermic reactions) as well as combustion reactions (exothermic reactions heat).

The decomposition reaction rate is calculated using the Arrhenius kinetic rate equation that determines the mass loss rate and it is assumed that the rate of decomposition $k(T)$ of the resin matrix follows a single-step modelled by Arrhenius equation [73, 238-239]

$$k(T) = A \cdot \exp\left(\frac{-E}{RT}\right) \quad (Eqn 6.2)$$

And the mass flow rate of volatile is defined as:

$$\dot{m}_g = \rho \cdot k(T)$$

With the conservation of mass in x axis as:

$$\frac{\partial \dot{m}_g}{\partial x} = -\frac{\partial \rho}{\partial t} \quad (\text{Eqn 6.3})$$

Where \dot{m}_g is the mass flow of volatile, ρ is the density, A pre-exponential factor, E activation energy and R is the universal gas constant.

The initial condition:

$$\text{At } T = T_a, \text{ gives rise to } \rho = \rho_0, \quad \dot{m}_g = 0, \quad \rho_i = 0.$$

With the following boundary conditions:

$$x = L, \quad \frac{\partial T}{\partial x} = 0, \quad \frac{\partial \rho_i}{\partial t} = 0, \quad \dot{m}_g = 0$$

$$x = 0, \quad k \frac{\partial T}{\partial x} = q_{net}$$

Also when:

$$t < t_{ig}$$

$$q_{net} = \alpha q_{inc} - q_c - q_{rr}$$

$$t > t_{ig}$$

$$q_{net} = (1 - \alpha_f) \alpha_s q_{inc} + q_f - q_{rr}$$

With,

$$q_c = h_c(T_s - T_\infty)$$

$$q_{rr} = \epsilon \sigma (T_s^4 - T_\infty^4)$$

Where q_{inc} is the external heat flux provided by the cone calorimeter, t_{ign} is the ignition time, T_{ign} is the ignition temperature, h_c is the convection coefficient, T_∞ is the ambient temperature, σ is the Stefan-Boltzmann constant, α_f is the flame absorptivity, q_{net} is the net heat flux penetrating through the composite laminates surface and q_f is the total incident heat flux from the flame, q_{rr} is the heat flux lost by re-radiation from the heated composite surface, q_c is the heat flux lost by convection from the heated composite surface, ϵ_s is the emissivity of the material surface, α_s is the absorptivity of the material surface, T_s is the surface temperature of the material. The surface emissivity of burning composite laminates is

normally around 0.96 however when the surface starts to darken it is assumed to be equal to 1 [72]; as the materials will darken, deform, melt and even char when burning, this is a reasonable approximation.

6.3 Temperature dependent thermophysical properties

The thermophysical properties, namely specific thermal conductivity, specific heat capacity and density which form part of Eqn 6.1 are temperature dependent. These properties are included in the numerical model as functions of temperature during the heating process of the GRE. Therefore the numerical modelling depends up the ability to predict the thermophysical properties that are already measured experimentally as they vary with temperatures as presented in Chapter 3, Section 3.4.3, and Table 3.5. Figure 6.4, 6.5 and 6.6 show respectively the graphs representing the conductivity, the specific heat capacity and the density in function of temperatures and average values which are then embedded in the Matlab programme as shown in Table 6.1. Below is shown in Figures 6.4, 6.5 and 6.6 the experimental and Matlab (The averaged values shown as solid lines) data representing the behaviour of conductivity, heat capacity and density against temperature. The average values are used in designed Matlab programme for simulations.

(i) Thermal conductivity, $k(T)$

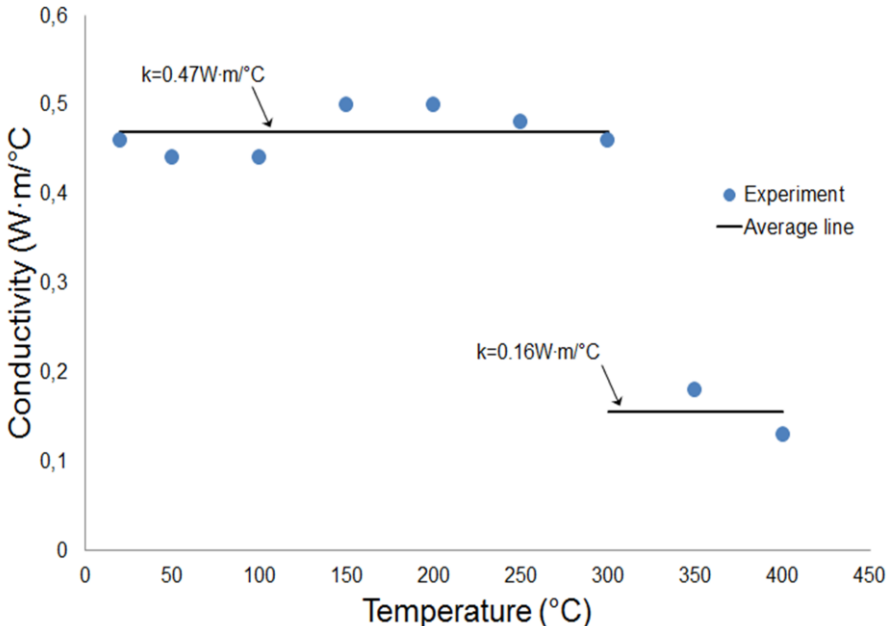


Figure 6.4: Thermal conductivity of GRE as a function of temperature and the averaged value (solid line) used in designed Matlab programme.

(ii) Heat capacity, $C_p(T)$

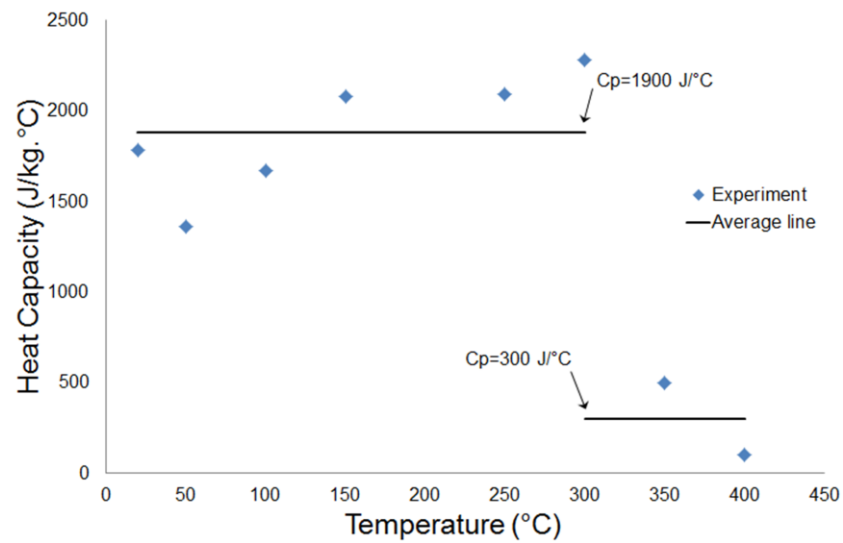


Figure 6.5: Heat capacity of GRE as a function of temperature and the averaged value (solid line) used in designed Matlab programme.

(iii) Density, $\rho(T)$

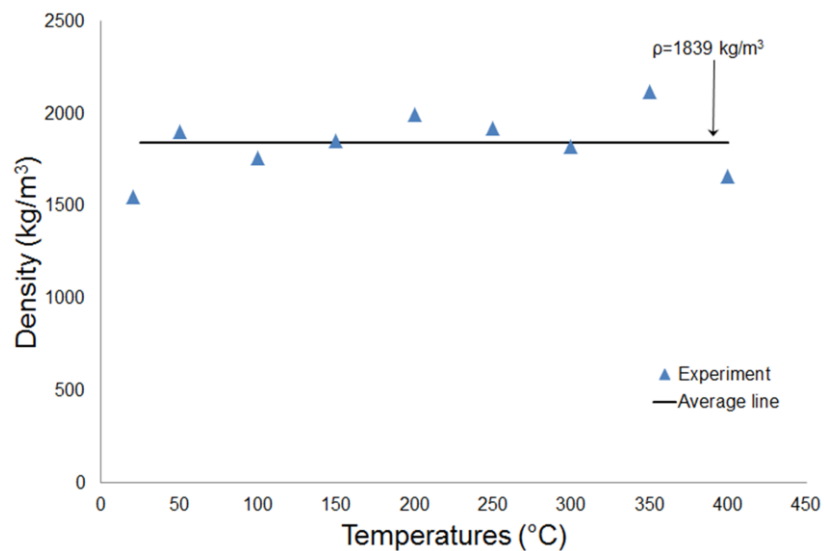


Figure 6.6: Density of GRE as a function of temperature and the averaged value (solid line) used in designed Matlab programme.

Table 6.1 summaries the values used in the Matlab code:

Temperature (°C)	Specific thermal conductivity (Wm/°C)	Specific heat capacity (J/kg)	Density (kg/m ³)
20<T<300	0.47	1900	1839
T>300	0.16	300	1839

Table 6.1: Thermophysical values embedded in designed Matlab programme.

6.4 Numerical resolution

There is no analytical solution for Eqn 6.1. Therefore, the approach is to solve the expression numerically using the finite difference method (FDM). In order to assume a 1D heat transfer the GRE sample represented by $(n + 1)$ layers insulated at the bottom and at the sides as shown in the Figure 6.7 below.

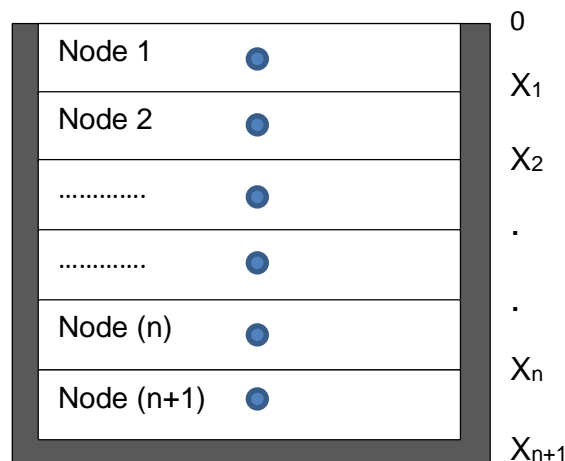


Figure 6.7: Schematically discretised sample

The temperature profiles within the GRE sample are unknown and therefore have to be determined. This is done by employing the explicit scheme method formulation for FDM as follows:

For $i = 1$,

$$\frac{c_i (T_i^{t+\Delta t} - T_i^t)}{\Delta t} = q_{net} \cdot S + \frac{k \cdot S \cdot (T_{i+1}^t - T_i^t)}{\Delta x_i} + \frac{(\dot{m}_{g_{i+1}} - \dot{m}_{g_i}) H_g}{x_{i+1} - x_i} + \dot{m}_g H_g + \dot{m}_g H_{comb} \quad (Eqns 6.4)$$

For $2 < i \leq n$,

$$\frac{(T_i^{t+\Delta t} - T_i^t)}{\Delta t} = \frac{k \cdot S \cdot (T_{i+1}^t - T_i^t)}{\Delta x_i} + \frac{k \cdot S \cdot (T_{i+2}^t - T_i^t)}{\Delta x_i} + \dot{m}_g H_g + \dot{m}_g H_{comb} \quad (\text{Eqns 6.5})$$

For $i = (n + 1)$.

$$\frac{C_i (T_i^{t+\Delta t} - T_i^t)}{\Delta t} = \frac{k \cdot S \cdot (T_{n+1}^t - T_n^t)}{\Delta x_i} + \dot{m}_g H_g + \dot{m}_g H_{comb} \quad (\text{Eqns 6.6})$$

Where c_p , \dot{m}_g , H_g , H_{comb} , S , ρ , Δx_i and $C_i = \Delta x_i S \rho c_p$ are respectively heat capacity, gas mass rate, gas enthalpy, combustion enthalpy, exposed surface of the sample, sample density, distance between two nodes and net heat capacity. Eqns 6.2, 6.3 and 6.4 are solved simultaneously by writing the appropriate code using Matlab software. The pre-set Matlab programme algorithm is as following:

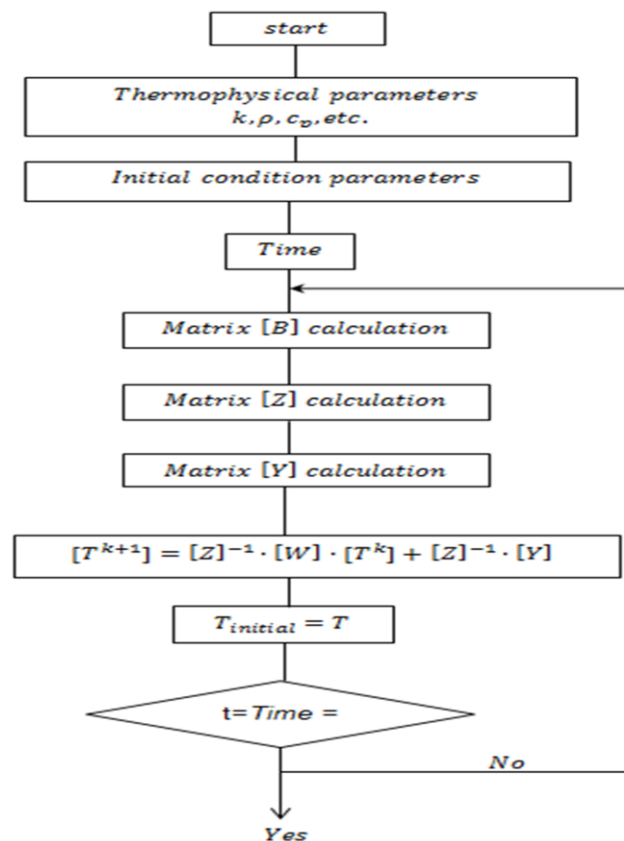


Figure 6.8: Matlab programme algorithm

6.4.1 Simulations and sensitivity analysis

The model was run using parameters in Table 6.1 to obtain temperature profiles at the top and bottom surface of a 3 mm GRE thickness exposed to 50kW/m^2 in a cone calorimeter and the results are shown in Figure 6.9.

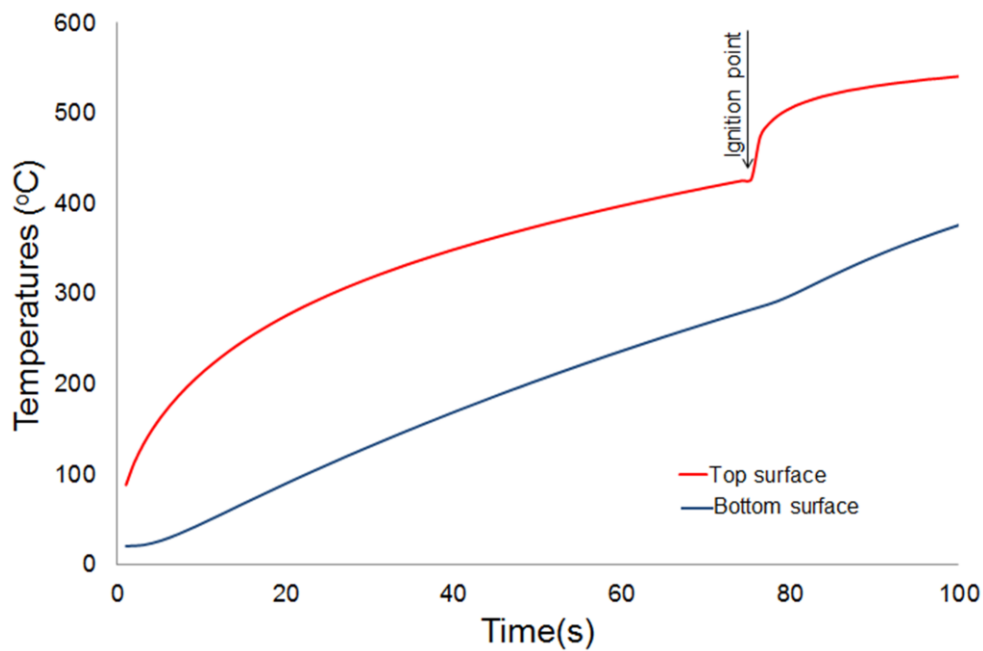


Figure 6.9: Simulated temperature profiles of GRE exposed to 50kW/m^2 heat flux.

In order to understand the sensitivity of the model to different parameters, sensitivity analysis was performed similar to the one discussed in Chapter 5 Section 5.3. The specific thermal conductivity k and the specific heat capacity C_p values varying with temperature given in Table 6.1 used in the model are considered to be the reference values in the process of performing the sensitivity analysis.

The first step was to vary the reference value of k and C_p in Table 6.1, by steps of 10% up to 30% to investigate the influence these parameters have on the predicted temperature as a function of time profiles. The results are shown in Figures 6.10 and 6.11 below:

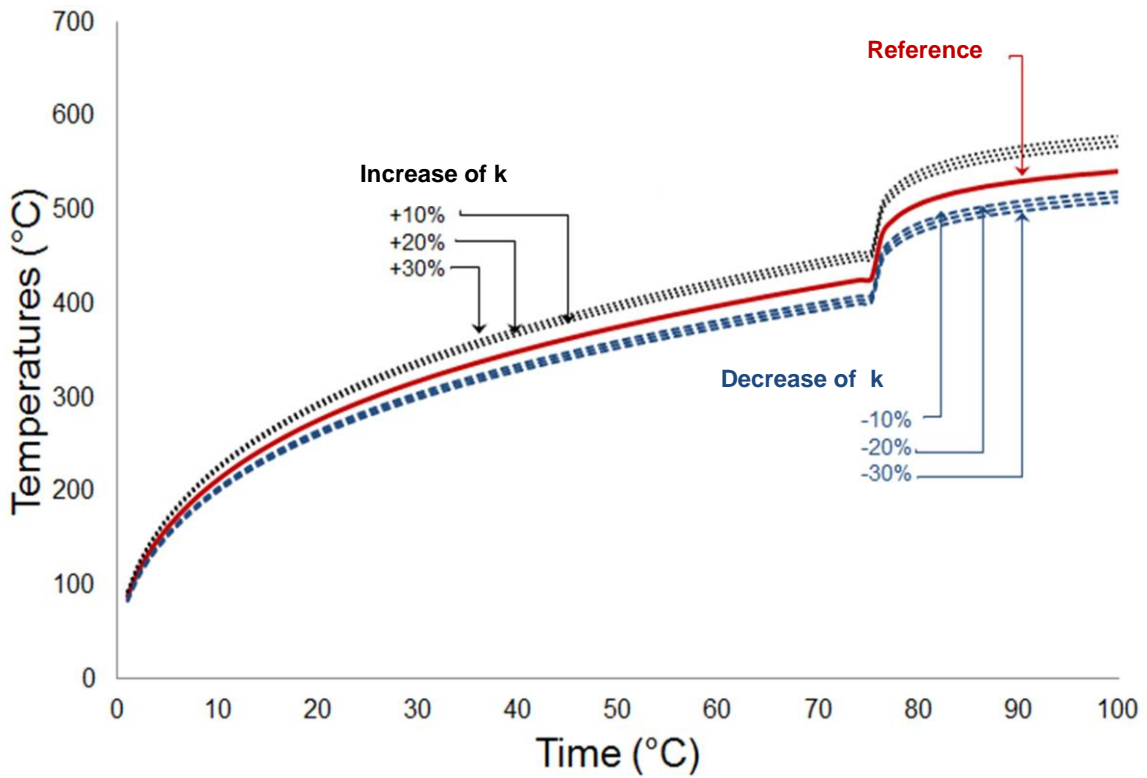


Figure 6.10: Change of temperature profiles with respect to time when the thermal conductivity is increased or decreased by step of 10% up to 30% from its reference value.

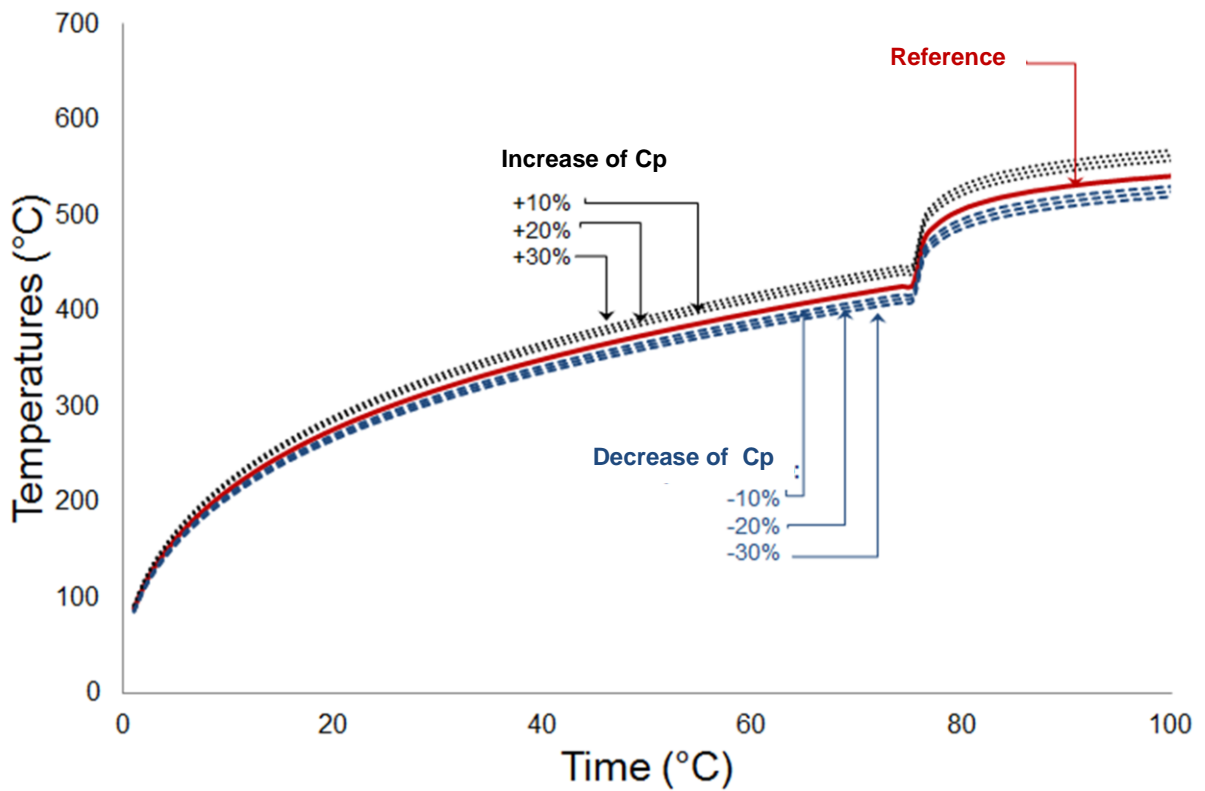


Figure 6.11: Change of temperature profiles with respect to time when the heat capacity is increased or decreased by step of 10% up to 30% from its reference value.

The second step is to carry out a sensitivity analysis based on the 'normalised sensitivity function' $S(k,T)$ or $S(C_p,T)$ [8] which indicates the respectively the change in percentage of k or C_p as an input and the change in percentage of the temperature profile as an output according to Figures 6.10 and 6.11. $S(k,T)$ and $S(C_p,T)$ are represented in Figure 6.12 below.

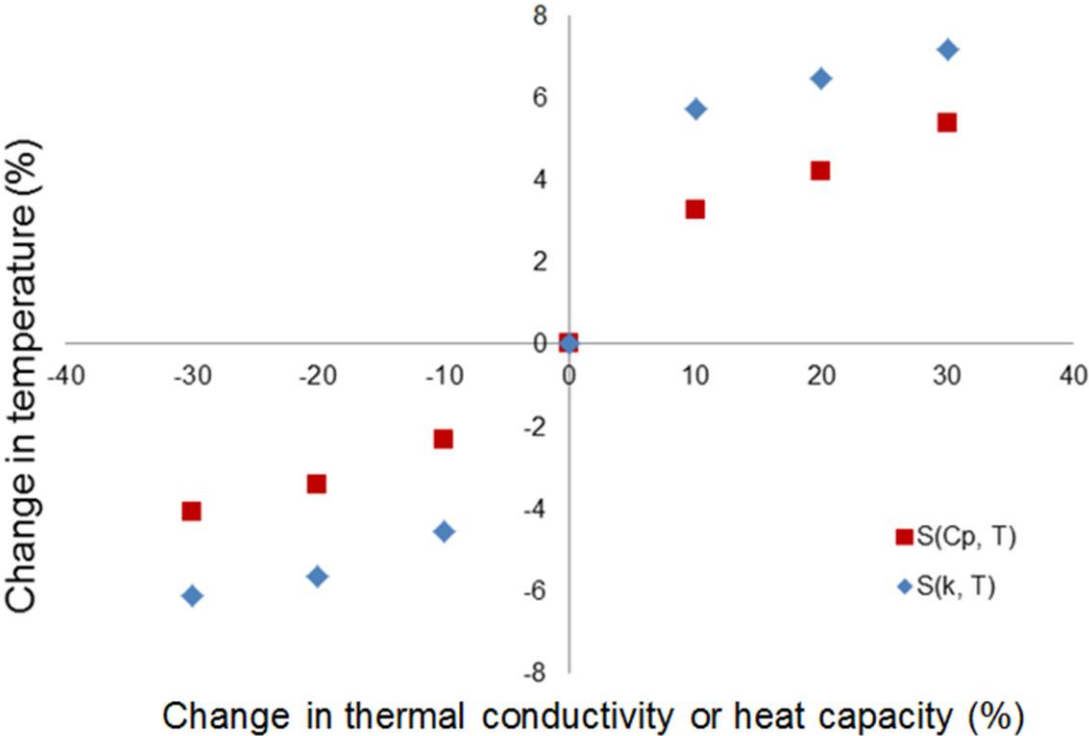


Figure 6.12: Change in temperatures (%) when the thermal conductivity (k) or the heat capacity (C_p) changes by +/- 10%.

According to Figure 6.9, 6.10 and 6.11 the following observations are noticed.

The temperatures profile increases or decreases when thermophysical parameters, specific thermal conductivity (k) and specific heat capacity (C_p), increase or decrease (Figure 6.9 and 6.10). The specific thermal conductivity (k) influences the output temperature profile giving rise to a change of approximately 7% whereas the specific heat capacity only induces a change of 4.5% , see Figure 6.12.

Since the thermal conductivity and the specific heat capacity values are experimentally measured as discussed in Chapter 3, Section 3.4.3 and the values might not be accurate due to experimental errors and different heating conditions used on those applied here. Hence, the variations are expected. The changes to the temperature dependent thermal conductivity have an impact on the heat transfer and hence, temperature profiles through the thickness of the laminate as well.

6.4.2 Simulation results

A set of simulations was performed with three different incident heat flux: 15, 35 and 50 kW/m² on a GRE sample of 3mm thickness. The temperature distribution in the model after simulation with previously discussed boundary conditions is shown in Figures 6.13, 6.14 and 6.15. The temperature is seen gradually decreasing from top to bottom due to the boundary conditions as expected: The top surface being exposed to the incident heat flux while the bottom side is insulated. The thermal decomposition of the resin matrix of the laminate begins at the exposed surfaces where the temperature is highest and progresses through the thickness to the insulated reverse (unexposed) side of the composite. Therefore, the heat transfer by conduction (rate of temperature increase) through the thickness of the laminate is not uniform; it decreases with the distance from the exposed surface affected by the thermal decomposition and the mass gas transfer.

Figure 6.13 shows the predicted temperatures profile for an incident heat flux of 15 kW/m² measured by thermocouples placed on the top and the bottom of the sample. It can be noticed that ignition does not occur because at the incident heat flux of 15 kW/m², the resin matrix does not degrade sufficiently to produce enough flammable volatile to have ignition, i.e., 15 kW/m² is below the critical incident heat flux defined as the minimum incident heat flux causing ignition. The conduction heat transfer within the composite reaches a steady state after 160s where the temperature gradient between the top and the bottom surface is approximately 100°C.

However, Figures 6.14 and 6.15 show that at incident heat fluxes of 35 and 50 kW/m² ignition occurs. Incident heat flux of 35 and 50 kW/m² are above the critical heat flux. The ignition point for a 50 kW/m² occurs after 75 s; the polymer degradation occurs faster due to the high intensity of the heat flux as well as the heat transfer between the top and the bottom surface of the sample. The same phenomenon happen with the incident heat flux of 35 kW/m² with a less thermal diffusivity of the heat within the sample denoted by the ignition occurring at the exposed side after 110 s.

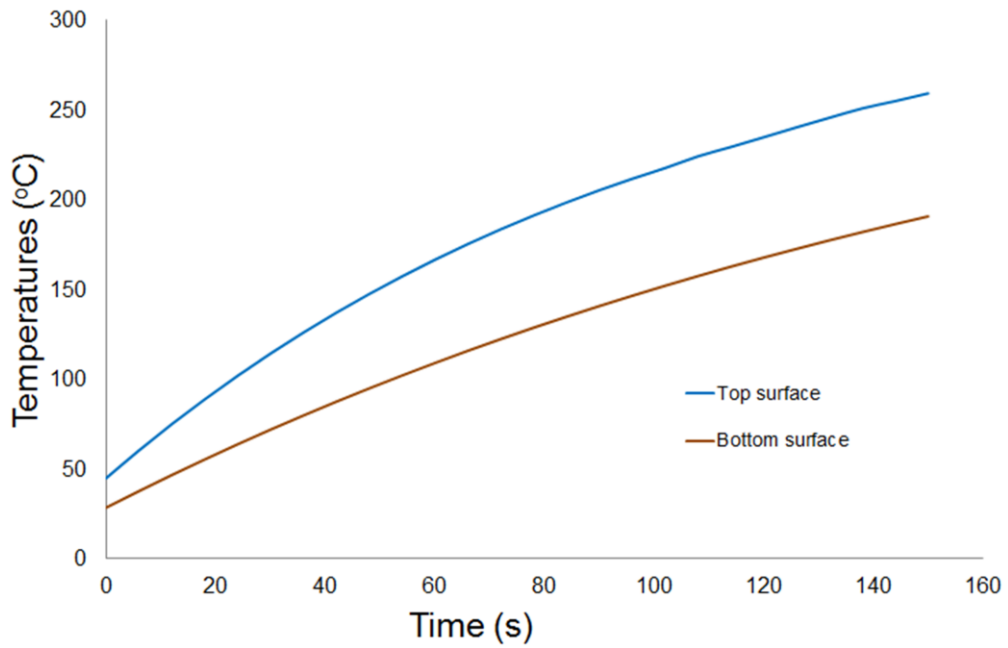


Figure 6.13: Simulated surface and bottom temperature profiles of GRE exposed to 15 kW/m² heat flux.

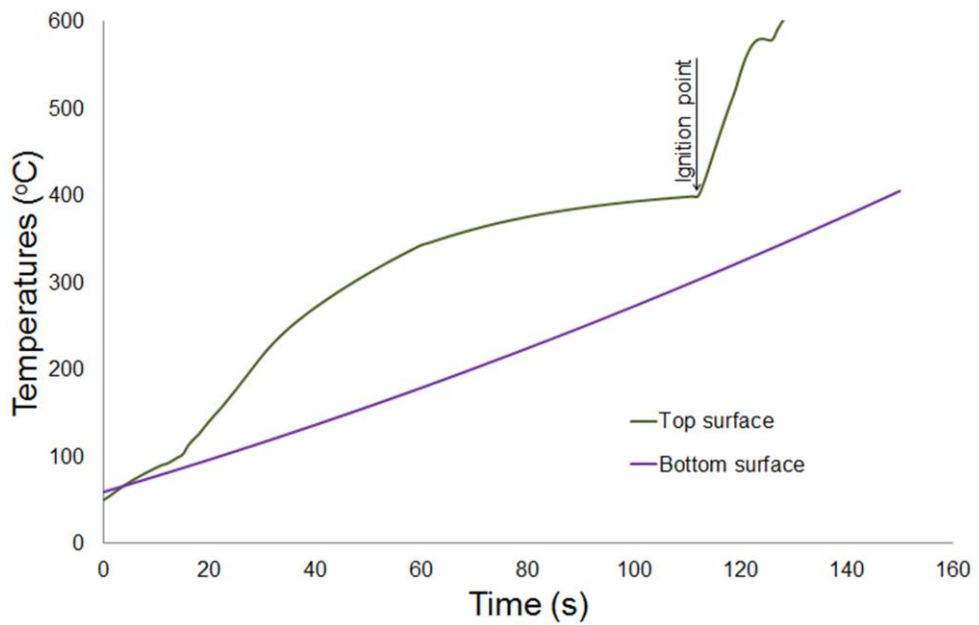


Figure 6.14: Simulated surface and bottom temperature profiles of GRE exposed to 35 kW/m² heat flux.

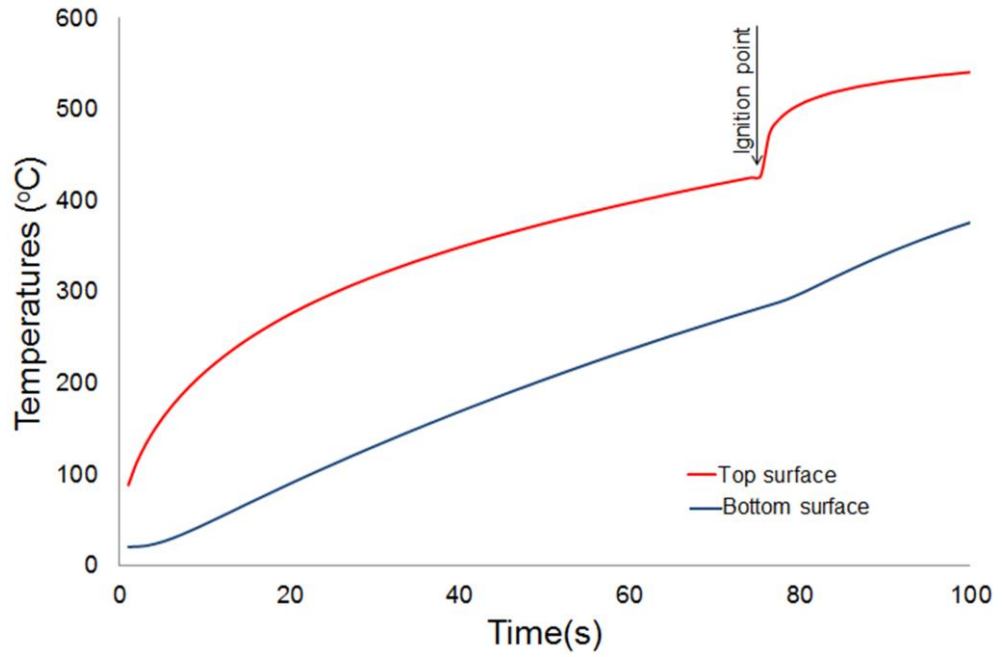


Figure 6.15: Simulated surface and bottom temperature profiles of GRE exposed to 50 kW/m² heat flux.

Subsequently in order to carry out an analysis of the effect of the thickness changes on the temperature profile when the composite is subjected to an incident heat flux of 35 kW/m², simulations are performed using different GRE sample thicknesses: 3 mm, 4.5 mm, 6 mm and 7.5 mm. The results are shown in Figure 6.16 and 6.17 below.

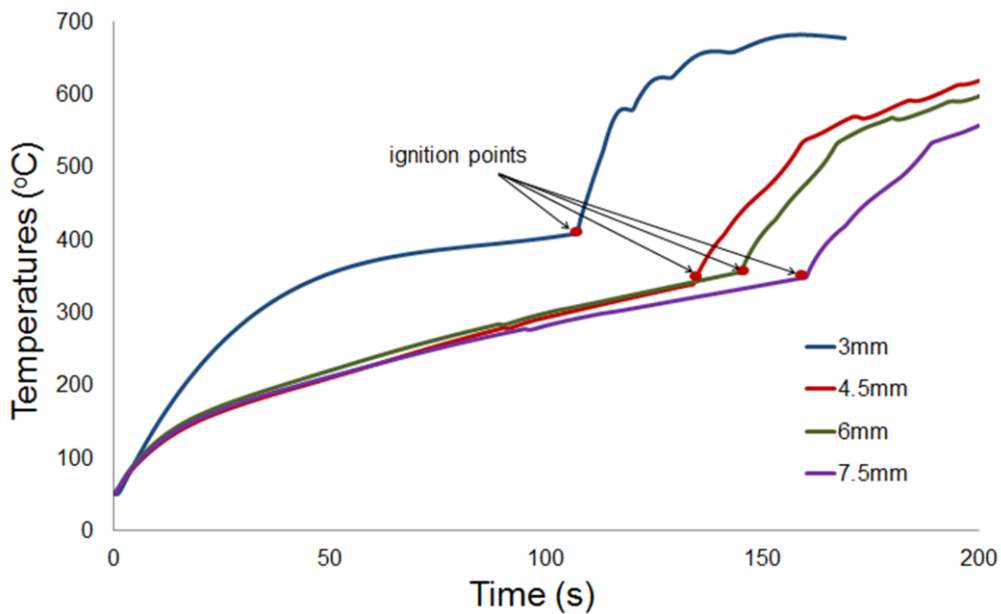


Figure 6.16: Simulated top surface temperature profiles of GRE for different samples thicknesses exposed to 35kW/m² heat flux.

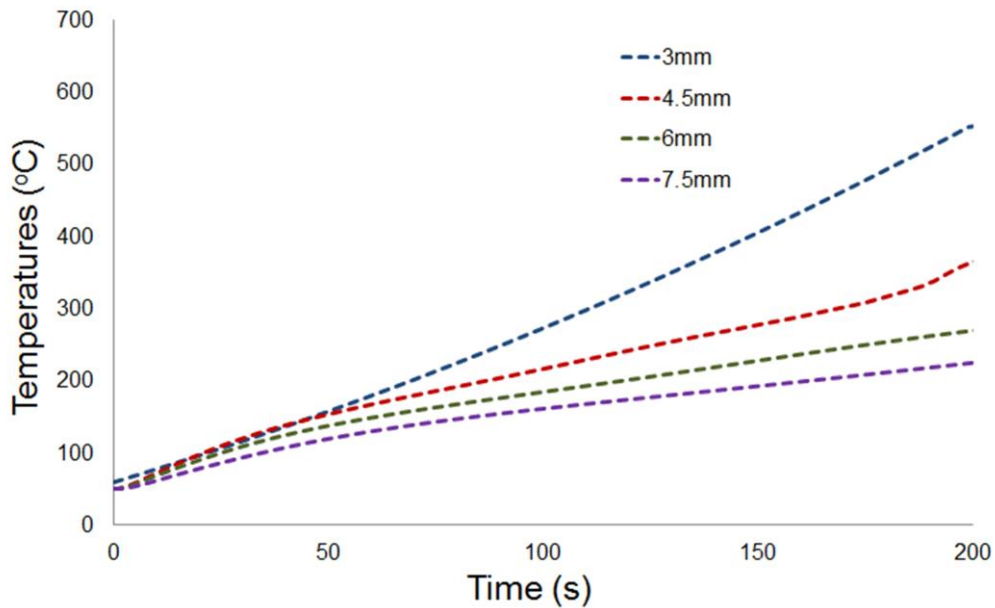


Figure 6.17: Simulated bottom surface temperature profiles of GRE for different samples thicknesses exposed to 35kW/m² heat flux.

6.5 Model validation

The predicted temperature profiles for localised one-sided radiant heating using Eqn 6.1 to 6.6 are shown together with the experimentally measured data for the composite at heat flux levels of 15, 25 and 35kW/m² in Figures 6.18 and 6.20, respectively. The data points show the measured values while solid lines show predicted temperature profiles at both the exposed and insulated surfaces of the specimen. While predicted temperature profiles are available for the finite difference mesh points through the thickness, only the surface profiles are shown to demonstrate the overall predictive ability, while maintaining the clarity of the graphs. In general, given the complexity of this problem and vast assumptions made, there is good agreement between the experimental data and the predicted temperature profiles. This degree of agreement is similar to that reported by other researchers on the same subject of thermal responses of fibre-reinforced composites [198-199].

However, for the 3mm thickness at 35 and 50 kW/m² the temperatures at the top surface are apparently underestimated by the model as shown in Figures 6.19 and 6.20. That could be explained partly due to the difficulty in experimentally measure the temperature over the duration of the experiment due to the problem of maintaining the thermocouples in permanent contact with the surface, hence inaccuracy in the experimental values. As the resin at the surface of the laminates is burnt off, the exposed surface thermocouples get

detached from the surfaces. While efforts were taken to mechanically weigh down the thermocouples, the thermocouples get detached and read the air temperature rather than the true surface temperature; hence the sudden take off of temperature profiles. The other source of error is the complexity to estimate the coefficient of convection that affects the heat transfer by convection close to the top surface. However, the increase in temperature happens close to the conclusion of the experiment and this is assumed to have no significant implications on the overall models.

The temperature-time profiles for the laminates compared at an incident heat flux of 15 kWm², Figure 6.18, show that the temperatures at the exposed and the rear are well predicted. A low incident heat flux in the order of 15 kWm² is not enough thermal energy to increase the laminate temperatures beyond 300 °C where the thermal decomposition of the epoxy resin formulation matrix as revealed by TGA measurements. The through thickness temperatures reached by the laminates during thermal exposure are below the decomposition temperature of 400 °C which means that the char formation enhancement is not maximised as a means of preserving material at this heat flux level.

Figures 6.21 to 6.24 show the measured and predicted surface thermal profiles for laminate glass fibre reinforced composite with 3, 4.5, 6 and 7.5 mm thickness and exposed to an incident heat flux of 35kW/m². These results show that the heat transfer through the laminate thickness is slower while the sample thickness is thicker because the thermal resistance is increasing with the sample thickness. Therefore, the exposed surface samples of the laminates ignite after 110, 140, 148 and 160s; each corresponding to a sample thickness ranked from the lowest to the highest. Predicted temperatures profiles from the numerical model and experiment temperature profiles show consistency in both cases; with and without ignition. The small discrepancies between the predicted and experimental temperatures of the top surface, particularly after the ignition of the sample can be explained partly due to experimental error in measurements of the surface temperature due to the difficulties to maintain the thermocouples in contact with the surface when ignition occurs. In addition, inaccuracies in measurements of thermophysical properties (specific thermal conductivity, specific heat capacity and density) affect the model.

As mentioned previously those parameters were measured experimentally as a function of temperature and inputted in the model [201-202, 209-210]. It is likely that the improvement of experimental processes to minimise errors would lead to a more precise measurement of these physical quantities and thus increase the precision of the results. Moreover, the relevance of thermophysical parameters measured is difficult to establish because they are specific to each composite and values found in scientific literature are always different from a

publication to another [160-161, 201-202, 209-210]. Moreover the numerical model used is a one-dimensional (1D) model while the experiment undertaken is in three dimensions (3D) therefore this may induce some errors in the modelling although the assumptions taken for the situation are consistent.

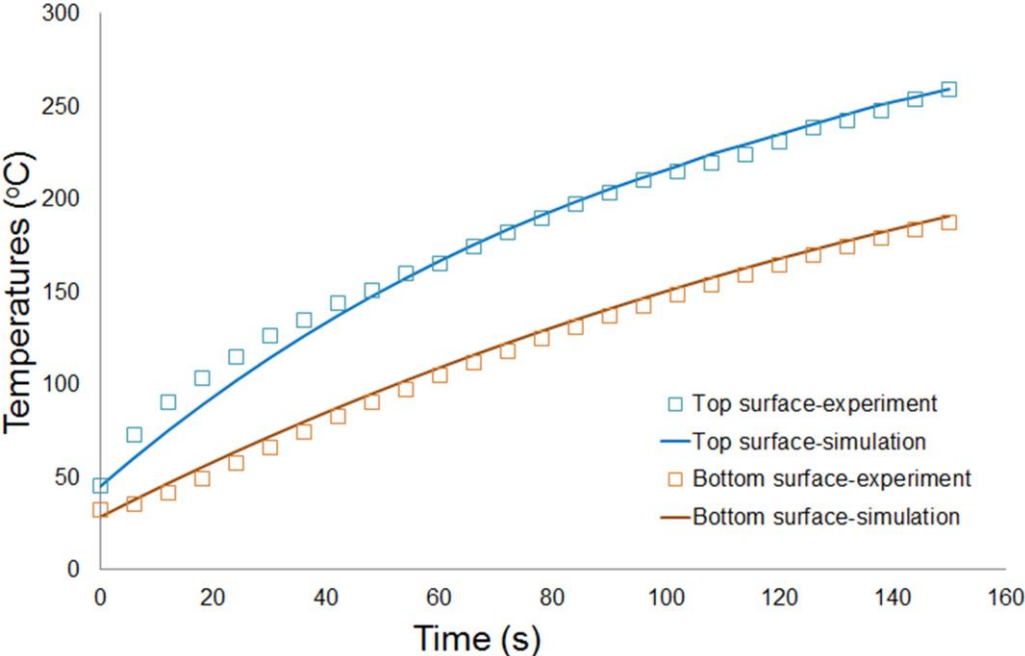


Figure 6.18: Simulated and experimental temperature profiles of top and bottom surfaces of GRE exposed to 15kW/m² heat flux.

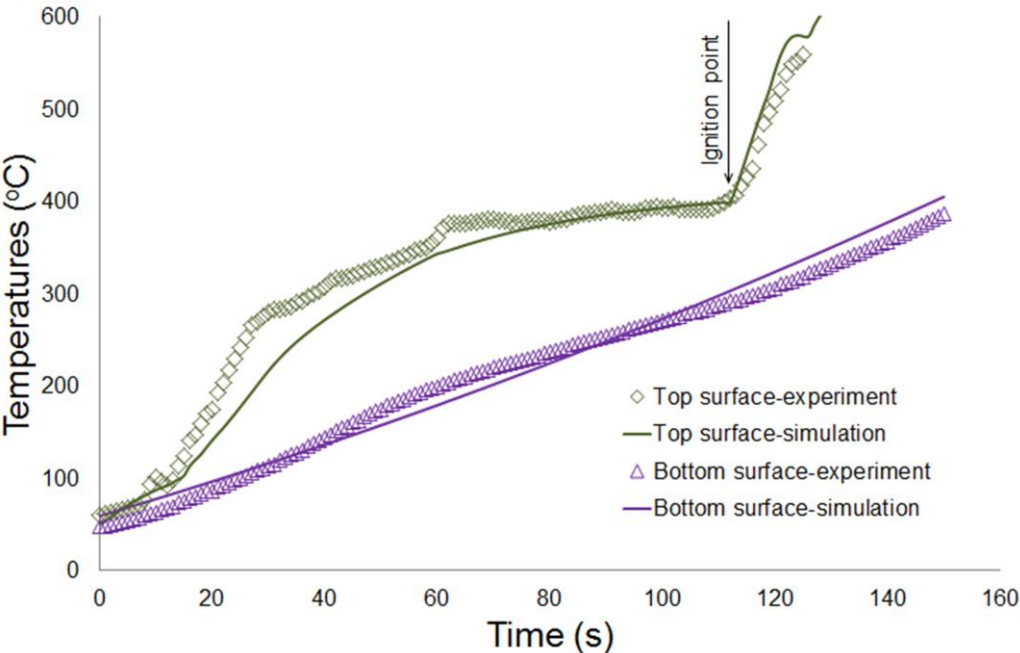


Figure 6.19: Simulated and experimental temperature profiles of top and bottom surfaces of GRE exposed to 35kW/m² heat flux.

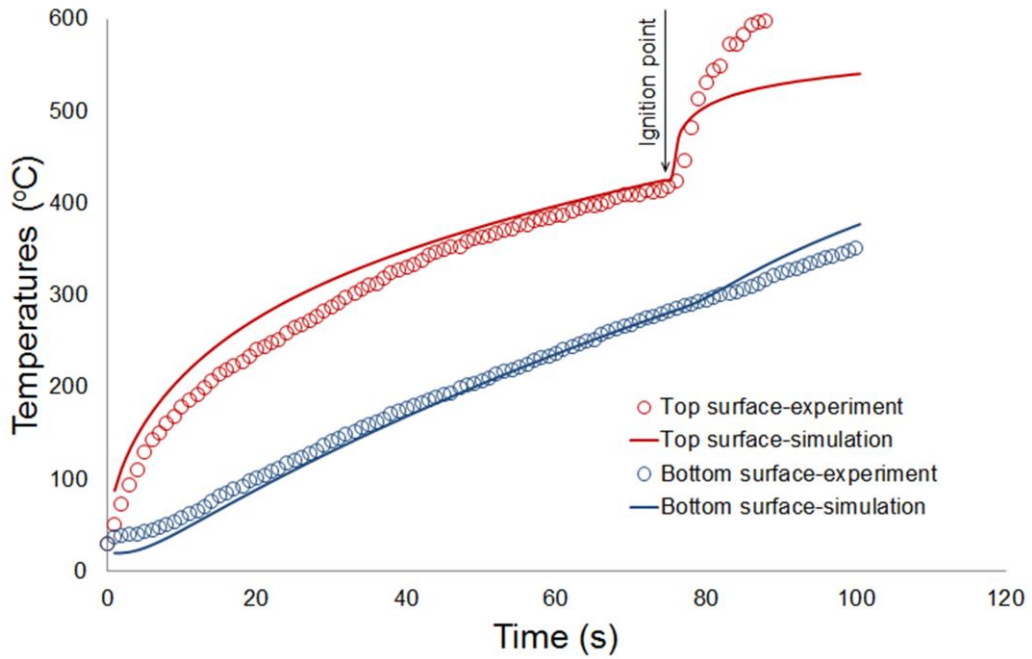


Figure 6.20: Simulated and experimental temperature profiles of top and bottom surfaces of GRE exposed to 50kW/m² heat flux.

Likewise to validate the mathematical model predicted and experimental temperature – time profiles (see Chapter 3, Section 3.3.3) are compared. Shown below are the Predicted and experimental temperature profiles of top and bottom surfaces of GRE at a heat flux of 35 kW/m² for different sample thickness indicated in Figures 6.21, 6.22, 6.23 and 6.24:

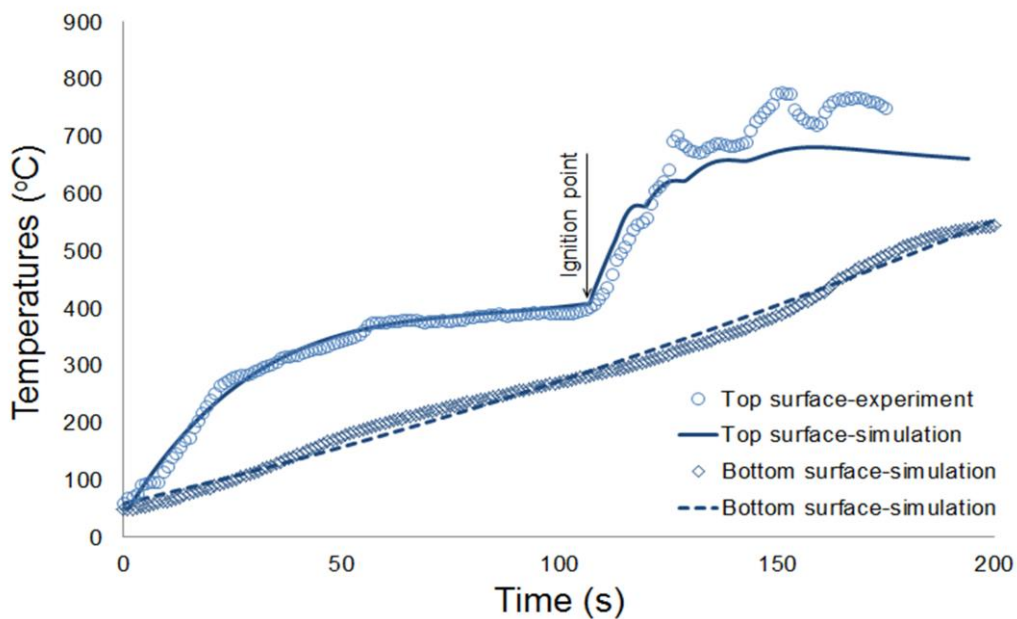


Figure 6.21: Simulated and experimental temperature profiles of top and bottom surfaces of 3 mm GRE sample thickness exposed to 35 kW/m² heat flux.

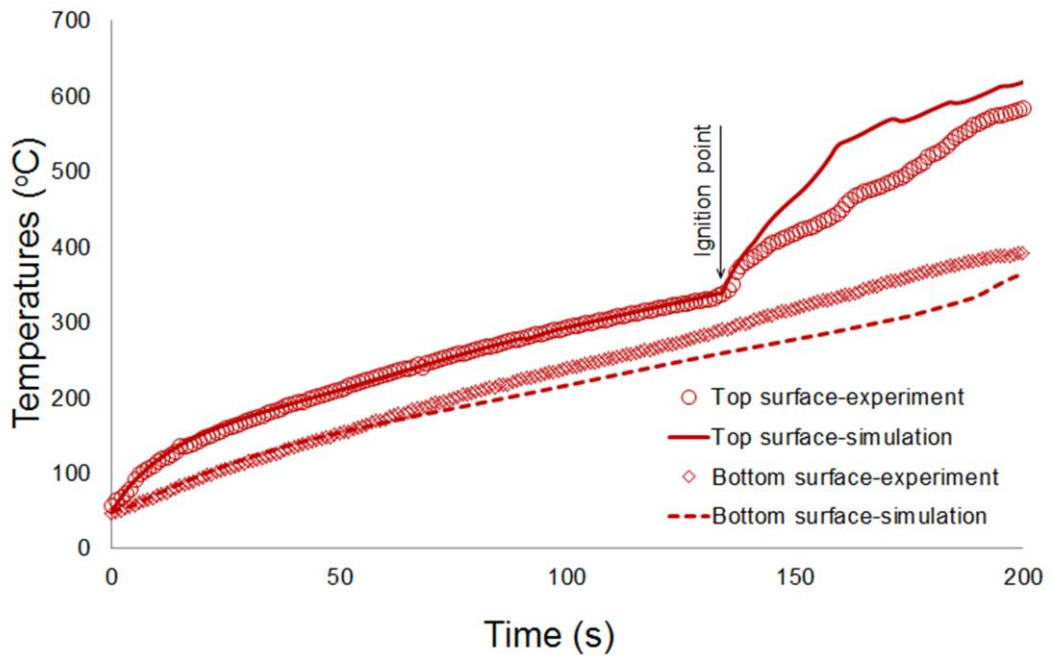


Figure 6.22: Simulated and experimental temperature profiles of top and bottom surfaces of 4.5 mm GRE sample thickness exposed to 35 kW/m² heat flux.

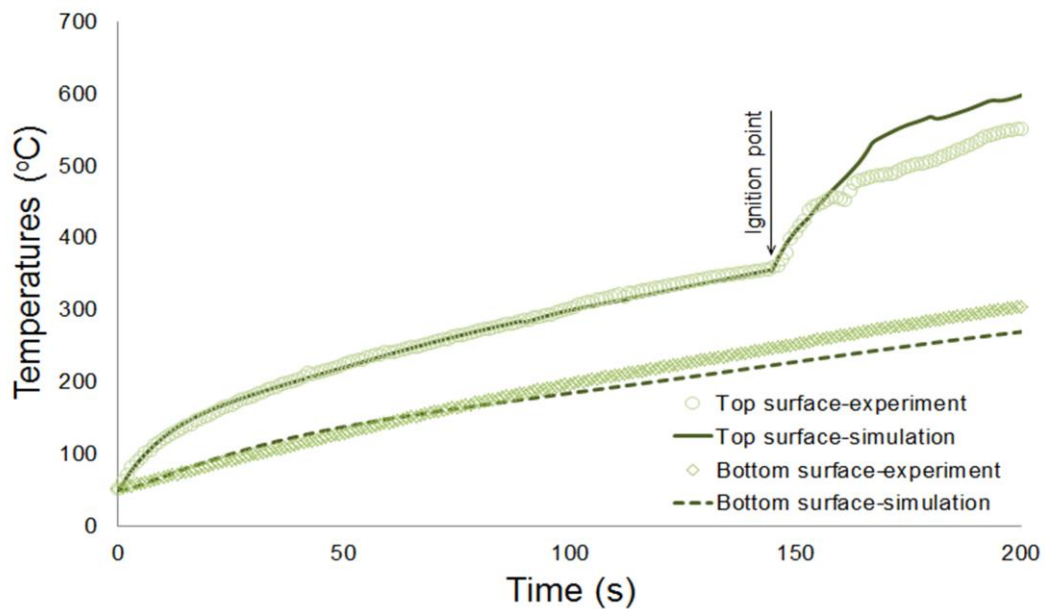


Figure 6.23: Simulated and experimental temperature profiles of top and bottom surfaces of 6 mm GRE sample thickness exposed to 35 kW/m² heat flux.

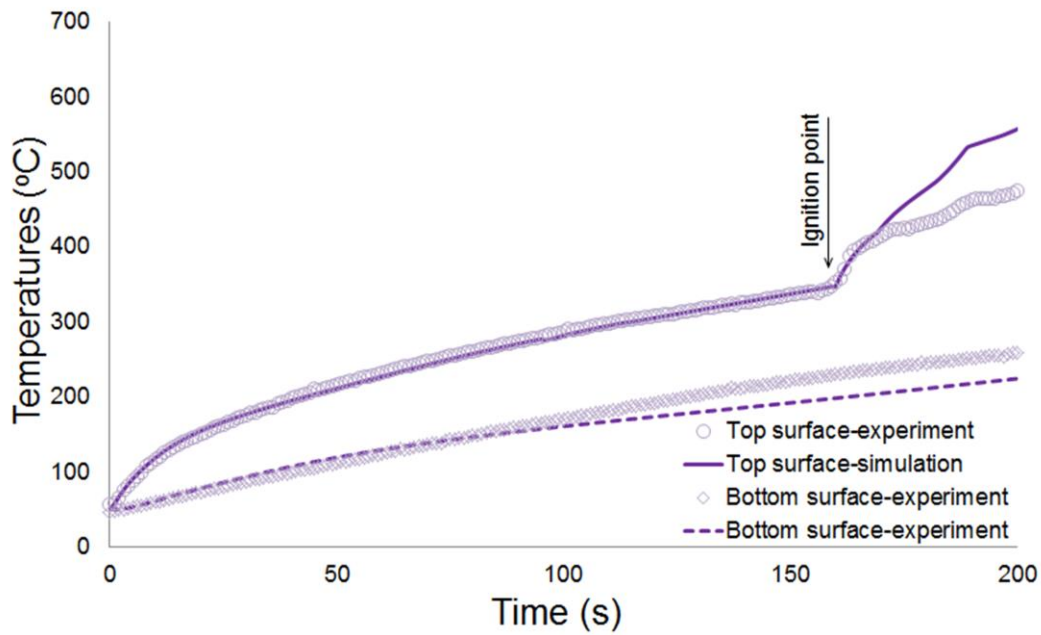


Figure 6.24: Simulated and experimental temperature profiles of top and bottom surfaces of 7.5 mm GRE sample thickness exposed to 35 kW/m² heat flux.

6.6 Effect of sample thickness and incident heat on time-to-ignition (TTI).

Firstly the effect of the sample thickness is analysed from the temperatures profiles obtained with different thicknesses at the incident heat flux of 35 kW/m² as shown in Figure 6.25 and 6.26, and secondly a methodology performing simulations by increasing and decreasing the incident flux from $Q_0=35\text{ kW/m}^2$ taken as a reference is carried out in order to analyse the effect on the TTI on samples with different thicknesses.

6.6.1 Effect of the sample thickness changes.

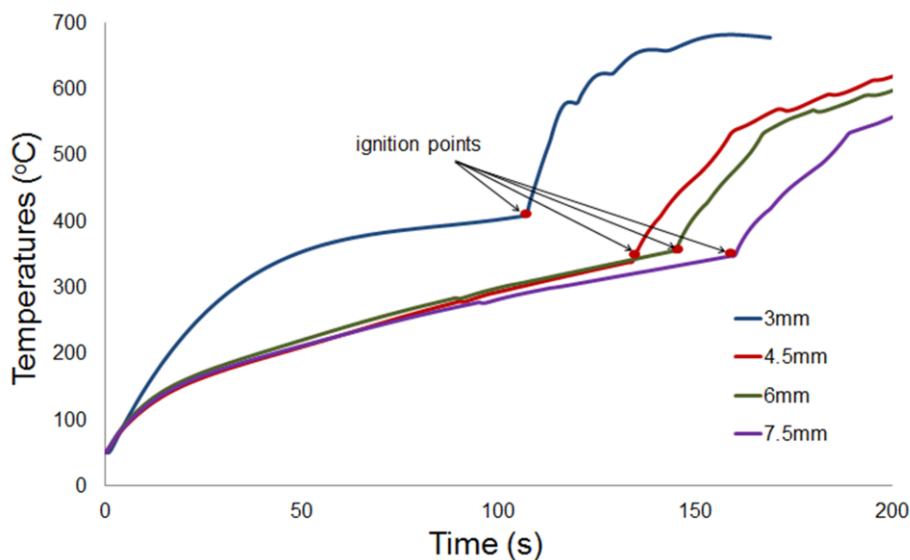


Figure 6.25: Simulated top surface temperature profiles of GRE for 3, 4.5, 6 and 7.5 mm samples thicknesses exposed to 35 kW/m² heat flux.

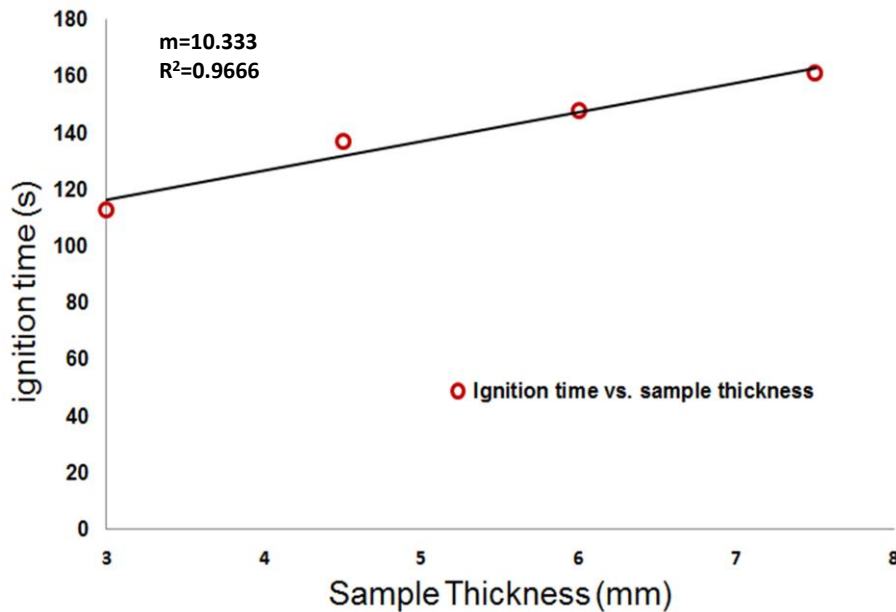


Figure 6.26: Time-to-ignition vs. sample thickness exposed to 35 kW/m² heat flux.

In Figure 6.25 it can be observed that the TTI increases linearly with the sample thickness when the same incident heat flux applied. That observation is confirmed in Figure 6.26 and the following equation is established for GRE at incident heat flux of 35 kW/m²:

$$TTI = 10.333 \times \text{sample thickness} + 85.6 \text{ s}$$

6.6.2 Relationship between TTI and incident heat flux.

The objective of this section is to find potential analytical relationships between the time required for the material to catch fire (i.e. TTI). This depends upon: the composition of the glass fibre epoxy resin composite sample, its thermophysical parameters and geometrical characteristics along with the various incident heat fluxes applied to the four different thicknesses: 3, 4.5, 6 and 7.5 mm.

A set of simulations is performed using the validated numerical Matlab programme as outlined in the previous sections of this chapter. The methodology of the simulations consist firstly in varying the values of the incident heat flux Q so that Q is equal to $2/5$, $1/2$, $2/3$, 1 , $3/2$, 2 or $5/2 \cdot Q_0$. ($Q_0 = 35 \text{ kW/m}^2$) in order to obtain the TTI for each sample as shown in Figures 6.27, 6.29, 6.31 and 6.33 below. Secondly the TTI is plotted against the corresponding incident heat flux in Figures 6.28, 6.30, 6.32 and 6.34. The values of the thermophysical properties taken at room temperature are as following:

$\rho = 1500 \text{ kg/m}^3$
 $C_p = 1540 \text{ J/kg}$
 $k = 0.4 \text{ W/m} \cdot ^\circ\text{C}$

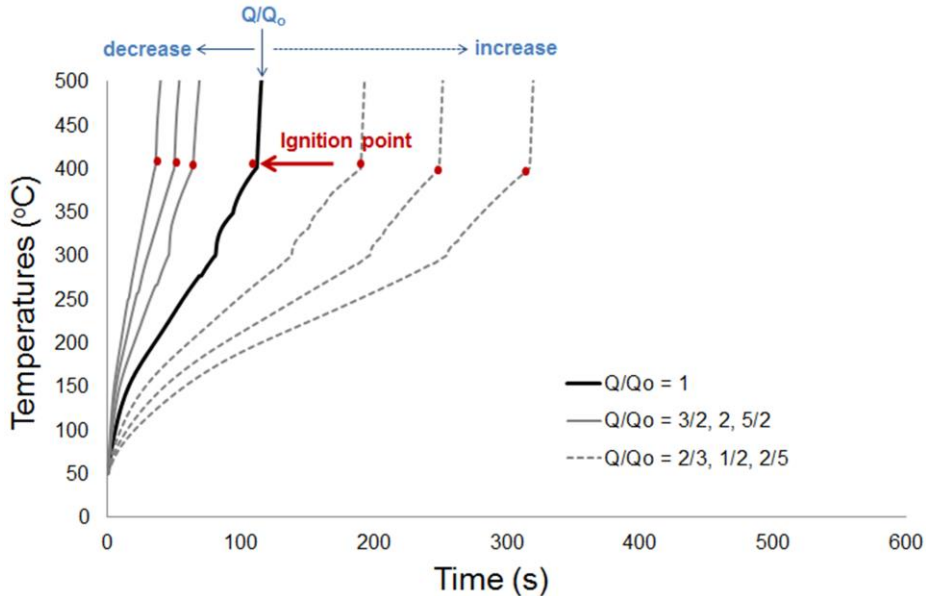


Figure 6.27: Effects of incident heat flux on the temperature profiles versus time of 3 mm GRE sample thickness.

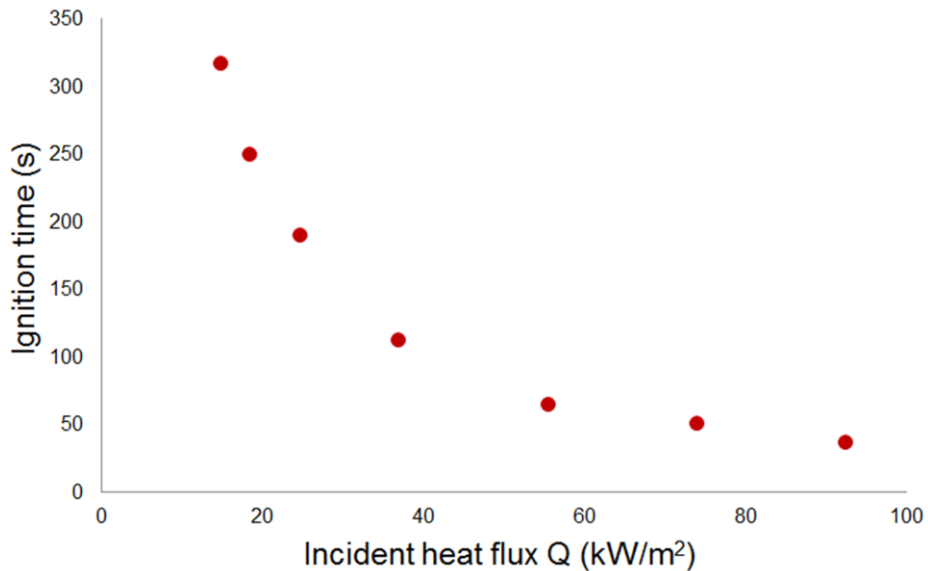


Figure 6.28: Simulation of TTI vs. incident heat flux of 3 mm GRE thickness.

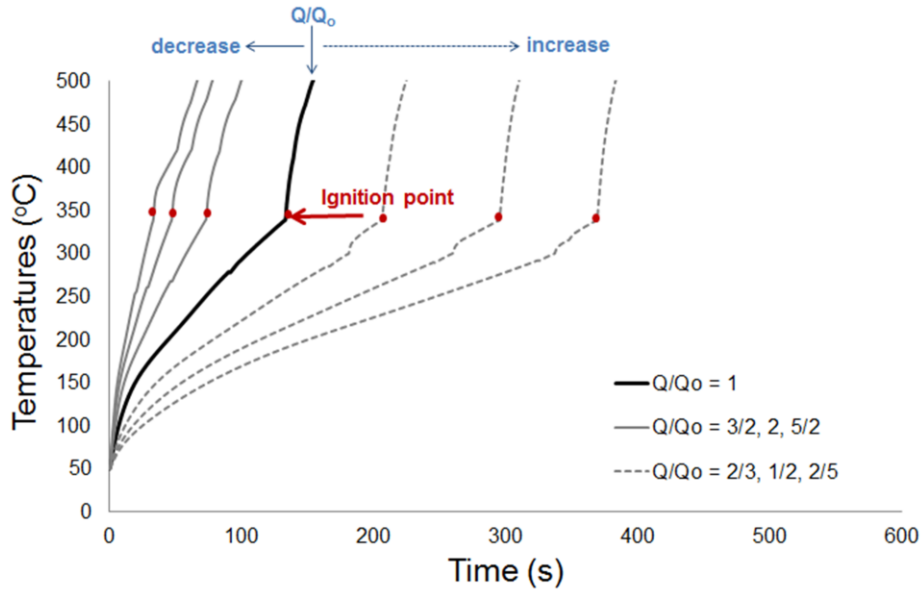


Figure 6.29: Effects of incident heat flux on the temperature profiles versus time of 4.5 mm GRE sample thickness.

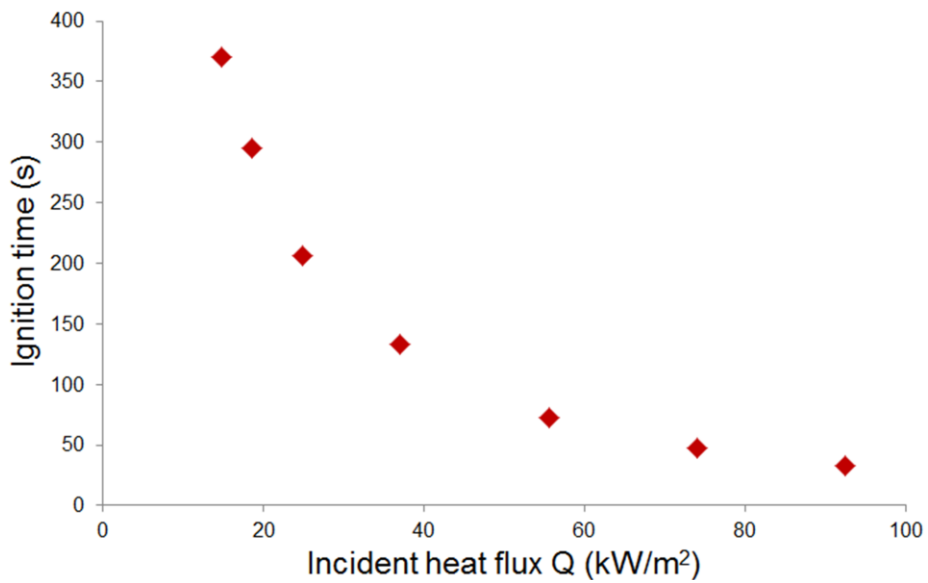


Figure 6.30: Simulation of TTI vs. incident heat flux of 4.5 mm GRE thickness.

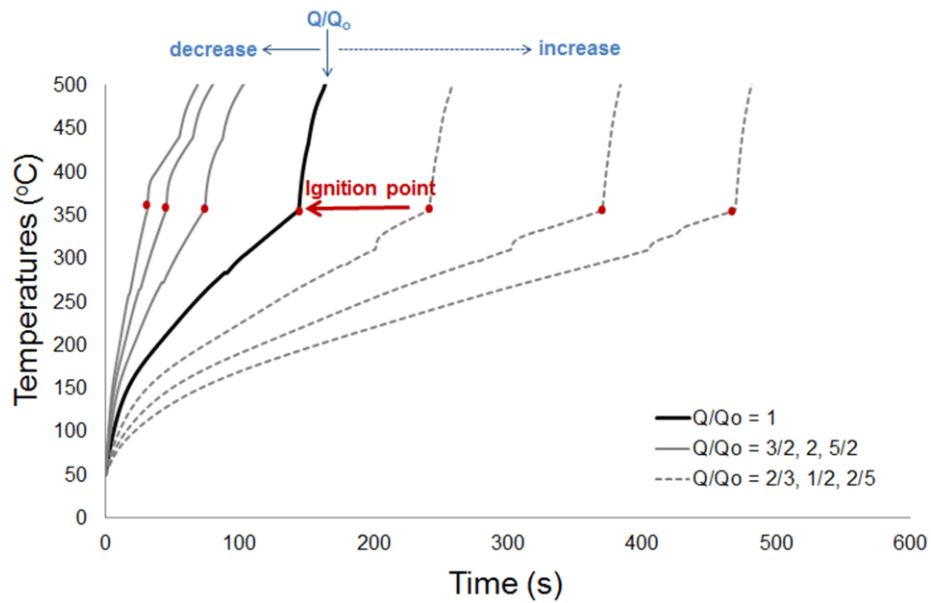


Figure 6.31: Effects of incident heat flux on the temperature profiles versus time of 6 mm GRE sample thickness.

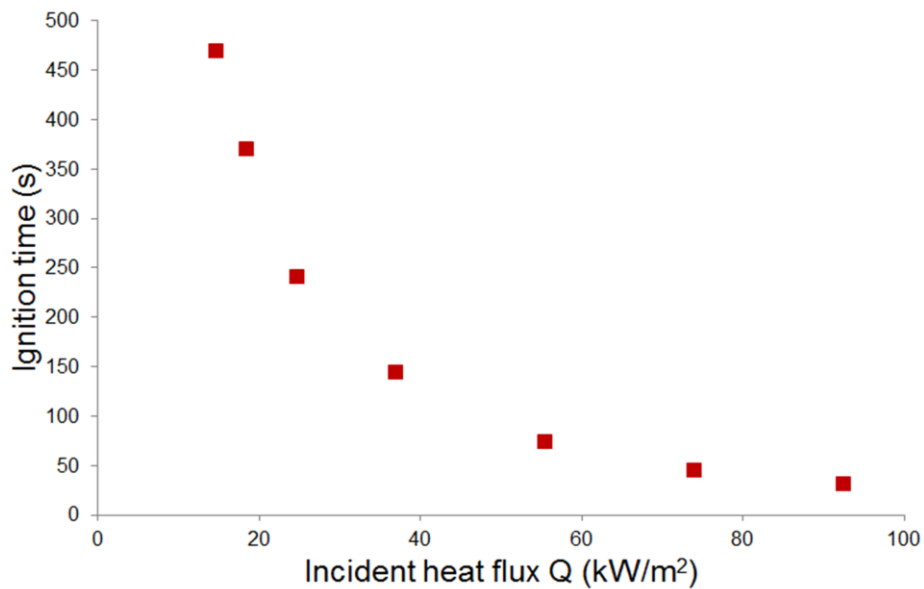


Figure 6.32: Simulation of TTI vs. incident heat flux of GRE of 6 mm thickness

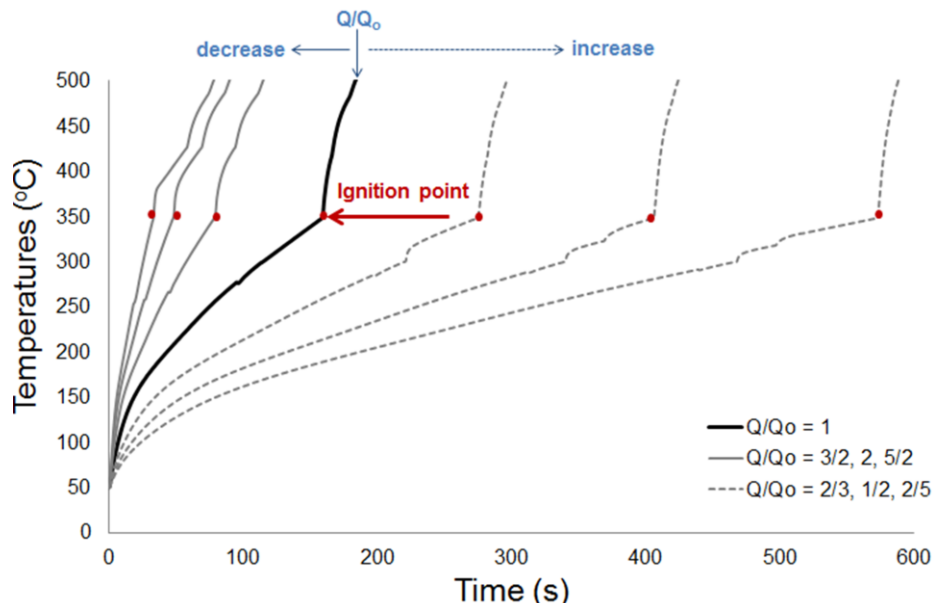


Figure 6.33 Effects of incident heat flux on the temperature profiles versus time of 7.5 mm GRE sample thickness.

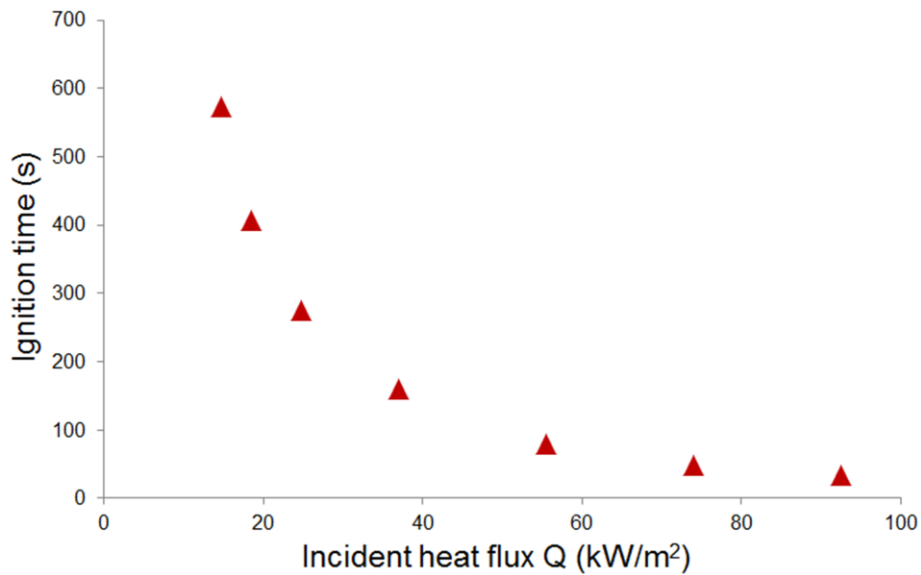


Figure 6.34: Simulation of TTI vs. incident heat flux of GRE of 7.5 mm thickness

In Figure 6.35, TTI versus heat flux of samples of different thicknesses have been compiled.

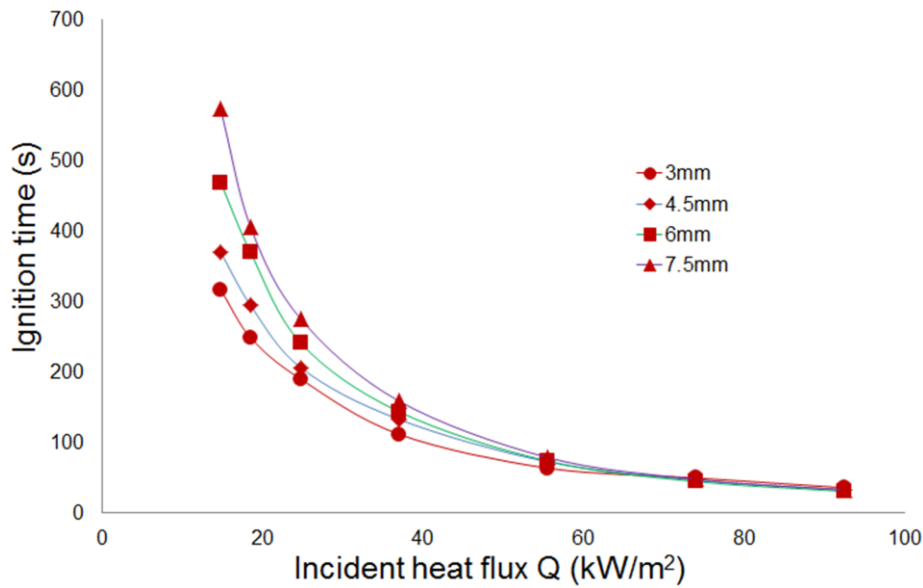


Figure 6.35: TTI vs. incident heat flux for 3, 4.5, 6 and 7.5 mm GRE sample thicknesses

The results in Figure 6.35 shows that beyond an incident heat flux of $Q = 50 \text{ kW/m}^2$ the TTI is almost the same regardless of the sample thickness value. In the literature a simple theory for the ignition of material, developed by Quintiere [3] is based on a pure heat transfer by conduction without degradation with a fixed ignition temperature, T_{ign} , which is equivalent to the flashpoint of liquid fuels. The flashpoint corresponds to the surface temperature sufficient to cause an evaporating vapour concentration equal to the lower flammable limit. Hence, submitted to a suitable heat source or pilot flame, this mixture will ignite and propagate fire. Once a flaming starts, the additional heating reflected to the polymer surface is usually sufficient to cause sustained burning. Since lower flammable limit concentrations are very low. Therefore, it is expected that a solid under the same circumstance will require little degradation to cause piloted ignition. Based on the concept of a fixed ignition temperature of a material, Lyon and Quintiere derived an expression for the time- to- ignition [237]:

$$t_{ign} = \frac{\pi}{4} \frac{k\rho C_p (T_{ign}-T_a)^2}{Q^2} \quad (\text{Eqn 6.5})$$

Where:

k : Specific thermal conductivity,

ρ : Specific density,

C_p : Specific heat capacity,

T_{ign} : Ignition temperature,

T_a : Ambient temperature,

Q : Incident heat flux

This equation is approximate and holds only under the following conditions:

- The solid is homogeneous,
- Thermal properties are constant,
- Its surface emissivity and absorptivity are both unity,
- The incident heat flux is much greater than the surface heat losses,
- The polymer thickness is greater than 1 mm.

For this work, in order to find an analytical mathematical relationship between the time required for the material to catch fire (i.e. TTI) depending on the composition of the glass fibre epoxy resin composite sample, its thermophysical parameters and geometrical characteristics, and the incident heat flux applied, the following equation is defined by dimension analysis extending Quintiere's equation (Eqn 6.5):

$$t_{ign} = \frac{\sqrt{kx_{th}} \cdot \rho C_p (T_{ign} - T_a)^{3/2}}{(1 - V_f) Q^{3/2}} \quad (Eqn 6.6)$$

Where in addition to the parameters in Eqn 6.5, x_{th} is the sample thickness and V_f is the volume fraction of fibre (0.32). The ignition temperature is defines as following [185]:

$$T_{ign} = \left[\frac{T_o H_g}{C_o} \right]^{0.5}$$

Where:

C_o : Heat capacity of the composite at 25°C (1500 J/kg.K)

T_o : Ambient temperature 298 K.

H_g : Heat of gasification (1.98*10⁶ J/kg)

Furthermore in order to verify the consistency of Eqn 6.6, the predicted TTI as a function of the incident heat flux for each thickness shown in Figure 6.35 are used for validation. Therefore shown below are the various response of ignition temperature in relation to heat flux for different thickness using both equation Eqn 6.6 and the computer predict TTI. All sets of data show good agreement.

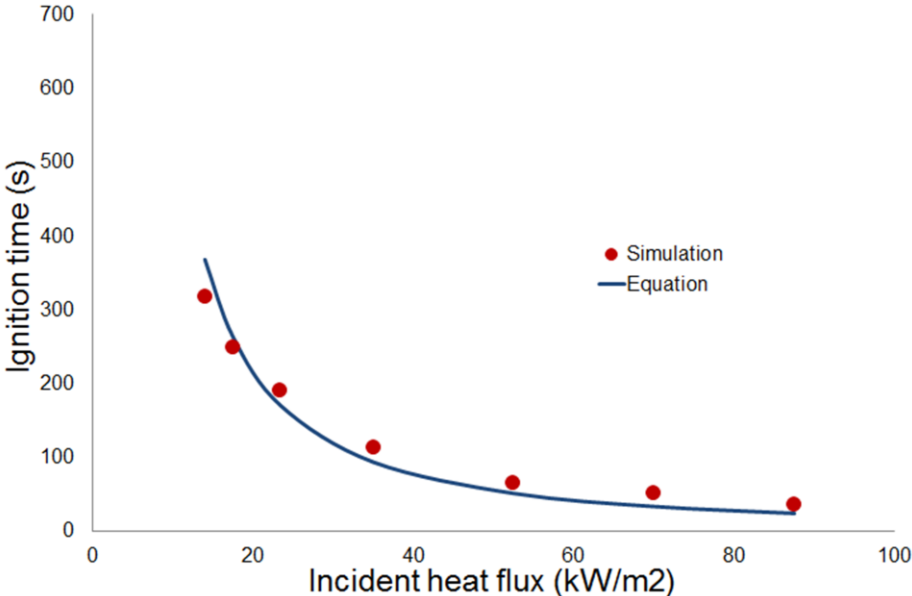


Figure 6.36: Predicted TTI and calculated TTI from Eqn 6.6 vs. incident heat flux for 3mm sample thickness

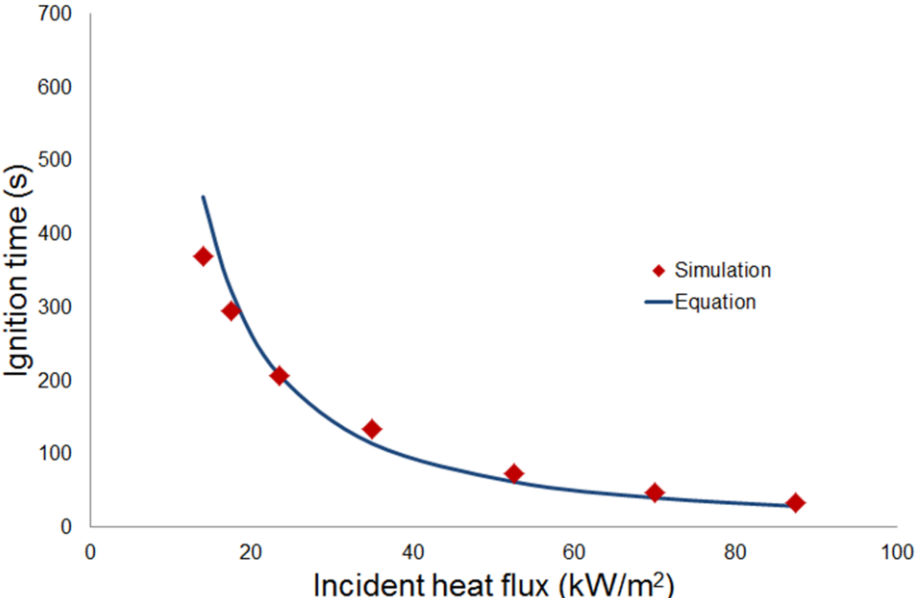


Figure 6.37: Predicted TTI and calculated TTI from Eqn 6.6 vs. incident heat flux for 4.5 mm sample thickness

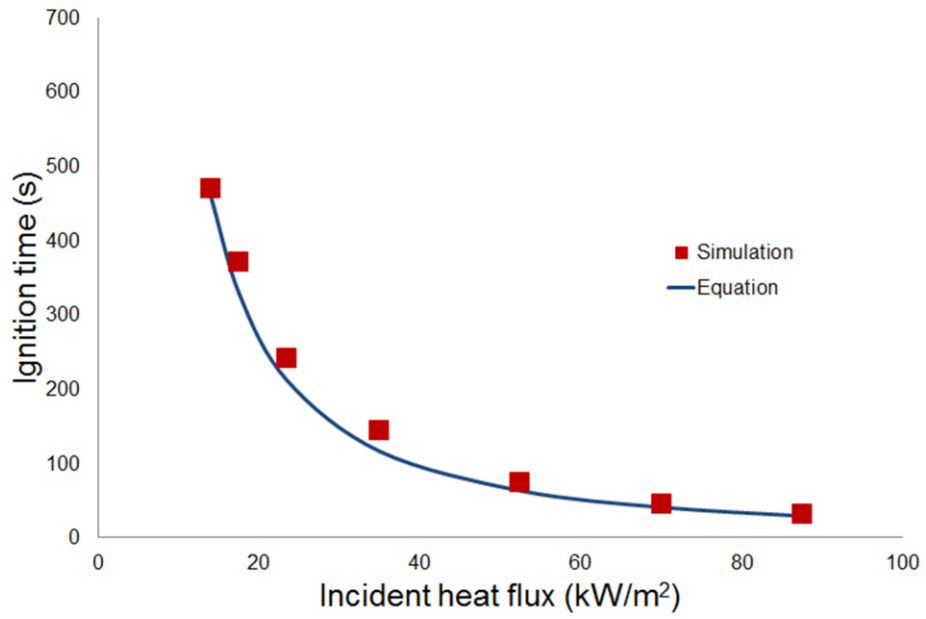


Figure 6.38: Predicted TTI and calculated TTI from Eqn 6.6 vs. incident heat flux for 6mm sample thickness

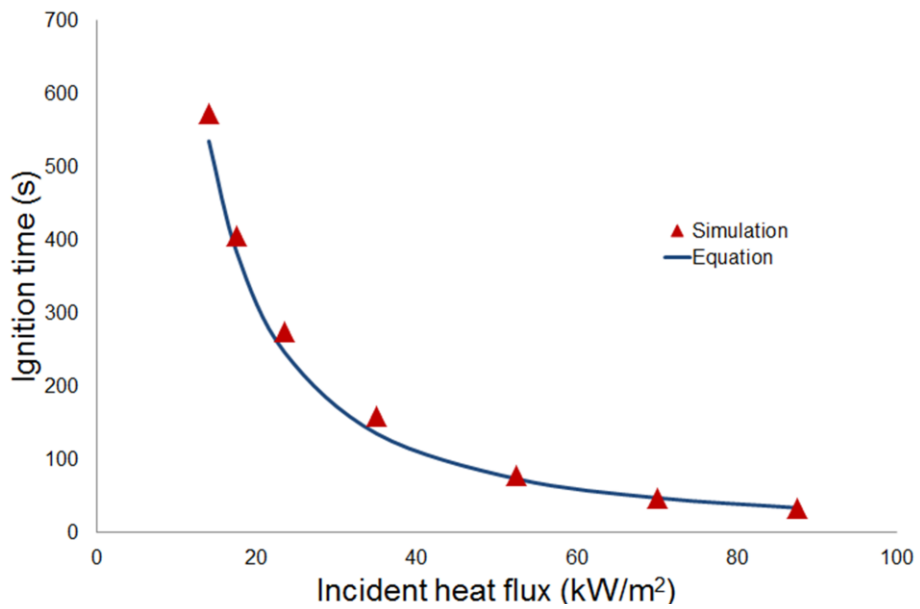


Figure 6.39: Predicted TTI and calculated TTI from Eqn 6.6 vs. incident heat flux for 7 mm sample thickness

6.6.3 Analysis and comments

Figure 6.36 to 6.39 show good agreements between simulation and calculated TTI, derived from the *Eqn 6.6* despite some minor differences which can be attributed to the overall sum of errors and the approximation due to the Finite Difference Method calculations. TTI increases as the incident heat flux decreases. That tendency is confirmed for samples of different thicknesses. The formula described by *Eqn 6.6*, is a useful approximation and provides acceptable results so that expensive lab experiments can be reduced.

6.7 Conclusions

In this chapter a numerical model was established and validated using experimental data. The novelty in this approach is the use of energy of activation in the equation defining the ignition temperature, T_{ig} , in order to obtain an acceptable simulated temperature profile. It has shown good agreement between simulated and experimental temperature versus time profiles of top and bottom surfaces of GFREP samples exposed to various incident heat fluxes and for samples of different thicknesses. Ignition phenomenon is well composed by the model showing a sudden step when the composite's polymer ignites and burns. Sensitivity analysis using analytical method (sensitivity function) is also used to find out which parameter influences the model most and the main information is that the temperature profile is more sensitive to the variation in thermal conductivity than to that of the heat capacity.

Moreover by using an experimentally validated Matlab programme based on the numerical model, an equation relating to the time-to-ignition and the incident heat flux is derived. This equation is extension of Quintiere's equation and is based upon the composition of the glass fibre epoxy resin composite sample, its thermophysical parameters and geometrical characteristics. The numerical model developed provides acceptable and is in good agreement with proposed theories.

Chapter 7: Heat transfer in intumescent coated glass reinforced epoxy composite (GRE).

7.1 Introduction

In Chapter 6 heat transfer in glass fibre reinforced epoxy resin composites (GRE) was studied. It was discussed that when these composites are exposed to high heat fluxes, the resin component tends to degrade on reaching its decomposition temperature, producing flammable volatiles, which then ignite. Therefore the structural integrity of the composite becomes difficult to be maintained once the resin softens / degrades. One of the solutions of such problem is to use an intumescent paint on the surface of the composite to provide a thermal barrier protective coating.

In this chapter the heat transfer in GRE composite sample (same as the one used previously in Chapter 6) coated with three different intumescent paints has been studied. A numerical model using Matlab software, capable of simulating the temperature profile inside the GFREP surface protected by a thermally insulative, intumesced char structure has been developed. The comparison between the simulated temperature profiles and the experimental results given in Chapter 3 is used to validate the model.

7.2 Model description

A one-dimensional heat and mass transfer model through an intumescent coated Glass Fibre Reinforced Epoxy Resin (GRE) composite laminates sample is schematically represented in the Figure 7.1 below.

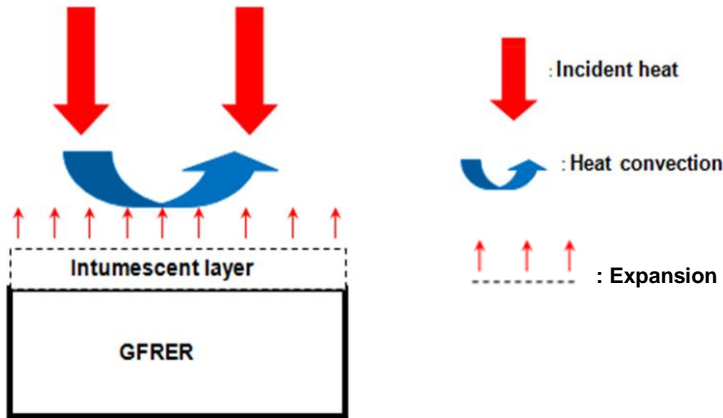


Figure 7.1: Schematic representation of heat transfer in intumescent coated GRE when the heating starts.

The system is taken as two layered structure: the GRE to be protected (the substrate) and the virgin intumescent coating. When exposed to elevated temperature intumescent chemicals expand and produce a thick layer of char which is the final barrier of protection against fire. The expanded layer is ablative and with time reduces its thickness. For the purpose of modelling the intumescent paint thickness, 1mm, is negligible comparing to the thickness of the charring layer and the GRE layer over the heating time. The gradual appearance of the carbonised layer in the expanding phase leads to the progressive change of the thermal properties of the system, which constitutes an effective thermal barrier. This dynamic process is schematically shown in Figure 7.2 below.

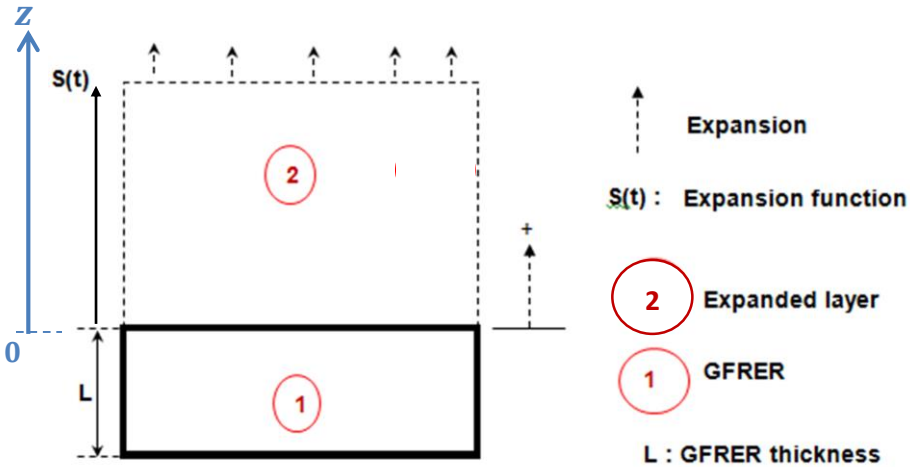


Figure 7.2: Schematic representation of heat transfer in intumescent coated GRE when the intumescent layer expands.

In Figure 7.2 above, from the Interface “GRE/intumescent paint” the intumescent layer is expanding according to the function $z = S(t)$. The assumption of perfect contact line between layers does not take into account the thermal contact resistance which could have an influence on the different flux (heat and gas) moving between layers of different nature. The modelling approach adopted assigns a sub-area for each of the layers, resulting in the appearance and disappearance of certain sub-domains under computational calculation.

7.3 Modelling heat transfer throughout the expanded layer

7.3.1 Balance equation

This expanded intumescent layer corresponds to the three intumescent layers (WI, EDI and EI) of thickness z such as $S(t)$ as shown in Figure 7.2. The heat transfer balance equation is given by [159, 240-241]:

$$\rho c_p \frac{\partial T(S(t), t)}{\partial t} = \nabla \cdot (k \cdot \nabla T(S(t), t)) + \dot{m} H_r \quad (\text{Eqn 7.1})$$

The left hand side and the right hand side of *Eqns 7.1* are respectively the variation of internal energy and the energy exchanged by conduction within the expanded layer where:

ρ , c_p , k , $S(t)$ and H_r are respectively the specific density, the specific heat capacity, the specific conductivity, the expansive intumescent function and the enthalpy of decomposition. The reaction rate of decomposition is modelled using the Arrhenius kinetic rate. As in Chapter 6, Section 6.2 it is assumed that the rate of decomposition $k(T)$ of the resin matrix follows a single-step [46-50]:

$$k(T) = A \cdot \exp\left(\frac{-E_a}{RT}\right)$$

And the mass flow rate of the expanding layer is defined as:

$$\dot{m} = \rho \cdot k(T)$$

Where, \dot{m} is the rate of mass decomposition ρ is the density, A pre-exponential factor, E_a activation energy and R is the universal gas constant. Moreover values for A and E are from reference [159, 242-243] for each intumescent coating material.

The thermal boundary condition is as following:

At $z = S(t)$ and $t > 0$,

$$k \frac{\partial T(S(t), t)}{\partial z} = \alpha \varphi_{inc} - h_c (T(S(t), t) - T_a) - \varepsilon \sigma (T^4(S(t), t) - T_a^4)$$

At $z = L$ and $t > 0$,

$$\frac{\partial T(S(t), t)}{\partial z} = \frac{\partial T(L, t)}{\partial z}$$

Where α , φ_{inc} , h_c , T_a , ε and σ are respectively the absorptivity coefficient of the intumescent layer, the incident heat flux from the cone calorimeter, the convection coefficient, the ambient temperature and Stefan Boltzmann coefficient.

7.3.2 Moving boundary condition

Three different coating types are studied: EI, EDI and WI with an initial thickness L_0 of 1, 3 and 5 mm. The expansion of each intumescent layer was experimentally measured at the end of a cone calorimeter experiment under an incident flux of 50kW/m² by Luangtriratana as discussed in Chapter 3, Section 3.4.2, Table 3.4), which is taken from reference [202].

Under conditions where intumescence occurred the thickness of the coating, $S(t)$, as it expands is calculated numerically using the equation as follows [150-155]:

$$S_i(t_i) = S_{i-1}(t_{i-1}) + m_{ex} \cdot (t_i - t_{i-1}) \quad (\text{Eqn 7.2})$$

Where m_{ex} is a variable expansion factor. In previous researchers' models, the expansion factor is purely determined by the overall conversion of gas-forming components or approximated as occurring over some period of gas evolution which matched when the molten matrix had reached a conversion such that the polymer viscosity was appropriate to trap the evolved gases [8, 9]. Here, m_{ex} is simply calculated as follows:

$$m_{ex} = \frac{\text{Char thickness}}{\text{Exposure time}}$$

The experimental values of 'char thickness' and 'exposure time' are taken from Table 3.4 in Chapter 3, Section 3.4.2., the values of m_{ex} are given in Table 7.2 below:

Samples	Char thickness (mm)	Exposure time (s)	m_{ex} (mm/s)
EI-1	6.8	400	0.02
EI-3	10	900	0.01
EI-5	15.8	1400	0.01
EDI-1	9.8	500	0.02
EDI-3	20.7	900	0.02
EDI-5	27	1600	0.02
WI-1	24.1	800	0.03
WI-3	41.7	800	0.05
WI-5	36.3	1200	0.03

Table 7.2: Char thickness, exposure time and calculated expansion factor.

7.4 Modelling heat transfer through the GRE substrate.

GRE corresponds to the layer of thickness $z = L$ such as $0 < z < S(t)$. The initial thickness is $L = 3 \text{ mm}$ in the present work. The corresponding balance equation is as following [149-151]:

$$\rho_{GP} c_{p_{GP}} \frac{\partial T(z, t)}{\partial t} + \dot{m}_{GP} H_{GP} = \nabla \cdot (k_{GP} \cdot \nabla T(z, t)) \quad (\text{Eqn 7.3})$$

The left hand side of *eqn 7.2* is the variation of internal energy stored in addition to the endothermic energy from pyrolysis of resin within the GRFP and the right hand side is the energy exchanged by conduction within the substrate . ρ_{GP} , $c_{p_{GP}}$, k_{GP} , \dot{m}_{GP} and H_{GP} are respectively the density, the specific heat capacity, the specific heat conductivity, the resin degradation mass rate and the enthalpy due to the resin degradation. The resin decomposition is modelled by Arrhenius equation previously mentioned in Chapter 6. The thermal boundary conditions are as following:

At $z = L$ and $t > 0$,

$$\frac{\partial T(S(t), t)}{\partial z} = \frac{\partial T(L, t)}{\partial z}$$

At $z = 0$ and $t > 0$,

$$\frac{\partial T(0, t)}{\partial z} = 0$$

7.5 Equation of thermophysical parameters

The experimental data of the specific conductivity, the specific heat capacity and the density of GRE have already been given in Table 6.1 in Chapter 6, Section 6.3.4.

The thermophysical experimental data of the intumescent coating paints WI, ED-I and EI Taken from Chapter 3 Section 3.4.3.2 are plotted and the graphs are shown in Figures 7.6 to 7.14. Matlab package of Matlab software is used to fit those curves in order to obtain their representative equations which are inputted in the numerical model based Matlab programme.

It is clearly observed in Figures 7.6 to 7.14 that the first drop in the thermophysical values of all intumescent coatings is due to the beginning of char expansion, at around 200 °C. Further

heating promotes a greater expanded char, which also means structural changes in the char (high porosity) leading to the lowest thermal conductivity and heat capacity values at 400°C in all coatings, especially the WI coating. After 400°C, the thermal conductivities start to increase again as a function of temperature as well as the densities. During the experiment it was observed that a reduction of the volume with little change in mass of the expanded layer above 300°C hence producing a more compact structure. This is the reason for the observed increase in the densities and the thermal conductivities. The heat capacities show little change, which indicates that, the composition of the char structure of EI and EDI changes little. The lowest thermal conductivity at 400°C is reflected by the maximum char expansion observed for WI coating. It must be noted that while the increase in char expansion is related to further heating it can also be co-related with the thermophysical properties despite the difficulties to correlate direct relationship between the two values due to different test conditions.

Figures 7.6 to 7.14 show respectively the fitted and experimental curves of the specific conductivity, the specific heat capacity and the specific density following by their derived polynomials equations with the constant given in Tables 7.1 to 7.3. Matlab gave a high degree of polynomial equation (13th order) to include all the experimental data in the equation. In order to simplify the expression of the equations, only the significant polynomial constants will be taken into account in the Matlab programme and the chosen constants are italicised and made bold in Table 7.2 to 7.4.

7.5.1 WI intumescent coating

(i) Thermal conductivity, $k(T)$

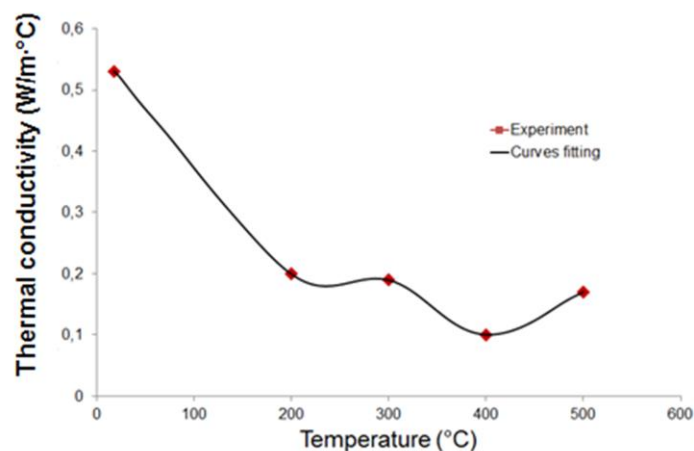


Figure 7.3: Thermal conductivity vs temperature curve fitted using Matlab.

(ii) Heat capacity, $C_p(T)$

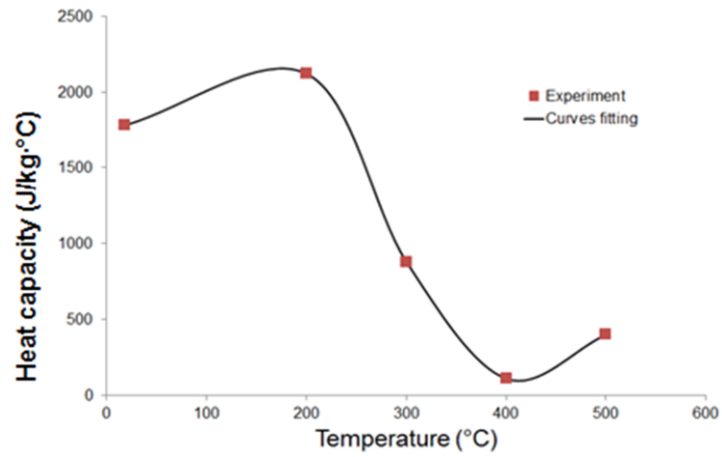


Figure 7.4: Heat capacity vs temperature curve fitted using Matlab.

(iii) Density, $\rho(T)$

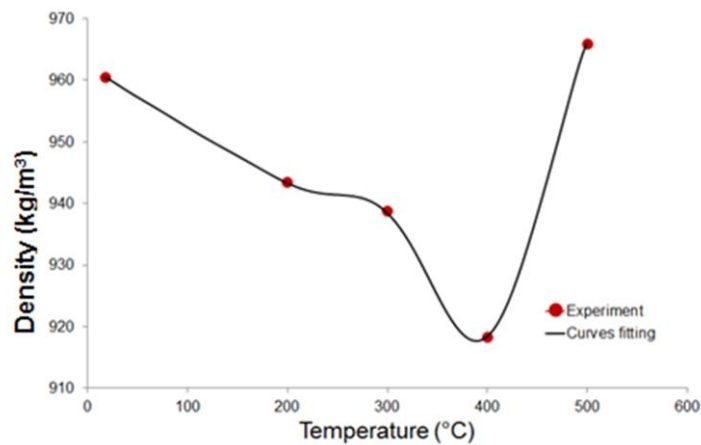


Figure 7.5: Density vs temperature curve fitted using Matlab.

From the data in Figure 7.3 to 7.5, $k(T)$, $C_p(T)$ and $\rho(T)$ are modelled in polynomial equations of 13 degrees as follows:

$$k, C_p \text{ or } \rho = A \times T^{13} + B \times T^{12} + C \times T^{11} + D \times T^{10} + E \times T^9 + F \times T^8 + G \times T^7 + H \times T^6 + I \times T^5 + J \times T^4 + K \times T^3 + L \times T^2 + M \times T + N$$

However, only the coefficients K, L, M and N (in bolt) are taken to be significant as shown in table 7.3 below:

Constants	Specific thermal conductivity	Specific heat capacity	Density
A	$6 \cdot 10^{-31}$	$-5 \cdot 10^{-27}$	-10^{-29}
B	$-2 \cdot 10^{-27}$	$2 \cdot 10^{-23}$	$2 \cdot 10^{-26}$
C	$3 \cdot 10^{-24}$	$-3 \cdot 10^{-20}$	-10^{-23}
D	$-2 \cdot 10^{-21}$	$2 \cdot 10^{-17}$	-10^{-20}
E	10^{-18}	-10^{-14}	$1,6 \cdot 10^{-17}$
F	$-6 \cdot 10^{-16}$	$5 \cdot 10^{-12}$	-10^{-14}
G	10^{-13}	$-1,5 \cdot 10^{-9}$	$3,64 \cdot 10^{-12}$
H	$-3 \cdot 10^{-11}$	$3 \cdot 10^{-7}$	$-8 \cdot 10^{-10}$
I	$4 \cdot 10^{-9}$	$-3,5 \cdot 10^{-5}$	10^{-7}
J	$-3 \cdot 10^{-7}$	$3 \cdot 10^{-3}$	-10^{-5}
K	$2 \cdot 10^{-5}$	$-1,6 \cdot 10^{-1}$	$7 \cdot 10^{-4}$
L	$-6 \cdot 10^{-4}$	5	$-3 \cdot 10^{-2}$
M	10^{-2}	-90	0.4
N	10^{-1}	$2,368 \cdot 10^3$	960

Table 7.3: Polynomial constant of k(T), Cp(T) and ρ(T) equations.

The same assumptions for EI in Table 7.3 above are also applied for EDI and WI in Table 7.4 and 7.5 respectively.

7.5.2 EDI intumescent coating

(i) Thermal conductivity, k(T)

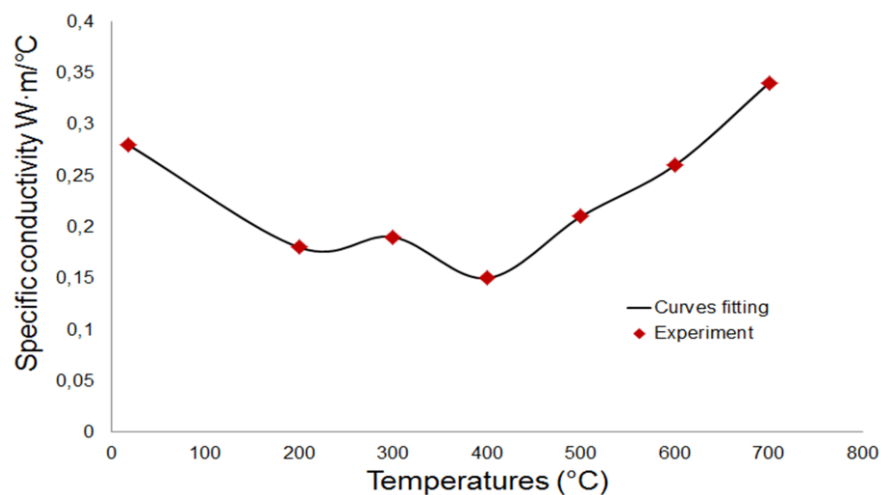


Figure 7.6: Thermal conductivity vs temperature curve fitted using Matlab.

(ii) Heat capacity, $C_p(T)$

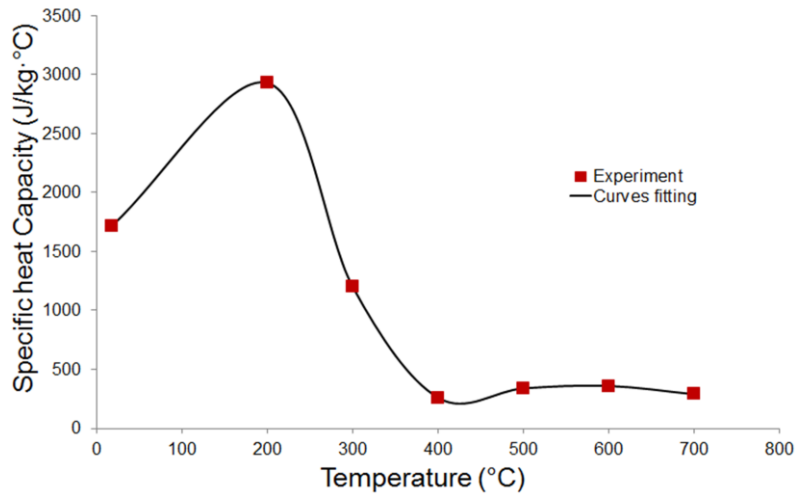


Figure 7.7: Heat capacity vs temperature curve fitted using Matlab.

(iii) Density, $\rho(T)$

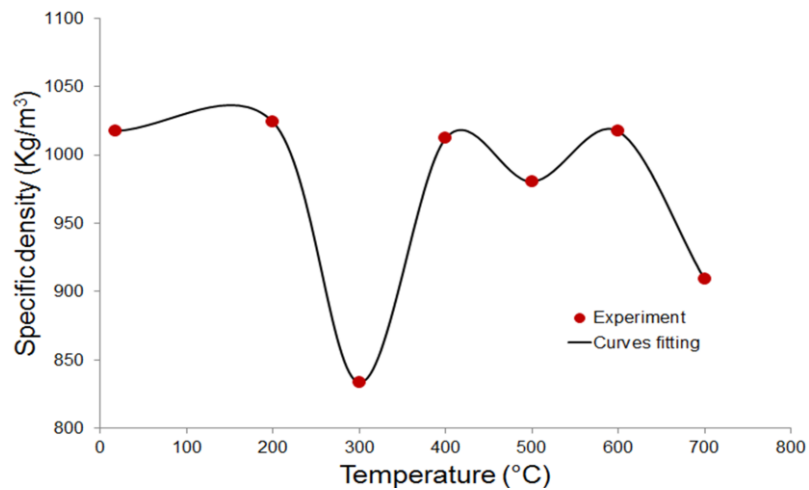


Figure 7.8: Density vs temperature curve fitted using Matlab.

Equation form for $k(T)$, $C_p(T)$ and $\rho(T)$:

$$k, C_p \text{ or } \rho = A \times T^{13} + B \times T^{12} + C \times T^{11} + D \times T^{10} + E \times T^9 + F \times T^8 + G \times T^7 + H \times T^6 + I \times T^5 + J \times T^4 + K \times T^3 + L \times T^2 + M \times T + N$$

Constants	Specific thermal conductivity	Specific heat capacity	Density
A	$-4 \cdot 10^{-32}$	10^{-28}	$5 \cdot 10^{-29}$
B	$2 \cdot 10^{-28}$	$-5 \cdot 10^{-25}$	$-2 \cdot 10^{-25}$
C	$-3 \cdot 10^{-25}$	10^{-21}	$5 \cdot 10^{-22}$
D	$4 \cdot 10^{-22}$	-10^{-18}	$-5,5 \cdot 10^{-19}$
E	$-3 \cdot 10^{-19}$	$8 \cdot 10^{-16}$	$4 \cdot 10^{-16}$
F	$1.6 \cdot 10^{-16}$	$-4 \cdot 10^{-13}$	$-2 \cdot 10^{-13}$
G	$-5.7 \cdot 10^{-14}$	10^{-10}	$7 \cdot 10^{-11}$
H	$1.4 \cdot 10^{-11}$	$-2.66 \cdot 10^{-8}$	$-2 \cdot 10^{-8}$
I	$-2.4 \cdot 10^{-9}$	$3.6 \cdot 10^{-6}$	$3 \cdot 10^{-6}$
J	$2.7 \cdot 10^{-7}$	$-3 \cdot 10^{-4}$	$-3 \cdot 10^{-4}$
K	$-2 \cdot 10^{-5}$	10^{-2}	$2 \cdot 10^{-2}$
L	$8 \cdot 10^{-4}$	$4.5 \cdot 10^{-2}$	-0.7
M	$-2 \cdot 10^{-2}$	-3	13
N	0.5	1733	1501

Table 7.4: Polynomial constant of $k(T)$, $C_p(T)$ and $\rho(T)$ of equations.

7.5.3 EI intumescent coating

(i) Thermal conductivity, $k(T)$

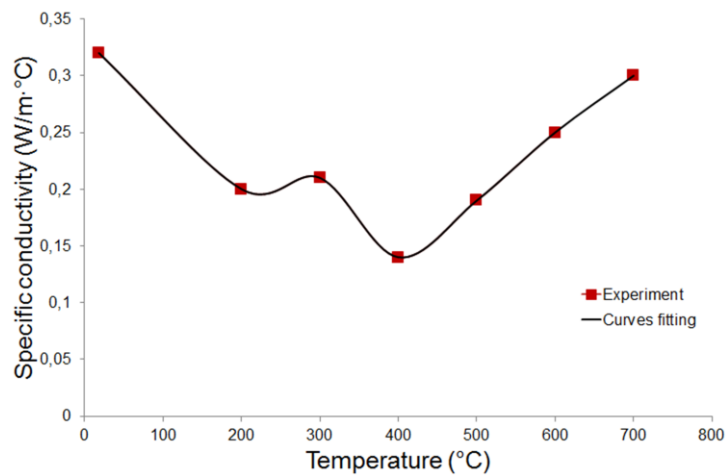


Figure 7.9: Thermal conductivity vs temperature curve fitted using Matlab.

(ii) Specific heat capacity, $C_p(T)$

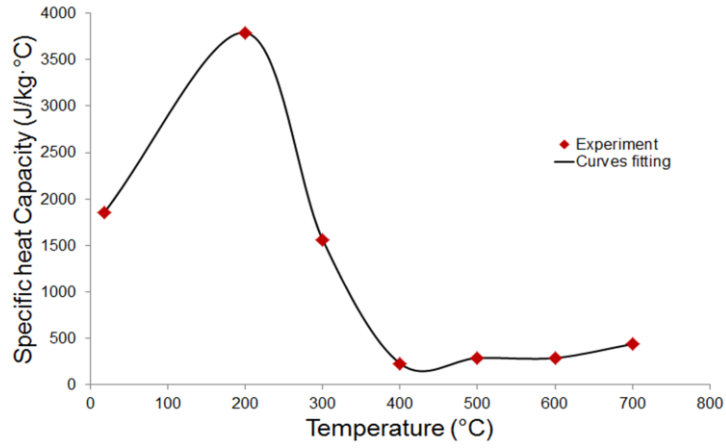


Figure 7.10: Heat capacity vs temperature curve fitted using Matlab.

(iii) Density, $\rho(T)$

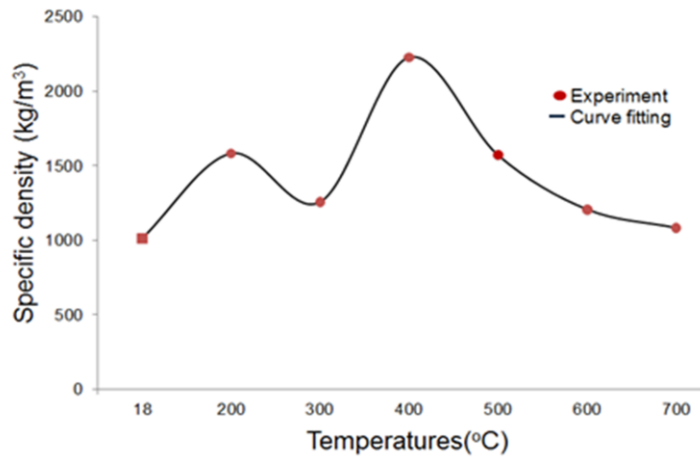


Figure 7.11: Density vs temperature curve fitted using Matlab.

Equation form for $k(T)$, $C_p(T)$ and $\rho(T)$:

$$k, C_p \text{ or } \rho = A \times T^{13} + B \times T^{12} + C \times T^{11} + D \times T^{10} + E \times T^9 + F \times T^8 + G \times T^7 + H \times T^6 + I \times T^5 + J \times T^4 + K \times T^3 + L \times T^2 + M \times T + N$$

Constants	Specific thermal conductivity	Specific heat capacity	Density
A	$-4 \cdot 10^{-32}$	$8.7 \cdot 10^{-29}$	$3 \cdot 10^{-28}$
B	$1.74 \cdot 10^{-28}$	$-3,6 \cdot 10^{-25}$	-10^{-24}
C	$-3.5 \cdot 10^{-25}$	$6.6 \cdot 10^{-22}$	$3 \cdot 10^{-21}$
D	$4 \cdot 10^{-22}$	$-6.6 \cdot 10^{-19}$	$-3.5 \cdot 10^{-18}$
E	$-3 \cdot 10^{-19}$	$4 \cdot 10^{-16}$	$3 \cdot 10^{-15}$
F	$1.6 \cdot 10^{-16}$	$-1.2 \cdot 10^{-14}$	-10^{-12}
G	$-5.7 \cdot 10^{-14}$	$5 \cdot 10^{-12}$	$5 \cdot 10^{-10}$
H	$1.4 \cdot 10^{-11}$	10^{-8}	-10^{-7}
I	$-2 \cdot 10^{-9}$	$-4.6 \cdot 10^{-6}$	$2 \cdot 10^{-5}$
J	$3 \cdot 10^{-7}$	$9 \cdot 10^{-4}$	$-2 \cdot 10^{-3}$
K	$-2 \cdot 10^{-5}$	-0.1	0.2
L	$8.7 \cdot 10^{-4}$	6	-8
M	$-2 \cdot 10^{-2}$	-154	177
N	0.5	3235	-486

Table 7.5: Polynomial constant of $k(T)$, $C_p(T)$ and $\rho(T)$ equations.

7.6 Numerical resolution

Eqn 7.1 and Eqn 7.3 are nonlinear equations due to the differential term in temperature T . Therefore, these equations need to be solved numerically using the Finite Difference Method (FDM). The temperature profiles within the char layer and the GRE will be determined from a purposely developed Matlab computer program based upon numerical nodal equations according the sample discretisation shown in Figure 7.12 below:

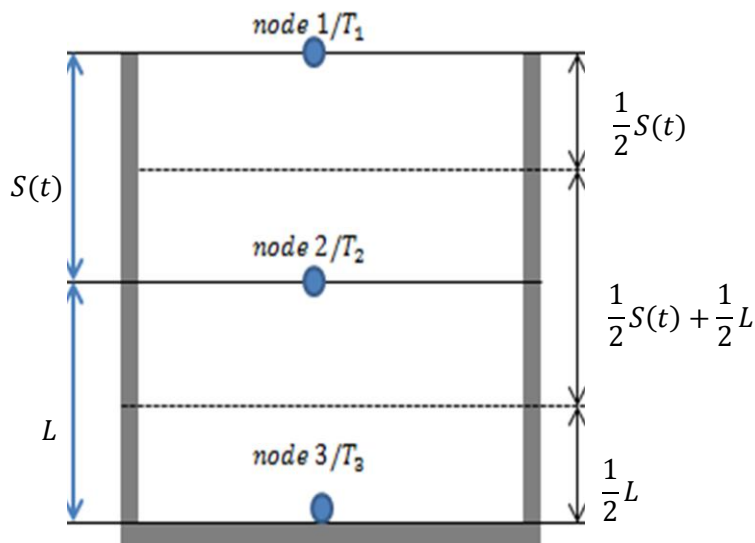


Figure 7.12: Discretised GRE substrate protected by intumescent coating

The finite difference approximation of Eqn 7.1 and Eqn 7.3 for a numerical resolution is as following:

$$\text{Node 1: } z = \frac{1}{2} S(t)$$

$$\left(\frac{1}{2}\rho_r c_{p_r}\right)\left(\frac{T_1^{t+\Delta t} - T_1^t}{\Delta t}\right) = \dot{q}_{ef} + k_c \frac{T_2^t - T_1^t}{S(t)} + \dot{m}_r H_r \quad (\text{Eqn 7.4})$$

$$\text{Node 2: } \frac{1}{2} S(t) \leq z \leq \frac{1}{2} L$$

$$\begin{aligned} \left(\frac{1}{2}\rho_r c_{p_r} + \frac{1}{2}\rho_{GP} c_{p_{GP}}\right)\left(\frac{T_2^{t+\Delta t} - T_2^t}{\Delta t}\right) \\ = k_r \frac{T_1^t - T_2^t}{S(t)} + k_{GP} \frac{T_3^t - T_2^t}{L} + \dot{m}_r H_r + \dot{m}_{GP} H_{GP} \quad (\text{Eqns 7.5}) \end{aligned}$$

$$\text{Node 3: } z = \frac{1}{2} L$$

$$\left(\frac{1}{2}\rho_{GP} c_{p_{GP}}\right)\left(\frac{T_3^{t+\Delta t} - T_3^t}{\Delta t}\right) = k_{GP} \frac{T_2^t - T_3^t}{L} + \frac{1}{2}\dot{m}_{GP} H_{GP} \quad (\text{Eqns 7.6})$$

The simultaneous numerical equations (Eqns 7.3) , (Eqns 7.4) and (Eqns 7.5) are solved by developing a computational programme code using Matlab software in order to find out the predicted temperature profile within the intumescent coated glass fibre reinforced epoxy resin samples.

7.7 Simulation results

The predicted temperature profiles in the three intumescent coated samples are shown on Figures 7.13 to 7.18.

(i) GRE substrate protected by EI intumescent coating

Figure 7.13 and 7.14 show the predicted temperature profiles GRE sample coated with WI intumescent coating.

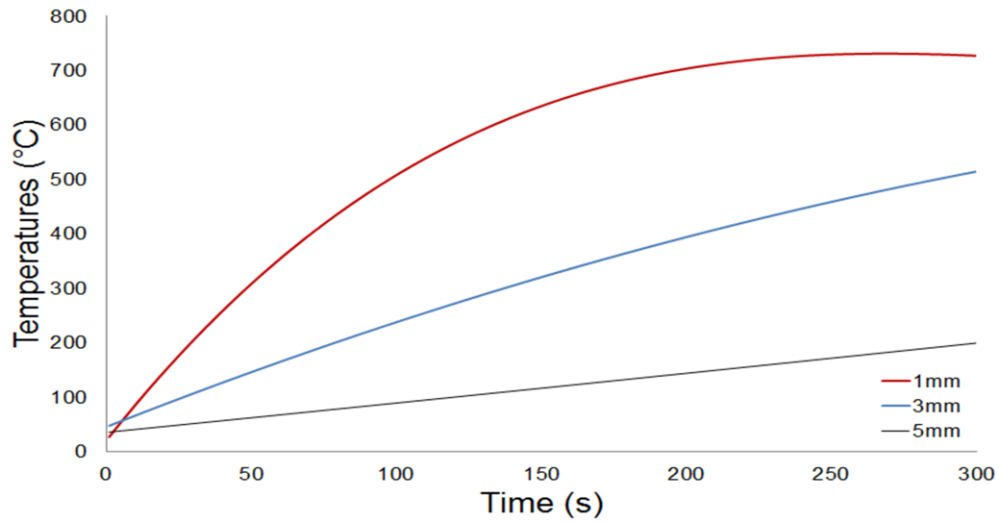


Figure 7.13: Simulated temperatures at the top side of the GRE coated with 1, 3 and 5mm thicknesses of EI exposed to 50 kW/m² heat flux.

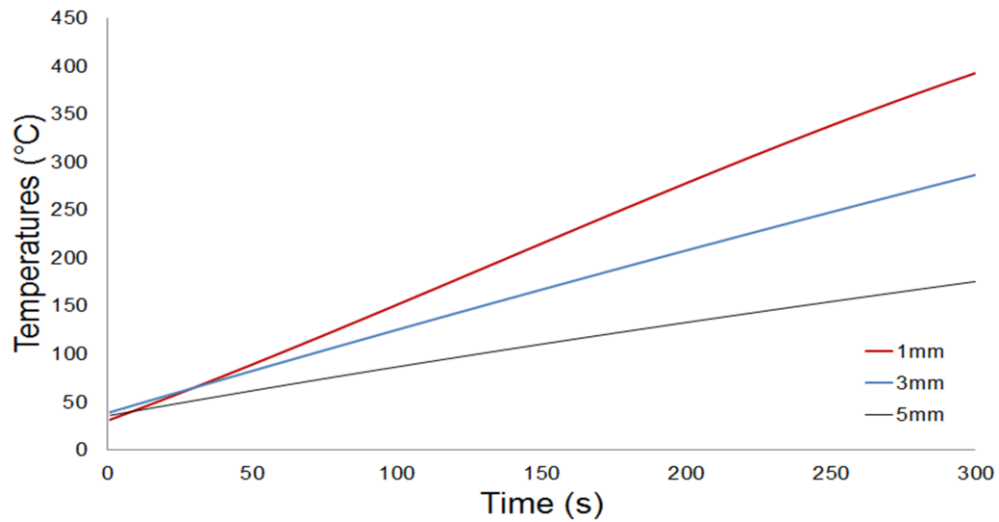


Figure 7.14: Simulated temperatures at the bottom side of the GRE coated with 1, 3 and 5mm thicknesses of EI exposed to 50kW/m² heat flux.

(ii) GRE substrate protected by EDI intumescent coating

Figure 7.15 and 7.16 show the predicted temperature profiles GRE sample coated with EDI intumescent paint.

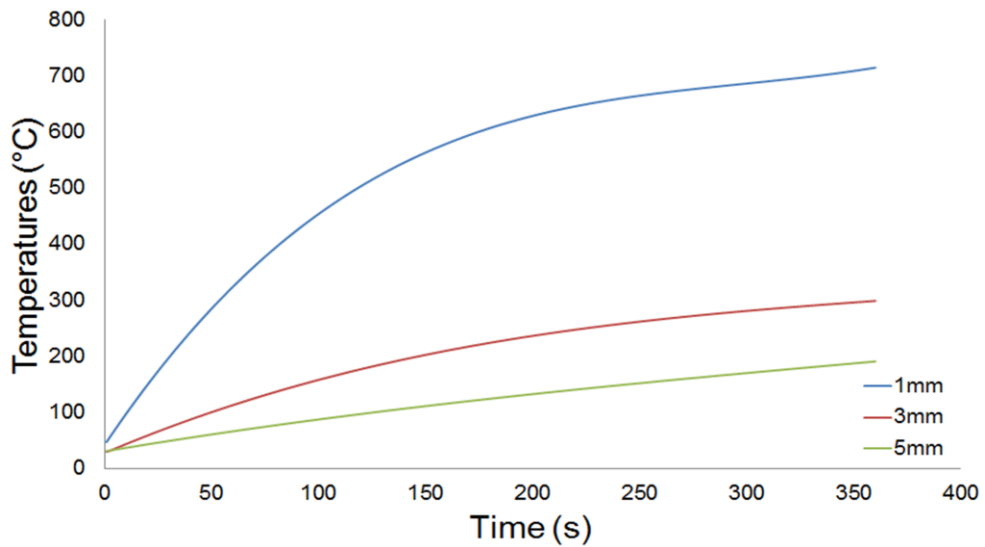


Figure 7.15: Simulated temperatures at the top side of the GRE coated with 1, 3 and 5mm thicknesses of EDI exposed to 50kW/m² heat flux.

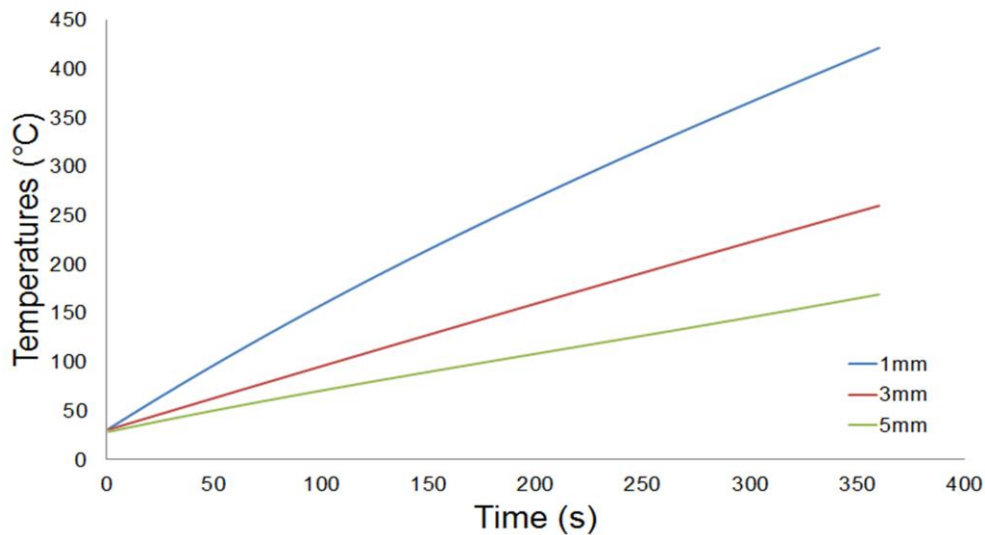


Figure 7.16: Simulated temperatures at the bottom side of the GRE coated with 1, 3 and 5mm thicknesses of EDI exposed to 50kW/m² heat flux.

(iii) GRE substrate protected by WI intumescent coating

Figure 7.17 and 7.18 show the predicted temperature profiles GRE sample coated with WI intumescent paint.

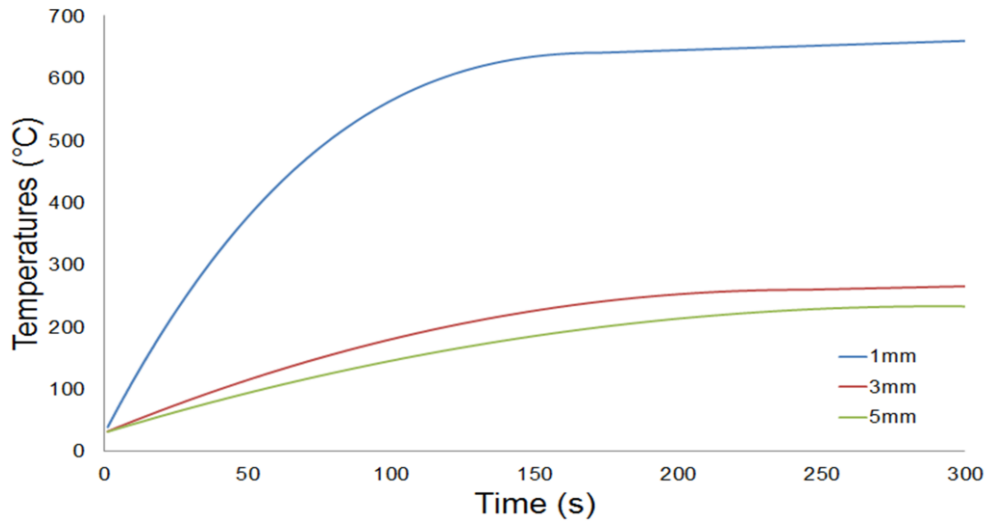


Figure 7.17 Simulated temperatures at the top side of the GRE coated with 1, 3 and 5mm thicknesses of WI exposed to 50kW/m² heat flux.

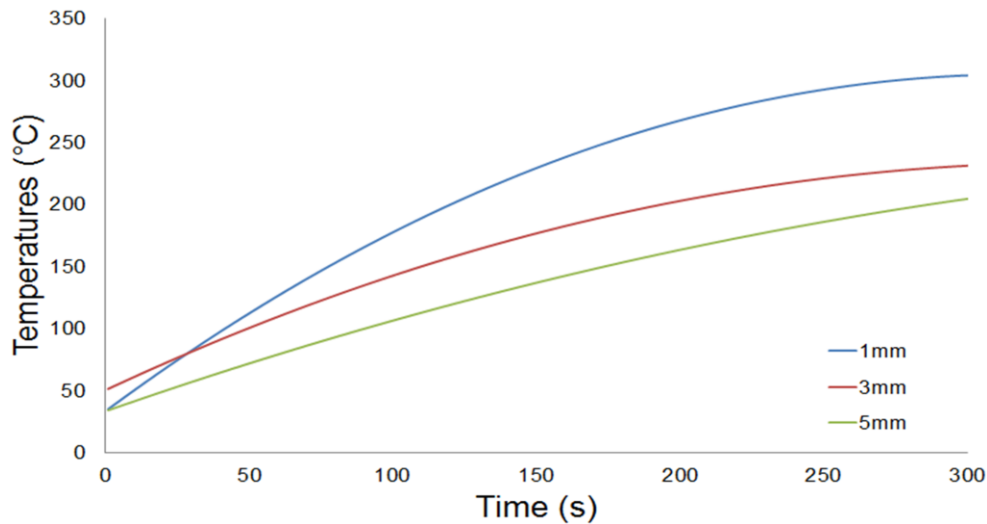


Figure 7.18: Simulated temperatures at the bottom side of the GRE coated with 1, 3 and 5mm thicknesses of WI exposed to 50kW/m² heat flux

7.8 Model validation

7.8.1 Comparison between predicted and experimental results.

Figures 7.19 to 7.24 inclusive show the comparison between experimental and simulation curves of the GRE sample coated with WI, EDI and EI intumescent coating paint.at an incident heat flux of 50kW/m^2 .

(i) GRE substrate protected by EI intumescent coating,

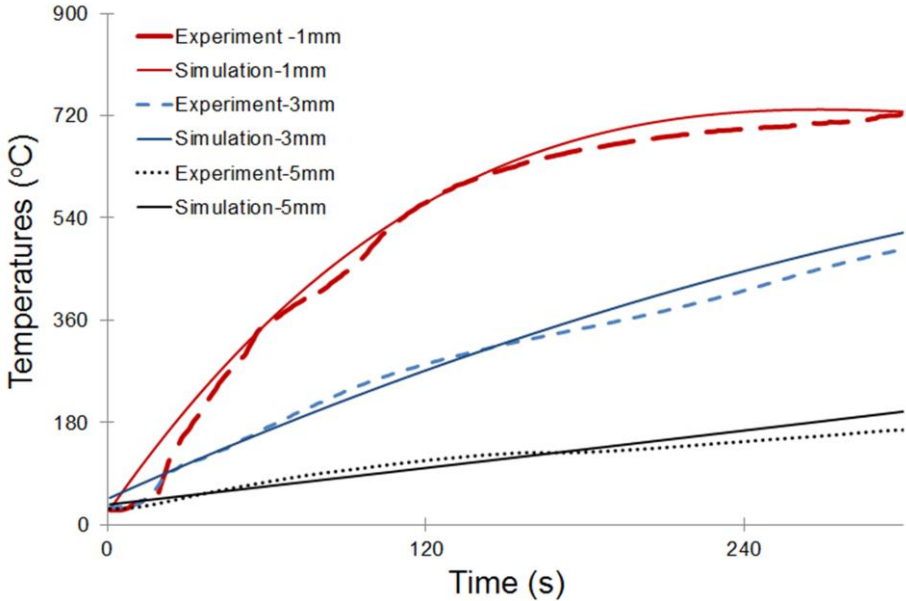


Figure 7.19: Simulated and Experimental temperatures at the top side of the GRE coated with 1, 3 and 5mm thicknesses of EI exposed to 50kW/m^2 heat flux

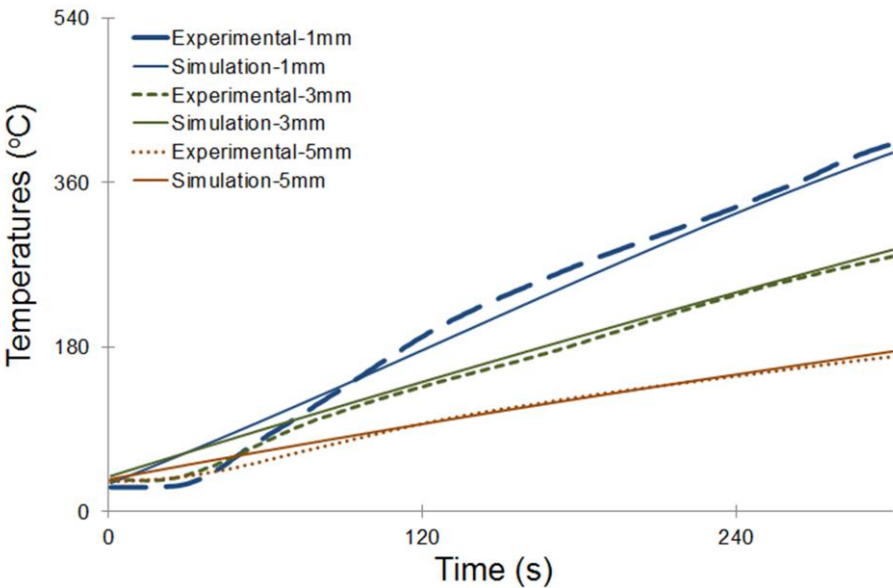


Figure 7.20: Simulated and Experimental temperatures at the bottom side of the GRE coated with 1, 3 and 5mm thicknesses of EI exposed to 50kW/m^2 heat flux

(ii) GRE substrate protected by EDI intumescent coating,

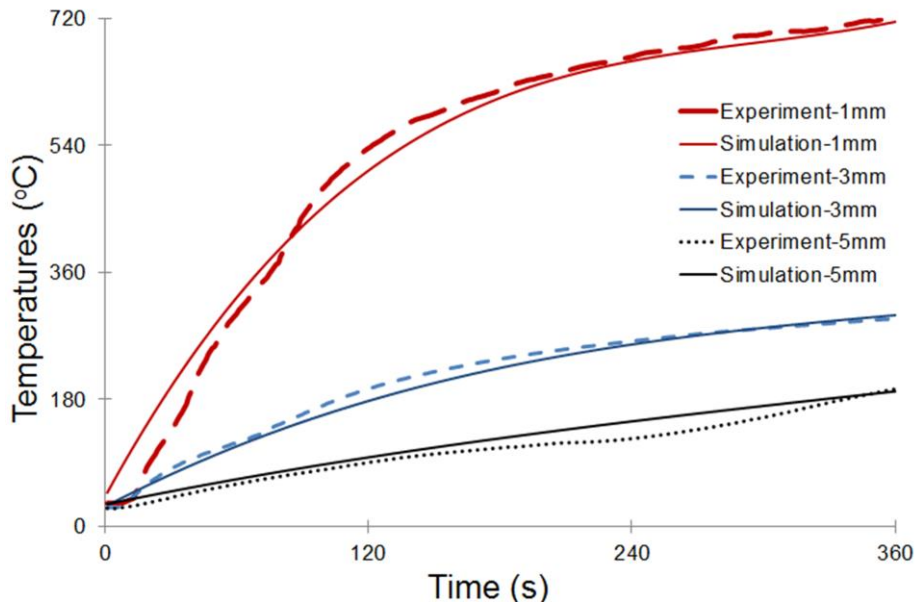


Figure 7.21: Simulated and Experimental temperatures at the top side of the GRE coated with 1, 3 and 5mm thicknesses of EDI exposed to 50kW/m² heat flux.

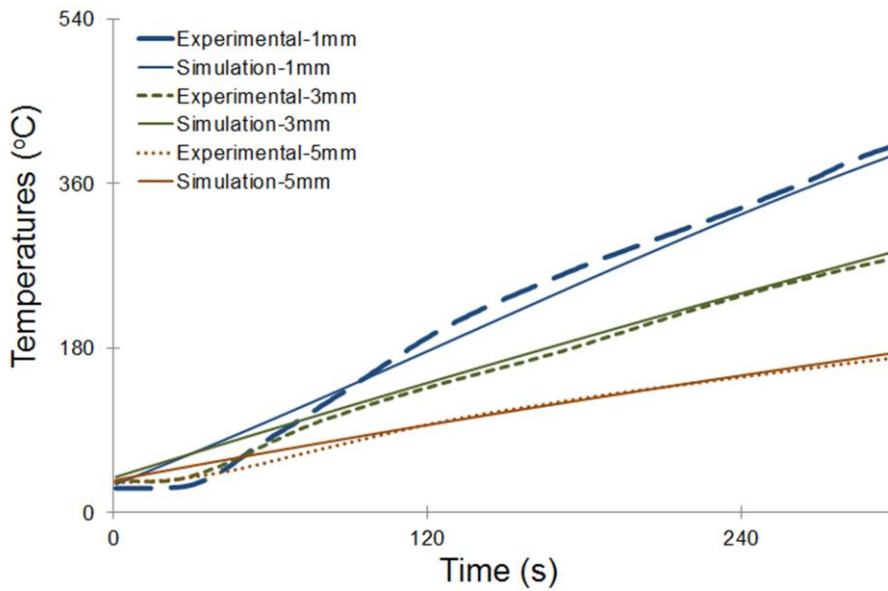


Figure 7.22: Simulated vs. Experimental temperatures at the bottom side of the GRE coated with 1, 3 and 5mm thicknesses of EDI exposed to 50kW/m² heat flux.

(iii) GRE substrate protected by WI intumescent coating.

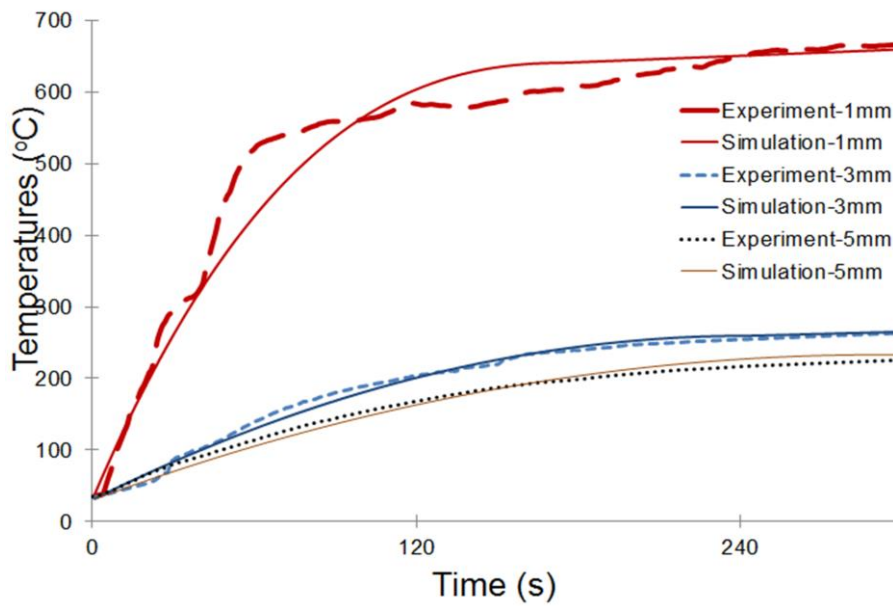


Figure 7.23: Simulated and Experimental temperatures at the top side of the GRE coated with 1, 3 and 5mm thicknesses of WI exposed to 50kW/m² heat flux.

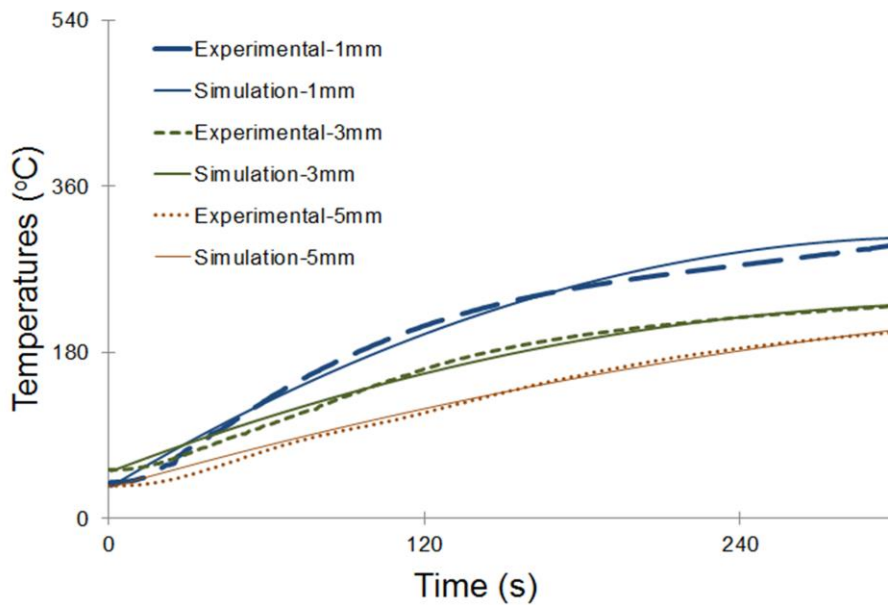


Figure 7.24: Simulated and Experimental temperatures at the bottom side of the GRE coated with 1, 3 and 5mm thicknesses of WI exposed to 50kW/m² heat flux.

Figure 7.19 to 7.24 show results both comparable in magnitude and trend for predicted and measured temperatures. However there are differences between simulation and experimental temperatures. The temperature gradient can be attributed to a combination of errors from the experiment process (thermocouple setting and reading) and from the parameters used to run the numerical model.

7.8.2 Comments

The validation of the model by comparing experimental and simulation temperature profiles shows constancy between predicted and measured temperature for the GFREPs with three types of intumescent coatings studied. Indeed, for both experimental temperatures and those from numerical simulations, there are differences between the temperature at the surface of the composite (under the coating) and those at the bottom; the temperature gradient is small and negligible. According to the balance equations used to build the model, thermophysical properties (the specific thermal conductivity, specific heat capacity and density) have a crucial effect. Those parameters were measured experimentally as a function of temperature [6] and inputted into the model. It is likely that the improvement of processes to minimize experimental errors would lead to a more precise measurements of these physical quantities and thus increase its accuracy. Indeed, the composition of an intumescent coating depends on the manufacturer and is confidential in most cases. The majority of the characteristics data of a specific intumescent coating are not directly accessible, and the uncertainty relating to their exact values is a potential source of error for the model.

7.9 Conclusion

In this chapter, heat transfer model of GRE coated with intumescent materials (WI, ED-I and EI), which respond to heat by expanding producing a char thickness between 5 and 100 times greater than their initial coating thickness. The intumescent coating provide thermal protection to the substrate after undergoing endothermic chemical reactions providing structural char formation that inhibits the transport of volatiles to the environment and the transport of oxygen to unburned region beneath the char; and the retention of mass in the char limits further involvement of the underlying materials in fire [202].

Also, the predicted behaviour of GRE with three different intumescent coating exposed to an incident heat flux is performed and a mathematical model is presented. This model is based on the one-dimensional (1D) representation of physical phenomena accompanying the reaction of intumescent coating applied to a GRE composite as a substrate and it is also based on the one-dimensional heat transfer phenomenon throughout the intumescent coating and through the Glass Fibre Reinforced Polymer composite.

All these phenomena are described by a balance equation which is a nonlinear Partial Differential Equation (PDE). That equation is solved numerically by the Finite Difference Method (FDM) for the one-dimensional (1D) domain (intumescent coating / GRE as a substrate). The simulated temperatures obtained through the intumescent coating layer and the temperatures through the GRE are presented and compared with experimental temperatures obtained in the corresponding conditions for model validation. The observation of these comparisons shows that the temperature profiles predicted by the model are consistent.

This work extends some previous works [159-166, 244-246] that can be found in literature in the same area of research by inputting in the mathematical modelling, thermophysical parameters varying as a function of temperatures. This method improves the accuracy and potentially increases the reliability of the model. However, the results may suffer from small inaccuracies in describing the dynamics of the phenomena due to the assumption made by taking the top surfaces of the samples as flat surfaces while in reality they are not.

Chapter 8: Conclusions

This thesis has focused on the design and development of theoretical and numerical heat transfer models, undertaken to simulate and experimentally validate temperature variations during melting, decomposition, charring and ignition phases of polymeric materials in different heating scenarios.

In the case of melting, thermoplastic polymers (polypropylene, polyester, polyamide 6, polymethyl methacrylate, polycarbonate and polystyrene) have been used, whereas for decomposition, charring and ignition glass fibre reinforced epoxy composites have been chosen.

Another aspect of the work was to simulate heat transfer in intumescent coated glass fibre - reinforced epoxy composites exposed to heat under a cone calorimeter. The emphasis was to understand the thermal barrier efficiency of the expanded char, however changes to the surface, expansion of the local thickness and char region, when exposed to heat, were incorporated into the model, so as to achieve closer agreement with experiment values.

A one-dimensional finite difference method was adopted in the form of a coded program, using Matlab as the operator in all scenarios. The program was developed to determine the transient temperature distributions within the different types of polymeric materials. The convective and radiative heat transfer boundary conditions, at the exposed and unexposed sides of polymer samples, have also been taken into account accordingly. While some experimental results to validate the different numerical models developed, are from other researchers' work at Bolton University, other sets of experiments were specifically developed for this work.

The Matlab simulation programmes performed the calculations giving numerical solutions to the partial differential equations which are not possible to solve analytically. The obtained results, validated by experimental data, may be a potential source for the reduction in the number of expensive experiments in laboratory. Therefore, the outcomes provide a foundation for future research and development in this area.

In the course of this work, the contributions to knowledge are thus:

1. The numerical model developed and the predicted results contribute to improve the knowledge of temperature of the drops from which degree of thermoplastic degradation can be estimated in the area of polymer melt dripping.

The numerical model developed reported in this thesis estimates the instantaneous temperature of the molten drops under radiant heat. The actual temperatures were also measured with a locally positioned thermocouple and were reasonably close given the potential for experimental error. The knowledge of the temperature of the drops indicates the actual degree of thermoplastic degradation occurring in the region of polymer melt dripping.

2. The Stefan method, usually employed to solve phase change of water (ice, snow etc.), was adapted here to design a numerical model capable of predicting the temperature profile, including ignition phenomenon for the thermoplastic polymer melting subjected to cone calorimeter heat flux. This combined method highlights a new process to extend the Stefan Method applied thermoplastic polymers under heat flux load.

3 Using a validated model, a set of simulations were performed to establish a methodology based on Quintiere's equation. The model produces an analytical prediction of the ignition time for GRE taking into account: the volume fraction of the fibres and the thickness of the sample.

4. A numerical model was produced to predict the temperature profile within a GRE plate containing an intumescent coating. This methodology can also aid the determination of efficiency of such thermal barrier protection systems.

The different parts of the work undertaken in this thesis have led to a progression in the knowledge of the understanding of the polymers' behaviour in presence of fire. The laboratory testing scales, combined with the numerical simulations, identified the dominant phenomena and defined the range of variation of the polymers' thermal properties, when subjected to heat. However, the effect of heat on polymeric based materials also showed the extreme complexity of the relationship between the intensity of the heat flux and thermoplastic material in melt dripping condition and, in GRE with intumescent coating as thermal barrier. One of the main objectives assigned to the laboratory experiments was therefore to produce accurate temperature measurements, in order to better validate the numerical model designed. Hence, all the numerical models developed in this thesis have been validated by comparing with experimental measurements. The predicted temperature profiles contributed to an improved understanding of the physico-chemical processes involved within heated polymeric material.

The main design process and concluding remarks can be drawn from the research undertaken, and these are listed below for each heating scenario:

1) Melting/melt dripping of thermoplastic polymers in vertical orientation

In chapter 4 an adiabatic container was designed and combined to an existing 21 mm diameter tubular furnace rig to enable collecting and temperature measurement of polymer melt drops. The rig is also classified technically as a small scale laboratory experiment in vertical orientation therefore, for simplicity and without altering the accuracy, the mathematical modelling is performed in two dimensions rather than three dimensions. Consequently a study of melt dripping polymers (PP, PA6, PC, PMMA and PET) in the absence of flame was carried out to measure the temperature of the drops immediately after they descend from the heated polymer surface. The degree of any decomposition within the collected fallen drops was determined via TGA experiments. The temperature of the polymer surface has been estimated using a heat transfer model, which thus provides an estimate of the molten drop temperature as it leaves the heated polymer surface. Estimation of the extent of the decomposition at the approximate temperatures can be compared to the equivalent experimental values obtained from TGA experiments on the collected molten drops. Reasonable agreement between the temperature curves obtained via TGA with those estimated from the estimated surface temperatures, indicated that the model provides a good indication of the surface temperature.

2) Heat transfer in thermoplastic polymers in horizontal orientation

In Chapter 5 a mathematical model was developed in conjunction with an associated sensitivity analysis, relating to the predicting the melting behaviour of three thermoplastic materials (PP, PA6 and PET) in horizontal position under three different heat fluxes: 15kW/m^2 , 25kW/m^2 and 35kW/m^2 generated by a cone calorimeter values. This model was based on the one-dimensional (1D) representation of static melting phenomena in horizontal position using Stefan Method describing the material when it undergoes phase change. This is a challenging problem to model due to a moving boundary condition between the solid phase and the liquid phase. All these phenomena are described by a balance-equation which is a nonlinear Partial Differential Equation (PDE) that cannot be solved analytically. Therefore, the equation is solved numerically by the Finite Difference Method (FDM) for the one-dimensional (1D) domain. The simulated temperature profile, obtained for the thermoplastic polymers, is presented and compared with experimental temperatures obtained in the corresponding conditions to validate the simulations. The predicted

temperature profiles from the simulations show the same trend and behaviour as those measured from the laboratory experiments.

The model also simulated the movement of the melting front through the thickness of the material. This provides an indication on the development of a formation of molten pool which leads often to polymer degradation and fire.

3) Heat transfer in GRE

In Chapter 6 a numerical model was built and validated using existing data from experiments already carried out in University of Bolton's fire laboratory. The sensitivity analysis performed shows that the temperature profile is more sensitive to the thermal conductivity than its heat capacity. The novelty in this approach is to incorporate in the model the equation of the conductivity and the heat capacity varying as a function of temperature, in order to obtain a more accurate simulated temperature profile. The simulation shows good agreement between the predicted values and their distribution with the experimental temperature profile using various incident heat flux of 15, 25 and 35 kW/m². Ignition phenomenon is described by the model showing a sudden step change in the temperature when the composite polymer catches fire ignites and burns.

4) Heat transfer in GRE with coated surface.

In Chapter 7, intumescent Thermal Barrier Protective Coating provides a char layer preventing the increase of temperature in the GRE sample. GRE and the intumescent coating are modelled as two different parts embedded to form one unique entity taking into account that each part has its own thermophysical properties. A numerical model capable of simulating this temperature profile within each part and also has a complete entity with specified conditions at the interface of the two parts. Experimental temperature data was used to validate the numerical model. Thus, the predicted temperatures of three different intumescent paints subject to an incident heat flux were performed and a mathematical model presented. This model was based on the one-dimensional (1D) representation of physical phenomena accompanying the reaction of intumescent paint applied to a Glass Fibre Reinforced Polymer (GRE) as a substrate and it is also based on the heat transfer phenomenon throughout the swelling coating paint and through the Glass Fibre Reinforced Polymer composite. The resulting nonlinear Partial Differential Equation (PDE) describing the phenomenon has no known analytical solution. Therefore, this equation has to be solved numerically by the Finite Difference Method (FDM) for the domain specified. The simulated

temperatures obtained through the swelling coating layer and the temperatures through the Glass Fibre Reinforced composite are presented and compared with experimental temperatures obtained in the corresponding conditions for model validation. The predicted temperatures developed by the simulations show similar trends to those measured by the experiments, with the actual temperatures being of similar order.

Recommendation for futures Works:

Each model designed in this thesis is subjected to assumptions because it is related to constitutive equations, numerical resolutions, experimental conditions or homogenisation laws. Therefore, there is a limit in their area of validity. Moreover the thermal degradation of polymeric materials under fire is a complex problem with various thermophysical aspects, and, in the scientific approach of this thesis, several hypotheses have been advanced in order to limit the complexity of the subject. However, the elimination of some of these assumptions would further develop the modelling of polymeric materials under fire:

Based on the results obtained from this PhD work, some recommendations for future research are given below:

- The measurement of the thermal thermophysical properties can be improved in order to develop and extend the numerical models.
- The current computer models can be extended by incorporating the modelling of the kinetics parameters of polymer degradation.
- The simulation of mechanical behaviour can be combined with the thermal effect to achieve a thermo-mechanical numerical model to study in more complete manner the polymeric materials in more diverse conditions.
- 3D numerical modelling is a potential possibility to take into account the actual conditions. However, the consideration of 3D geometry can increase computational costs significantly.

References:

- [1] Drysdale, D., *An Introduction to Fire Dynamics*, John Wiley & Sons (1999)..
- [2] Lyon R.E, Quintiere J.G., 'Criteria for piloted ignition of combustible solids', *Combustion and Flame* 151, (2007), p. 551
- [3] Vovelle C., Delfau J.-L.; 'Techniques de l'Ingénieur, traité Plastiques et polymeric materials'.
- [4] Hilado C .J: 'The combustion of polymers, *Chem Tech*, 24,232 - 1972.
- [5] Gibson A.G., Mouritz A.P., 'Fire Properties Of Polymer Polymeric materials' in 'Solid Mechanics And Its Applications' Ed. Gladwell G.M.L., (2006), Springer, 143, p. 140-168, ISBN-13 978-1-4020-5355-9 (HB)
- [6] Galgano A., Di Blasi C., Branca C., Milella E., 'Thermal response to fire of a fibre-reinforced sandwich panel: Model formulation, selection of intrinsic properties and experimental validation' *Polymer Degradation and Stability*, 94, (2009), p. 1267.
- [7] Di Blasi C. Transition between regimes in the degradation of thermoplastic polymers. *Polymer Degradation and Stability* 1999;64: 359-367.
- [8] Sullivan RM, Salamon NJ. A finite element method for the thermochemical decomposition of polymeric materials - II. carbon phenolic polymeric materials. *International Journal of Engineering Science* 1992;30: 939-951.
- [9] Stoliarov SI, Crowley S, Walters RN, Lyon RE. Prediction of the burning rates of charring polymers. *Combustion and Flame* 2010;157: 2024-2034.
- [10] Lyon R.E., 'Pyrolysis kinetics of char-forming polymers', *Polymer Degradation and Stability* 61, (1998), p. 201
- [11] Mouritz AP, Feih S, Kandare E, Mathys Z, Gibson AG, Des Jardin PE, et al. Review of fire structural modelling of polymer polymeric materials. *Polymeric materials: Part A* 2009;40: 1800-1814.
- [12] Hilado C .J: 'The combustion of polymers, *Chem Tech*, 24,232 - 1972.
- [13] Alexiades, V., and Solomon, A. D., "Mathematical Modeling of Melting and Freezing Processes", Hemisphere Publishing Company, Washington, DC, 1993.
- [14] Vovelle C., Delfau J.-L.; 'Techniques de l'Ingénieur, traité Plastiques et polymeric materials'.
- [15] Di Blasi C, Crescitelli S, Russo G, Cinque G. Numerical model of ignition processes of polymeric materials including gas-phase absorption of radiation. *Combustion and Flame* 1991;83: 333-344.
- [16] Di Blasi C. Modeling of solid- and gas-phase processes during thermal degradation of composite materials. *Polymer Degradation and Stability* 1996;54: 241-248.
- [17] Di Blasi C. Numerical simulation of cellulose pyrolysis. *Biomass and Bioenergy* 1994;7: 87-98.
- [18] Di Blasi C. Kinetic and heat transfer control in the slow and flash pyrolysis of solids. *Industrial and Engineering Chemistry Research* 1996;35: 37-46.
- [19] Di Blasi C. Heat, momentum and mass transport through a shrinking biomass particle exposed to thermal radiation. *Chemical Engineering Science* 1996;51: 1121-1132.
- [20] Di Blasi C. Modeling intra- and extra-particle processes of wood fast pyrolysis. *AIChE Journal* 2002;48: 2386-2397.

- [21] Galgano A, Di Blasi C. Modeling the propagation of drying and decomposition fronts in wood. *Combustion and Flame* 2004;139: 16-27.
- [22] Di Blasi C. Linear pyrolysis of cellulosic and plastic waste. *Journal of Analytical and Applied Pyrolysis* 1997;40-41: 463-479.
- [23] Di Blasi C, Branca C. Mathematical model for the nonsteady decomposition of intumescent coatings. *AIChE Journal* 2001;47: 2359-2370.
- [24] Di Blasi C. Modeling the effects of high radiative heat fluxes on intumescent material decomposition. *Journal of Analytical and Applied Pyrolysis* 2004;71: 721-737.
- [25] Stoliarov SI, Crowley S, Walters RN, Lyon RE. Prediction of the burning rates of charring polymers. *Combustion and Flame* 2010;157: 2024-2034.
- [26] Stoliarov SI, Crowley S, Lyon RE, Linteris GT. Prediction of the burning rates of non-charring polymers. *Combustion and Flame* 2009;156: 1068-1083.
- [27] Stoliarov SI, Lyon RE. Thermo-Kinetic Model of Burning. Federal Aviation Administration; 2008: DOT/FAA/AR-TN08/17.
- [28] Stoliarov SI, Lyon RE. Thermo-Kinetic Model of Burning for Pyrolyzing Materials. In: *The ninth International Symposium on Fire Safety Science*; German; 2008. p. 38-50.
- [29] Lautenberger C, Rein G, Fernandez-Pello C. The application of a genetic algorithm to estimate material properties for fire modeling from bench-scale fire test data. *Fire Safety Journal* 2006;41: 204-214.
- [30] Lautenberger C. A generalized pyrolysis model for combustible solids. PhD thesis. University of California, Berkeley; 2007.
- [31] Janssens M, Douglas B. Wood and wood products. In: *Handbook of building materials for fire protection*, New York: McGraw-Hill; 2004, p. 7.1-7.58.
- [32] Di Blasi C. Modeling chemical and physical processes of wood and biomass pyrolysis. *Progress in Energy and Combustion Science* 2008;34: 47-90.
- [33] Stoliarov SI, Walters RN. Determination of the heats of gasification of polymers using differential scanning calorimetry. *Polymer Degradation and Stability* 2008;93: 422-427.
- [34] Stoliarov SI, Crowley S, Lyon RE, Linteris GT. Prediction of the burning rates of non-charring polymers. *Combustion and Flame* 2009;156: 1068-1083.
- [35] Hilado C .J: 'The combustion of polymers, *Chem Tech*, 24,232 - 1972.
- [36] Gibson A.G., Mouritz A.P., *Fire Properties Of Polymer Polymeric materials in Solid Mechanics And Its Applications*, Ed. Gladwell G.M.L., (2006), Springer, 143, p. 140-168, ISBN-13 978-1-4020-5355-9 (HB)
- [37] Staggs J.E.J., Whitelely R.H., 'Modelling the combustion of solid-phase fuels in cone calorimeter experiments', *Fire Mater.* 23, (1999), p. 63
- [38] Gibson A.G., Wu Y.S., Evans J.T., Mouritz A.P., *Polymeric material Theory Analysis of Composites under Load in Fire.* *Journal of Composite Materials*, 40(7):639{658, 2006.
- [39] ASTM Standard D792.; *Standard Test Methods for Density and Specific Gravity (Relative Density) of Plastics by Displacement.* ASTM International, pages 1-13, 2008.
- [40] Lyon R.E., 'Degradation kinetics of char-forming polymers', *Polymer Degradation and Stability* 61, (1998), p. 201

- [41] Staggs J.E.J., 'Ignition of char-forming polymers at a critical heat flux', *Polymer Degradation and Stability*, 74, (2001), p. 433
- [42] Staggs J.E.J., Watt S.D., McIntosh A.C., Brindley J., 'A theoretical explanation of the influence of char formation on the ignition of polymers', *Fire Safety Journal*, 26, (2001), p. 421
- [43] Staggs J.E.J., 'A simple model of polymer degradation including mass transport of volatiles', *Fire Safety Journal*, 34, (2000), p. 69
- [44] Staggs J.E.J., 'Modelling thermal degradation of polymers using first-order kinetics', *Fire Safety Journal* 32, (1999) p. 17
- [45] Aboulkasa A., El harfik., Study of the kinetics and mechanisms of thermal decomposition of Moroccan Tarfaya oil shale and its kerogen, *Oil Shale*, 2008, Vol. 25, No. 4, pp. 426–443. doi: 10.3176/oil.2008.4.04, ISSN 0208-189X - Estonian Academy Publishers.
- [46] Coats, A. W., Redfern, J. P. Kinetic parameters from thermogravimetric data // *Nature*. 1964. Vol. 201. P. 68–69.
- [47] Kissinger, H. E. Reaction kinetics in differential thermal analysis // *Anal. Chem.* 1957. Vol. 29, No. 11. P. 1702–1706.- Akahira, T., Sunose, T. Trans. Joint Convention of Four Electrical Institutes, Paper No. 246, 1969 Research Report // *Chiba Institute of Technology Sci. Technol.* 1971. Vol.16. P. 22–31.
- [48] Friedman, H. Kinetics of thermal degradation of char-forming plastics from thermogravimetry. Application to a phenolic plastic // *J. Polym. Sci., Part C.* 1964. Vol.6. P. 183–195.
- [49] Flynn, J. H., Wall, L. A. A quick, direct method for the determination of activation energy from thermogravimetric data // *Polym. Lett.* 1966. Vol. 4.P. 323–328.- Ozawa, T. A new method of analysing thermogravimetric data // *Bull. Chem. Soc. Jpn.* 1965. Vol. 38, No. 11. P. 1881–1886.
- [50] Criado, J. M. Kinetic analysis of DTG data from master curves // *Termochim. Acta.* 1978. Vol. 24, No. 1. P. 186–189.
- [51] Gabal M.A., Hoff D., Kasper G., *J. Thermal Anal. Calorim.*, 89 (2007) 109
- [52] García S.J., Serra A., Ramis X. and Suay J., *Thermal Anal. Calorim.*, 89 (2007) 223
- [53] Cadenato A., Morancho J.M., Fernández-Franco X., Salla J.M., Ramis X., *J. Thermal Anal. Calorim.*, 89 (2007) 233
- [54]. Hong-Kun Z., Cao T., Dao-Sen Z., Wen-Lin X., Ya-Quong W., Qi-Shu Q., *J. Thermal Anal. Calorim.*, 89 (2007) 531
- [55] Feher L., Jurconi B., Vlase G., Vlase T., Doca N., *J. Thermal Anal. Calorim.*, 88 (2007) 621
- [56] Kok M.V., *J. Thermal Anal. Calorim.*, 88 (2007) 663
- [57] Budugreac P., Segal E., *J. Thermal Anal. Calorim.*, 88 (2007) 703
- [58] Biedunkiewicz A., Gordon N., Straszko J., Tamir S., *J. Thermal Anal. Calorim.*, 88 (2007) 717
- [59] Pérez C.J., Alvarez V.A., Steffani P.M., Vazquez A., *J. Thermal Anal. Calorim.*, 88 (2007) 825
- [60] Criado J.M., Pérez-Maqueda L.A., Gotor F.J., Malek J., Koga N., *J. Thermal Anal. Calorim.*, 72 (2003) 901
- [61] Criado J.M., Pérez-Maqueda L.A., *J. Thermal Anal. Calorim.*, 80 (2005) 27
- [62] Vyazovkin S., Dollimore D., *J. Chem. Inf. Comput. Sci.*, 36 (1996) 42

- [63] Vyazovkin S., Wight C.A., *J. Phys. Chem. A*, 101 (1997) 8279
- [64] Vyazovkin S., *Int. Rev. Phys. Chem.*, 19 (2000)45
- [65] Vyazovkin S., *New J. Chem.*, 24 (2000) 913
- [66] Vyazovkin S., *J. Compt. Chem.*, 22 (2001) 178
- [67] Shi L., *Pyrolysis and combustion processes of combustible materials under external heat flux*, National university of Singapore, thesis, 2014.
- [68] Henderson J.B., Wiebelt J.A., Tant M.R. A model for the thermal response of polymer composite materials with experimental verification., *Journal of Composite Materials*, (19):579{595, 1985.
- [69] Gibson A.G., Mouritz A.P., 'Fire Properties Of Polymer Composites' in 'Solid Mechanics And Its Applications' Ed. Gladwell G.M.L., (2006), Springer, 143, p. 140-168, ISBN-13 978-1-4020-5355-9 (HB)
- [70] Drysdale D., Grant G., 'Numerical modelling of early flame spread in warehouse fires', *Fire Safety Journal* 14, (1995), p. 247
- [71] Drysdale D., Kuang-Chung, T., 'Using cone calorimeter data for the prediction of fire hazard', *Fire Safety Journal* 37, (2002), p. 697
- [72] Lyon R.E, Quintiere J.G., 'Criteria for piloted ignition of combustible solids', *Combustion and Flame* 151, (2007), p. 551
- [73] Galgano A., Di Blasi C., Branca C., Milella E., 'Thermal response to fire of a fibre-reinforced sandwich panel: Model formulation, selection of intrinsic properties and experimental validation' *Polymer Degradation and Stability*, 94, (2009), p. 1267
- [74] Mangalgiri P D., *Polymer-matrix Composites for High-temperature Applications*.55 (2):175{193, 2005.
- [75] Popescu CM, Singurel G, Popescu MC, Vasile C, Argyropoulos DS, Willfor S. Vibrational spectroscopy and X-ray diffraction methods to establish the differences between hardwood and softwood. *Carbohydrate Polymers* 2009; 77: 851-857.
- [76] Janssens M, Douglas B. Wood and wood products. In: *Handbook of building materials for fire protection*, New York: McGraw-Hill; 2004, p. 7.1-7.58.
- [77] Sullivan RM, Salamon NJ. A finite element method for the thermochemical decomposition of polymeric materials - II. carbon phenolic composites. *International Journal of Engineering Science* 1992; 30: 939-951.
- [78] Stoliarov SI, Crowley S, Walters RN, Lyon RE. Prediction of the burning rates of charring polymers. *Combustion and Flame* 2010; 157: 2024-2034
- [79] Di Blasi C. Transition between regimes in the degradation of thermoplastic polymers. *Polymer Degradation and Stability* 1999; 64: 359-367.
- [80] Pering GA, Farrell PV, Springer GS. Degradation of tensile and shear properties of composites exposed to fire or high temperatures. *J Compos Mater* 1980; 14:54-68.
- [81] Bamford CH, Crank J, Malan DH. The combustion of wood: Part I. *Cambridge Phil. Soc. Proc.*, 1946; 42: 166-182.].
- [82] Tinney ER., *The combustion of wooden dowels in heated air. Symposium (International) on Combustion*, 1965; 10: 925-930.]

- [83] Hadvig S, Paulsen O., One-dimensional charring rate in wood, *Journal of Fire and Flammability* 1976; 7: 433-449.]
- [84] Munson T.R., Spindler R.J., *Transient thermal behaviour of decomposing materials*, 1961, AVCO Corporation RAD-TR-1961; 61.
- [85] Panton, R.L. and Rittmann, J.G., *Analytical Study of Degradation Including Effects of Mass Loss and Competing Reactions*. 1969: La Jolla, California.
- [86] Kung HC, A mathematical model of wood degradation, *Combustion and Flame* 1972; 18: 185-195.].
- [87] Kansa EJ, Perlee HE, Chaiken RF. Mathematical model of wood degradation including internal forced convection. *Combustion and Flame* 1977; 29: 311-324.]
- [88] Munson T.R., Spindler R.J., *Transient thermal behaviour of decomposing materials*, 1961, AVCO Corporation RAD-TR-1961; 61.
- [89] Alerts PDJ, Rageland KW. Pressurized downdraft combustion of woodchips. In: *Twenty-Third Symposium (International) on Combustion*; Pittsburgh, USA; 1990. p. 1025-1032.]
- [90] Di Blasi C. Numerical simulation of cellulose pyrolysis. *Biomass and Bioenergy* 1994; 7: 87-98.
- [91] Spearpoint MJ. Predicting the ignition and burning rate of wood in the cone calorimeter using an integral model. Master thesis. University of Maryland, College Park; 199].
- [92] Swann, Robert T.; Pittman, Claud M.; and Smith, James C., Jr.: *One-Dimensional Numerical Analysis of the Transient Response of Thermal Protection Systems*. NASA TN D-2976, 1965.
- [93] Murty KA. Thermal decomposition kinetics of wood degradation. *Combustion Flame* 1977; 29:311–24.
- [94] Swann, Robert T.: *Composite Thermal Protection Systems for Manned Re-Entry Vehicles*. ARS Jour., vol. 32, no. 2, Feb. 1962, pp. 221-226.
- [95] Swann, Robert T.: *Composite Thermal Protection Systems for Manned Re-entry I Vehicles*. Keprinq 1569-60, American Rocket Soc., Dec 1960. d
- [96] Swann, Robert T., and Pittman, Claud M.: *Numerical Analysis of the Transient Response of Advanced Thermal Protection Systems for Atmospheric Re-entry*. NASA TN D-1370, 1962.
- [97] Brooks, William A., Jr., Swann, Robert T., and Wadlin, Kenneth L.: *Thermal Protection for Spacecraft Entering at Escape Velocity*. SOC. Automotive Erg., Apr. 1962.
- [98] Swann, Robert T.; Pittman, Claud M.; and Smith, James C., Jr.: *One-Dimensional Numerical Analysis of the Transient Response of Thermal Protection Systems*. NASA TN D-2976, 1965.
- [99] Pittman C. M., Brewer W. D., *Analytical Determination of the Effect of Thermal Property Variations on the Performance of a Charring Ablator*, NASA TN D-3486 Volume 3486, National Aeronautics and Space Administration, 1966
- [100] McManus LN, Coyne DC. A TRAP4-A digital computer program for calculating the response of mechanically and thermally loaded aircraft structures to the thermal radiation of a nuclear explosion or high energy laser. Kaman Avidyne Technical Memorandum; 1982. TM-141.
- [101] Pering GA, Farrell PV, Springer GS. Degradation of tensile and shear properties of composites exposed to fire or high temperatures. *J Compos Mater* 1980; 14:54–68.
- [102] Griffis CA, Masumra RA, Chang Cl. Thermal response of graphite epoxy composite subjected to rapid heating. *J Compos Mater* 1981; 15:427–42.

- [103] Chen JK, Sun CT, Chang CI. Failure analysis of a graphite/epoxy laminates subjected to combined thermal and mechanical loading. *J. Compos Mater* 1985;19(5):216–35.
- [104] Griffis CA, Nemes JA, Stonesfiser FR, Chang CI. Degradation in strength of laminated composites subjected to intense heating and mechanical loading. *J Compos Mater* 1986; 20(3):216–35.
- [105] Chang CI. Thermal effects on polymer composite structures. *Theor Appl Fract Mech* 1986;6(2):113–20.
- [106] Milke JA, Vizzini AJ. Thermal response of fire, exposed composites. *J Compos Technol Res* 1991; 13(3):145–51.
- [107] Fanucci JP. Thermal response of radiantly heated kevlar and graphite/epoxy composites. *J Compos Mater* 1987; 21(2):129–39.
- [108] J.B. Henderson, T.E. Wiecek, A numerical study of the thermally-induced response of decomposing, expanding polymer composites. *Warme- und Stoffubertragung* 1988;22: 275-284].
- [109] Henderson JB, Verma YP, Tant MR, Moore GR. Measurement of the thermal conductivity of polymer composites to high temperature using the line source techniques. *Polym Compos* 1983; 4(4):219–24.
- [110] Henderson JB, Wiebelt JA, Tant MR, Moore GR. A method for the determination of the specific heat and heat of decomposition of composite materials. *Thermochimica Acta* 1982;57:161–71.
- [111] Springer GS. A model for predicting the mechanical properties of composites at elevated temperatures. *J Reinf Plast Compos* 1984; 3(1):85–95.)
- [112] Henderson, J. B., M. R. Tant, G. R. Moore and J. A. Wiebelt (1981). "Determination of kinetic parameters for the thermal decomposition of phenolic ablative materials by a multiple heating rate method." *Thermochimica Acta* 44: 253-264.
- [113] Henderson, J. B., J. A. Wiebelt, M. R. Tant and G. R. Moore (1982). "A method for the determination of the specific heat and heat of decomposition of composite materials." *Thermochimica Acta* 57: 161-171.
- [114] Henderson, J. B., Y. P. Verma, M. R. Tant and G. R. Moore (1983). "Measurement of the Thermal Conductivity of Polymer Composites to High Temperatures Using the Line Source Technique." *Polymer Composites* 4(4): 219-224.
- [115] Henderson J.B., Wiecek T.E.: A mathematical model to predict the thermal response of decomposing, expanding polymer composites. *Journal of Composite Materials*, 21(4):373–393, 1987.
- [116] Florio J., Henderson J.B., F.L. TEST et R. HARIHARAN: A study of the effects of the assumption of local-thermal equilibrium on the overall thermally-induced response of a decomposing, glass-filled polymer composite. *International Journal of Heat and Mass Transfer*, 34(1):135–147, 1991.
- [117] Milke, J.A., and A.J. Vizzini, "Thermal Response of Fire-Exposed Composites", *Journal of Composites Technology and Research*, Vol. 13, Fall 1991, pp. 145-151.
- [118] McManus LN, Springer GS. High temperature thermo-mechanical behaviour of carbon-phenolic and carbon–carbon composites, I. Analysis. *J Compos Mater* 1992;26(2):206–29.
- [119] McManus LN, Springer GS. High temperature thermo-mechanical behavior of carbon-phenolic and carbon–carbon composites, II. Results. *J Compos Mater* 1992;26(2):230–51.
- [120] Sullivan RM, Salamon NJ. A finite element method for the thermochemical decomposition of polymeric materials – I. Theory. *Int J Eng Sci* 1992;30(4):431–41.

- [121] Sullivan RM, Salamon NJ. A finite element method for the thermochemical decomposition of polymeric materials – II. Carbon Phenolic Laminates. *Int J Eng Sci* 1992;30(7):939–51.
- [122] Dimitrienko YI. Thermo-mechanical behavior of composite materials and structures under high temperatures: 1. Materials. *Compos: Part A* 1997;28(5):453–61.
- [123] Gibson AG, Wu YS, Chandler HW, Wilcox JAD. A model for the thermal performance of thick composites laminates in hydrocarbon fires. *Revue de l'Institut du Pe'trol* 1995;50(1):69–74..
- [124] Crank, J. (1975) *The Mathematics of Diffusion*, 2nd ed., Clarendon Press, Oxford.
- [125] Dhingra, S.S., and Marand, E. (1998) Mixed Gas Transport Study through Polymeric Membranes. *J. Membrane Sci.*, 141, 45-63.
- [126] Aminabhavi, T.M., and Aithal, U.S. (1988) An Overview of the Theoretical Models Used to Predict Transport of Small Molecules through Polymer Membranes. *JMS-Rev. Macromol. Chem. Phys.*, C28, 421-474.
- [127] Stern, S.A. and Trohalaki, S. (1990) Gas Diffusion in Rubbery and Glassy Polymers. *ACS Symp. Ser.*, 423, 22-59.
- [128] Stern, S.A. (1994) Polymers for Gas Separations: the Next Decade. *J. Memb. Sci.*, 94, 1-65.)
- [129] Di Blasi C., The state of the art of transport models for charring solid degradation. *Polymer International (UK)*, 49:1133–1146, 2000.
- [130] Puiroux N. : Transferts Thermiques et d'Humidité dans les Matériaux Composites Ablatables : Effet des Hétérogénéités. Thèse de doctorat, Institut National Polytechnique de Toulouse, 2004.
- [131] Di Blasi C., Heat, momentum and mass transport through a shrinking biomass particle exposed to thermal radiation. *Chemical Engineering Science* 1996; 51: 1121-1132.
- [132] Lautenberger C., Fernandez-Pello C., A model for the oxidative degradation of wood, *Combustion and Flame* 2009; 156: 1503-1513.
- [133] Ratte J., Marias F., Vaxelaire J., Bernada P., Mathematical modelling of slow degradation of a particle of treated wood waste. *Journal of Hazardous Materials* 2009; 170: 1023-1040.
- [134] R. Vije R., Gerun L., Tazerout M., Castelain C., Bellettre J., Dimensional modelling of wood degradation using a nodal approach. *Fuel* 2008;87: 3292-3303.
- [135] Wang Y.F., Yang L.Z., Zhou X.D., Dai J.K., Zhou Y.P., Deng Z.H., Experiment study of the altitude effects on spontaneous ignition characteristics of wood. *Fuel* 2010; 89: 1029-1034.
- [136] Staggs J.E.J., Heat and mass transport in developing chars, *Polymer Degradation and Stability* 82 (2003) p. 297.
- [137]. Lyon R. E., Degradation kinetics of char forming polymers, *Polymer Degradation and Stability*, N° 61, pp. 201-210, 1998.
- [138] Kanury A.M. 'Introduction to Combustion Phenomena' from 'Combustion Science and Technology Book Series', Ed. Glassman, I., Gordon & Breach, London, 1975, ISBN 067702690.
- [139] Babrauskas V. Ignition of wood: a review of the state of the art. In: *The ninth Interflam*; Edinburgh, Scotland; 2001. p. 71-88.
- [140] Babrauskas V. *Ignition handbook: principles and applications to fire safety engineering, fire investigation, risk management and forensic science*. Issaquah: Fire Science Publishers; 2003.

- [141] Delichatsios MA, Panagiotou TH, Kiley F. The use of time to ignition data for characterizing the thermal inertia and the minimum (critical) heat flux for ignition or degradation. *Combustion and Flame* 1991; 84: 323-332.
- [142] Atreya A, Abu-Zaid M. Effect of environmental variables on piloted ignition. In: The third International Symposium on Fire Safety Science; University of Edinburgh, Scotland; 1991. p. 177-186.
- [143] Mikkola E, Wichman IS. On the thermal ignition of combustible materials. *Fire and Materials* 1989;14: 87-96.
- [144] Carslaw HS, Jaeger JC. Conduction of heat in solids. Oxford: The Clarendon Press; 1959.
- [145] Janssens M. Fundamental thermophysical characteristics of wood and their role in enclosure fire growth. PhD thesis. University of Gent; 1991.
- [146] Harada T. Time to ignition, heat release rate and fire endurance time of wood in cone calorimeter test. *Fire and Materials* 2001; 25: 161-167.
- [147] Camina G., Lomakin S., Intumescent materials . In: Horrocks AR., Price D., editos., Fire Retardants., Cambridge, England: Woodhead Publishing Ltd; 2001. P. 318-336.
- [148] Mouritz AP, Feih S, Kandare E, Gibson AG, Thermal mechanical modelling of laminates with fire protection coating. *Composites Part B: Engineering*, 48-68-78,2013.
- [149] Griffin GJ, The therma modelling of heat transfer across intumescent polymer coatings. *Journal of fire science*, 28(3):249-277, 2009.
- [150] Zverev VG, Goléidin VD, Nesselov V.V., Modeling heat and mass transfer in intumescent fire-retardant coatings. *Combust Explos Shock Waves*, 34(2):198-205,1998.
- [151] Isakov GN and Kuzin AY, Modeling of heat and mass transfer in multilayer heat –and fire insulating coatings under interaction with a high-temperature gas flow. *Combust Explos Shock Waves*, 34(2):197,1998.
- [152] Di Blasi C and Branca C, Mathematical model for the nonsteady decomposition of intumescent coatings. *AIChE Journal*, 47(10):2359-2370,2001.
- [153] Di Blasi C., Modeling the effects of high radiative heat fluxes on intumescent material decomposition. *Journal of Analytical and Applied Pyrolysis*, 71(2):721-737, 2004.
- [154] Gillet M., Autrique L., and Perez L., Mathematical model for intumescent coatings growth: application to fire retardant systems evaluation. *Journal of physics D: Applied physics*, 40(3):883-899,2007.
- [155] Zhang F., Zhang J., and Wang Y., Modeling study on the combustion of intumescent fire-retardant polypropylene. *Expresspolymlett*, 1(3): 157-165, 2007.]
- [156] Staggs EJ, Crewe RJ, and Butler R., A theoretical and experimental investigation of intumescent behaviour in protective coatings for structural steel. *Chemical Engineering Science*, 71:239-251, 2012.
- [157] Asaro RJ, Lattimer B., Mealy C., and Steele G., Thermo-physical performance of a fire protective coating for naval ship structures. *Composites Part A: Applied Science and anufacturing*, 40(1):11-18, 2009.
- [158] Kandare E., Griffin G., Feih S., Gibson AG., Lattimer BY., and Mouritz AP., Fire structural modelling of fibre-polymer laminates protected with an intumescent coating. *Composite part A: Applied science and anufacturing*, 43(5):793-802, 2012.
- [159] Jiminez M., Duquesne S., and Bourbigot ., Kinetics analysis of the thermal degradation of an epoxy-based intumescent coating. *Polymer Degradation and Stability*, 92(10):1778-1787, 2007.

- [160] Neininger S., Staggs J.E.J., Horrocks R.E., Hill N.J., 'A study of the global kinetics of thermal degradation of a fibre-intumescent mixture', *Polymer Degradation and Stability* 77 (2002) p. 187.
- [161] Kandare E., Kandola B.K., Staggs J.E.J., 'Global kinetics of flame-retarded epoxy resin formulations', *Polymer Degradation and Stability* 92 (2007) p. 1778.
- [162] Butler KM, Baum HR, Kashiwagi T., Heat transfer in an intumescent material using a three-dimensional Lagrange model, Lund DP, Angell EA, editors, Proceedings, International Conference on Fire Research and Engineering, September 10-15, 1995, Orlando, FL. Boston, MA: Society of Fire Protection Engineering (SFPE); 1995. P.261-266.
- [163] Butler KM, Physical modelling of intumescent fire retardant polymers. IN: Khemani KC, editor. Polymeric Foams: Science and Technology. Proceedings. American Chemical Society. ACS Symposium Series 669. Chapter 15. Washington DC: American Chemical Society, 1997. P. 214-230.
- [164] Butler KM, Baum HR, Kashiwagi T., Three-dimensional modelling of intumescent behavior in fires, IN: Hasemi Y, editor. Fire Safety Science. Proceedings. Fifth (5th) International Symposium. March 3-7, 1997, Melbourne, Australia. Boston, MA: International Association for Fire Safety Science; 1997. P.523-534.
- [165] Carslaw HS, Jaeger JC., Conduction of heat in Solids., 2nd edition: Oxford University Press; 1959.
- [166] Butler KM, Mixed layer pyrolysis model for polypropylene., In: Curtat M., editor. Fire Safety Science. Proceedings. Sixth (6th) International Association for the Fire Safety Science. July 5-9, 1999, Poitiers, France. Boston, MA: Int. Assoc. for Fire Safety Science; 2000. P. 313-324.
- [167] Bourbigot S., Jimenez M., Duquesne S., Modelling Heat Barrier Efficiency of Flame Retarded Materials, Excerpt from the Proceedings of the COMSOL Users Conference 2006 Paris.
- [168] [Stefan J., Ueber die theorie der eisbildung, insbesondere uber die eisbildung im polaemeere, Annalen der Physik and Chemie 1891; 42:269-286].
- [169] Crank j., Two method for the numerical solution of moving-boundary problems in diffusion and heat flow., Quarterly journal of mechanics and applied mathematics 1957; X(2); 220-231.-
- [170] Crank J., How to deal with moving boundaries in thermal problems., Inc. Lewis RW, Morgan K, Zankiewicz OC, editors. Numerical method in heat transfer.- Crank J., Fire and moving boundary problem., Oxford: Clarendon Press; 1984.]
- [171] Poirier D., Salcudean M., On numerical methods used in mathematical modelling of phase change in liquid metal, Trans ASME, Journal of heat transfer 1995. 1988; 110:562-569.
- [172] Bradean R, Ingham DB, Heggs PJ, Stefan in blow moulding operations., In: Tupholme GE, Wood AS, editors. Mathematics of heat transfer. Oxford Clarendon Press; 1998.bp. 89-96.,
- [173] Andrews JG, Atthey DR., On the motion of an intensively heated evaporation boundary., Journal of the institute of mathematics and its application. 1975; 19:59-72.]
- [174]. Landau, H. G., "Heat Conduction in a Melting Solid," Quart, of Appl. Math., Vol. VIII, No. 1, April 1950, pp 81-9U.]
- [175]. Dewey, K.F., Schlesinger S. I., Saahkin L., "Temperature Profiles in a Finite Solid with Moving Boundary," Journ. Aero/Space Science, Vol. 27, No. 1, Jan. 1960, p 59.
- [176] Lotkin M., "The Calculation of Heat Flow in Melting Solids," Quart, of Appl. Math., Vol. XVIII, No. 1, April 1960, pp. 79-85.]
- [177] Citron S. J., "Heat Conduction in a Melting Slab," Journ. Aero/Space Science, Vol. 27, No. 3, March 1960, p. 219.

- [178] Zhang, J., Shields, T.J., and Silcock, G.W.H., "Fire Hazard Assessment of Polypropylene Wall Linings Subjected to Small Ignition Sources," *Journal of Fire Sciences*, 14: pp. 67-84, (1996).
- [179] Zhang, J., Shields, T.J., and Silcock, G.W.H., "Effect of Melting Behavior on Upward Flame Spread of Thermoplastics," *Fire and Materials*, 21: pp. 1-6, (1997).
- [180] Zhang J., Wang Y., Lu X., Yu J., Study on Melting Behavior of Polymers during burning, Fire safety science – Proceedings of the eighth international symposium, pp. 637-646, (2005).
- [181] Idelsohn, S.R., Oñate, E., Del Pin, F., "The particle finite element method: a powerful tool to solve incompressible flows with free-surfaces and breaking waves", *Int. J. Num. Meth. Engng.*, Vol. 61, 2004, pp. 964-989.
- [182] Idelsohn, S.R., Oñate, E., Del Pin, F., "A lagrangian meshless finite element method applied to fluidstructure interaction problems", *Computer and Structures*, Vol. 81, 2003a, pp. 655-671.
- [183] Oñate, E., Rojek, J., Chiuimenti, M., Idelsohn, S.R., Del Pin, F., Aubry, R., "Advances in stabilized finite element and particle methods for bulk forming processes", *Comput. Methods Appl. Mech.Engng.*, Vol. 195, 2006, pp. 6750-6777.
- [184] Ohlemiller, T.J., Shields, J.R., Butler, K.M., Collins, B., Seck, M., "Exploring the role of polymer melt viscosity in melt flow and flammability behavior", *Proceedings of the Fall Conference of the Fire Retardant Chemicals Association*, Oct 2000, pp. 1-28.].
- [185] Butler, K., Onate, E. and Rossi, R., "Modeling Polymer Melt Flow Using the Particle Finite Element Method," paper presented at Interflam 2007, Edinburgh Scotland (July 2007)).
- [186] Butler, K., Ohlemiller, T. and Linteris, G., "A Progress Report on Numerical Modelling of Experimental Polymer Melt Flow Behavior," *Proceeding of the Interflam 2004*, Interscience Communications, London (2004) pp. 937-948).
- [187] Ohlemiller T.J., Butler K.M., Influence of polymer melt behavior on flammability, *Proceedings of the 15th Joint Panel Meeting on Fire Research and Safety of the US/Japan Government Cooperative Program on Natural Resources (UJNR)*, Vol. 1, Mar 2000, pp. 81-88.
- [188] (Butler, K. and Ohlemiller, T., "Some Difficult Problems in the Modeling of Fire Spread," paper presented to the 7th World Congress on Computational Mathematics, Los Angeles, CA (July 2006)).
- [189] Lautenberger C, Rein G, Fernandez-Pello C. The application of a genetic algorithm to estimate material properties for fire modeling from bench-scale fire test data. *Fire Safety Journal* 2006;41: 204-214.
- [190] Lautenberger C. A generalized degradation model for combustible solids. PhD thesis. University of California, Berkeley; 2007.
- [191] Lautenberger C, Fernandez-Pello C. Generalized degradation model for combustible solids. *Fire Safety Journal* 2009;44: 819-839.
- [192] Lautenberger C, Fernandez-Pello C. A model for the oxidative degradation of wood. *Combustion and Flame* 2009;156: 1503-1513.
- [193] Stoliarov SI, Crowley S, Walters RN, Lyon RE. Prediction of the burning rates of charring polymers. *Combustion and Flame* 2010;157: 2024-2034.
- [194] Stoliarov SI, Crowley S, Lyon RE, Linteris GT. Prediction of the burning rates of non-charring polymers. *Combustion and Flame* 2009;156: 1068-1083.
- [195] Stoliarov SI, Lyon RE., Thermo-Kinetic Model of Burning. Federal Aviation Administration; 2008: DOT/FAA/AR-TN08/17.

- [196] Stoliarov SI, Lyon RE. Thermo-Kinetic Model of Burning for Pyrolyzing Materials. In: The ninth International Symposium on Fire Safety Science; German; 2008. p. 38-50.
- [197] Kandola B.K., Price D., Milnes G.J., Da Silva A., Development of a novel experimental technique for quantitative study of melt dripping of thermoplastic polymers, *Polymer Degradation and Stability* 98 (2013) 52-63.
- [198] Kandare E., Kandola B.K., Myler P. and Edwards G., Thermo-mechanical Responses of Fibre-reinforced Epoxy Composites Exposed to High Temperature Environments. Part I: Experimental Data Acquisition, *Journal of Composite materials*, Vol. 44, page 3093-3114, No. 26/2010.
- [199] Kandola B. K., Kandare E., Myler P., McCarthy E., Edwards G., Yuan J. F., Wang Y.C., Thermo-mechanical response of flame-retarded fibre reinforced composite after exposure to convective and radiative heat. *Journal of Composite materials*, page 1-10, 2009.
- [200] Kandola B.K., Ndiaye M., Price D., Quantification of polymer degradation during melt dripping of thermoplastic polymers, *Polymer Degradation and Stability* 106 (2014) 16-25.
- [201] Kandola B.K., Price D., Milnes G.J., Da Silva A., Gao F., Nigmatullin R., Fire Behaviour Characterization of Melt Dripping Thermoplastics'. In: Morgan A, Nelson GL, Willkie CA, editors, *Fire and Polymers*, American Chemical Society Symposium Series, 1118, 2012, Washington DC, Chapter 21, 311-325.
- [202] Luangtriratana P., Kandola B.K, Duquesne S., Bourbigot S., Quantification of thermal barrier efficiency of intumescent coatings on Glass Fibre-Reinforced Epoxy Composites, 'Flame Retardancy and Protection of Materials: Recent Advances and Current Perspectives', Eds. S Duquesne et al, Springer, in press, 2015
- [203] Technical datasheet. Polypropylene (PP), Moplen HP516R, Basell. LyondellBasell Industries Holdings, Australia Pty Ltd.
- [204] Technical datasheet. Polyamide 6 (PA6), Technyl C 301 Natural, Rhodia, France.
- [205] Technical datasheet. Polyethylene terephthalate (PET, polyester), Fibre Extrusion Technology, UK.
- [206] Technical datasheet. Polycarbonate (PC), Bayer MaterialScience AG D-51368 Leverkusen, Germany
- [207] Technical datasheet. Polystyrene (PS), Total Petrochemicals Research, Feluy, Belgium.
- [208] Technical datasheet. Polymethyl methacrylate (PMMA), Piedmont Plastics, CYRO Industries, USA.
- [209] Kanury A.M., Introduction to Combustion Phenomena, Combustion Science and Technology. Book Series, Ed. Glassman, I., Gordon & Breach, London, 1975, ISBN 067702690.
- [210] Kandola B.K., Luangtriratana P., Duquesne S., Bourbigot S., The Effects of Thermophysical Properties and Environmental Conditions on Fire Performance of Intumescent Coatings on Glass Fibre-Reinforced Epoxy Composites. *Materials* 2015, 8, 5216-5237; doi:10.3390/ma8085216.
- [211] ASTM E119-00a (2001). Standard Test Methods for Fire Tests of Building Construction and Materials, 2001 ASTM Standards on Disc, 4.07, ASTM, Pennsylvania.
- [212] Elliott, C. M., and Ockendon, J. R., "Weak and Variational Methods for Moving Boundary Problems", Pitman Advanced Publishing Program, Boston, MA, 1982.198

- [213] Šarler, B., "Stefan's Work on Solid-Liquid Phase Change", *Engineering Analysis with Boundary Elements*, 16, pp. 83-92, 1995.
- [214] Rubinstein, L. I., "The Stefan Problem", *Translations of Mathematical Monographs*, 27, American Mathematical Society, 1971.
- [215] Alexiades, V., and Solomon, A. D., "Mathematical Modeling of Melting and Freezing Processes", Hemisphere Publishing Company, Washington, DC, 1993.
- [216] Wang YZ, Chen XT, Tang XD, Du XH. A new approach for the simultaneous improvement of fire retardancy, tensile strength and melt dripping of poly(ethylene terephthalate). *J Mater. Chem.* 2003; 13:1248–1249.
- [217] Oñate E, Rossi R, Idelsohn SR, Butler KM. Melting and spread of polymers in fire with the particle finite element method. *International Journal for Numerical Methods in Engineering*, 2009; 81 (8): 1046-1072.
- [218] Wang Y, Jow J, Su K, Zhang J. Dripping behaviour of polymers under UL94 vertical test conditions, *J Fire Sci.* 2012; 30(6): 477-501.
- [219] ASTM E698-11 Standard Test Method for Arrhenius Kinetic Constants for thermally unstable materials using DSC and the Flynn-Wall-Ozawa method. P8
- [220] Mark JE, editor. *Physical properties of polymers handbook*. Second edition. New York: Springer Science, 2007. ISBN-13:978-0-387-31235-4.
- [221] F. Gallez, R. Legras, J. P. Mercier, *Polym Engr. Sci.*, 1976, 16, 276.
- [222] G. E. Wissler, B. Crist. Jr, *J. Polym Sci., Polym.Phys.*, 1980, 18, 1257.
- [223] Abramowitz, M., and Stegun, I.A. 1964, *Handbook of Mathematical Functions*, Applied Mathematics Series, Volume 55 (Washington: National Bureau of Standards; reprinted 1968 by Dover Publications, New York), Chapters 6, 7, and 26.
- [224] Pearson, K. (ed.) 1951, *Tables of the Incomplete Gamma Function* (Cambridge: Cambridge University Press).
- [225] Wisniak J., Josef Stefan: Radiation, conductivity, diffusion, and other phenomena, *Revista CENIC. Ciencias Químicas*, vol. 37, núm. 3, 2006, pp. 188-195.
- [226] Salva N. N., Tarzia D. A., 'A sensitivity analysis for the determination of unknown thermal coefficients through a phase-change process with temperature-dependent thermal conductivity', *International Communications in Heat and Mass Transfer* 38 (2011) 418–424.
- [227] Thompson, E.V., "Thermal Properties, *Encyclopedia of Polymer Science and Engineering*, Vol. 16, Mark, H.F. (ed.), John Wiley & Sons, New York, 1989, pp. 711-747.
- [228] Chartoff, R.C., "Thermoplastic Polymers, *Thermal Characterization of Polymeric materials* (2nd ed.), Turi, E. A. (ed.), Academic Press, New York, 1997, pp. 621-625.
- [229] Zhang, J., Shields, T. and Silcock, G., "Effect of Melting Behavior on Upward Flame Spread Behavior of Thermoplastics," *Fire and Materials*, 21, (1997) pp 1-6.
- [230] Ohlemiller, T., Shields, J., Butler, K., Collins, B. and Seck, M. "Exploring the Role of Polymer Melt Viscosity in Melt Flow and Flammability Behavior," *Proceedings of the Fall Conference of the Fire Retardant Chemicals Association*, Ponte Vedra, Florida, October, 2000.
- [231] Kurschner P., Maki-Marttunen T., Vestergaard S., Wandl S., *Modelling and Simulation of Ice/Snow Melting*, The 22nd ECMI Modelling Week in Eindhoven, The Netherlands, October 31, 2008.

- [232] R.E. Lyon, M.L. Janssens, Polymer Flammability, Final Report DOT/FAA/AR-05/14, Federal Aviation Administration, 2005.
- [233] Tian, M. Ph.D. thesis, Eindhoven University of Technology, Understanding the Organization and Reorganization of Polymer Crystal ISBN 90-386-2705-x.
<http://alexandria.tue.nl/extra2/200412853.pdf>
- [234] Onate E., Marti J., Ryzhakov P., Riccardo Rossi R., Idelsohn S.R., Analysis of the melting, burning and flame spread of polymers with the particle finite element method, Computer Assisted Methods in Engineering and Science, 20: 165–184, 2013.
- [235] Horrocks A.R., Kandola B., Flammability and Fire Resistance of Composites, Chapter 9 in A.C.Long (ed), Design and Manufacture of textile composites, Woodhead Publishing Ltd, Cambridge, 2005.
- [236] Phillips L N (Ed), 'Design with Advanced Composite Materials', London, Springer-Verlag, 1989.
- [237] Quintiere J., Fundamentals of fire phenomena, Edition John Wiley & Sons Ltd, Copyright 2006.
- [238] Kandare E., Kandola B.K., Staggs J.E.J., 'Global kinetics of flame retarded epoxy resin formulations', *Polymer Degradation and Stability* 92 (2007) p. 1778
- [239] Drysdale D.D., *An introduction to Fire Dynamics*, Second Edition, John Wiley & Sons, Chichester, 1998.
- [240] Kuznetsov, G. V., Rudzinskii, V. P., "Heat transfer in intumescent heat- and fire-insulating coatings", *Journal of Applied Mechanics and Technical Physics*, Vol. 40, No. 3, 1999.
- [241] Bartholmai M., Schriever R., Scharfel B., "Influence of external heat flux and coating thickness on the thermal insulation properties of two different intumescent coatings using cone calorimeter and numerical analysis", *Fire and Materials*, Vol. 27, Issue 4, 151 – 162, 2003.
- [242] Gómez-Mares M., Tugnoli A., Larcher S., Landucci G., Cozzani V., " Experimental Study and Numerical Simulation of Epoxy Intumescent Passive Fire Protection Performance", Conference paper. January 2011. DOI: 10.3303/CET1124194. Conference: 10th International Conference on Chemical and Process Engineering, Volume: 24
- [243] Mesquita, L.M.R.; Piloto, P.A.G.; Vaz, M.A.P.; Pinto, T.; "Decomposition of intumescent coatings: comparison between numerical method and experimental results", *Application of Structural Fire Design*, ISBN: 978-80-01-04266-3, pp. 140-145, Prague, Czech Republic, 19-20 February 2009.
- [244] Giuseppe V. Di Filippo, Maria E. Gonzalez, Maria T. Gasiba, A.V. Müller, *J. Appl. Polym. Sci.*, 1987, 34, 1959.
- [245] J.E J. Staggs, "Thermal conductivity estimates of intumescent chars by direct numerical simulation", *Fire Safety Journal*, 45(4), pp. 228-237 (2010)
- [246] B. Gardelle, S. Duquesne, V. Rerat and S. Bourbigot, "Thermal degradation and fire performance of intumescent silicone-based coatings", *Polymers for Advanced Technologies*, 24(1), pp. 62-69 (2013).

Appendix 1: Numerical computation of heat transfer

A.1 Finite Difference Method (FDM)

This is the oldest known method introduced by Euler in 1750 to find numerical solutions of Partial Differential Equations (PDE's). In the mathematical modelling process, the Finite Difference method (FDM) is one useful mathematical technique among several different others for obtaining numerical solutions to partial differential equation (PDE) which are generally too difficult to solve by standard analytical techniques. Taylor series expansions are used to have approximations of the derivatives appearing in the PDE's and the continuous function in PDE's is replaced by a discrete approximation. The word "discrete" means that the numerical solution is known only at a finite number of points. In general, increasing the number of points not only increases the degree of resolution, but also the accuracy of the numerical solution.

FDM discrete approximation results in a set of algebraic equations that are evaluated for the values of the discrete unknowns. The mesh is the set of locations where the discrete solution is computed. These points are called nodes. Two key parameters of the mesh are Δx , the local distance between adjacent points in space, and Δt , the local time between adjacent time steps. The numerical derivatives are called difference formulas that involve only the discrete values associated with positions on the mesh. Thus, using the FDM to solve a PDE means replacing all derivatives with difference formulas [1].

The first step of the method is to discretise the domain by defining a partition grid with two families of lines:

- Grid lines of same family do not intercept.
- Grid lines of different families intercept only once.

In two dimensions (2D) each node is identified by (i, j) as shown in Figure 3.14. The unknown variable of each node of the field depends on neighbouring nodes providing then a set of algebraic equations covering the whole domain.

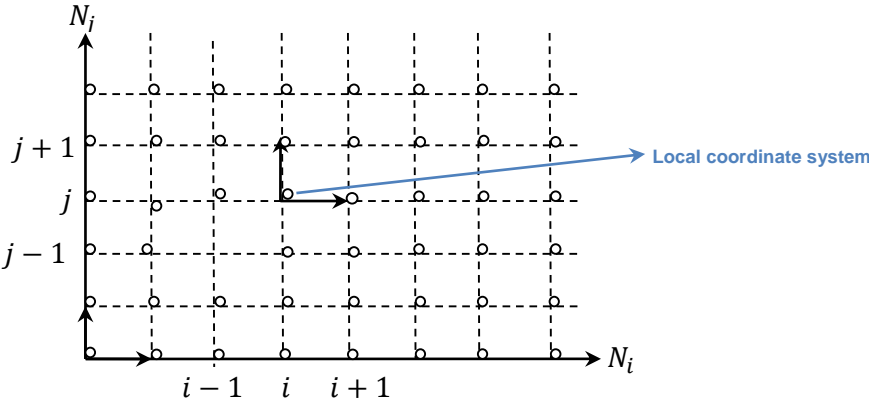


Figure A1: Domain discretisation by nodes

A. 2 One dimension (1D) continuous derivatives function.

The derivative or slope at x_i in 1D according is schematically described on the following Figure 3.15 [1-2].

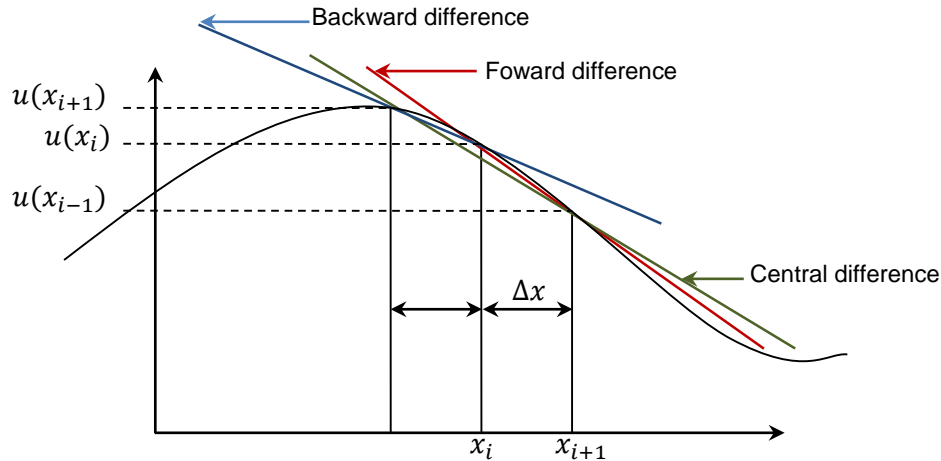


Figure A2: Different geometric interpretations of the first-order approximation

The derivative at x_i can be calculated analytically by:

$$\left(\frac{\partial u}{\partial x}\right)_{x_i} = \lim_{\Delta x \rightarrow 0} \left(\frac{u(x_{i+1}) - u(x_i)}{\Delta x}\right) = \lim_{\Delta x \rightarrow 0} \left(\frac{u(x_i) - u(x_{i-1})}{\Delta x}\right) = \lim_{\Delta x \rightarrow 0} \left(\frac{u(x_{i+1}) - u(x_{i-1})}{2\Delta x}\right)$$

One of those three approximate calculations is better than another according to the situation considered. Quality of approximation improves as Δx is made smaller. Assuming that Δx is uniform on the whole grid (1D uniform grid):

$$\Delta x = x_i - x_{i-1} = x_{i+1} - x_i$$

The following definitions are adopted:

- Forward Difference (FD) uses x_i and x_{i+1} :

$$\left(\frac{\partial u}{\partial x}\right)_{x_i} = \lim_{\Delta x \rightarrow 0} \left(\frac{u(x_{i+1}) - u(x_i)}{\Delta x}\right)$$

- Backward Difference (BD) uses x_i and x_{i-1} :

$$\left(\frac{\partial u}{\partial x}\right)_{x_i} = \lim_{\Delta x \rightarrow 0} \left(\frac{u(x_i) - u(x_{i-1})}{\Delta x}\right)$$

- Central Difference (CD) uses x_{i-1} and x_{i+1} :

$$\left(\frac{\partial u}{\partial x}\right)_{x_i} = \lim_{\Delta x \rightarrow 0} \left(\frac{u(x_{i+1}) - u(x_{i-1}))}{2\Delta x} \right)$$

A.3 One dimension (1D) Taylor series expansions

To use computer to solve differential equations derivatives are replaced by appropriate differential quotients. If it is assumed that the function can be differentiated many times then Taylor's Theorem is a very useful device in determining the appropriate difference quotient to use. Finite difference approximations of $u(x)$ near x_i using Taylor expansion at order n is given by [1-3]:

$$u(x) = u(x_i) + \frac{(x - x_i)}{1!} \left. \frac{\partial u}{\partial x} \right|_{x_i} + \frac{(x - x_i)^2}{2!} \left. \frac{\partial^2 u}{\partial x^2} \right|_{x_i} + \dots + \frac{(x - x_i)^n}{n!} \left. \frac{\partial^n u}{\partial x^n} \right|_{x_i}$$

Thus by replacing in that previous equation, x by x_{i+1} or x by x_{i-1} respectively, $u(x_{i+1})$ and $u(x_{i-1})$ can be expressed in term of $u(x_i)$ and the first different derivatives are:

- FD uses x_i and x_{i+1} :

$$\left(\frac{\partial u}{\partial x}\right)_{x_i} = \frac{u(x_{i+1}) - u(x_i)}{\Delta x} - \frac{\Delta x}{2} \left. \frac{\partial^2 u}{\partial x^2} \right|_{x_i} - \frac{\Delta x^2}{6} \left. \frac{\partial^3 u}{\partial x^3} \right|_{x_i} + \text{high order terms (h.o.t)}$$

- FD uses x_i and x_{i-1} :

$$\left(\frac{\partial u}{\partial x}\right)_{x_i} = \frac{u(x_i) - u(x_{i-1}))}{\Delta x} + \frac{\Delta x}{2} \left. \frac{\partial^2 u}{\partial x^2} \right|_{x_i} - \frac{\Delta x^2}{6} \left. \frac{\partial^3 u}{\partial x^3} \right|_{x_i} + \text{high order terms (h.o.t)}$$

- CD uses x_{i-1} and x_{i+1} :

$$\left(\frac{\partial u}{\partial x}\right)_{x_i} = \frac{u(x_{i+1}) - u(x_{i-1}))}{\Delta x} - \frac{\Delta x^2}{3} \left. \frac{\partial^3 u}{\partial x^3} \right|_{x_i} + \text{high order terms (h.o.t)}$$

$\left(\pm \frac{\Delta x}{2} \left. \frac{\partial^2 u}{\partial x^2} \right|_{x_i} - \frac{\Delta x^2}{6} \left. \frac{\partial^3 u}{\partial x^3} \right|_{x_i}\right)$ and $\left(-\frac{\Delta x^2}{3} \left. \frac{\partial^3 u}{\partial x^3} \right|_{x_i}\right)$ are called first or second order approximation truncation error and their notations are respectively $\theta(\Delta x)$ and $\theta(\Delta x^2)$. As Δx is small $\theta(\Delta x)$, $\theta(\Delta x^2)$ and *h.o.t* can be neglected and formulas similar to those are determined by geometrical approach. Moreover as Δx tends to zero, the errors tend to zero and the

approximation of the derivatives by using Taylor series expansions is improved in convergence but errors are always introduced mainly by truncation errors.

By definition FD and BD formulas for the first derivatives are called “one-sided” formulas and the power of Δx with which the truncation error tends to zero is called the order of accuracy of the finite difference approximation.

Three remarks can be introduced;

- The second derivative can be calculated by subtracting FD from BD

$$\left(\frac{\partial^2 u}{\partial x^2}\right)_{x_i} = \frac{u(x_{i+1}) - 2u(x_i) + u(x_{i-1}))}{\Delta x^2} + \theta(\Delta x^2)$$

- Considering the interval [0,1] discretised in 11 mesh points in 1D domain, Δx is then equal to 0.1 and the first order approximation has a truncation error $\theta(\Delta x)$ around $\theta(10\%)$ while the second order approximation has a truncation error $\theta(\Delta x^2)$ around $\theta(1\%)$. To obtain a first order approximation with $\theta(1\%)$, Δx has to be equal to 0.01 that corresponds to a discretisation of 101 mesh points.
- The first Finite Difference (FD) formulas for $\left.\frac{\partial u}{\partial x}\right|_{x_i}$ can be considered as a central difference with respect to the midpoint so that:

- For FD:

$$\left(\frac{\partial u}{\partial x}\right)_{x_{i+\frac{1}{2}}} = \frac{u(x_{i+1}) - u(x_i)}{\Delta x} + \theta(\Delta x^2)$$

- For BF:

$$\left(\frac{\partial u}{\partial x}\right)_{x_{i-\frac{1}{2}}} = \frac{u(x_i) - u(x_{i-1}))}{\Delta x} + \theta(\Delta x^2)$$

In this case an order of accuracy is gained using the same formulas [4].

A.4 FDM for 1D heat transfer equation

For example, in the one dimensional heat equation eqn (3.1) there are derivatives with respect to time, t , and derivatives with respect to space, z [4].

$$\frac{\partial T(x, t)}{\partial t} = \alpha \left(\frac{\partial^2 T(x, t)}{\partial x^2} \right), \quad 0 \leq x \leq L, \quad t \geq 0 \quad (\text{Eqn A1})$$

Where $T(x, t)$ is the temperature, $\alpha = \frac{k}{\rho c_p}$ is the thermal diffusivity, k is the specific thermal conductivity, ρ is the specific density and c_p is the specific heat capacity. Equation eqn(3.1) is a transient heat conduction equation in a material slab of width L . In a practical computation, the solution is obtained only for a finite time, t_{max} . Numerical solution of eqn(3.1) requires specification of boundary conditions at $x = 0$ and $x = L$, and initial conditions at $t = 0$. Boundary and initial conditions of slab heated by an incident heat flux φ_{inc} on the top surface and all the others side being insulated are:

$$\varphi(0, t) = 0, \quad \varphi(L, t) = \varphi_{inc}, \quad T(x, 0) = T_a.$$

A.4.1 Explicit Scheme Method.

The explicit scheme is forward-time and a centred-space (FTCS) method where subscripts denote location in space and superscripts denote location in time ($T(x_i, t_n) = T_i^n$). Then the approximation for the equation at x_i is [4-5]:

$$\frac{T_i^{n+1} - T_i^n}{\Delta t} = \alpha \left(\frac{T_{i+1}^n - 2T_i^n + T_{i-1}^n}{\Delta x^2} \right)$$

Where the truncation error is $\theta(\Delta t, \Delta x^2)$ and $\alpha = \frac{k}{\rho c_p}$ is the diffusivity coefficient. With the Fourier number ($F = \frac{\alpha \Delta t}{\Delta x^2}$) the simplified update is:

$$T_i^{n+1} = FT_{i-1}^n + (1 - 2F)T_i^n + FT_{i+1}^n$$

Notice that the next time step ($n + 1$) at x_i is updated from the values at the previous time step (n) at x_{i-1} , x_i and x_{i+1} .

A.4.2 Stability of Explicit Scheme

As a general rule, for explicit FTCS scheme (Euler's method for time) to be stable, the value of F has to be less than 0.5 ($F \leq 0.5$). This restriction is called a Courant-Friedrich-Levy (CFL) condition on grid sizes. For smaller numbers of time steps (larger time steps), temperature solutions quickly blew up because of $F \geq 0.5$. Therefore an explicit scheme typically requires many more time steps to achieve the convergence desired than an implicit

scheme but it is typically a simple update. Because of the CFL condition, implicit method is much preferred than explicit methods for conduction heat transfer equation [4].

A.4.3 Implicit Scheme Method.

Implicit scheme is a backward-time and a centred-space (BTCS) and the approximation of the diffusion heat equation at x_i is [6]:

$$\frac{T_i^{n+1} - T_i^n}{\Delta t} = \alpha \left(\frac{T_{i+1}^{n+1} - 2T_i^{n+1} + T_{i-1}^{n+1}}{\Delta x^2} \right)$$

Where the truncation error is $\theta(\Delta t, \Delta x^2)$ and $\alpha = \frac{k}{\rho c_p}$ is the diffusivity coefficient. With the Fourier number ($F = \frac{\alpha \Delta t}{\Delta x^2}$) the simplified update is:

$$T_i^n = -FT_{i+1}^{n+1} + (1 + 2F)T_i^{n+1} - FT_{i-1}^{n+1}$$

Where the next time step (n) at x_i is updated from the values at the next time step ($n + 1$) at x_{i-1} , x_i and x_{i+1} .

A.4.4 Stability of Implicit Scheme.

The implicit scheme is stable and so there is no CFL condition on the time steps like in the explicit scheme. The inverse system is stable for any size time steps or space steps so the accuracy desired will dictate how small of grid size steps is needed to use.

A.4.5 Crank-Nicholson Scheme Method.

Explicit and implicit schemes have a temporal truncation error of $\theta(\Delta x)$. When a time accurate solution is needed, the Crank-Nicolson scheme has significant advantages. The Crank-Nicolson scheme is not significantly more difficult to implement than the implicit scheme, and it has a temporal truncation error that is $\theta(\Delta x^2)$. The Crank-Nicolson scheme is implicit and unconditional stable.

The left hand side of the heat equation is approximated with the forward time difference used in the FTCS scheme. The right hand side of the heat equation is approximated with the average of the central difference scheme evaluated at the current and the previous time step. Therefore the heat conduction equation is approximated by [2-5]:

$$\frac{T_i^{n+1} - T_i^n}{\Delta t} = \frac{\alpha}{2} \left(\frac{T_{i+1}^{n+1} - 2T_i^{n+1} + T_{i-1}^{n+1}}{\Delta x^2} + \frac{T_{i+1}^n - 2T_i^n + T_{i-1}^n}{\Delta x^2} \right)$$

Rewritten as:

$$-\frac{1}{2}FT_{i+1}^{n+1} + (1+F)T_i^{n+1} - \frac{1}{2}FT_{i-1}^{n+1} = \frac{1}{2}FT_{i-1}^n + (1-F)T_i^n + \frac{1}{2}FT_{i+1}^n$$

The Crank-Nicolson scheme is implicit and a system of equations for the temperature T must be solved at each time step. The system of equations is identical to those of the implicit FTCS scheme. Algorithmically, the implicit FTCS scheme and Crank-Nicolson scheme are very similar but Crank-Nicolson scheme has a truncation error of $(\theta(\Delta x^2) + \theta(\Delta x^2))$ that means its temporal truncation error is significantly smaller than the temporal truncation error of the implicit FTCS scheme.

A.5 All FDM schemes in one.

It can be considered instead $\left(\frac{T_i^{n+1}-T_i^n}{\Delta t}\right)$ as an approximation of $\left(\frac{\partial T_i^{n+a}}{\partial t}\right)$, $0 \leq a \leq 1$, then:

- $a = 0$ leads to explicit scheme.
- $a = 1$ leads to implicit scheme.

Note that:

$$\frac{T_i^{n+1} - T_i^n}{\Delta t} = \frac{\partial T_i^{n+a}}{\partial t} + \theta(\Delta x^2)$$

Where $T_i^{n+a} = T_i^n + a\Delta t$. This suggests the following general scheme:

$$\frac{T_i^{n+1} - T_i^n}{\Delta t} - \alpha\alpha \left(\frac{T_{i+1}^{n+1} - 2T_i^{n+1} + T_{i-1}^{n+1}}{\Delta x^2} \right) - \alpha(1-a) \left(\frac{T_{i+1}^n - 2T_i^n + T_{i-1}^n}{\Delta x^2} \right) = 0$$

Re-written as:

$$(1 + 2aF)T_i^{n+1} - aFT_{i-1}^{n+1} - aFT_{i+1}^{n+1} = (1 - 2(1-a)F)T_i^n + (1-a)FT_{i-1}^n + (1-a)FT_{i+1}^n$$

So for (m) nodes, a simultaneous equation of (m) equations is derived from the above equation and they have to be solved for T . Also, those simultaneous equations can be written in matrices form as following:

$$[C][\dot{T}] = [A][T]$$

Recall that the temperature at time t is denoted by the exponent n and the temperature at time $(t + \Delta t)$ is denoted by the superscript $(n + 1)$. So let define the temperature T variation from t to $(t + \Delta t)$ as a combination of T^n and T^{n+1} as following:

$$T = a \cdot T^{n+1} + (1 - a)T^n$$

Matrices equation can be written as:

$$[C] \left[\frac{T^{n+1} - T^n}{\Delta t} \right] = [A][a \cdot T^{n+1} + (1 - a)T^n]$$

Rearranging the above equation becomes:

$$\left(\frac{[C]}{\Delta t} - a \cdot [A] \right) \cdot [T^{k+1}] = \left(\frac{[C]}{\Delta t} - (1 - a) \cdot [A] \right)$$

Simplifying the notations as following:

$$\left(\frac{[C]}{\Delta t} - a \cdot [A] \right) = [Z], \left(\frac{[C]}{\Delta t} - (1 - a) \cdot [A] \right) = [W]$$

Finally:

$$[Z][T^{k+1}] = [W] \cdot [T^k]$$

Depending on the value of 'a' the previous equation can be compute easily according to the explicit or implicit.

Then:

- If $\frac{1}{2} < a < 1$, the conductive heat equation is approximated with the 'implicit scheme method'.
- If $a = 1$, the conductive heat equation is approximated with the pure implicit scheme method.
- For $a = \frac{1}{2}$, the conductive heat equation is approximated with the 'Crank-Nicholson scheme method'.
- For $a = 0$, the conductive heat equation is approximated with the 'implicit scheme method'.

In the following Figure 3.20, the temperature variation is represented according to each scheme formulation.

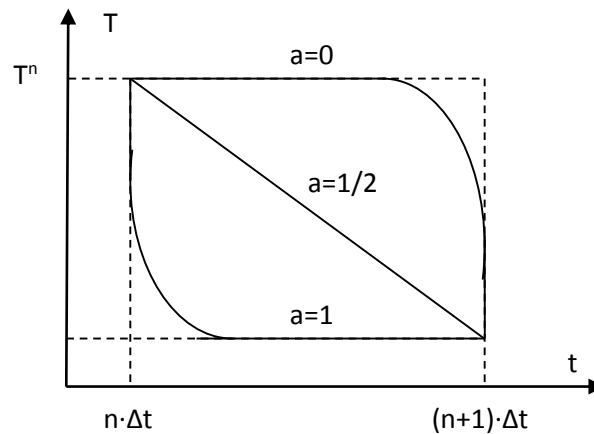


Figure A3: Temporal scheme formulation

Using the matrix equation computed with Matlab software the temperature profile can be obtained for each node by computing the temperature at any time t over a chosen duration and for the chosen scheme formulation (Implicit, Explicit or Crank-Nicholson). The numerical resolution of PDEs involving the heat equation is treated in many research works. Some of them provide a more mathematical development of finite difference methods [7-8]. Others take a more applied approach that also introduces implementation issues [9-10].

A.6 Sensitivity analysis.

How heat transfer phenomenon within a polymeric material depends to parameters such as specific thermal conductivity, specific heat capacity or specific density. If one of those parameters value changes, how will this affect the temperature?

Sensitivity analysis helps to evaluate how important the influence of each parameter can have onto the rise of temperatures. That is key information to improve fire resistance of polymeric material. It is therefore necessary to quantify the material sensitivity by using a sensitivity function.

A sensitivity function $S(T, x)$ is define as a quantity called sensitivity of T to x . The variable x represents the parameter whose influence is being evaluated n [6].

$$S(T, x) = \frac{\text{Relative change in } T}{\text{Relative change in } x} = \frac{\left(\frac{\Delta T}{T}\right)}{\left(\frac{\Delta x}{x}\right)} = \frac{\Delta T}{\Delta x} \cdot \frac{x}{T}$$

If Δx tends to zero, $S(T, x)$ is then:

$$S(T, x) = \frac{dT}{dx} \cdot \frac{x}{T} \quad (\text{Eqn A2})$$

Graphically $S(T, x)$ is illustrated in Figure 3.16:

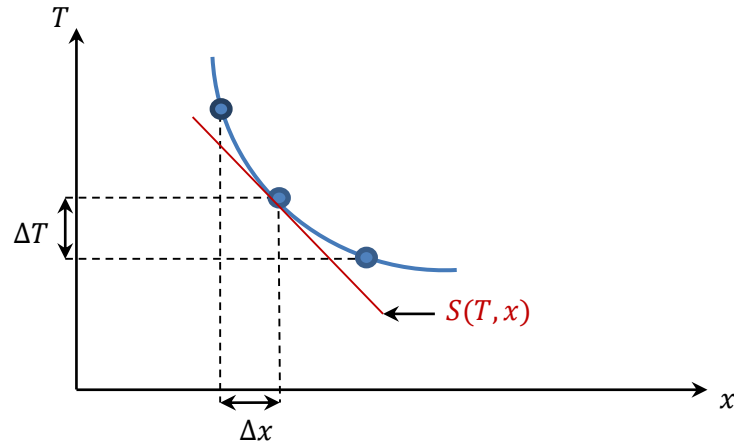


Figure A4: Geometrical representation of $S(T, x)$

Appendix references

- [1] Belotserkovskii O. M., Forsythe G. E., Wasow W. R., Finite-difference methods for partial differential equations. Book Review”, Zh. Vychisl. Mat. Mat. Fiz. 2:3 (1962), 508–509.
- [2] Thom A., Apelt C. J., ‘Field Computations in Engineering and Physics’, London: D.Van Nostrand, 1961.
- [3] Matthew, Sadiku, "Numerical Techniques in Electromagnetics," by, CRC Press, Inc. (1992)
- [4] Hoffman J. D., ‘Numerical Methods for Engineers and Scientists’, McGraw-Hill, New York, 1992.
- [5] Cooper J., ‘Introduction to Partial Differential Equations with Matlab’, Birkhauser, Boston, 1998.
- [6] Salva N. N., Tarzia D. A., ‘A sensitivity analysis for the determination of unknown thermal coefficients through a phase-change process with temperature-dependent thermal conductivity’, International Communications in Heat and Mass Transfer 38 (2011) 418–424.